Fermilab Recycler Ring

Technical Design Report

November 1996

Revision 1.2

Table of Contents

1. Introduction

This report describes the technical design of the Fermilab Recycler Ring. The purpose of the Recycler is to augment the luminosity increase anticipated from the implementation of the Fermi III upgrade project, which has as its main component the Fermilab Main Injector construction project.

The Recycler is a fixed 8 GeV kinetic energy storage ring. It is located in the Main Injector tunnel directly above the Main Injector beamline, near the ceiling. The construction schedule calls for the installation of the Recycler ring during the installation of the Main Injector. This aggressive construction schedule is made possible by the exclusive use of permanent magnets in the ring lattice, removing the need for expensive conventional iron/copper magnet construction along with the related power supplies, cooling water system, and electrical safety systems. The location, operating energy, and mode of construction are chosen to minimize operational impacts on both Fermilab's ongoing High Energy Physics program and the Main Injector construction project.

1.1 Role in the Fermilab III Program

The Tevatron Collider provides the highest energy collisions in the world. To fully exploit this unique tool, Fermilab is committed to a program of accelerator upgrades for the purpose of increasing the Collider luminosity. Over the past 7 years the luminosity has been increased from a typical peak of 1.6×10^{30} $cm^{-2}sec^{-1}$ in 1989 to over 2×10^{31} $cm^{-2}sec^{-1}$ during 1995. Note that the original design peak luminosity of the Tevatron Collider was 1.0×10^{30} $cm^{-2}sec^{-1}$.

The Main Injector will supply a larger flux of protons for antiproton production, more intense proton bunches for use in the Collider, and a higher efficiency acceleration of antiprotons. The role of the Recycler ring is to provide more antiprotons for the Tevatron, which proportionally increases the luminosity. This is accomplished by acting as a high reliability post-Accumulator and receptacle for recycled antiprotons from the previous Collider store. Prior to the development of the Recycler ring, the peak luminosity goal of the Fermi III upgrade program was 8×10^{31} cm^{-2} sec^{-1}. With the construction of the Recycler ring, a typical peak luminosity of 2×10^{32} cm^{-2} sec^{-1} is expected. This factor of 2-3 increase in luminosity comes from the availability of more antiprotons at Tevatron injection. The Reycler is also the foundation of future accelerator upgrades which can generate another order of magnitude luminosity increase up to an ultimate goal of greater than 1×10^{33} $cm^{-2}sec^{-1}$. This report documents the design of the new fixed-energy Recycler storage ring to be placed in the Main Injector tunnel.

Figure 1.1 displays the history of the typical peak luminosity as a function of time since 1989, which shows an exponential growth with a doubling time of 1.5 years. With the addition of the Recycler ring and its commissioning along with the Main Injector, the Tevatron Collider will be able to remain on this exponential slope. The first open point represents the initial typical peak luminosity goal of the Main Injector project. The second open point represents the luminosity goal of 2×10^{32} $cm^{-2}sec^{-1}$ during Collider Run II when the Recycler is added to the picture. It should be possible, with further

accelerator upgrades, to achieve a luminosity of $1x10^{33}$ $cm^{-2}sec^{-1}$, which is the highest luminosity open point in figure 1.1.

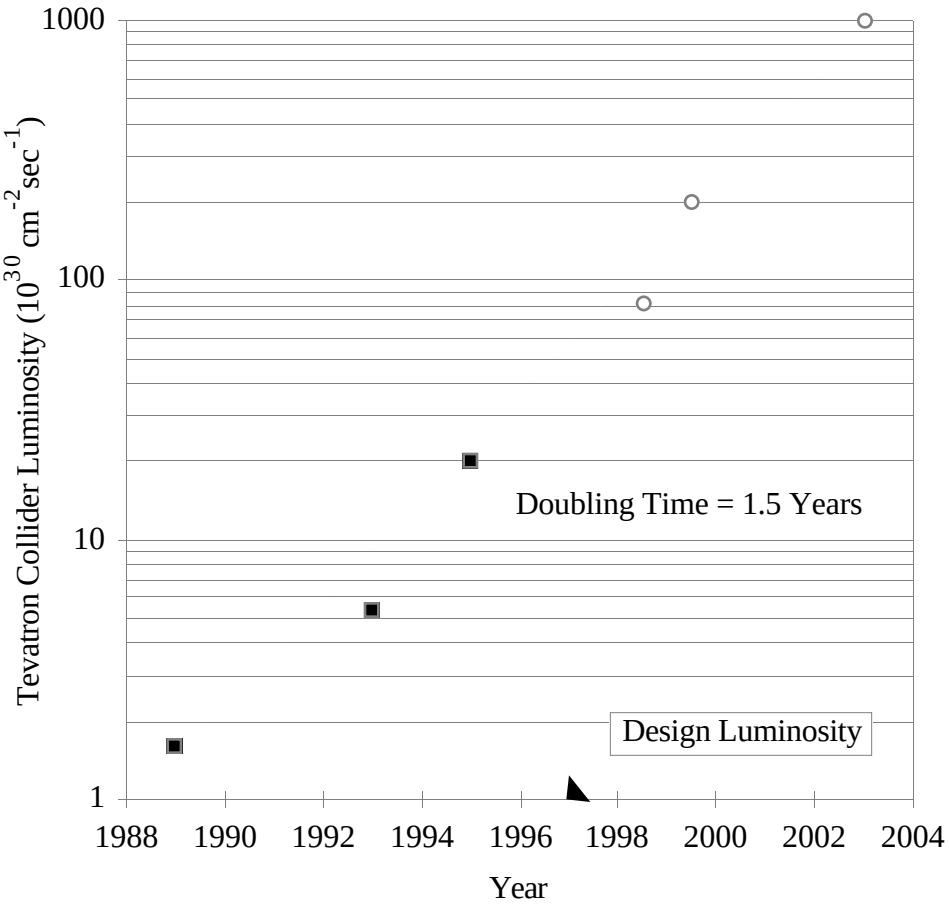

Figure 1.1: Tevatron Collider luminosity as a function of time. The filled circles are measured "best typical" peak luminosities, the line is an exponential fit to the data, and the open points represent goals for the future.

1.2. Performance

The Recycler ring parameter list is given in table 1.1. The placement and design of the ring were chosen to minimize its impact on the existing high energy physics program. This minimization takes place mostly in the areas of project cost and schedule. After the end of the present fixed target run, the only scheduled prolonged accelerator shutdown before the start of LHC operations at CERN is the 1998 Main Injector connection to the Tevatron. In the interest of accumulating the maximum amount of integrated luminosity before the LHC is publishing high energy physics results, an additional Tevatron shutdown for installation of the Recycler would be highly undesirable. By using as many of the already established Main Injector subsystem and lattice designs as possible, the ability to finish the Recycler installation before the completion of the Main Injector is made possible.

Table 1.1: Recycler ring parameter list.

Circumference	3319.400	m
Momentum	8.889	GeV/c
Number of Antiprotons	2.5×10^{12}	
Maximum Beta Function	55	m
Maximum Dispersion Function	2.0	m
Horizontal Phase Advance per Cell	86.8	degrees
Vertical Phase Advance per Cell	79.3	degrees
Nominal Horizontal Tune	25.425	
Nominal Vertical Tune	24.415	
Nominal Horizontal Chromaticity	-2	
Nominal Vertical Chromaticity	-2	
Transition Gamma	20.7	
Transverse Admittance	40	π mmmr
Fractional Momentum Aperture	1%	
Superperiodicity	2	
Number of Straight Sections	8	
Number of Standard Cells in Straight Sections	18	
Number of Standard Cells in Arcs	54	
Number of Dispersion Suppression Cells	32	
Length of Standard Cells	34.576	m
Length of Dispersion Suppression Cells	25.933	m
Number of Gradient Magnets	108/108/128	
Magnetic Length of Gradient Magnets	4.267/4.267/2.845	m
Bend Field of Gradient Magnets	1.45/1.45/1.45	kG
Quadrupole Field of Gradient Magnets	3.6/-3.6/7.1	kG/m
Sextupole Field of Gradient Magnets	3.3/-5.9/0	kG/m^2
Number of Lattice Quadrupoles	72	
Magnetic Length of Quadrupoles	0.5	m
Strength of Quadrupoles	30	kG/m

The other, more important, means of insuring prompt construction of the Recycler ring is to keep the cost very low. In order to achieve this feat, all subsystems must be designed to be simultaneously lower cost. For instance, the biggest cost savings comes from placing the Recycler ring in the Main Injector tunnel and avoiding civil construction. Taking advantage of the fact that this ring operates at a fixed momentum, the magnets are built using permanent strontium ferrite magnets. By designing the

magnets to require very little human labor in their construction, a substantial cost reduction is realized. Minimizing the number of magnets is accomplished by merging the quadrupole and dipole functions into gradient magnets. Because the magnetic field is permanent, no power supplies, LCW cooling systems, power distribution cables, or electrical safety systems are required. Since the permanent magnets are very stable against time and temperature, distributed correction magnets are also not needed.

In addition, technological advancements in beam pipe preparation have led to superior vacuum pressures at lower cost. Stochastic cooling is employed to provide the phase space density necessary for Tevatron Collider operations. By recycling many of the components used in the Tevatron bunched beam stochastic cooling R&D project, and minimizing the design costs for the pickup and kicker tanks by copying old Accumulator tanks, the cost of this subsystem is also minimized. The cost of instrumentation is also reduced through technological innovation, but these saving are reinvested back into the ring to provide more detailed and precise measurements of beam parameters.

The design kinetic energy of the Recycler ring is precisely 8.000 GeV. This is the design kinetic energy of the Accumulator, as well as the injection kinetic energy of the Main Injector and extraction kinetic energy of the Booster. In the past considerable debate has occurred regarding the measurement and synchronization of this energy between these accelerators. With the planned construction of the Recycler with fixed field permanent magnets, an unambiguous energy reference is installed into the Fermilab accelerator complex. All other accelerators will be energy matched to the Recycler.

1.3. Operational Roles

The purpose of the Recycler is to further increase the luminosity of the Tevatron Collider over the luminosity goals of the Main Injector by itself. The majority of the luminosity improvement comes from the ability to inject more antiprotons into the Tevatron each store.

The first role of the Recycler is to act as a high reliability storage ring for antiprotons. Because there are few power sensitive components, there are virtually no mechanisms for inadvertent beam loss. Studying the data from the existing Antiproton Source complex, composed of the Debuncher and Accumulator rings, a couple of recent statistics ratify this concern.

In 35 weeks of running, the total number of antiprotons stacked was 16.72×10^{13}. In the same time interval, the total number of antiprotons lost or dumped was 2.42×10^{13}, which is 14.5% of antiprotons stacked. Additionally, there were 506 hours of Antiproton Source downtime out of a total of 9552 hours of operation (5.3% downtime). It is not impossible to lose the beam in the Recycler, so some of the types of failures found in the Accumulator will also occur in the Recycler. Therefore, the percentage improvement in antiproton availability with the use of the Recycler will not be the full 14.5%.

The second role of the Recycler is to act like a post-Accumulator ring. As the stack size in the Accumulator ring increases, there comes a point when the stacking rate starts to decrease. By emptying the contents of the Accumulator into the Recycler periodically, the Accumulator is always operating in its optimum antiproton intensity regime.

The third role of the Recycler, and by far the leading factor in luminosity increase, is to act as a receptacle for antiprotons left over at the end of Tevatron stores. By cooling these antiprotons and reintegrating them into the Recycler stack, the effective stacking rate, and hence the luminosity, is more than doubled.

1.4. Organization of this Report

This report is organized into four chapters. Chapter 1 is the introduction. Chapter 2 is the summary of the accelerator physics issues of the Recycler ring and beamlines. Chapter 3 contains a description of the technical component subsystems as well as overviews of design specifications. Discussions and descriptions of technical component subsystems are organized to follow the Work Breakdown Structure (WBS) of the project. All technical components are contained in WBS category 3.1. The third digit of the WBS describes the component type: 1=magnets, 2=vacuum, 3=power supplies, etc. Chapter 4 summarizes the civil construction for the Recycler.

2. Accelerator Physics

The purpose of the Recycler ring is to improve the luminosity performance of the Tevatron Collider during Run II. The design luminosity of 2×10^{32} cm^{-2} sec^{-1} is accomplished by creating more antiprotons at a faster rate, storing existing antiprotons in a more reliable fashion, and recycling antiprotons remaining in the Tevatron at the end of stores. The Recycler ring plays a major role in each of these three areas of improvement.

In this chapter the role of accelerator physics and novel technologies in the Recycler are reviewed. This discussion starts with a detailed overview of the operational role of the Recycler during Run II. Next, the beam manipulations and accelerator technology crucial to the Recycler are described.

2.1. Operational Overview

In order to describe the operational role of the Recycler ring, it is necessary to explain the intricately interweaved operation of all of the particle accelerators in the entire accelerator complex. It is convenient to start this discussion when the Tevatron has just started a new store.

2.1.1. Operational Goals

The purpose of the Fermi III accelerator upgrades is to maximize the luminosity of the Tevatron Collider. In the absence of a crossing angle the luminosity per interaction region L is determined by the equation

$$L = \frac{N_p (N_a B) f_o (6\beta_r \gamma_r)}{2\pi \beta^* (\varepsilon_{np} + \varepsilon_{na})} H\left(\frac{\beta^*}{\sqrt{\frac{1}{2}\left(\sigma_{sp}^2 + \sigma_{sa}^2\right)}} \right) \quad , \quad (2.1.1)$$

in which $N_{p,a}$ is the number of protons and antiprotons per bunch, B is the number of bunches per beam, f_o is the revolution frequency of the Tevatron, β_r and γ_r are the relativistic velocity and energy of the beam, β^* is the value of the beta function at the interaction points, $\varepsilon_{np,na}$ are the proton and antiproton 95% normalized transverse emittances, σ_s is the rms bunch length, and the hour-glass luminosity form factor has the form

$$H(x) = \sqrt{\pi}\, x [1 - \Phi(x)]\, e^{x^2} \quad , \quad (2.1.2)$$

where $\Phi(x)$ is the error function. The transverse emittance is defined so that the transverse rms bunch widths are calculated using the equation

$$\sigma_{a,p}^2 = \beta^* \frac{\varepsilon_{na,np}}{(6\beta_r \gamma_r)} \quad . \quad (2.1.3)$$

The values for all of these parameters at the beginning of a store for Run I operations, anticipated after completion of the original Main Injector project, and after commissioning of the Recycler ring are listed in table 2.1.1.

Table 2.1.1: Initial Beam conditions for Run I (recently completed), originally anticipated post-Main Injector Run II, and Run II in which the Recycler ring is operational.

Initial Store Parameters	Run I	MI only	Recycler
N_p Proton Intensity/Bunch (10^9)	250	330	270
N_a Antiproton Intensity/Bunch (10^9)	60	36	66
B Number of Bunches/Beam	6	36	36
Minimum Time between Bunches (ns)	3500	395	395 (132)
E_o Beam Energy (GeV)	900	1000	1000
β^* Interaction Point Beta (cm)	35	35	35
ε_{np} Proton 95% Emittance (π mmmr)	24	30	18
ε_{na} Antiproton 95% Emittance (π mmmr)	15	15	15
σ_{sp} Rms Proton Bunch Length (cm)	50	45	45
σ_{sa} Rms Antiproton Bunch Length (cm)	50	45	33
f_o Revolution Frequency (kHz)	47.7	47.7	47.7
(N_aB) Total Antiproton Intensity (10^{10})	36	130	238
($\beta r \gamma r$) Relativistic Momentum	959	1066	1066
H Hour Glass Form Factor	0.65	0.69	0.72
L Peak Luminosity (10^{32} cm^{-2} sec^{-1})	0.19	0.8	2.0
$\int$L Integrated Luminosity (pb^{-1}/week)	3.8	17	40
N_{IR} Number of interaction Regions	2	2	2

The quantity N_aB (called the stack size) in equation (2.1.1) is just the total antiproton intensity injected into the Tevatron Collider, independent of the number of bunches that charge is divided into. Note that the luminosity grows proportionally with this number, the fact which is the basis of the luminosity improvement generated by the Recycler ring. This relationship between luminosity and antiproton availability is due to the fact that the proton intensity is limited.

The limit on the proton intensity comes from the observation that the maximum allowable total antiproton linear beam-beam tune shift from all bunch crossings with the proton bunches is approximately 0.026. The equation relating this maximum antiproton total tune shift ξ_{max} and the proton intensity is

$$\xi_{max} = \frac{r_o}{4\pi}\frac{N_p}{\varepsilon_{np}} N_{IR} \quad . \quad (2.1.4)$$

The quantity r_o is the classical radius of the proton (1.53×10^{-18} m). The number of interaction regions N_{IR} is at a minimum equal to the number of high energy physics

detectors operating in the collider. Plugging this equation for the tune shift into the equation for luminosity per interaction region (2.1.1) yields the result

$$L = \frac{(N_a B)}{N_{IR}\beta^*} \frac{2\xi_{max} f_o(6\beta_r\gamma_r)}{r_o\left(1+\frac{\varepsilon_{na}}{\varepsilon_{np}}\right)} H\left(\frac{\beta^*}{\sqrt{\frac{1}{2}\left(\sigma_{sp}^2+\sigma_{sa}^2\right)}}\right) \quad , \quad (2.1.5)$$

where the factors whose values can be significantly modified appear in the left fraction on the right hand side of the equation. The emittances of the protons and antiprotons can be changed, but the ratio of the proton to antiproton emittances is always near unity due to nonlinear beam dynamics concerns. Therefore, reducing the emittances of the beams is not helpful once the beam-beam limit has been reached.

Even though β^* can be changed, eventually the length of the bunch and the sensitivity of the lattice to errors in low-β quadrupole strengths limits the extent to which β^* can be reduced. The number of interaction regions is chosen by the high energy physics community. Note that for a uniform β^* in all detectors, the sum of the luminosity available in the Tevatron Collider at all interaction regions is conserved as the number of interaction regions is changed.

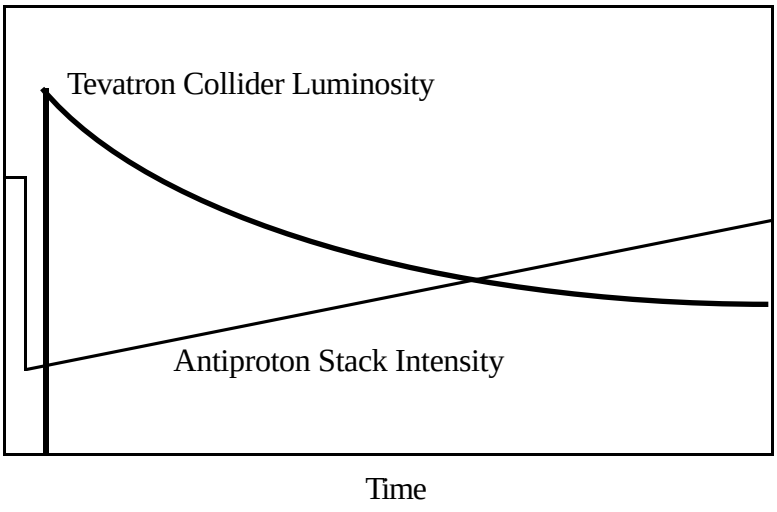

Figure 2.1.1: Sketch of antiproton stacking during Tevatron Collider stores. At the beginning of each store some of the stacked antiprotons are delivered to the Tevatron. During the store those antiprotons are replenished via continuous Main Injector operations.

2.1.2. Antiproton Stacking

As demonstrated in the previous section, the dominant limitation to high luminosity operations in proton-antiproton colliders is the availability of bright (high current and low emittance) antiproton beams. Antiprotons are produced by aiming 120 GeV protons from

the Main Injector onto a metallic target. For every million protons, approximately 15 antiprotons are captured, cooled, and stored for future use. Because of this very small yield, antiproton production must occur continuously while the Tevatron is storing beam and creating proton-antiproton collisions for high energy physicists.

While the Tevatron is storing beam at an energy of 1 TeV, the Main Injector is continuously cycling. Every ~2 seconds the Main Injector accelerates protons from a kinetic energy of 8 GeV to the required 120 GeV for antiproton production. The 8 GeV kinetic energy antiprotons from the target are cooled and stored (stacked) in the Debuncher and Accumulator rings. As the Tevatron stores the beam the luminosity decreases due to particle loss and emittance growth. Therefore, a certain antiproton stacking rate is required to keep the Tevatron operating at a determined typical peak luminosity level. Figure 2.1.1 contains a sketch of the Tevatron luminosity and antiproton stack size during collider operations.

2.1.3. Luminosity Evolution

The evolution of the luminosity and antiproton intensity during a Tevatron Collider store is determined by the luminosity itself, intrabeam scattering, external transverse and longitudinal emittance growth mechanisms, and the length of the store. The parameters which depend on luminosity itself are the proton and antiproton intensity lifetimes. The central purpose of the Tevatron Collider is to collide protons and antiprotons, using them up at the rate of

$$R_{lost} = N_{IR}\, L\, \sigma_{lost} \quad , \qquad (2.1.6)$$

where σ_{lost} is the 78 mb cross-section [E811 collaboration] for losing protons and antiprotons due to both inelastic and large elastic interactions and N_{IR} is the number of interaction regions in the Collider. The proton and antiproton intensity lifetimes due to this mechanism are calculated using the equation

$$\tau_{Lp,La} = \frac{N_{p,a}\, B}{R_{lost}} \quad . \qquad (2.1.7)$$

Another limit to beam intensity lifetime is the residual vacuum in the Tevatron. The vacuum intensity lifetime τ_{vac} is approximately 200 hours at the present time.

The other parameters which vary during a store are the bunch length and the transverse emittance. One mechanism observed to induce emittance growth during a store was external noise. When noise driven coherent betatron and synchrotron oscillations decohere due to nonlinearities, a constant emittance growth rate is established. Over the years this emittance growth rate has been lowered to a fairly insignificant level of 0.3 π mmmr/hr 95% normalized transversely and 0.01 eV-sec/hr 95% normalized longitudinally. Another mechanism is multiple Coulomb scattering against the residual molecules in the vacuum chamber.

The growth times of the transverse and longitudinal emittances due to intrabeam scattering in the Tevatron are described by the equations [D. Finley, TM-1646 (1989)]

$$\tau_{\varepsilon_p} = 0.054\left(\frac{6x10^{10}}{N_P}\right)\varepsilon_{nP}^{2.24}\ A_P^{0.68} \quad , \quad (2.1.8)$$

$$\tau_{A_p} = 0.103\left(\frac{6x10^{10}}{N_P}\right)\varepsilon_{nP}^{1.24}\ A_P^{1.68} \quad , \quad (2.1.9)$$

where ε_{np} and A_p are the normalized 95% transverse (π mmmr) and longitudinal (eV-sec) emittances of the protons and the times are in hours. The antiproton growth times are calculated similarly. This equation assumes the Tevatron Collider lattice and an RF voltage of 1 MV/turn.

By including all of the above effects into a calculation of the evolution of the luminosity and beam properties during a collider beam store, predictions can be made. In order to confirm that the factors affecting luminosity evolution are understood, these calculations were applied to the recently completed collider Run I. This model is quantitatively in agreement in all beam parameters in all measured stores in which comparisons have been performed. Therefore, it is with confidence that predictions of Run II performance are presented below.

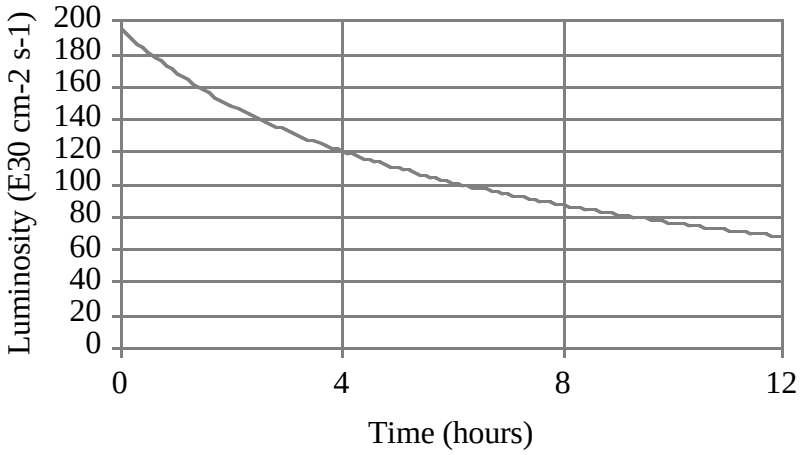

Figure 2.1.2: Prediction of the time evolution of luminosity during a Tevatron Collider store during Run II with the Recycler ring.

The prediction of Run II luminosity evolution appears in figure 2.1.2. The luminosity drops by a factor of two in about six hours. The next factor of two drop requires more than an additional 12 hours. The principal reason for this increase in the luminosity lifetime with elapsed time in the store is intrabeam scattering. The transverse emittance time evolution of both the protons and antiprotons are shown in figure 2.1.3. The emittance growth rates are initially steep and decrease with time in the store. In addition, the longitudinal emittance of the protons and antiprotons also grow during a store due to intrabeam scattering. The predictions for this effect of intrabeam scattering are displayed in figure 2.1.4.

The longitudinal emittance of the antiproton bunches in figure 2.1.4 start out small due to the fact that the Recycler ring is capable of forming the required intensity bunches without the use of coalescing. The 11 proton and antiproton bunches before coalescing in the present collider run have a longitudinal emittance of approximately 0.2 eV-s each. Instead of the expected longitudinal emittance of 2.2 eV-s for the coalesced bunch, the initial emittance ends up as ~3 eV-sec. The process of coalescing dilutes the longitudinal emittance by approximately 50%.

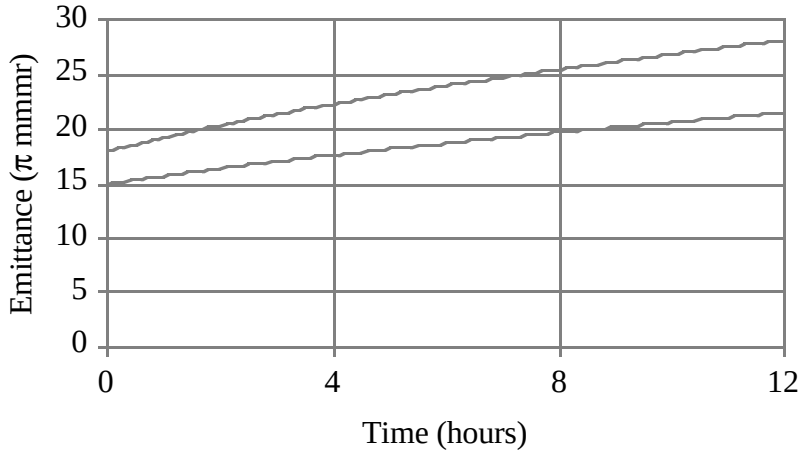

Figure 2.1.3: Predictions of the proton (upper) and antiproton (lower) transverse 95% invariant emittances as a function of time during Run II with the Recycler ring.

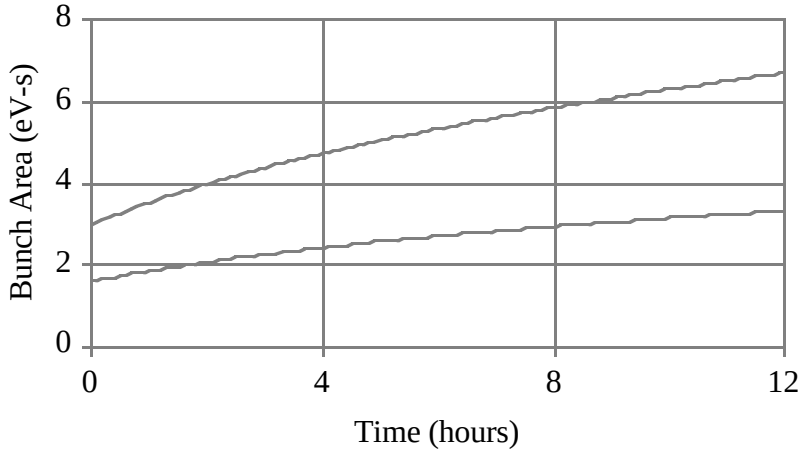

Figure 2.1.4: Predictions of the proton (upper) and antiproton (lower) longitudinal 95% invariant emittances as a function of time during Run II with the Recycler ring.

For 36x36 bunch operations, the total longitudinal emittance of the antiprotons stored in the Recycler ring must be partitioned into 36 equal portions. The total invariant 95% longitudinal emittance of the Recycler ring A_r is

$$A_r = 4\, T_o\, \sigma_e \qquad , \quad (2.1.10)$$

where T_o is the revolution period of the Recycler and σ_e is the rms energy spread. Given the Main Injector longitudinal admittance of 0.5 eV-s (at transition crossing) for a single bunch in a 53 MHz RF bucket, the total Recycler longitudinal emittance must be less than 18 eV-sec. For reference, this 18 eV-sec emittance corresponds to an rms energy spread of 0.4 MeV, or a fractional energy spread of approximately 5×10^{-5}. Because the stochastic cooling system cannot generate such small longitudinal emittances in the presence of the expected intrabeam scattering growth rates, the 2.5 MHz RF system normally used for coalescing will be used to accelerate and decelerate the beam through transition. The backup plan is to use the traditional coalescing manipulation, which has the disadvantages of larger final longitudinal emittance and lower charge efficiency.

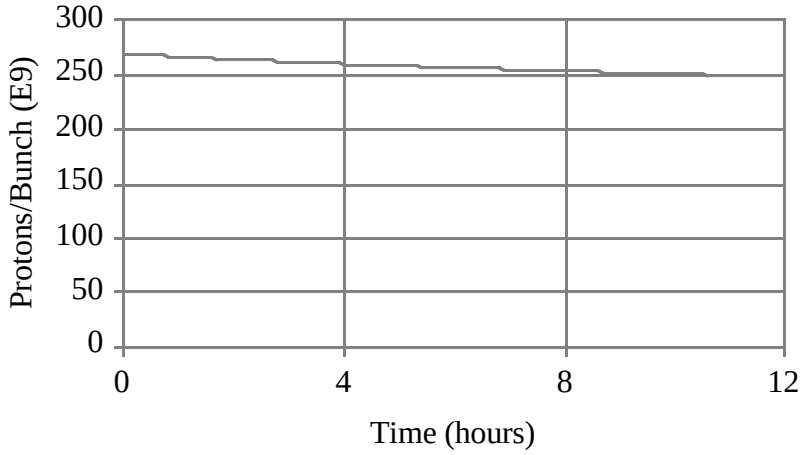

Figure 2.1.5: Prediction of the proton bunch intensity as a function of time during Run II with the Recycler ring.

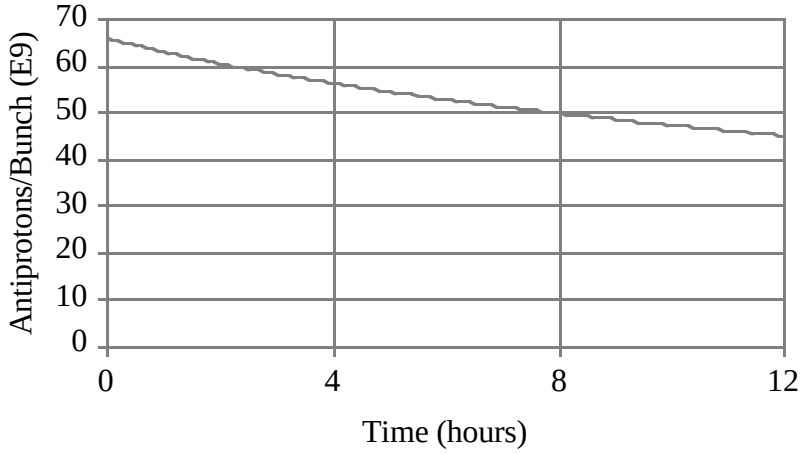

Figure 2.1.6: Prediction of the antiproton bunch intensity as a function of time during Run II with the Recycler.

The time evolution of the proton and antiproton bunch intensities are shown in figures 2.1.5 and 2.1.6. As expected, because the rate of particle loss for both beams is equal and the antiproton total intensity is much lower than that of the protons, the proton intensity lifetime is much longer than the antiproton lifetime. The third major benefit of the Recycler ring is the ability to recycle antiprotons remaining at the end of a store. In order to assess the benefit of antiproton recycling, the percentage of the original antiproton intensity remaining at the end of the store is critical. The next task is to consider the optimum length of a store.

2.1.4. Optimum Store Length

The goal of the Tevatron Collider is to integrate luminosity at the highest rate possible. In order to achieve this goal, high initial luminosities, long luminosity lifetimes, and high stacking rates are required. The store length T_s is also equal to the time available for stacking between injections. The filling time T_f is determined by a number of factors not relevant to this discussion. In present operations using the Accumulator to stack antiprotons the time evolution of the luminosity and antiproton stack size have the dependencies sketched in figure 2.1.7. The total Tevatron Collider cycle time T_c is the sum of the store time and the fill time.

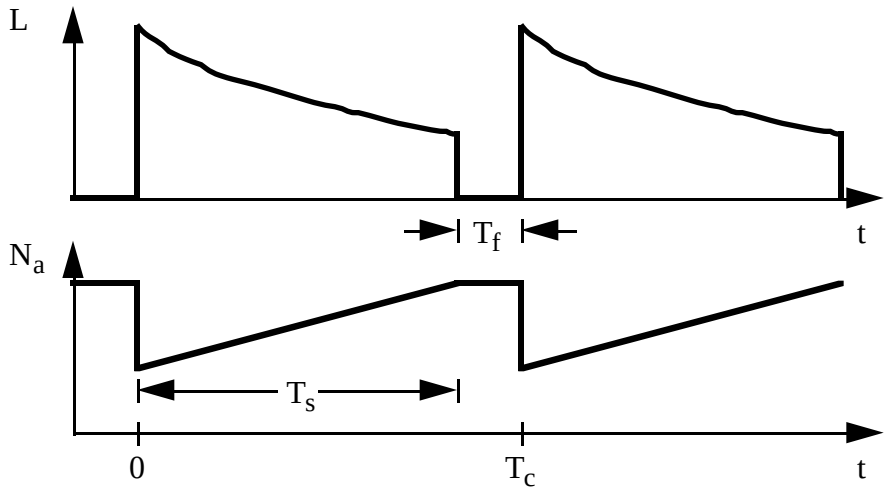

Figure 2.1.7: Sketch of the time dependence of luminosity and accumulated antiproton stack intensity during Collider Run I. The store time T_s plus the fill time T_f equals the total collider cycle time of T_c.

To maximize the rate at which integrated luminosity is delivered, it is necessary to maximize the average luminosity <L>, which is defined as

$$\langle L \rangle = \frac{1}{T_s + T_f} \int_0^{T_s} L(t)\,dt \qquad . \quad (2.1.11)$$

Because antiproton recycling is assumed, T_s plus the deceleration efficiency partially determine the initial number of available antiprotons. The recycled antiprotons are not immediately recooled, but stored and cooled for an entire Tevatron Collider store. The model used to predict the luminosity and other beam parameters during Run II operations also generates the integrated luminosity vs. time during a store. It assumes steady state operations with no Collider failures. By allowing the store duration to be the independent variable, the dependence of the average luminosity on store length for a number of choices for the fill time is plotted in figure 2.1.8. As expected, shorter fill times correspond to high average luminosities and shorter optimum store lengths. Even though fill times of one half hour are possible, it is more likely that fill times around 1 hour will be operationally feasible. At that choice of fill time, there is only a 10% difference in average luminosity between the optimum of 3.5 hours and 8 hours. A store length of 7 hours will be used as the reference store length for discussions below.

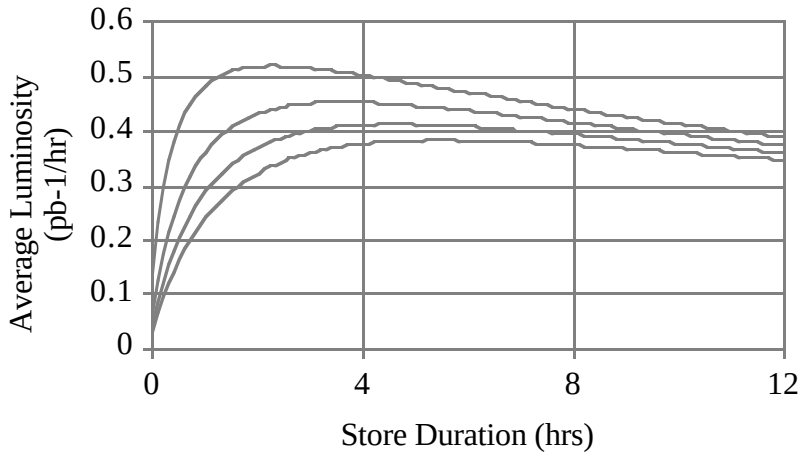

Figure 2.1.8: Prediction of the average luminosity vs. store duration for fill times of 0.5 (top), 1.0, 1.5, and 2.0 (bottom) hours. The longer the fill time, the longer is the optimum store duration. The above calculation assumes the existence of the Recycler during Run II.

The main impact of the store length is the antiproton stacking rate required to maintain the design luminosity of 2×10^{32} cm^{-2} sec^{-1} during Run II. In order to understand how the curve in figure 2.1.9 describing the required stacking rate vs. store duration was generated, refer to table 2.1.2.

The values in the rows labeled "Antiprotons at End of Store" and "Integrated Luminosity" were generated by the luminosity evolution calculations described above. The fill time for the MI and the MI with the Recycler ring are estimates. The Main Injector fill time is longer since without recycling the optimum store length is longer, making fill time less critical to average luminosity and putting less pressure on efforts aimed at shortening the injection time. The acceleration efficiency is the same as the value of 90% chosen in the original Main Injector design. The deceleration efficiency of 80% is basically the acceleration efficiency plus a factor due to the initially novel nature of this operation. Plugging in all of these parameter values, one can generate the subsequent numbers.

Figure 2.1.9: Prediction of the stacking rate required to achieve repeated stores at the peak luminosity of $2x10^{32}$ cm^{-2} s^{-1}.

Table 2.1.2: Parameters which describe the effect of recycling antiprotons on antiproton stacking and average luminosity during Run II. Comparisons are made with Run I operations (without both the Main Injector and the Recycler).

Parameter	Run I	MI only	Recycler
Store Duration T_s (hr)	12	12	7
Injection Time T_f (hr)	2.5	1	1
Antiprotons at End of Store	73%	65%	78%
Deceleration Efficiency	0%	0%	80%
Acceleration Efficiency	75%	90%	90%
Integrated Luminosity (pb^{-1}/store)	0.56	2.9	3.4
Required Usable Stack (10^{10})	48	144	264
Antiprotons Recycled (10^{10})	0	0	148
New Antiprotons Stacked (10^{10})	48	144	116
Required Stacking Rate (10^{10}/hr)	4	12	17
Average Luminosity (pb-1/hr)	0.04	0.21	0.43
Store Hours Needed to Achieve the Snowmass Criterion Between Integrated and Peak Luminosity	98 (typical)	101	93

The required usable stack is simply the initial total antiproton intensity in the Tevatron divided by the acceleration efficiency. In other words, it is the number of antiprotons which must be extracted from the Accumulator now or the Recycler in the future in order to attain the number of antiprotons called for in table 2.1.1. The number of antiprotons recycled is the initial antiproton intensity times the fraction of antiprotons remaining at the end of the store times the deceleration efficiency. The number of antiprotons stacked is simply the difference between the required stack size and the number of antiprotons recycled. In the case of Run II with the Recycler, recycling

contributes more than a factor of two to the luminosity. The stacking rate is just the number of stacked antiprotons divided by the store duration.

2.1.5. Luminosity Leveling

At a given luminosity, the maximum number of interactions per crossing which the HEP detectors can absorb while still performing physics research determines the number of bunches per beam. Table 2.1.3 contains a summary of the average number of interaction per crossing for Run I and anticipated with the Main Injector alone and with the addition of the Recycler. The purpose of the Tevatron Collider is to record useful HEP interactions on tape at the fastest possible rate. From the perspective of an accelerator physicist, this requires the delivery of integrated luminosity at the fastest rate possible. In other words, the average luminosity in equation 2.1.11 must be maximized. From the perspective of an HEP physicist, a high average luminosity is desired only if the number of interactions per crossing is at a "reasonable" level. Too many interactions in a given crossing increases the chances of mistaking tracks associated with a given vertex, thereby decreasing trigger and off-line analysis efficiencies. The problem is that the word "reasonable' is very soft, depending on the type of particle tracking and identification required for a given class of measurements. The general consensus is an average number of interactions per crossing below 5-6 are probably reasonable for Run II.

Table 2.1.3: Average number of interactions per crossing at each HEP detectors at the beginning of stores for the same three scenarios summarized in tables 2.1.1 and 2.1.2. These rates occur at the peak luminosities listed in table 2.1.1.

Parameter	Run I	MI only	Recycler
Average Number of Interactions per Crossing (@ 49 mb)	3.2	2.4	5.7

One method for controlling the interactions per crossing problem while still delivering a high average luminosity is called luminosity leveling. In this plan the peak luminosity at the beginning of a store is sacrificed in order to maintain a stable average luminosity for a longer period of time. The method for achieving this luminosity profile calls for slowly decreasing the β^* at the interaction period, starting at a larger initial value. For example, in figure 2.1.2 a constant value of $\beta^* = 35$ cm was assumed. Using the same simulation of Tevatron Collider performance, the time dependence for β^* shown in figure 2.1.10 was assumed.

Of course the primary effect of this continuous low beta squeeze is on the luminosity, shown in figure 2.1.11. In this example the peak luminosity was decrease by almost a factor of two, bringing the average number of interactions per crossing down to the peak value experienced in Run I. The β^* is decreased until the minimum value of 35 cm is reached. Because the low beta squeeze has no effect on the beam sizes around the ring, the emittance growth mechanisms are not affected. In addition, with the exception of particle losses due to these interaction region collisions, the beam intensity evolution is also unaffected. In fact, for the luminosity leveling example investigated here the

evolution of emittances and intensities are identical to those shown in figures 2.1.3 through 2.1.5.

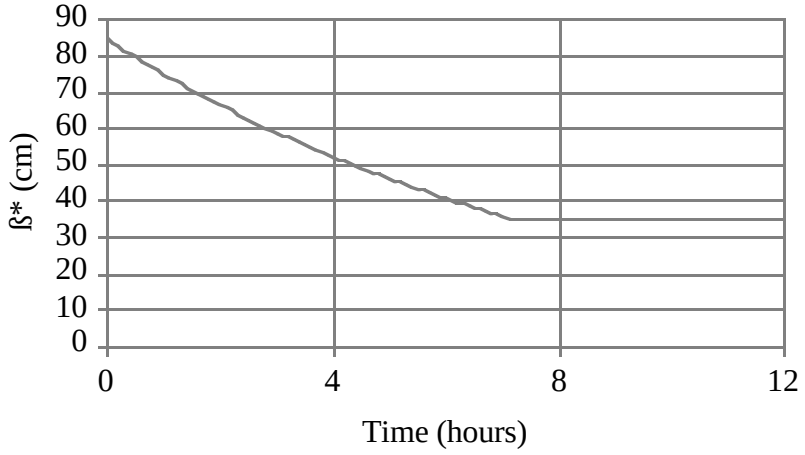

Figure 2.1.10: Continuous low beta squeeze during a Tevatron Collider store which produces a constant luminosity. The squeeze ends at 35 cm, which is considered the minimum for Run II.

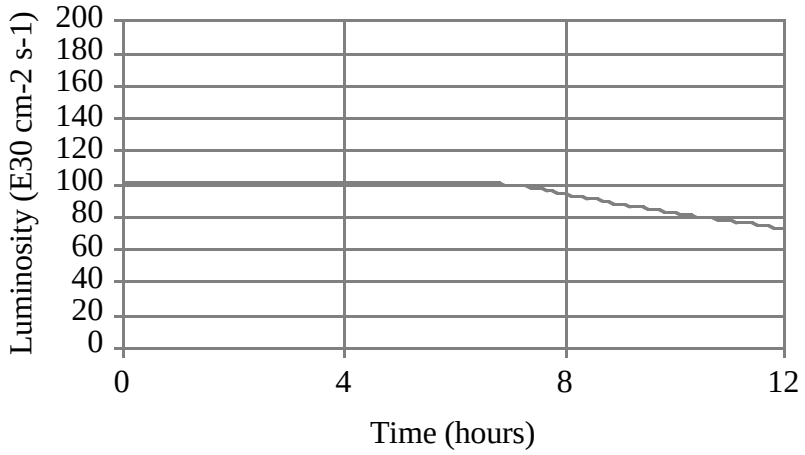

Figure 2.1.11: Luminosity as a function of time for the same initial values of beam intensity and emittance, but employing the continuous low beta squeeze to level the luminosity.

The only noticeable change is in the antiproton intensity lifetime, which is dominated by the rate of proton-antiproton collisions. The antiproton intensity evolution with time is shown in figure 2.1.12. It is this improvement in antiproton lifetime which explains why the luminosity curve in figure 2.1.10 is higher than the constant β^* curve in figure 2.1.1 after 6 hours.

Since the luminosity lifetime is improved, the loss in average luminosity is not as severe as might at first be expected. As shown in figure 2.1.13, the biggest impact is to push the optimum store length out by 2-3x to values which were typical in Run I. In fact,

assuming a 1 hour injection time, the optimum store length is 10-11 hours. On the other hand, comparing with figure 2.1.8, the optimum average luminosity decreased by 25%.

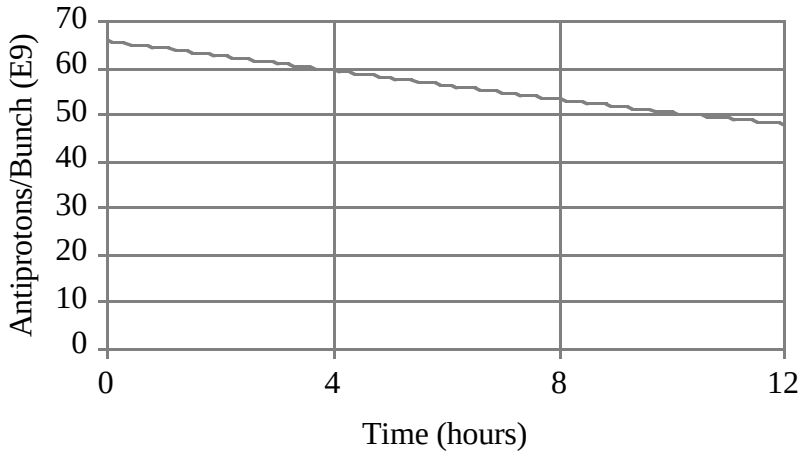

Figure 2.1.12: Time evolution of the antiproton intensity per bunch when luminosity leveling is employed. At the end of 8 hours there are approximately 10% more antiprotons in the Tevatron as compared with the case of constant β^*.

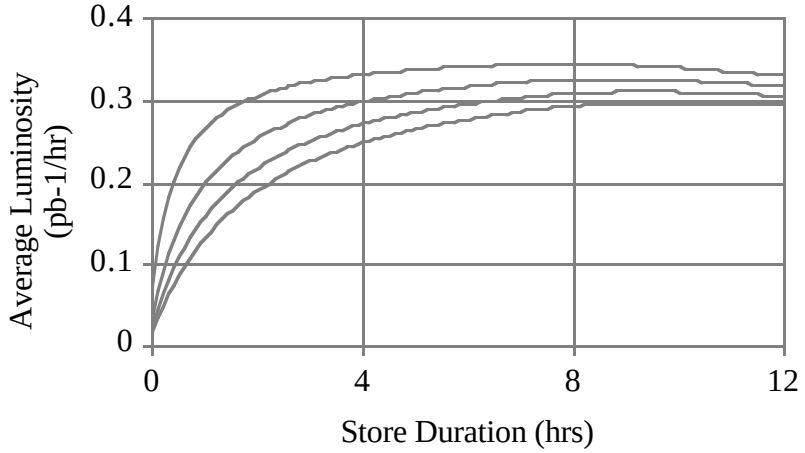

Figure 2.1.13: Prediction of the average luminosity as a function of store duration for fill times of 0.5 (top), 1.0, 1.5, and 2.0 (bottom) hours. In this example luminosity leveling in which the peak luminosity is decreased by a factor of 2 is assumed.

The impact of luminosity leveling on the stacking rate required to achieve a steady state condition of repetitive stores is small but positive. Displayed in figure 2.1.14, the required stacking rate is slightly smaller for all choices of store length. But what if the stacking rate does reach it's design goal of 16×10^{10} antiprotons/hour?

Figure 2.1.14: Prediction of the stacking rate required to achieve steady state luminosity performance assuming luminosity leveling. As found in the case of constant β^*, longer store lengths mean that a lower antiproton stacking rate still produces the same peak luminosity.

This was the stacking rate needed to achieve the 7 hour store lengths assumed in the case of constant β^*, so it is a reasonable assumption. At the same time, relax the interaction per crossing criterion and require that the optimum average luminosity be the same as the constant β^* case. In this case the initial antiproton intensity per bunch in the Tevatron increases from 66×10^9 to 100×10^9, the initial luminosity is 1.3×10^{32} cm^{-2} sec^{-1}, and the peak average number of interactions per crossing is the manageable value of 3.7!

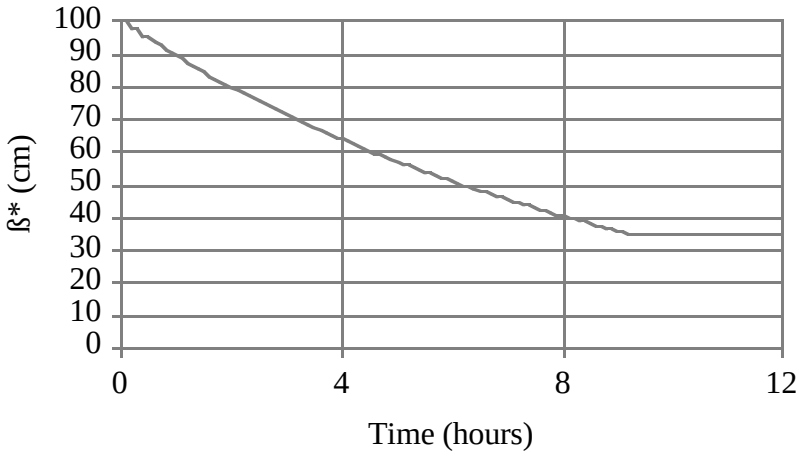

Figure 2.1.15: Continuous low beta squeeze which generates a constant luminosity at 65% of peak with an antiproton stacking rate of 16×10^{10} antiprotons/hour.

Figure 2.1.15 shows the continuous low beta squeeze needed to maintain a constant luminosity at the higher initial antiproton intensity. Since the goal is to end up with the

same optimum average luminosity, the peak luminosity shown in figure 2.1.6 is 65% of the peak design luminosity of $2x10^{30}$ cm^{-2} sec^{-1} in the absence of luminosity leveling.

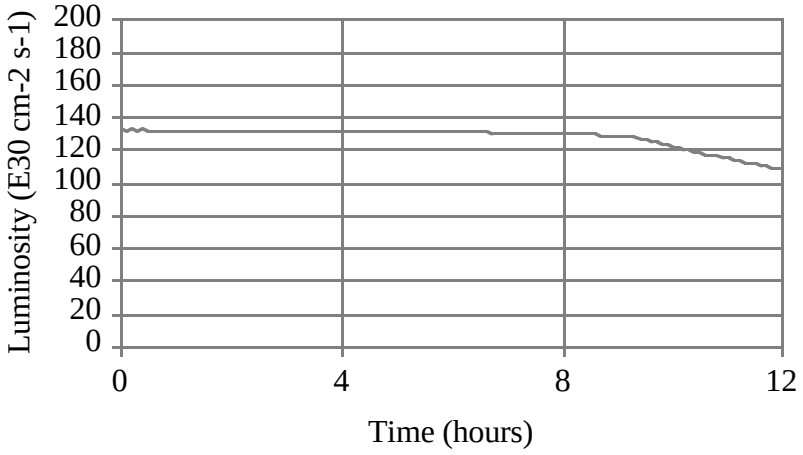

Figure 2.1.16: Prediction of the time dependence of Run II luminosity assuming luminosity leveling at 65% of peak with an antiproton stacking rate of $16x10^{10}$ antiprotons/hour at an optimum store length of 11 hours.

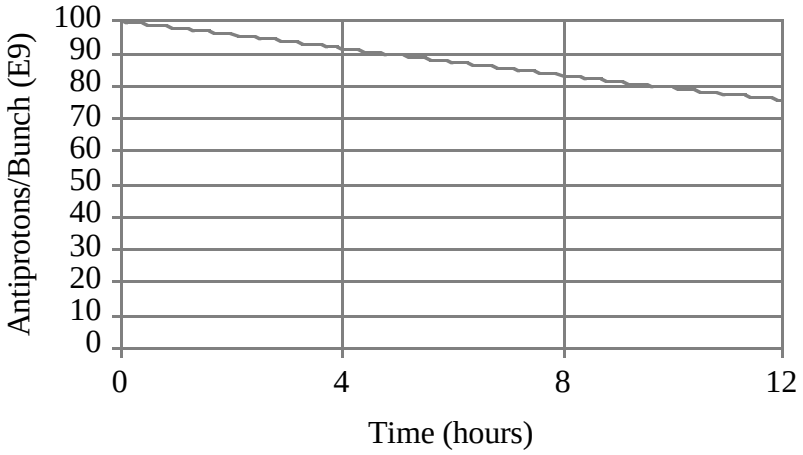

Figure 2.1.17: Prediction of the time dependence of the antiproton intensity/bunch assuming luminosity leveling at 65% of peak with an antiproton stacking rate of $16x10^{10}$ antiprotons/hour at an optimum store length of 11 hours.

Because there are more antiprotons and a lower peak luminosity, the antiproton intensity lifetime is considerably longer than in the case of no luminosity leveling (see figure 2.1.17). So even for double the store length the percentage of antiprotons left at the end of the store is the same. But because the antiproton intensity is higher for longer, the transverse and longitudinal emittance growth of the antiprotons are also larger. The updated emittance evolution curves are displayed in figure 2.1.18 and 2.1.19. Note that because of the greater growth rates and the longer stores, the recycled antiprotons will

have transverse emittances approaching 25 π mmmr and longitudinal emittances of 4 eV-sec.

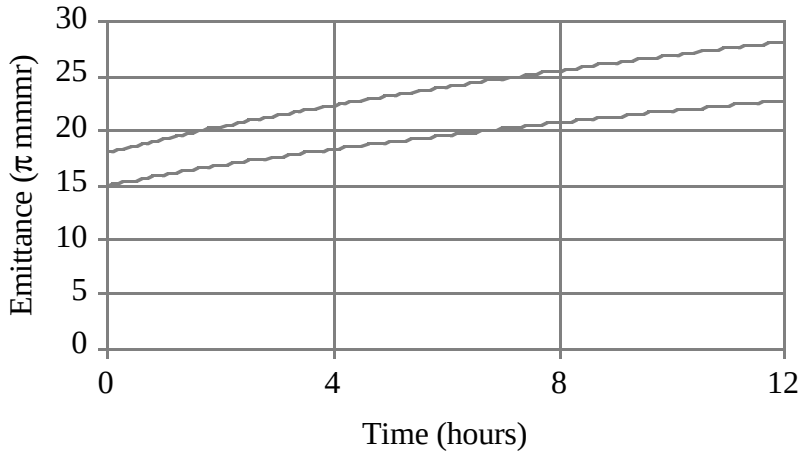

Figure 2.1.18: Prediction of the time dependence of the proton (top) and antiproton (bottom) transverse normalized 95% emittance assuming luminosity leveling at 65% of peak with an antiproton stacking rate of $16x10^{10}$ antiprotons/hour at an optimum store length of 11 hours.

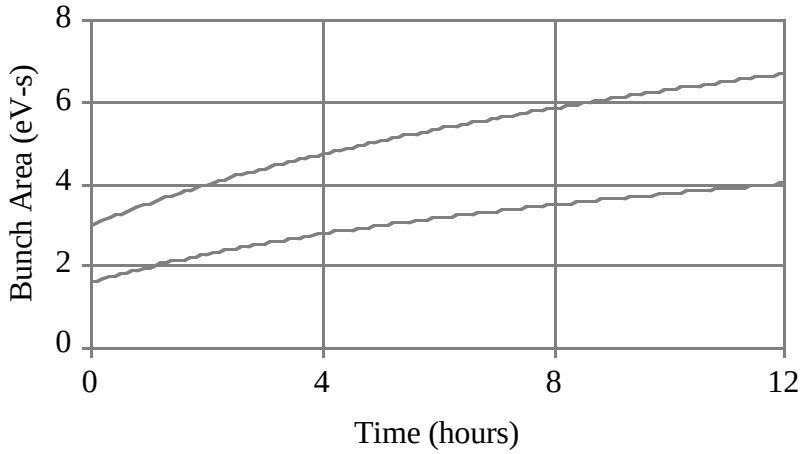

Figure 2.1.19: Prediction of the time dependence of the proton (top) and antiproton (bottom) longitudinal normalized 95% emittance assuming luminosity leveling at 65% of peak with an antiproton stacking rate of $16x10^{10}$ antiprotons/hour at an optimum store length of 11 hours.

By design, the average luminosity (figure 2.1.20) and stacking rate (figure 2.1.21) at a store length of 11 hours is equal to the constant β^* case at a store length of 7 hours. There are some advantages with this luminosity leveling scenario beyond the arguments concerning interactions per crossing. For example, the longer store lengths reduces the sensitivity to unanticipated increases in the fill time. It also gives the Recycler more time to cool the recycled antiprotons.

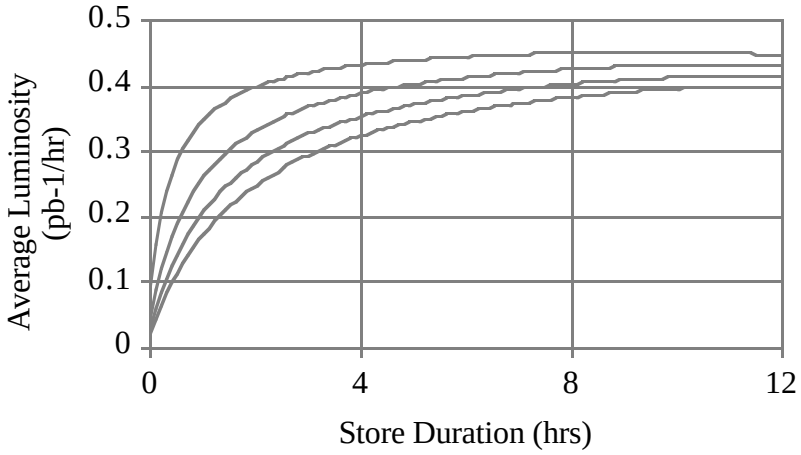

Figure 2.1.20: Average luminosity assuming luminosity leveling at 65% of peak with an antiproton stacking rate of $16x10^{10}$ antiprotons/hour at an optimum store length of 11 hours. The four curves are for injection times of 0.5 (top), 1.0, 1.5, and 2.0 (bottom) hours.

Figure 2.1.21: Required antiproton stacking rate to support luminosity leveling at 65% of peak with an antiproton stacking rate of $16x10^{10}$ antiprotons/hour at an optimum store length of 11 hours.

2.1.6. Antiproton Recycling

In order to achieve the luminosity goal of Fermi III with the Recycler, the proton and antiproton beams will have to be extracted from the Tevatron. This section is a review of the beam parameter values and issues associated with the transfers from Tevatron Collider end-of-store to storage in the Recycler.

The process of recycling starts in the Tevatron at 1 TeV in the low-β lattice configuration. The first step is to eliminate the protons. Computer controlled collimators are used to scrape away the protons (which are on one strand of the separated orbit helix) without intercepting antiprotons and without quenching Tevatron magnets. It is

anticipated that once some experience has been gain that this operation can take as little time as 5 minutes.

Once the protons are eliminated, the electrostatic separators can be turned off, dramatically increasing the available aperture for the larger emittance antiprotons. The antiprotons can then be decelerated while remaining in the low-β lattice, or the low-β lattice can be unsqueezed back into the injection lattice. Changing β^* from its injection value to 35 cm and back to its injection value has already been performed at 900 GeV. The resulting tune change was only 0.004 from the value before reducing β^*. The decision of whether or not to unsqueeze from the low-β lattice should depend on which approach provides the brightest antiproton bunches to the Main Injector.

The maximum deceleration rate expected is 16 GeV/sec which is the acceleration rate used for Collider Run I. This acceleration rate was chosen so that acceleration would still be possible with a single RF station non-operational. If the deceleration ramp is constructed to be a mirror image of the acceleration ramp from Collider Run I, the RF system can still produce a 3 eV-sec bucket with a missing station. The regulation of the main power supply and low beta quadrupole systems is not a problem. The current main power supply regulation error coming out of flattop is about 100 mA, about a factor of 2 higher than the error at the start of ramp. Regulation parameters can be adjusted to try to improve this regulation. With a single beam in the machine, this regulation error is not a problem. With a deceleration ramp that mirrors the acceleration ramp, the low-β quadrupole power supplies will need no modification. If the rate of deceleration is increased near the injection energy, four of the power supplies will need to be given the ability to invert.

The waveform generators used to control most Tevatron power supplies have enough capability to produce the additional ramps needed. The correction dipoles, however, have an older waveform generator that may need to be reloaded for the deceleration process. This will be operationally awkward, but is not technically difficult. Replacement of these generators with newer models is under present consideration.

The biggest challenge will be correctly compensating for the changing sextupole component in the main dipoles. Some magnet measurements have been made to analyze these fields so that compensation ramps can be calculated. The expected current needed from the chromaticity sextupoles is well within the capabilities of the existing circuits. The exact shape of the deceleration ramp will be finalized after all results of the magnet measurements are available.

The antiprotons will be decelerated to a DC energy of 150 GeV. The exact number of bunches transferred at a time will depend on the proton injection kicker used. It is likely that this kicker will have a flattop long enough to transfer 4 bunches at a time. Nine Main Injector cycles would then be needed to transfer all antiproton bunches to the Recycler. The Tevatron needs to be at 150 GeV for no more than 3 minutes to complete the transfers to the Main Injector. The main issue at this point will be compensating the time varying sextupole fields in the Tevatron during this period. The exact scheme for this will be determined after more Tevatron magnet measurements are complete.

The transverse aperture in the Tevatron at 150 GeV is approximately 25 π mmmr with the electrostatic separators turned on. Since the separators are off during recycling, the transverse aperture is even larger and once measured at approximately 40 π mmmr.

Therefore, since the antiprotons are expected to increase in emittance to less than 25 π mmmr, no problems with transverse aperture are anticipated. In table 2.1.4 the longitudinal aperture of the Tevatron is explored. At 150 GeV the maximum RF voltage is 1 MV. This is also the maximum voltage at the flattop energy of 1 TeV. Note that the bucket area decreases from 11 eV-sec to 4.2 eV-sec as the antiprotons are decelerated. This bucket area is sufficient to accommodate the 4 eV-sec bunches expected at the end of a store, even if luminosity leveling is employed.

Table 2.1.4: Longitudinal parameters relevant to antiproton deceleration in the Tevatron during the recycling process.

Parameter	Tevatron FT	Tevatron Inj
Beam Kinetic Energy (GeV)	1000	150
RF Voltage (MV)	1	1
RF Frequency (MHz)	53	53
Momentum Compaction Factor	0.0028	0.0028
RF Bucket Half Length (nsec)	9.4	9.4
RF Bucket Half Height (MeV)	450	175
Invariant RF Bucket Area (eV-sec)	11	4.2
Synchrotron Frequency (Hz)	34	87
Invariant 95% Longitudinal Emittance (eV-sec)	3	3
Matched RMS Bunch Length (nsec)	1.5	2.3
Matched RMS Energy Spread (MeV)	110	68
Fractional RMS Momentum Spread (%)	0.011	0.045
Ratio of Emittance to Bucket Area	0.28	0.71

The Main Injector has a design transverse aperture of 40 π mmmr. The Recycler ring has been chosen to have the same aperture. Therefore, at no point in the remainder of the recycling process is transverse aperture envisioned to cause any difficulties, even assuming 1-2 π mmmr of invariant emittance growth per transfer between accelerators.

Since the Tevatron and the Main Injector have different circumferences, the RF voltage in each ring at Tevatron to Main Injector transfer must be different in order to generate matched RF buckets. Otherwise, longitudinal emittance growth will occur just after the transfer. As can be seen in table 2.1.5, a Main Injector RF voltage of 0.4 MV generates a bucket height and area equal to a Tevatron voltage of 1.0 MV. Based on present operational experience, the transfer between the Tevatron and Main Injector should only increase the already large bunch area by approximately 0.1-0.2 eV-sec.

The maximum 53 MHz RF voltage in the Main Injector is approximately 4 MV. This voltage is required for fast deceleration when the synchronous phase must be limited in order to maintain bucket area. In table 2.1.5 deceleration in the Main Injector to 25 GeV using the standard 53 MHz RF system is described. The energy of 25 GeV is far enough above transition that longitudinal beam dynamics are not distorted by the strong energy dependence of the momentum compaction factor near transition.

Table 2.1.5: Longitudinal parameters relevant to antiproton deceleration in the Main Injector during the recycling process. This table describes the standard deceleration phase from Tevatron transfer down to 25 GeV, just before transition crossing.

Parameter	MI Flattop	MI 25 GeV
Beam Kinetic Energy (GeV)	150	25
RF Voltage (MV)	0.4	1.2
RF Frequency (MHz)	53	53
Momentum Compaction Factor	0.0021	0.0008
RF Bucket Half Length (nsec)	9.4	9.4
RF Bucket Half Height (MeV)	178	206
Invariant RF Bucket Area (eV-sec)	4.2	4.9
Synchrotron Frequency (Hz)	65	168
Invariant 95% Longitudinal Emittance (eV-sec)	4	4
Matched RMS Bunch Length (nsec)	2.7	2.5
Matched RMS Energy Spread (MeV)	80	85
Fractional RMS Momentum Spread (%)	0.053	0.33
Ratio of Emittance to Bucket Area	0.93	0.81

The problem with transition crossing is that the longitudinal admittance hits its minimum at 0.5 eV-sec. This aperture limitation is caused by the normal increase in momentum spread (and conjugate decrease in the bunch length) during transition crossing. Assuming a nominal longitudinal emittance of 4 eV-sec, it is clear that antiproton recycling via the 53 MHz RF system alone is not possible. But if the RF frequency were decreased by a factor of 8 or more, then the matched bunch length would be longer and momentum spread decreased correspondingly. Since the Main Injector contains a 2.5 MHz RF system, it is natural to investigate using that system for transition crossing and the remaining deceleration to the base kinetic energy of 8 GeV.

The transition from one RF system to the other can take place relatively easily by turning on the 2.5 MHz system and then adiabatically lowering the 53 MHz voltage to zero. The maximum sustainable voltage in the 2.5 MHz system is 60 kV. Table 2.1.6 contains the parameter values for transfer to the 2.5 MHz system. Once the transfer has taken place, the antiprotons can be decelerated at a rate of the peak voltage times the sine of the synchronous phase angle. Assuming a phase angle of 53°, the beam can be decelerated at a rate of 48 keV/turn, or 4.25 GeV/sec. At this rate it takes 4 seconds to decelerate the beam down to a kinetic energy of 8 GeV.

In order to deliver the smallest possible momentum spread beam to the Recycler, at 8 GeV the RF voltage is reduced adiabatically until the bunch longitudinal emittance equals the bucket area. Table 2.1.7 contains the longitudinal parameters just before transfer to the Recycler. The beam delivered to the Recycler has an energy spread less than 4 MeV, even for the large longitudinal emittance of 4 eV-sec.

The act of transition crossing has been simulated using the ESME program. Figure 2.1.22 contains the resultant phase space distribution of a 3 eV-sec bunch after crossing transition with only an instantaneous RF phase change. No special RF or gamma-t jump manipulations are involved. Note that the longitudinal emittance grew by approximately 10%, and no test particles out of the original 1000 were lost. The case of 4 eV-sec

transition crossing was also studied with ESME. The result is that for an identical deceleration as in the previous 3 eV-sec case, the longitudinal emittance is diluted to 5.1 eV-sec, which represents a 25% growth. On the other hand, no beam loss was observed. Repeating the 4 eV-sec transition crossing simulation but this time with a gamma-t jump, the longitudinal emittance dilution was reduced to less than 10%.

Table 2.1.6: Longitudinal parameters relevant to antiproton deceleration in the Main Injector during the recycling process. This table documents the transfer of RF systems to the 2.5 MHz system for deceleration through transition to a kinetic energy of 8 GeV.

Parameter	RF Handoff
Beam Kinetic Energy (GeV)	25
RF Voltage (kV)	60
RF Frequency (MHz)	2.5
Momentum Compaction Factor	0.0008
RF Bucket Half Length (nsec)	198
RF Bucket Half Height (MeV)	211
Invariant RF Bucket Area (eV-sec)	106
Synchrotron Frequency (Hz)	8.2
Invariant 95% Longitudinal Emittance (eV-sec)	4
Matched RMS Bunch Length (nsec)	11.2
Matched RMS Energy Spread (MeV)	18.8
Fractional RMS Momentum Spread (%)	0.073
Ratio of Emittance to Bucket Area	0.037

Table 2.1.7: Longitudinal parameters relevant to antiproton deceleration in the Main Injector during the recycling process. This table documents the remaining deceleration to the kinetic energy of 8 GeV and transfer into the rectangular barrier bucket RF system of the Recycler ring, where the energy spread must be minimized.

Parameter	MI @ 8 GeV
Beam Kinetic Energy (GeV)	8
RF Voltage (kV)	2.8
RF Frequency (MHz)	2.5
Momentum Compaction Factor	-0.0089
RF Bucket Half Length (nsec)	198
RF Bucket Half Height (MeV)	8.0
Invariant RF Bucket Area (eV-sec)	4.04
Synchrotron Frequency (Hz)	10
Invariant 95% Longitudinal Emittance (eV-sec)	4
Matched RMS Bunch Length (nsec)	58
Matched RMS Energy Spread (MeV)	3.7
Fractional RMS Momentum Spread (%)	0.041
Ratio of Emittance to Bucket Area	0.99

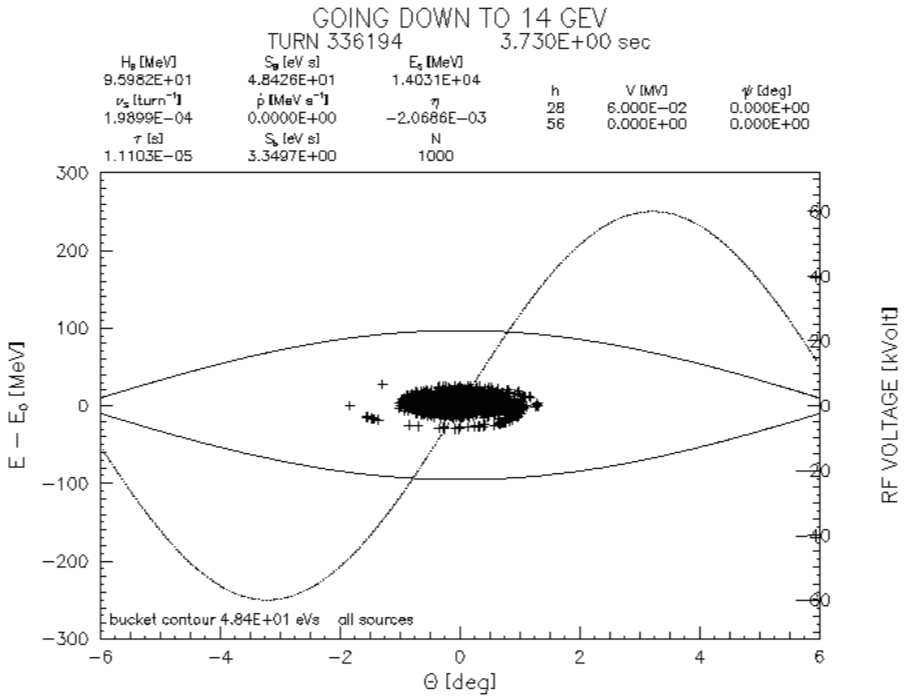

Figure 2.1.22:Simulation of longitudinal phase space of a 3 eV-sec bunch after crossing transition with a simple RF phase change and no gamma-t jump.

The recycled antiproton beam in the Tevatron are handled as 9 batches each composed of 4 bunches spaced at a 2.5 MHz frequency. The entire recycling process repeats the Main Injector deceleration and transfer process 9 times, once per batch. The next issue to address is how the transfers and RF manipulations are handled during the recycling process between the Main Injector and the Recycler.

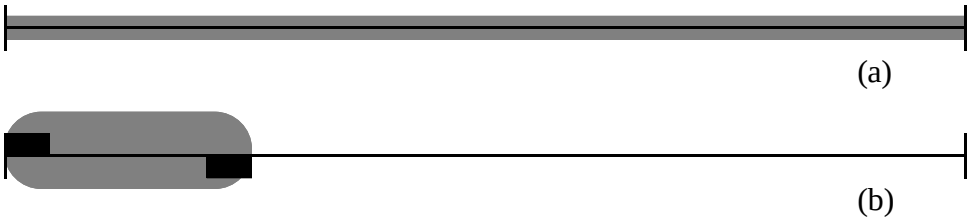

Figure 2.1.23: Full ring phase space sketches of the initial steps of antiproton recycling in the Recycler. In the top drawing (a) the cooled beam starts off basically unbunched (unless an azimuthal gap is necessary for ion clearing reasons). In the bottom drawing (b) a rectangular barrier voltage system adiabatically squeezes the beam into a small fraction of the circumference.

In the remainder of this discussion luminosity leveling is not assumed. When luminosity leveling is included some quantitative values may change, but the qualitative flavor of the operations and concerns remains unchanged.

When the entire recycling process starts, the Recycler already contains 264×10^{10} antiprotons (116×10^{10} newly stacked, 148×10^{10} from the recycling process of the previous store). Given calculations of intrabeam scattering and the choice of stochastic momentum cooling system, the longitudinal emittance is cooled to approximately 54 eV-sec, which according to equation (2.1.10) corresponds to a fully occupied ring with an rms energy spread of 1.2 MeV (see figure 2.1.23a). The first step is to generate a barrier bucket [J.E. Griffin, C. Ankenbrandt, J.A. MacLachlan, and A. Moretti, "Isolated Bucket RF Systems in the Fermilab Antiproton Facility", IEEE Trans. Nucl. Sci. **NS-30**, 3502 (1983)] voltage waveform which constrains the cooled beam distribution to one quarter of the circumference, as shown in figure 2.1.23b. In figure 2.1.24 the phase space capture bucket generated by a pair of rectangular voltage pulses is shown. Because of the intrinsic wide bandwidth of modern power amplifiers, rectangular pulses are desirable for generating the largest bucket height for the smallest pulse width and voltage. The bucket half height $\Delta E_{1/2}$ given a pulse voltage of V_o, a beam total energy of E_o, a pulse width of T, a revolution period of T_o, and a momentum compaction factor η is

$$\Delta E_{1/2} = \sqrt{\frac{T}{T_o}\frac{2\beta_r^2}{\eta} e V_o E_o} \quad . \quad (2.1.12)$$

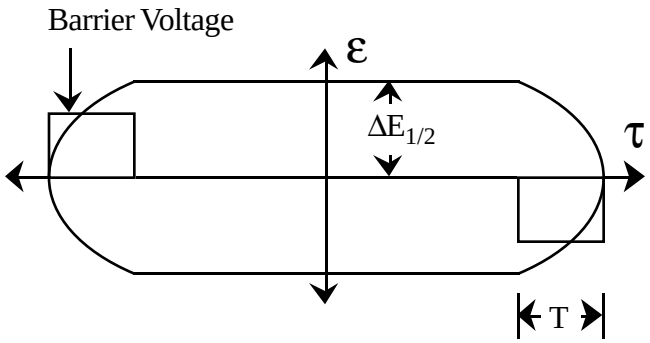

Figure 2.1.24: Phase space sketch associated with a rectangular barrier bucket accelerating voltage system. Inside the voltage pulse the trajectory of energy vs. longitudinal position is quadratic.

Assuming that one wants to longitudinally compress this beam distribution so that the momentum span of the bunch grows out to the momentum aperture of the stochastic cooling systems, the rms momentum spread has grown to approximately 4.8 MeV and charge length has been compressed into 1/4 of the ring circumference. Assuming $\pm 2\ \sigma_e$ of bucket height to constrain most of the beam to that portion of the circumference, table 2.1.8 describes the required voltage and pulse length necessary to produce the minimum bucket height. The final beam distribution length is approximately 2.8 μsec out of 11.2 μsec, so 8.4 μsec of free circumference is available for the recycling process.

Table 2.1.8: Parameters which produce the minimum bucket height necessary to constrain a beam distribution with an rms energy spread of 4.5 MeV.

Parameter	σ_e=4.5 MeV
Beam Total Energy (GeV)	8.938
Relativistic Velocity	0.9945
RF Voltage (kV)	1.2
RF Pulse Length (μsec)	0.5
Momentum Compaction Factor	-0.008683
Revolution Period (μsec)	11.2
RF Bucket Half Height (MeV)	10

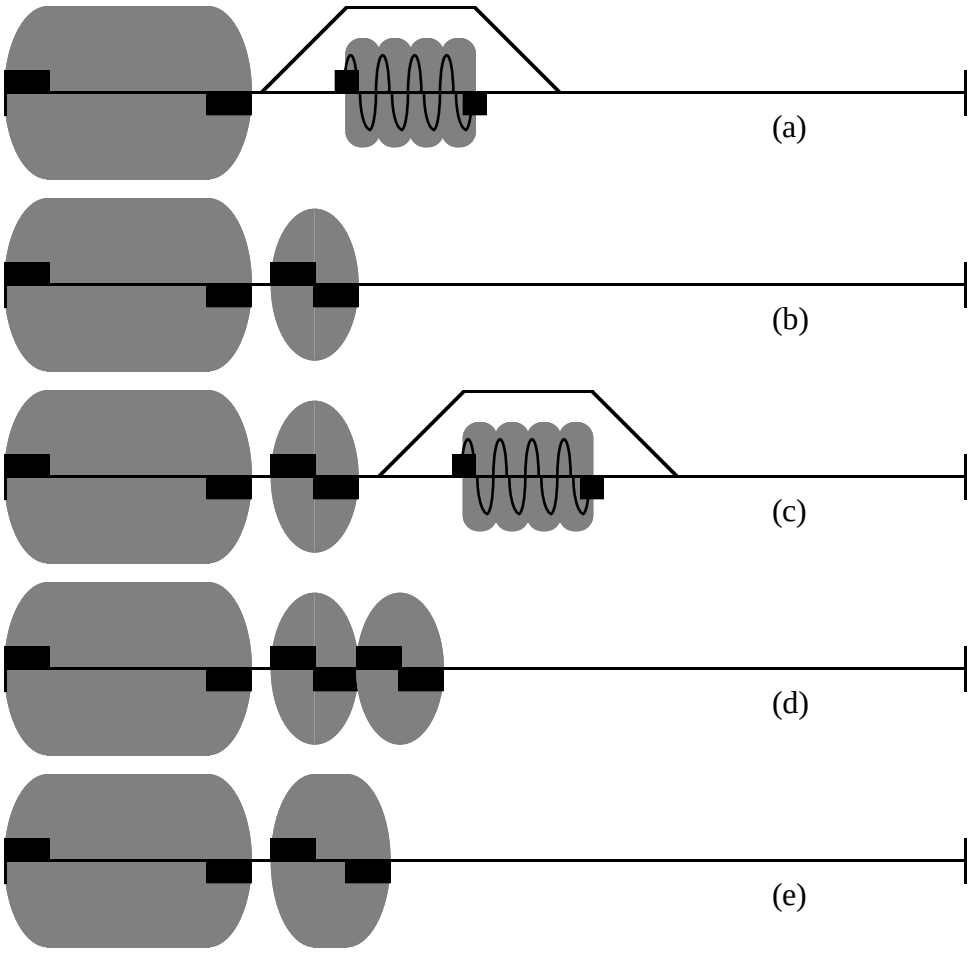

Figure 2.1.25: Recycling of antiproton batches from the Main Injector. The leftmost charge distribution is always the cooled antiprotons. The shown Recycler injection kicker waveform has a rise-time and fall-time of 1 μsec. The recycling process never requires more than 3 pairs of barrier voltage pulses.

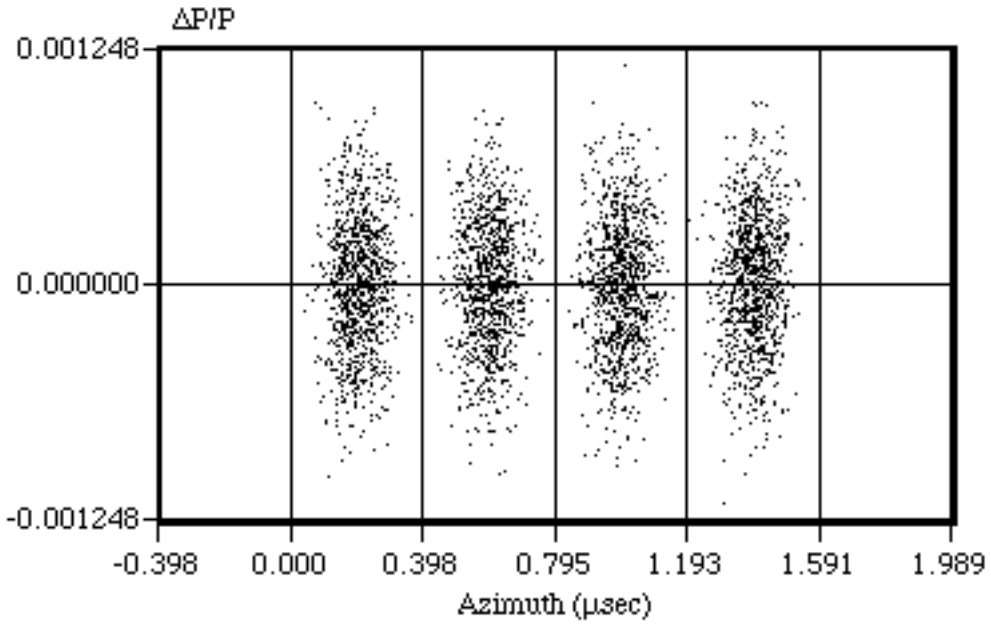

Figure 2.1.26: Simulation result of the adiabatic debunching of the 2.5 MHz bunch structure into a barrier bucket. In this figure the initial distribution with an rms fractional momentum spread of 0.00033 is shown.

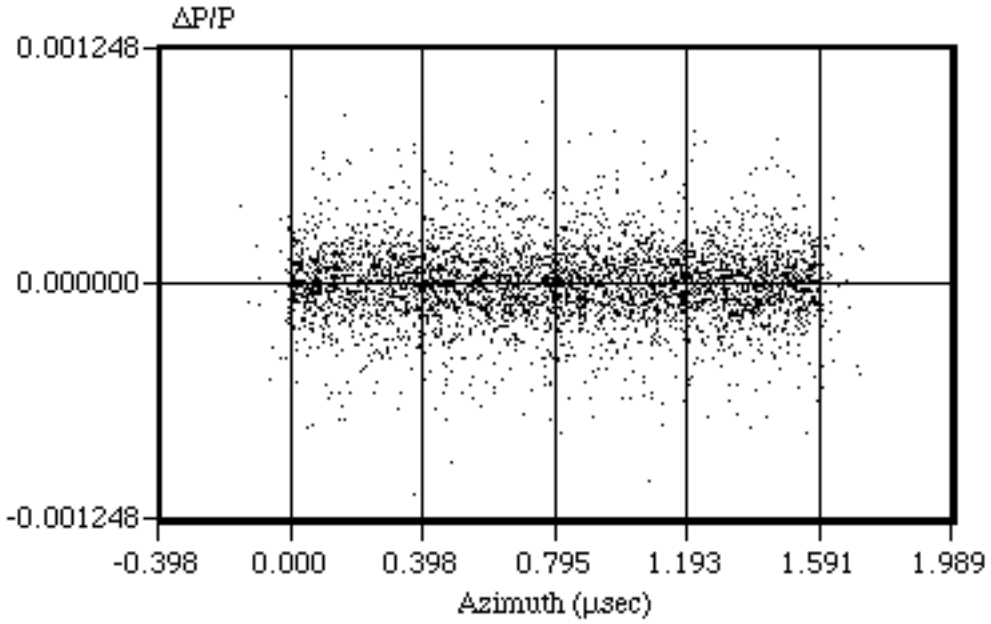

Figure 2.1.26: Simulation result of the adiabatic debunching of the 2.5 MHz bunch structure into a barrier bucket. In this figure the final distribution with an rms fractional momentum spread of 0.00020 is shown. The 2.5 MHz sinusoidal matching waveform was reduced in voltage linearly in 1 second.

The transfers of bunches from each batch from the Main Injector to the Recycler ring is performed 4 bunches at a time. The length of a series of 4 recycled collider bunches in the Recycler ring just after transfer is 1.6 μsec. According to table 2.1.7 the rms energy spread of this distribution at 3 eV-sec per bunch is 2.8 MeV. A sketch of this injection in longitudinal phase space is shown in figure 2.1.25a.

At the time of beam transfer the Recycler RF system is generating a pair of constraining barrier voltage pulses. In addition, between these pulses 4 wavelengths of 2.5 MHz with a matching voltage of 1.6 kV (matched to the 3 eV-sec bucket in the Main Injector) provides bucket-to-bucket RF transfer. After adiabatically turning the 2.5 MHz sinusoidal waveform to zero, the transferred charge is cogged azimuthally to its storage position (see figure 2.1.13b) and compressed. Figures 2.1.26 and 2.1.27 show the results of a ESME-like simulation of this operation, where the entire process takes approximately 1 second with no measurable longitudinal emittance growth..

The second antiproton batch transfer occurs similarly (see figure 2.1.25c). When the batch is moved to the left, it is merged with the first recycled batch. As shown in figure 2.1.25d and 2.1.25e, this merger is accomplished by adiabatically reducing the voltage of the inner voltage pulses to zero. At this point the distribution of recycled antiprotons can be compressed by moving the right barrier pulse to the left. This process was also simulated with an ESME-like computer program. The results are shown in figures 2.1.28 and 2.1.29. Reducing the middle pair of voltage pulses separating the 12 eV-sec distributions in 2 seconds with an emittance growth of less than 5%.

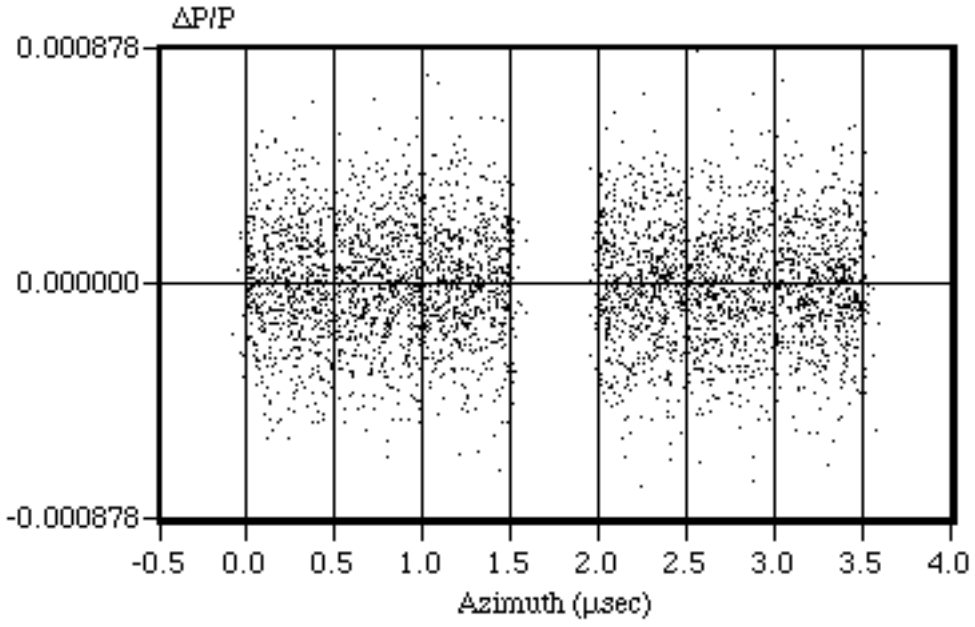

Figure 2.1.28: Initial distribution in which two 12 eV-sec distributions are constrained by a pair of 250 nsec long barrier RF pulse sets (not shown).

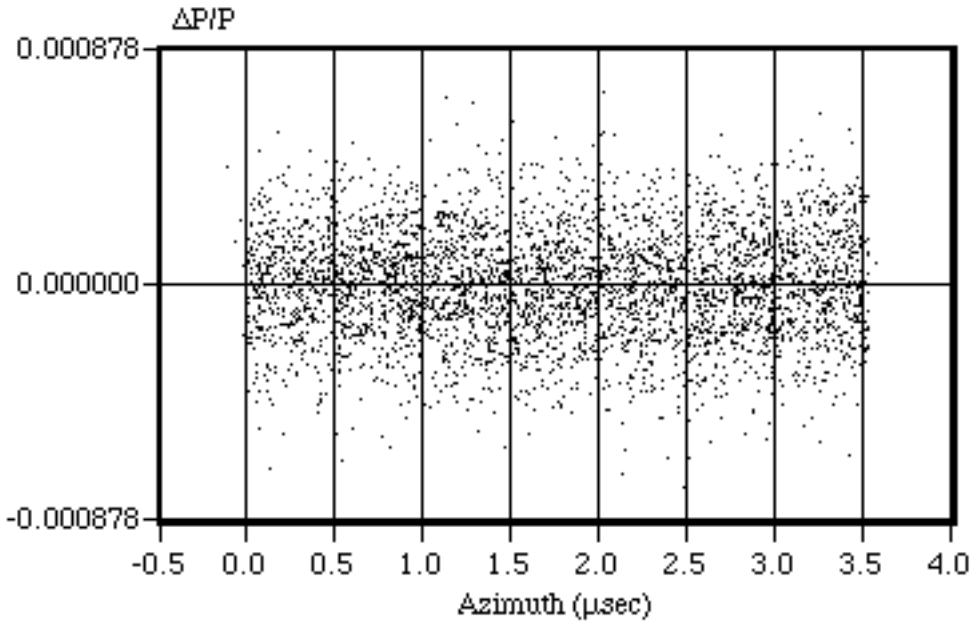

Figure 2.1.29: Final distribution in which the two 12 eV-sec distributions are merged by linearly reducing the voltage of the intermediate barrier pulses in 2 seconds. Less than 5% emittance growth is observed in the simulation.

This process of beam transfer continues until the last of 9 batches are injected. Figure 2.1.30a shows the compression of the previous 8 batches necessary to leave sufficient azimuthal aperture to fire the injection kicker. Note that a voltage of 2 kV and a pulse length of 1 μsec is now necessary to constrain the recycled beam. After merging the 9th batch (see figure 2.1.30b), the recycled beam is compressed into a pulse length of approximately 4 μsec, leaving sufficient room for the inverse operation of extracting the cooled antiprotons for injection into the next Tevatron Collider store (see figure 2.1.30c).

In a given allowed azimuthal time interval, the maximum bucket area is produced when the pair of barrier pulses have a total length equal to that interval. See figure 2.1.31 for a sketch of this situation. The equation for this bucket area A is

$$A = \frac{8}{3} \Delta E_{1/2} \, T \quad . \quad (2.1.13)$$

Table 2.1.9 contains parameters assuming storage of all of the recycled beam in 3.5 μsec assuming no emittance growth in any of the phase space manipulations above. By increasing the pulse width to 2 μsec each, equation (2.1.13) suggests that the bucket area would increase by a factor of 30%, enough to encompass a healthy emittance growth contingency.

It is anticipated that the minimum time between successive transfers of batches to the Recycler ring is approximately 20 sec. Therefore, the entire Main Injector deceleration cycle should be less than this time interval to keep the injection time as low as possible. Figure 2.1.32 contains a sketch of the timing of the Main Injector deceleration cycle.

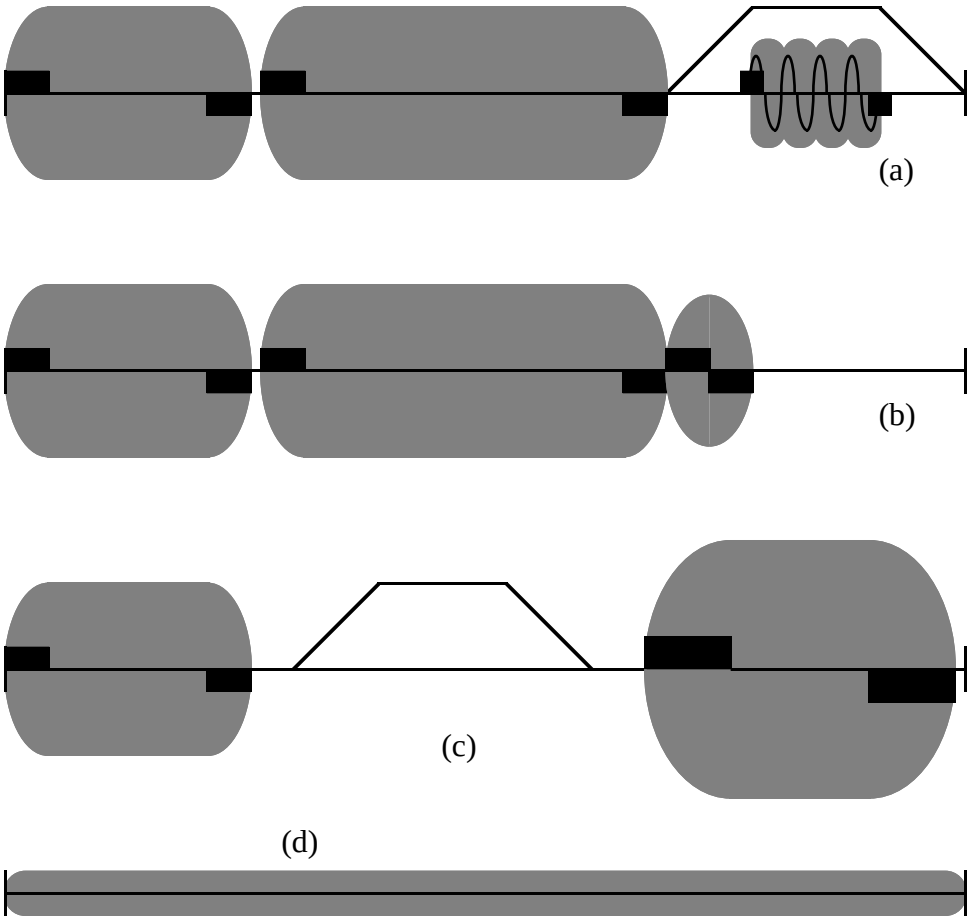

Figure 2.1.30: End of the process of antiproton recycling from the Main Injector. The leftmost charge distribution is always the cooled antiprotons. In (d) the cooled antiprotons have been injected into the Tevatron Collider and the recycled antiprotons have been debunched.

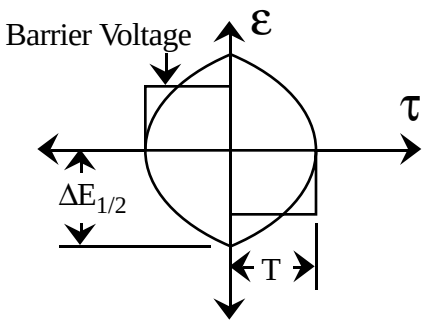

Figure 2.1.31: Sketch of the phase space configuration of the maximum bucket area generated in a given azimuthal time interval (=2T).

Table 2.1.9: Recycler and RF parameters which produce the maximum bucket area with a limited voltage inside a prescribed fraction of the circumference. The necessary RF bucket area is equal to the total invariant 95% longitudinal emittance of all the recycled antiprotons, which is equal to 36 x 3 eV-sec = 108 eV-sec.

Parameter	36 Bunches
Invariant 95% Longitudinal Emittance (eV-sec)	108
Beam Total Energy (GeV)	8.938
Relativistic Velocity	0.9945
RF Voltage (kV)	2
RF Pulse Length (μsec)	1.75
Momentum Compaction Factor	-0.008683
RF Bucket Length (μsec)	3.5
RF Bucket Half Height (MeV)	24
RF Bucket Area (eV-sec)	112
RMS Momentum Spread of the Beam (MeV)	12

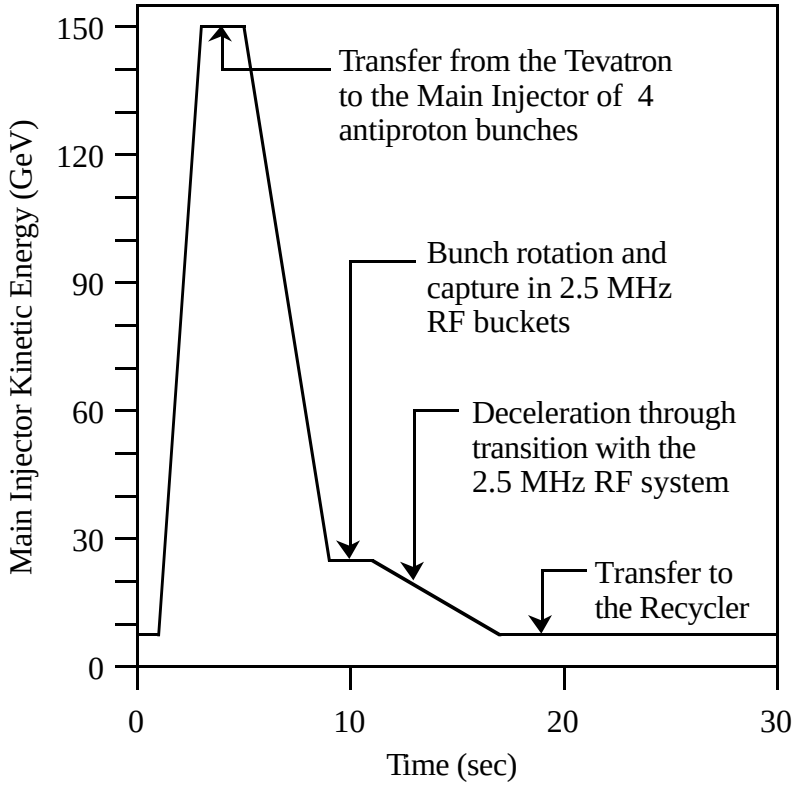

Figure 2.1.32: Sketch of the Main Injector deceleration cycle in which 4 recycled antiproton bunches are injected into the Recycler.

When all of the cooled antiprotons have been extracted, the recycled antiprotons can be adiabatically expanded to fill the ring. As shown in figure 2.1.30d, by slowly reducing the barrier pulse voltage to zero, the minimum momentum spread can be achieved.

Except for the portion of the azimuth carrying the overly compressed recycled antiprotons during extraction, the stochastic cooling is always turned on. In the above example calculations, assuming 3 eV-sec per recycled antiproton bunch and a healthy contingency of emittance growth through all of the RF manipulations, a maximum rms energy spread of approximately 3 MeV is expected.

2.1.7. Stacking from the Accumulator

In the Accumulator, a longitudinal emittance of 6.4 eV-sec is produced by the longitudinal stochastic cooling system at low stack intensities. This corresponds to an rms energy spread of 1 MeV. As the stack intensity increases, both the longitudinal emittance and rms energy spread increase linearly. Therefore, if short bunches are desired in the Tevatron Collider the Recycler ring acts as a necessary storage stage after the Accumulator.

It is anticipated that the optimum rate at which antiprotons are transferred from the Accumulator to the Recycler ring will be determined by a number of factors. First, as the stack size in the Accumulator increases the stacking rate eventually starts to decrease. Second, there will be considerable setup time preparing the transfer lines. This is because the 120 GeV proton transfer line to the antiproton target as an 8 GeV antiproton extraction line must be used. Changing the energy of the line and tuning up the steering between the Accumulator and the Main Injector could require up to 5 minutes for each transfer (in the mean time the Main Injector is not stacking, but still servicing other needs such as 120 GeV fixed target or NuMI beam delivery). Third, if the momentum spread of the Accumulator is large compared to the Recycler stack and/or the momentum acceptance of the stochastic cooling system, time will be required to cool the beam before the next transfer. At present the best estimate for the optimum transfer rate is once every 2 hours.

The actual transfer between the Accumulator and the Recycler should be quite straightforward. Once a gap of sufficient azimuth is opened in the Recycler beam distribution, the Accumulator beam can be injected via the Main Injector. According to data gathered from Accumulator operations, a 20×10^{10} antiproton/hour stacking rate and a 2 hour time between transfers generates an antiproton distribution each transfer with a pulse length of 1.5 μsec, an intensity of 40×10^{10} antiprotons, a transverse emittance of approximately 10 π mmmr, and a momentum spread of 1.6 MeV. This corresponds to a longitudinal emittance of 10 eV-sec.

Therefore, the overall intensity history of the Recycler should look like the sketch in figure 2.1.33. The peak current in the ring occurs after the recycled antiprotons are injected but before the cooled antiprotons are extracted. Since the transverse diffusion mechanisms are quite small and the Accumulator beam is already injected at the target invariant 95% transverse emittance of 10 π mmmr, transverse cooling times on the order of a few hours are sufficient. In order to understand the demands on the momentum cooling system, an integrated model of the entire time evolution of antiproton distributions shown in figure 2.1.33 must be synthesized.

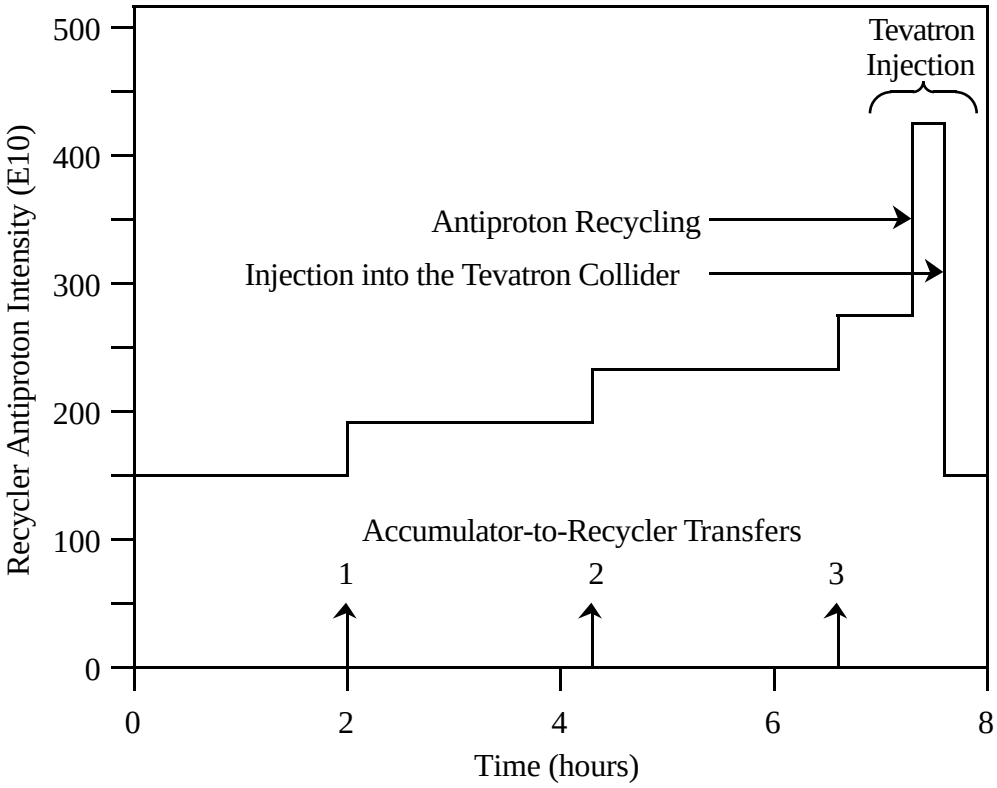

Figure 2.1.33: Anticipated time evolution of the intensity in the Recycler ring.

2.1.8. Antiproton Injection into the Tevatron Collider

In figure 2.1.30c the cooled antiprotons (left) and recycled antiprotons (right) are stored in the Recycler. At this point it is necessary to extract the cooled antiprotons. The empty space occupied in figure 2.1.30c by the extraction kicker waveform is the location where pulses of antiprotons are extracted into the Main Injector for injection into the Tevatron Collider.

A total of 36 collider bunches must be extracted in 9 batches of 4 bunches. Therefore, the 1/9th of the cooled distribution is extracted at a time. The extraction process for each batch starts with the formation of a pair of barrier pulses formed adiabatically inside of the cooled beam distribution. By placing the pulses at the correct azimuth, the correct fraction of antiprotons are segmented into a separate distribution. This separate distribution is then accelerated into the extraction azimuth.

Before the extraction kicker fires, the opposite adiabatic operation to that shown in figures 2.1.26 and 2.1.27 is implemented. The RF and beam parameters at this stage are summarized in table 2.1.10. In this way 4 bunches spaced into separate 2.5 MHz RF buckets are formed in the Recycler. When the extraction kicker is fired the Recycler and Main Injector 2.5 MHz waveforms are synchronized in amplitude and phase in order to avoid longitudinal emittance growth.

Once the transfer of 4 antiproton bunches into the Main Injector is accomplished, the 2.5 MHz RF system in the Main Injector then accelerates the beam through transition to

25 GeV. At 25 GeV the antiproton distribution is bunch rotated, similar to the operation performed on protons just before they are sent into the antiproton target. The purpose of this operation is to shorten the antiproton bunches sufficiently to allow capture into 53 MHz RF buckets. Once the RF handoff is complete, the beam is accelerated the rest of the way to 150 GeV and transferred into the Tevatron Collider. This entire process is summarized in figure 2.1.34.

Table 2.1.10: Recycler and RF parameters which produce the 2.5 MHz bucket just before injection of cooled antiprotons into the Main Injector.

Parameter	per Bunch
Invariant 95% Longitudinal Emittance (eV-sec)	1.5
Beam Total Energy (GeV)	8.938
Relativistic Velocity	0.9945
RF Voltage (kV)	2
RF Frequency (MHz)	2.5
Momentum Compaction Factor	-0.008683
RMS Bunch Length (μsec)	.038
RF Bucket Half Height (MeV)	6.9
RF Bucket Area (eV-sec)	3.5
Ratio of Bunch Area to Bucket Area	0.43

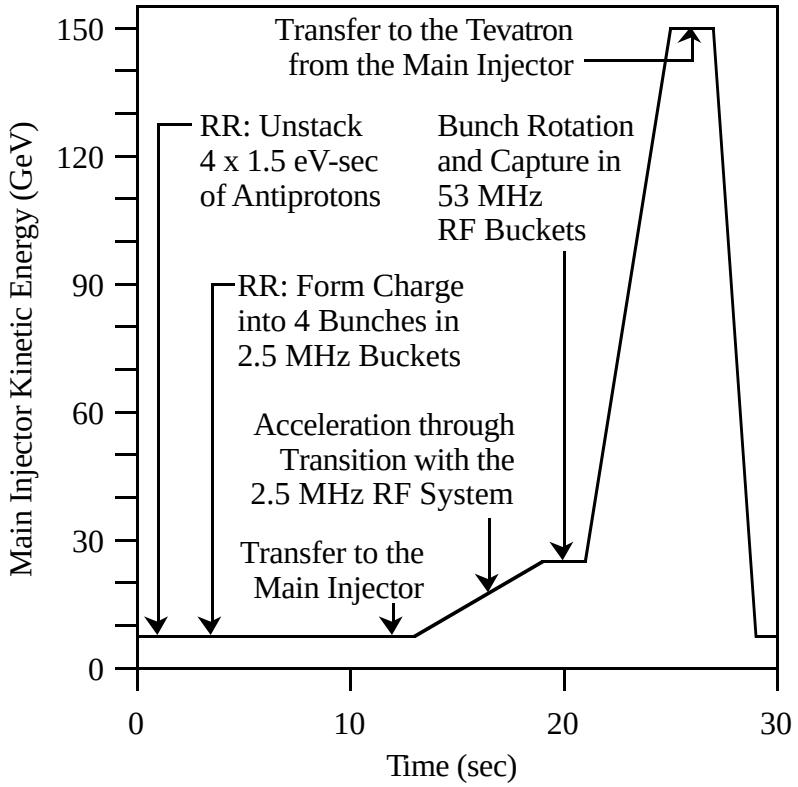

Figure 2.1.34: Sketch of the Recycler and Main Injector functions during each antiproton batch creation/extraction cycle.

2.1.9. Beam Cooling Requirements

In the above discussion the concept of stochastic cooling has been invoked but not explained. The requirements for beam cooling in the above Recycler operational scenario (where luminosity leveling is not invoked) are summarized below.

1. Produce a stacked beam of 2.6×10^{12} antiprotons in a longitudinal emittance of 54 eV-sec and a normalized transverse emittance of 10 π mmmr in an 8 hour cooling cycle (see table 2.1.2).

2. Accept recycled antiproton beams from the Tevatron at a nominal intensity of 1.5×10^{12} antiprotons, a maximum longitudinal emittance of 108 eV-sec and a maximum normalized transverse emittance of 30 π mmmr. This beam is the basis for forming the stacked beam for the next cooling cycle.

3. Accept beam from the Accumulator and add it to the stack at the rate of 0.2×10^{12} antiprotons per hour. The Accumulator beam has a longitudinal emittance of 10 eV-sec and a normalized transverse emittance of 10 π mmmr.

The design of the cooling systems to accomplish these functions is described in more detail in section 2.9.

2.1.10. Nominal Cooling/Recycling Cycle

In order to better understand the following discussion, refer to figure 2.1.33. The simulation begins at 0:00 (hours:minutes) with a beam of 1.5×10^{12} antiprotons that has been recycled from the Tevatron and is contained in a longitudinal emittance of 108 eV-sec. A remnant of the cold antiproton beam which was in the tails of the momentum distribution and not transferred to the Tevatron collider contains 0.3×10^{12} antiprotons in 85 eV-sec. The recycled and remnant antiprotons have been previously merged and are contained between a pair of 2 kV barrier bucket pulses 1 μsec wide and separated by 5.5 μsec. The recycled beam has a maximum normalized 95% transverse emittance of 30 π mmmr.

During the stacking cycle the barrier bucket holding the recycled beam is compressed to 2.3 μsec and beam is added from the Accumulator. Transfers from the Accumulator occur at 2:00, 4:20, and 6:40 in the stacking cycle. Each transfer contains 4.66×10^{12} antiprotons in 10 eV-sec longitudinally and 10 π mmmr transversely.

At 7:20 a new batch of recycled antiprotons are injected and stored in a separate barrier bucket in the Recycler. These antiprotons can be cooling, but for simplicity the simulation assumes that the recycled beam is neither cooled nor heated until the beginning of the next cycle. The cooling of the stacked beam continues until 7:40, when the outer (unusable) 85 eV-sec of the cooled antiproton momentum distribution are combined with the recycled beam and the central 54 eV-sec are transferred to the

Tevatron. At this point the stacked beam has a normalized 95% transverse emittance of 10 π mmmr. At 8:00, the cooling cycle repeats.

A technical description of the cooling system is given in section 2.9.

2.1.11. Effect of Failures

The average luminosity is calculated using equation (2.1.11) and the parameter values for the store duration, fill time, and integrated luminosity per store. In tables such as 2.1.1 there is typically a row which contains the predicted integrated luminosity per week or month. This number is usually the integrated luminosity assuming the store is always at the peak luminosity the entire time period, and then derated by a factor of 3. This is commonly referred to as the Snowmass criterion. Given the average luminosity, a certain number of store hours in a week are thus required in order to achieve the Snowmass criterion. It turns out that the recently completed Run I had a ratio of peak to integrated luminosity which was consistent with the Snowmass criterion. In the case of Run II with the Recycler ring the same number of store hours per week will insure that the accumulation rate of integrated luminosity predicted in table 2.1.1 will be achieved.

During Run II the dominant anticipated type of failure is unintended antiproton loss in the Tevatron (i.e. the store ends unintentionally). During Run I Tevatron stores ended unintentionally at an average rate of twice per week. The worst time for such a failure is just after injection, when the antiproton stack size is at its minimum. In the scenario with the Recycler, during the couple of hours in which the cause of the store loss is investigated and the Tevatron is returned to an operational state, the recycled antiprotons have been recooled and are ready for immediate injection into the Collider. Therefore, a store at approximately half of the nominal luminosity can occur almost immediately.

Using the same simulations as those shown above, this store would have an initial luminosity of 1.1×10^{32} cm^{-2} sec^{-1} and after 12 hours would have accumulated 2.8 pb-1 of integrated luminosity, almost identical to the MI case where a full store was underway. During this time the stack size has grown to 204×10^{10} antiprotons assuming a stacking rate of 17×10^{10}/hr. The number of antiprotons recycled at this point is 72×10^{10}, and the initial luminosity of the next store is only 25% below Recycler scenario nominal. Assuming a normal store duration for that store, the subsequent store will have an initial luminosity which is 99% of nominal. In the absence of the Recycler, where the Accumulator is emptied to 40% of peak current each transfer, that same 12 hour period would yield no integrated luminosity. Therefore, the Recycler adds a level of versatility which makes the Tevatron Collider complex much more tolerant of unintentional Tevatron store losses.

2.2. Lattice Issues

The Recycler ring lattice mimics closely the Main Injector lattice with two 4.267 m long 1.45 kG gradient magnets in each arc half cell. The ring was designed such that it replicated the Main Injector cell length and hence followed the footprint of the Main Injector. The center of the Recycler ring vacuum chamber is placed over Main Injector at a distance of 7' from the floor. The Recycler has been designed to have exactly the same radius as the Main Injector. Figures 2.2.1 and 2.2.2 show the beam's eye, plan, and elevation views of both the Recycler and Main Injector in a standard arc cell.

The only exception to the rule that the Recycler is placed over the Main Injector is at MI-60, the RF straight section. Because of the power tubes over the Main Injector RF cavities, the Recycler ring swings to the radial outside by 18" at that straight section. Figure 2.2.3 shows a tunnel cross-section of the geometry in the MI-60 region.

The other straight sections are identical to the Main Injector. In figures 2.2.4 and 2.2.5 plan and elevation tunnel views of a straight section and the dispersion cells which surround them are displayed.

The Recycler lattice is virtually indistinguishable from the Main Injector lattice, even with the bypass at MI-60 included. It is a strong focusing FODO lattice made up of either two gradient magnets or two quadrupoles (in the dispersion free straight sections) above each Main Injector quadrupole. The horizontal and vertical tunes of the Recycler are split by an integer to minimize transverse coupling effects. The lattice has been designed to have base tunes of Q_x=25.425 and Q_y=24.415 with a maximum horizontal dispersion of 2 m and a corrected chromaticity of -2 units in each plane. Figure 2.2.5 shows the lattice functions for the entire ring.

The Recycler is made of three basic cell structures. The first are the arc cells which have a horizontal phase advance of 86.8° and a vertical phase advance of 79.3°. There are 54 arc cells, each consisting of four 4.267 m magnetic length (add 88.9 mm to each end for a physical length of 4.445 m) permanent gradient magnets with a half-cell length of 17.288 m. The different horizontal and vertical phase advance require different gradients between the focusing and defocusing arc cell gradient magnets. In addition, pole faces of the arc gradient magnets include a sextupole component to reduce the chromaticity to -2 in each plane.

The second cell type is that of the (dispersion free) straight section cells with the same horizontal and vertical phase advance as the arc cells. There are three lengths of straight sections; four 3 half-cell, two 4 half-cell, and two 8 half-cell to make a total of 18 straight section cells, each made up of four 0.5 m long permanent magnet quadrupoles. The separation of the two quadrupoles at each focusing (defocusing) location was tuned to match the lattice amplitude functions of the arc cells.

The third basic cell type is that of the dispersion suppresser cell. These form a dispersion suppresser insert (2 cells) on either side of each straight section to make a total of 32 dispersion suppresser cells. The half-cell length of this insert is 12.966 m such that the product of the bend angle and cell length is exactly half that the arc cells, thus canceling the horizontal dispersion. There are actually two flavors of this insert because of the two different straight sections lengths (i.e. 3 or 4 half-cells in length). One matches between the arc and straight section focusing cells while the other matches between defocusing locations. The dispersion suppresser insert is made up of eight (2/3)*4.267 m

long (2.845 m magnetic, 3.023 physical) permanent gradient magnets and produce 180° of phase advance in both planes.

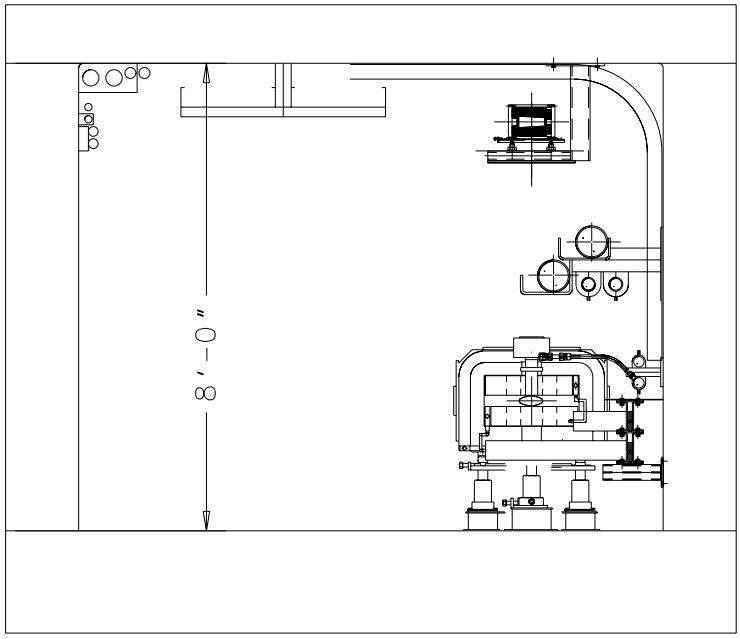

Figure 2.2.1: Tunnel cross-section in a standard arc cell showing a Main Injector dipole near the floor and a Recycler gradient magnet above it and near the ceiling.

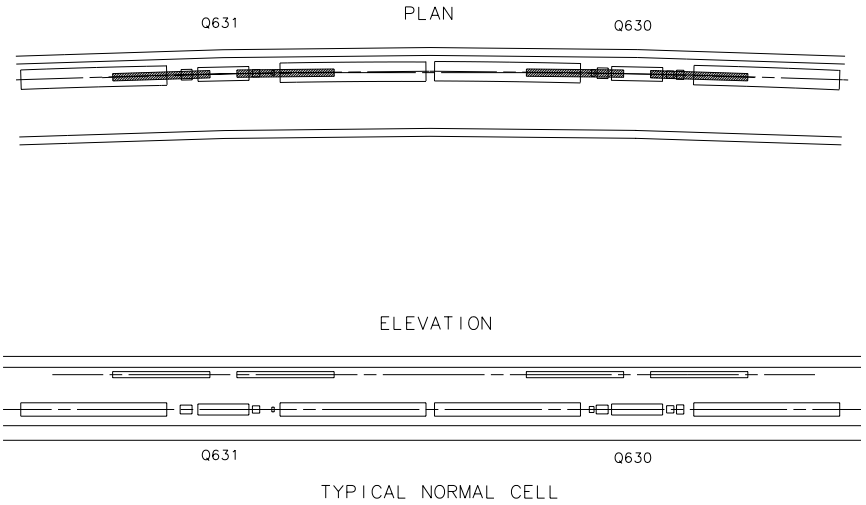

Figure 2.2.2: Plan and elevation views of both the Recycler and Main Injector beamlines. Note that the top magnets (shaded magnets in the plan view) are the Recycler gradient magnets.

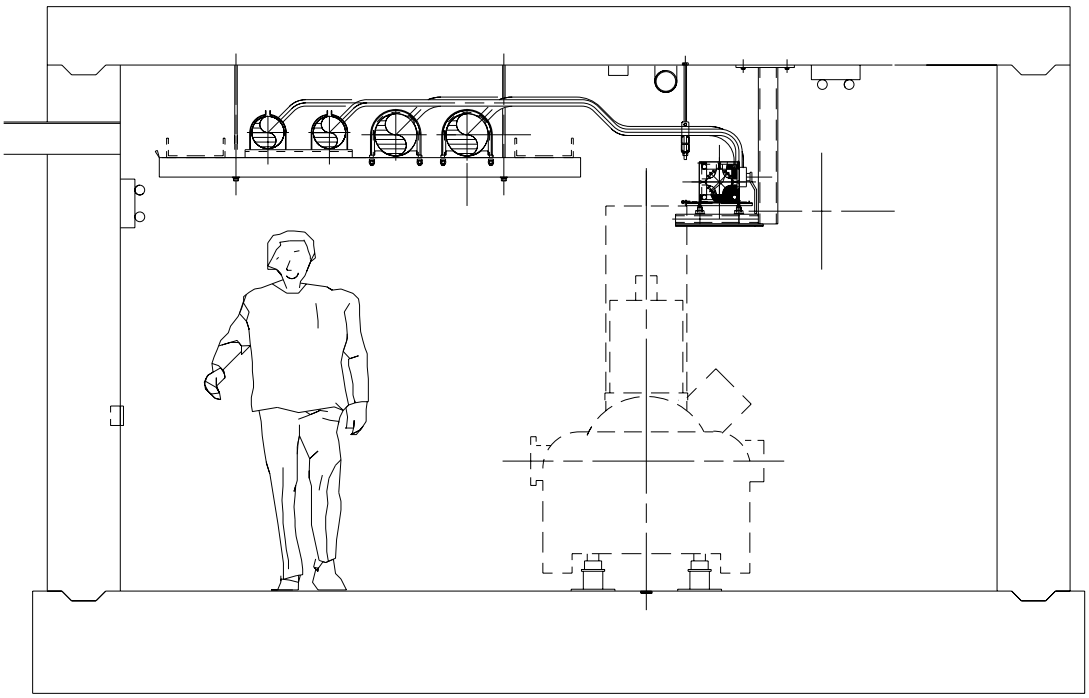

Figure 2.2.3: Tunnel cross-section at the MI-60 straight sections showing the Main Injector RF cavities with the Recycler ring quadrupoles above and to the radial outside.

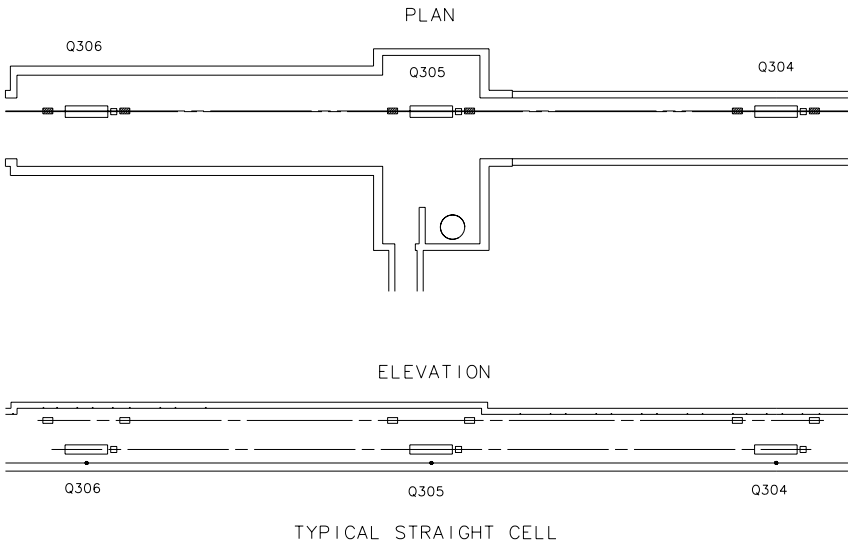

Figure 2.2.4: Plan and elevation views of the Main Injector (open frames) and Recycler (shaded rectangles) magnet deployments in a standard straight section.

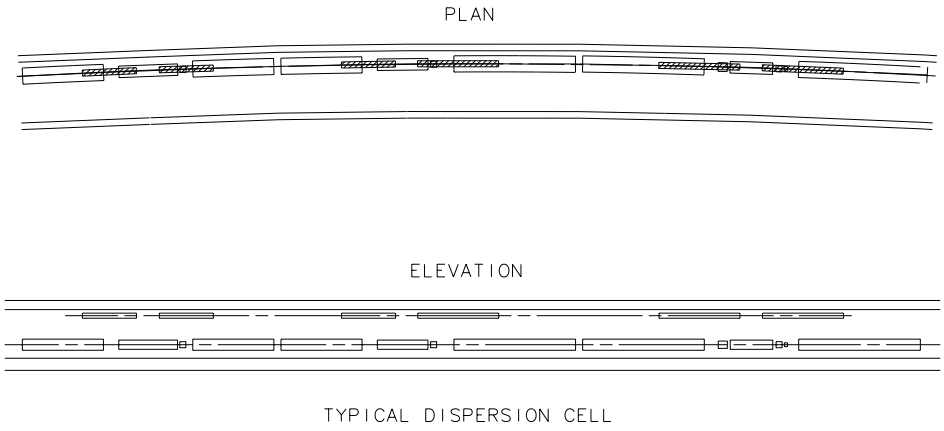

Figure 2.2.5: Plan and elevation views of the Main Injector (open frames) and Recycler (shaded rectangles) magnet deployments in a dispersion suppresser cell.

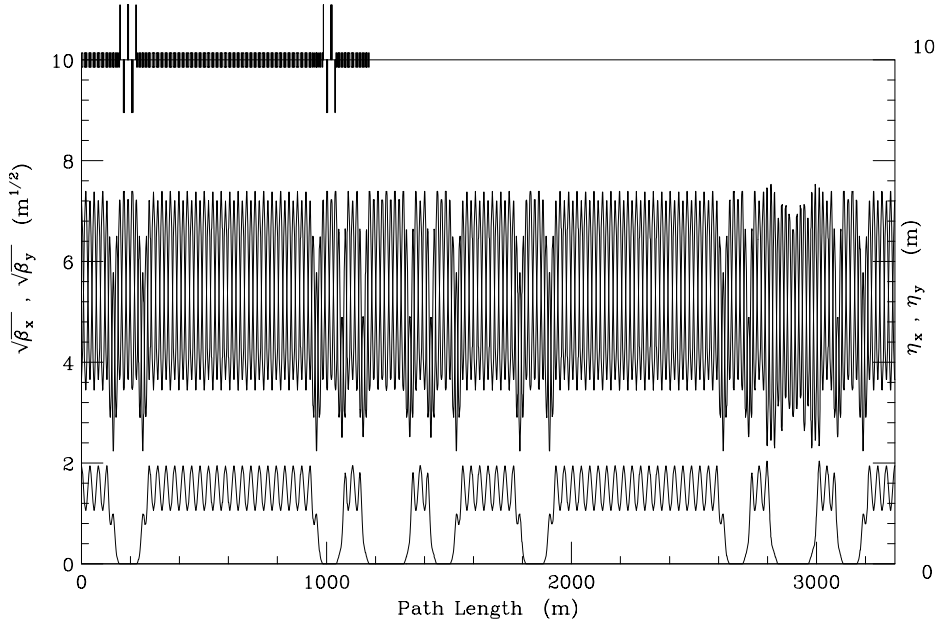

Figure 2.2.6: The Recycler lattice. Note that this lattice is virtually identical to that of the Main Injector.

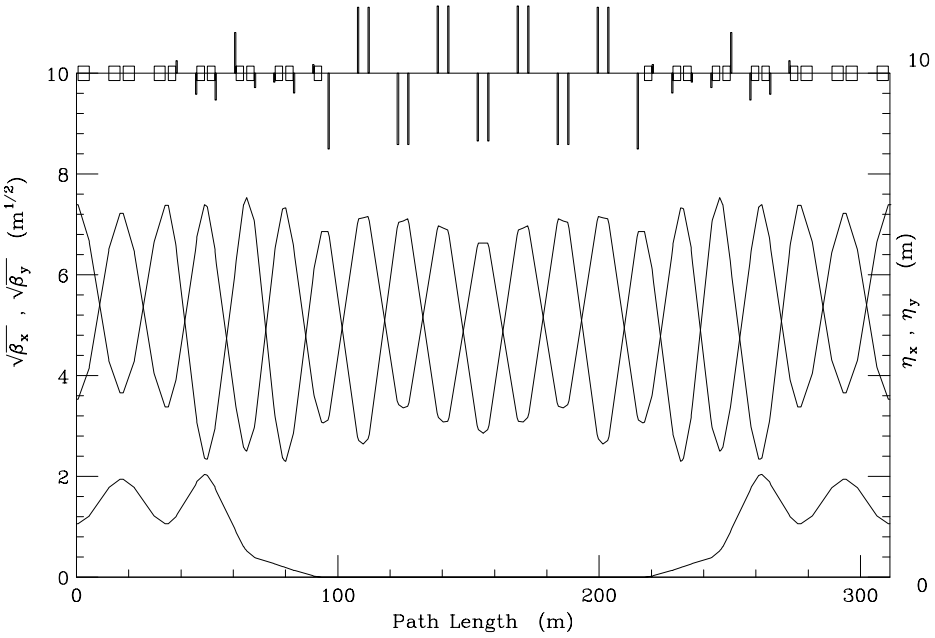

Figure 2.2.7 The Recycler lattice near MI-60. Note that 8 special quadrupoles have been placed around the dispersion suppresser gradient magnets in order to match Twiss and dispersion functions distorted by the magnet moves required to generate the 18" radial bypass of the Main Injector RF stations.

Given that there are 104 cells in the Recycler, the above cell descriptions would infer that the horizontal and vertical betatron tunes are 25.36 and 23.86, respectively. In actuality, the phase advance in the region of the MI-60 bypass is not the standard straight section or dispersion suppresser. The reason is that the half-cell length of the dispersion suppresser cells on either side of the RR-60 straight section were lengthened by 2 m and the RR-60 straight section half-cell length was shortened by the same amount to accomplish the 18" radial bypass of the MI RF stations. The shorter cell length in the straight section reduced the lattice functions in this region creating a greater demand on the dispersion suppresser insert to match between the arc and straight section lattice functions and cancel the dispersion. Figure 2.2.7 shows the lattice functions in the region of the MI-60 bypass. Note the extra 8 quadrupoles in the dispersion suppressers on either side of the straight section. These are used to aid in the match between the straight section and standard arc cells.

A special feature of the RR-60 straight section is its use as a phase trombone for Recycler tune control. Instead of distributing remotely adjustable quadrupoles around the ring, the RR-60 quadrupoles are segmented into 5 families. By adjusting these circuits, a tune variation of up to ±0.5 is attainable, although only a fraction of that is actually required and will be implemented in the initial phase of Recycler operations. The adjustments in these circuits are coordinated in such a way that the Twiss parameters at the ends of the straight section are unchanged. For the full tuning range from the base tune, the peak beta function inside the straight section can grow by about a factor of 3.

Therefore, the vacuum chamber will be round and have a 3" diameter in this region in order to preserve the Recycler aperture.

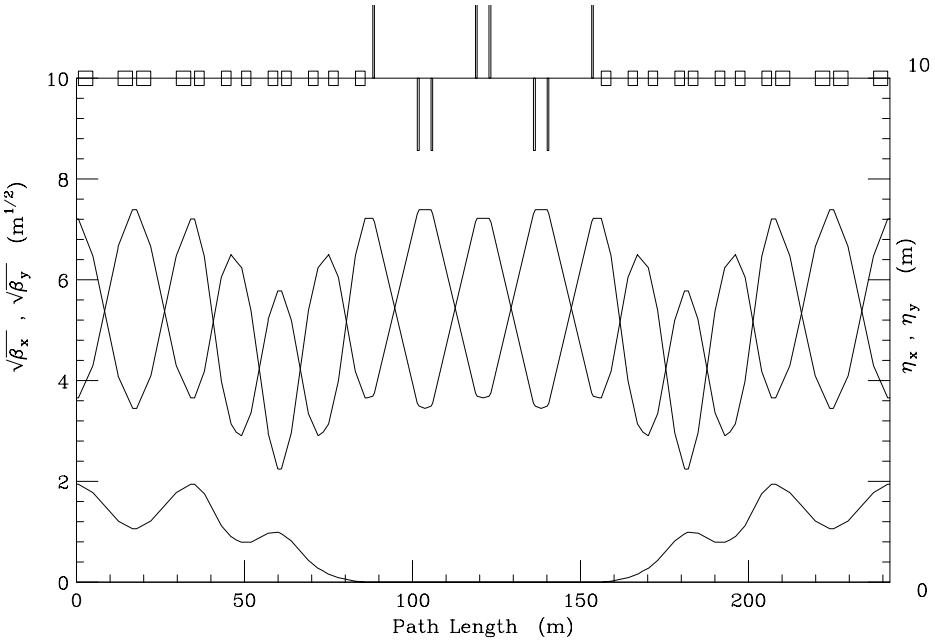

Figure 2.2.8: A standard Recycler long straight section.

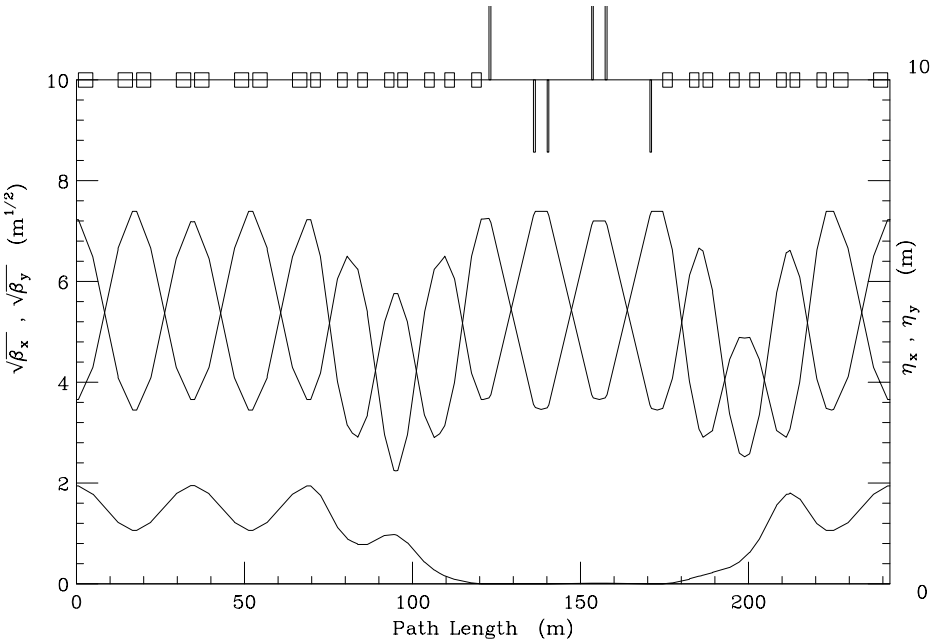

Figure 2.2.9: A standard Recycler short straight section.

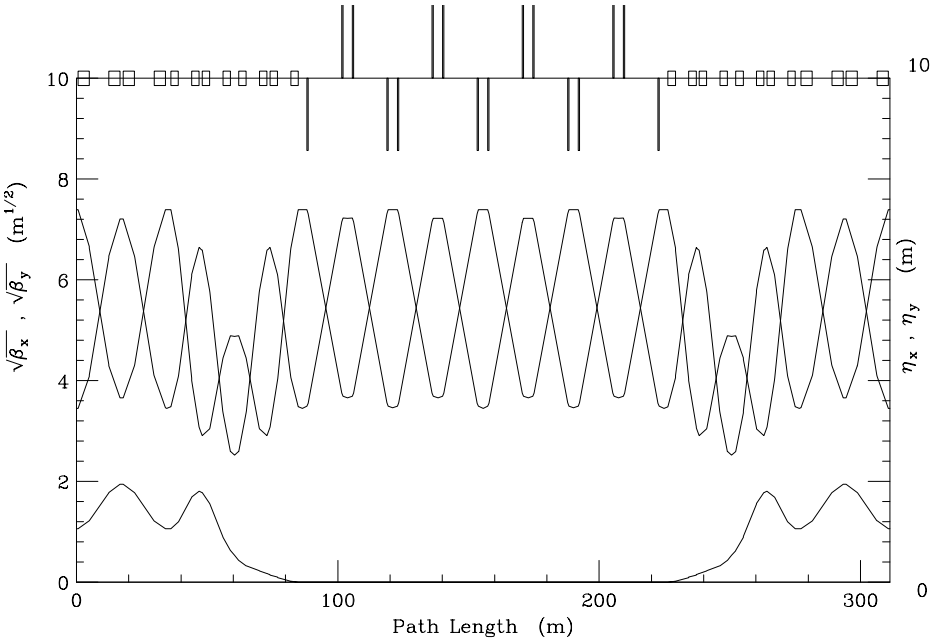

Figure 2.2.10: Lattice functions for the Recycler MI-30 straight section.

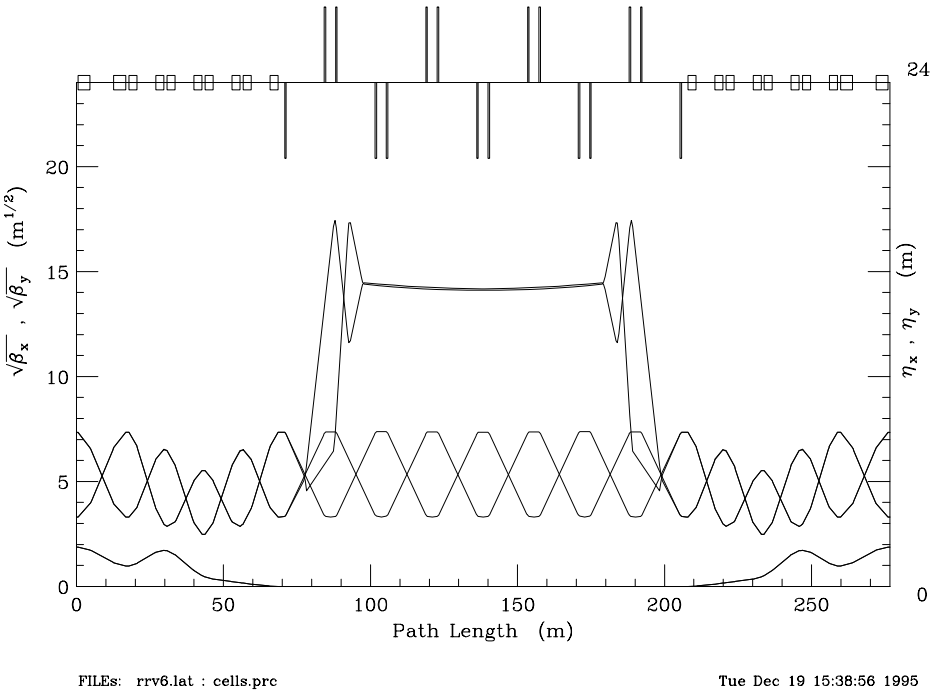

Figure 2.2.11: Lattice functions for the Recycler MI-30 straight section, with the future high-beta insertion for electron cooling superimposed.

With the exception of MI-30, the other long and short straight sections are quite unremarkable and similar to the Main Injector lattice. Figures 2.2.8 and 2.2.9 document their lattice configurations.

At MI-30 the intention at Recycler commissioning is to have the lattice shown in figure 2.2.10, which is basically identical to the Main Injector lattice. In the future, electron cooling is necessary to meet the more aggressive luminosity goals envisioned for the Tevatron Collider. Electron cooling requires a very long high-beta insertion in order to effectively transfer transverse emittance from the antiprotons to the electron beam. In figure 2.2.11 a β=200 m straight region approximately 80 m in length is superimposed over the commissioning lattice functions. In order to maintain the aperture of the Recycler ring with this high-beta insert, the round vacuum chamber at MI-30 will have to be 6" in diameter.

2.3. Performance Projections and Modeling

A series of calculations and simulations have been completed to assess the performance of the Recycler Ring. The Recycler is designed to accept antiprotons from the Accumulator and from the Main Injector at 8.9 GeV/c. The antiproton beam is required to be stored in the Recycler for many hours under the influence of a stochastic cooling systems with cooling times of approximately 2 hours. The long cooling time precludes the possibility of a complete tracking simulation of the entire accumulation scenario. Instead we rely on a combination of semi-analytic calculations and tracking of particles over a range of 10^5 to 10^6 turns (1-10 seconds of real time). In general the strategy is to use the calculations to suggest criteria for alignment and field quality requirements and then utilize tracking simulations to observe the survivability of particles in the model Recycler as a function of betatron oscillation amplitude and momentum offset.

Tracking calculations are performed using the thin element tracking program TEAPOT [L. Schachinger and R. Talman, Particle Accelerators 22, 1987]. Because of our inability to track particles for more than a few seconds we require survivability for particles with oscillation amplitudes corresponding to at least 70 π mmmr (normalized) over the full ±0.3% momentum aperture of the Recycler. This oscillation amplitude corresponds to the vertical physical vacuum chamber aperture and provides a 50% margin relative to the specified 40 π mmmr dynamic aperture. As Recycler prototype magnets become available it is assumed that these tracking calculations will continue utilizing measured field characteristics.

In this section we describe the sensitivity of the Recycler lattice (RRV10) to a variety of alignment and field non-uniformities that manifest themselves as closed orbit errors, betatron function errors, horizontal-vertical coupling, and finite dynamic aperture. The description of the Recycler lattice includes higher magnetic multipoles in combined function and quadrupole magnets, and both magnet and beam position monitor alignment errors. As described in section 2.2 this lattice is based on a ~90° phase advance cell, with a maximum beta function of 55 m and a maximum dispersion of about 2 m. The vertical dispersion in the Recycler is essentially zero and the nominal tune is $(Q_X,Q_Y)=(25.425, 24.415)$. The lattice functions for the Recycler ring are shown in figure 2.2.6.

2.3.1 Recycler error matrix and expected alignment tolerances

The Recycler Ring utilizes a total of 344 combined function (a.k.a. gradient) and 86 quadrupole magnets to provide bending and optical focusing. Construction of the ring with the expected optical characteristics depends upon the production and alignment of magnets with a high degree of accuracy. In addition, since these elements are all implemented as permanent magnets, the absolute strengths need to be well controlled.

In the presence of alignment and magnetic field errors the Recycler lattice will exhibit a number of effects including closed orbit distortion, variations from the nominal tune, beta function distortions, horizontal-vertical tune splits due to coupling, and limited dynamic aperture. Magnetic field errors will be of two generic types; systematic and random. Systematic errors are reflected in a variation of the average value for a type of magnet relative to a desired value, while random errors refer to the width of the

distribution around the mean. The effects of systematic and random errors are different and so we treat them separately here.

Two primary magnet classes are considered. The first class is represented by the long (4.3 m) and the short (2.8 m) gradient magnets, while the second class is represented by the total of all quadrupole magnets. The short gradient magnets differ from the long in total integrated bending strength, nominally 2/3 of the long magnets, in their gradient-to-dipole ratio, and in the absence of a built-in sextupole component. The quadrupole magnets come in 10 flavors representing a variety of strengths. Magnet strength requirements are summarized in section 3.1.

Orbit, tune, beta function, and coupling sensitivities of the Recycler lattice have been calculated for systematic and random magnetic and alignment errors for each class of magnet. Results are displayed in table 2.3.1 for systematic errors and in table 2.3.2 for random errors. Systematic sensitivities are calculated via direct application to the Recycler design lattice while random sensitivities are calculated via statistical expressions as given below. Examples of specific orbit and lattice variations can be found in sections 2.3.2 and 2.3.3.

Table 2.3.1: Sensitivity of the Recycler lattice to systematic errors. Root-mean-square orbit and beta function distortions, as well as tune shifts and global coupling strength are given for the indicated systematic errors. All effects are linear in the assumed underlying errors.

	Orbit (σ_x)	ΔQ_x	ΔQ_y	$\Delta\beta_x/\beta_x$ (rms)	$\Delta\beta_y/\beta_y$ (rms)	ΔQ_{min}
Gradient magnets						
integrated dipole strength $\Delta BL/BL=.0001$*	0.3 mm					
integrated gradient $\Delta B'L/BL=.0001$/inch		.037	-.037	38×10^{-4}	98×10^{-4}	
skew quadrupole $\Delta B'_sL/BL=.0001$/inch						.0218
Quadrupole magnets						
integrated strength $\Delta B'L/B'L=.0001$		.0004	-.0004	2.9×10^{-4}	5.1×10^{-4}	

* Orbit entry represents a systematic shift between the short magnet and the target of 2/3 the long magnet strength.

In table 2.3.1 it is assumed that the energy at which antiprotons are delivered to the Recycler will be adjusted to correspond to the average bending field in the long gradient magnets. Thus the only entry for a closed orbit error is associated with a mismatch between the strength of the short magnet and 2/3 the strength of the long magnet. As seen from the table a 10^{-4} systematic mismatch of these two magnets results in a 0.3 mm rms orbit distortion. The beta function distortion caused by gradient errors shows relatively suppressed sensitivity in the gradient magnets. This is because of the natural

suppression to systematic gradient errors provided by the ~90° cells making up the Recycler. The sensitivity of the tune split to a systematic skew quadrupole has been reduced by providing a one unit tune split between the horizontal and vertical tunes. It should be noted that table 2.3.1 makes no provision for any sort of systematic magnet misalignment.

Table 2.3.2 shows the sensitivity of the lattice to both random magnetic and alignment errors. Closed orbit errors are evaluated utilizing the expression:

$$\frac{\sigma_x^2(s)}{\beta_x(s)} = \frac{1}{8\sin^2(\pi\nu_x)} \sum_i \beta_{x_i} (\sigma_{\theta_i})^2 \quad , \quad (2.3.1)$$

where σ_{θ_i} is the rms bending angle error through the i^{th} element. For a dipole magnet σ_{θ_i} is $\sigma_{BL}/(B\rho)$ (horizontally) or $\sigma_\phi \times BL/(B\rho)$ where ϕ is the roll angle (vertically). For any magnet containing a field gradient, σ_{θ_i} is $\sigma_d \times B'L/(B\rho)$ where d is the transverse displacement. The interpretation of the numbers in table 2.3.2 is that at any given point in the ring, there would be a ~2/3 chance of observing an orbit distortion of $<(\sigma_x/\sqrt{\beta}) \times \sqrt{\beta}(s)$ if magnetic elements were fabricated and aligned to the noted tolerances. A total rms orbit distortion at any point due to a different set of errors can be calculated by noting that distortions are linear in the corresponding errors and that all distortions add in quadrature. For example, a magnet-to-magnet (rms) strength variation of 5×10^{-4}, accompanied by an rms displacement error of 0.25 mm and an rms roll angle of 0.5 mrad would produce an rms orbit distortion of 5.8 mm horizontally and 6.1 mm vertically (β_{av}=33 m).

Beta function distortions are calculated using the expression:

$$\sigma^2_{\frac{\Delta\beta}{\beta}} = \frac{1}{8\sin^2(2\pi\nu)} \sum_i (\sigma_{kl})_i^2 \beta_i^2 \quad , \quad (2.3.2)$$

where σ_{kl} is the integrated gradient error, or the transverse displacement times the integrated sextupole strength in the case of the long gradient magnets. The minimum tune split is calculated as

$$(\Delta\nu_{min})^2 = \frac{1}{2\pi^2} \sum_i (\sigma_{k_s l})_i^2 \beta_{x_i} \beta_{y_i} \quad , \quad (2.3.3)$$

where $\sigma_{k_s l}$ is taken as σ_ϕ times the nominal integrated gradient. For any set of errors the expected rms beta distortion or minimum tune split can be calculated by scaling the numbers listed in the tables and then adding in quadrature. For example, an rms integrated gradient error of 1×10^{-4}/inch as referenced to the dipole field, accompanied by an rms 0.25 mm transverse offset would produce a distortion of 3.8% in both the horizontal and vertical beta functions. It should be noted through a comparison of table 2.3.2 with 2.3.1 that systematic (normal) gradient errors are more benign than random errors.

Table 2.3.2: Sensitivity of the Recycler lattice to random errors. Root-mean-square orbit and beta function distortions, as well as global coupling strength are given for the indicated random errors. All effects are linear in the assumed underlying errors and results add in quadrature

	Orbit Error ($\sigma_x/\sqrt{\beta_x}$)	Orbit Error ($\sigma_y/\sqrt{\beta y}$)	$\Delta\beta_x/\beta_x$ (rms)	$\Delta\beta_y/\beta_y$ (rms)	ΔQ_{min}
Gradient magnets					
integrated dipole strength σ_{BL}/BL=.0001	$1.1x10^{-4}$				
integrated gradient $\sigma_{B'L}/BL$=.0001/inch			$386x10^{-4}$	$375x10^{-4}$	
skew quadrupole $\sigma_{B'sL}/BL$=.0001/inch					.0110
transverse displacement σ_d=.00025 m	$7.9x10^{-4}$	$8.4x10^{-4}$	$54x10^{-4}$	$84x10^{-4}$	
roll σ_ϕ=.0005		$4.6x10^{-4}$			.0040
Quadrupole magnets					
integrated strength $\sigma_{B'L}/B'L$=.0001			$10.x10^{-4}$	$9.8x10^{-4}$	
transverse displacement σ_d=.00025 m	$2.7x10^{-4}$	$2.9x10^{-4}$			
roll σ_ϕ=.0005					.0015

2.3.2 Closed orbit calculation and correction procedure

The Recycler contains 416 beam position monitors (BPMs), one horizontal and one vertical in each half cell. The closed orbit as observed on the BPM system is calculated for a random collection of alignment and bending strength errors as described in table 2.3.3. Orbit errors in the horizontal plane are generated by random transverse misalignments of the combined function and quadrupole magnets, and magnet-to-magnet bending strength variations, while in the vertical plane roll alignment errors replace strength variations as a contributor.

Table 2.3.3. Random misalignment errors used in Recycler orbit and tracking simulations.

Magnet Type	σ_{BL}/BL	σ_h (mm)	σ_v (mm)	σ_{roll} (mrad)
Gradient Magnet	.0005	0.25	0.25	0.50
Quadrupoles	-	0.25	0.25	0.50
Beam Position Monitors	-	0.25	0.25	-

Ten sets of Recycler closed orbits are generated using random distributions of strength and alignment errors with rms widths as given in table 2.3.3. Errors are generated in Gaussian distributions cut off at 3σ. The equality of the magnet-to-magnet and roll distribution widths implies that the vertical and horizontal orbits will be the same in a statistical sense. As a result only the horizontal orbit is studied here.

A histogram of the distribution of observed rms horizontal orbit distortions is given in figure 2.3.1. The figure shows that the most likely rms orbit distortion for tolerances given above lies in the 4-8 mm range. As can be deduced from table 2.3.2, magnet-to-magnet strength variation, transverse alignment, and roll errors all contribute approximately equally to the closed orbit distortion.

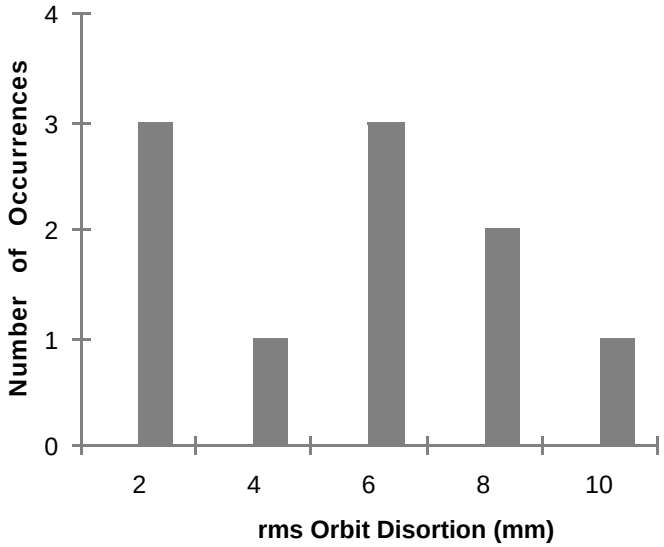

Figure 2.3.1: Probability distribution of expected uncorrected rms horizontal orbit distortion based on the alignment and strength errors given in table 2.3.3. Ten different ensembles of errors are calculated and entered into this histogram.

It will be desirable to correct the orbit to a residual distortion of under 1 mm. Because of the static nature of the Recycler it is possible to consider doing this by displacing the combined function magnets transversely in an appropriate manner. Several different strategies are possible for identifying a finite set of magnets that could and should be moved to correct the orbit. In the approach studied here a specific algorithm is applied to select a set of magnet moves that reduce the rms orbit distortion. This algorithm is believed to have originated in the CERN SPS and is implemented as follows:

1. For the closed orbit given, find the single magnetic element in the ring for which a move minimizes the rms orbit distortion. If an element has to be moved more than 5 mm in order to minimize the distortion that element is removed from consideration.

2. Find the second element that paired with the element identified in 1, is most effective in minimizing the rms orbit distortion. Again reject any element that requires a move of more than 5 mm to minimize the orbit distortion.

3. Repeat up to 15 times, always identifying the element to add to the previously defined list as most effective at minimizing the rms orbit distortion.

The effectiveness of the algorithm is demonstrated in table 2.3.4 and in figure 2.3.2. The table lists the rms and peak orbit distortions observed both before and after corrections for each of the ten generated orbits. In addition the maximum transverse magnet move is listed. The table indicates that in all cases the rms distortion can be reduced to less than 1 mm, with a peak distortion under 2.6 mm, by utilizing 15 suitably chosen magnet moves. In all instances the maximum magnet move is less than 3.3 mm. Figure 2.3.2 shows the entire uncorrected and corrected orbit for seed 8, the seed with the worst uncorrected orbit.

Table 2.3.4: Uncorrected and corrected orbit distortions for ten different randomly generated closed orbits. The column label "Δ_{max}" lists the maximum magnitude of the 15 magnet moves required to effect the correction.

Seed	Uncorrected		Corrected (15 moves)		
	σ_H (mm)	Peak (mm)	σ_H (mm)	Peak (mm)	Δ_{max} (mm)
1	2.87	6.85	0.65	2.61	2.54
2	5.69	13.45	0.66	2.17	2.23
3	7.83	17.57	0.65	2.04	2.80
4	2.69	6.35	0.52	1.66	3.28
5	7.55	17.27	0.75	2.04	2.72
6	2.49	6.02	0.73	2.08	3.06
7	6.06	11.01	0.56	1.52	2.89
8	9.00	16.40	0.73	1.79	2.69
9	5.67	11.33	0.77	1.84	2.82
10	3.69	8.87	0.59	1.77	2.06

2.3.3 Optical function errors

As discussed in section 2.3.1, combined function and quadrupole magnetic strength and alignment errors change the beta function around the Recycler from that of the ideal lattice. Figure 2.3.3 shows an example of the beta function distortion for a random distribution of gradient errors of 1×10^{-4}/inch (rms, relative to the nominal dipole field) in the combined function magnets and 8×10^{-4} of the nominal gradient in the quadrupole magnets. The rms beta function deviation is a few percent and is dominated by the contribution from the long combined function magnets. The relatively large (15%) variation on the right hand side of figure 2.3.3 is caused by adjustments in the phase trombone at MI-60 required to maintain the tune at its nominal values in the presence of the gradient errors modeled.

No special provision are currently planned for correcting beta function distortions. Magnet performance specifications will be tailored to keep uncorrected distortions less than 2%.

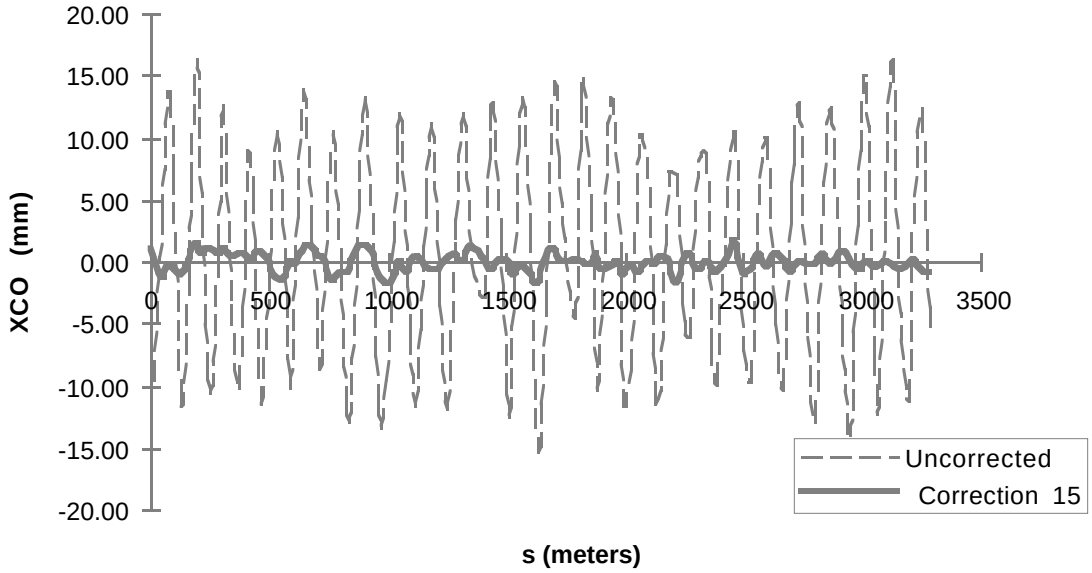

Figure 2.3.2: The uncorrected and corrected orbit corresponding to seed 8 in table 2.3.4. The corrected orbit is produced by transverse moves of fifteen magnets around the Recycler.

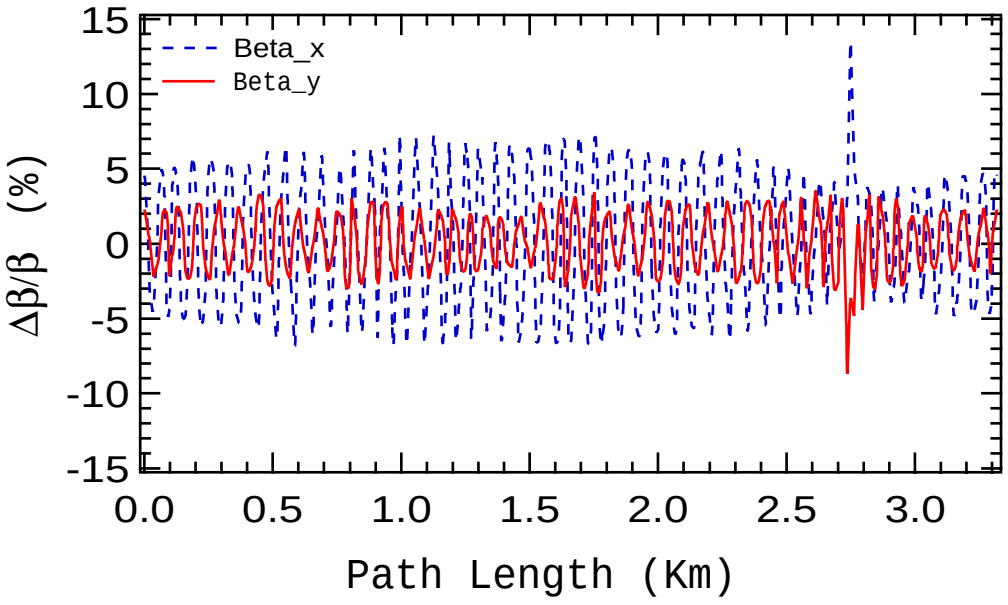

Figure 2.3.3: Typical beta function variation resulting from expected gradient strength errors.

2.3.4 Field Non-uniformities

Magnet field non-uniformities can be characterized in terms of field multipoles. This characterization is based on a description of the field in transverse coordinates via:

$$B_y + iB_x = B_0 \sum_{n=0}^{\infty} (b_n + ia_n)(x + iy)^n \quad , \quad (2.3.4)$$

where b_0, b_1, b_2 . . . are the normal dipole, quadrupole, sextupole, . . . field components, and a_0, a_1, a_2 . . . are the corresponding skew components. These higher-order field components can produce tune variations with particle oscillation amplitude and can produce unstable motion when the tune operating point comes close to fulfilling the relation

$$l\nu_x + m\nu_y = k \quad , \quad (2.3.5)$$

where l, m, and k are integers. The integers l and m are related to the field index n through the relation n=l+m-1.

The design tune of the Recycler is $(Q_X,Q_Y)=(25.425,24.415)$. This leaves it relatively isolated from resonances up to fifth order. Tune variations with amplitude and one dimensional resonance widths up to tenth order have been calculated for one Fermilab "unit" of multipole component, where Fermilab units are defined as the ratio of the multipole strength to the dipole strength, measured at 1", times 10,000, i.e.

$$1\text{unit} = b_n x^n\Big|_{x=1"} \times 10^4 = \frac{B^{(n)} x^n}{n! B_0}\Big|_{x=1"} \times 10^4 \quad . \quad (2.3.6)$$

In quadrupole magnets the multipole strengths are referred to the quadrupole, rather than the dipole field. Resonance widths generated by higher order multipoles are much less significant than tune variations with amplitude for the design tune point.

Sensitivity of the tune variation with amplitude to a given multipole contribution is computed using the expressions:

$$\Delta\nu_n = \frac{\varepsilon^{(n-1)/2}(n+1)!}{2^{n+2}\pi(\frac{n+1}{2})!^2} \sum_i b_{n,i}\theta_i\beta_i^{(n+1)/2}(39.37)^n \times 10^{-4} \quad , \quad (2.3.7)$$

$$\Delta\nu_n = \frac{\varepsilon^{(n-2)/2} n(n)!}{2^{n+1}\pi(\frac{n}{2})!^2} \frac{\Delta p}{p} \sum_i b_{n,i}\theta_i D_{x_i}\beta_i^{n/2}(39.37)^n \times 10^{-4} \quad . \quad (2.3.8)$$

Here all lengths are measured in meters, θ_i is the bend angle in the magnet, D_x is the horizontal dispersion function, and the particle oscillation amplitude is given by

$x(s) = A\sqrt{\beta(s)}\cos\phi(s) = \sqrt{\varepsilon\beta(s)}\cos\phi(s)$. Equation 2.3.7 applies only to n=odd multipoles and equation 2.3.8 to even multipoles. Equation 2.3.8 represents the feed down effect in the presence of non-zero dispersion and only leads to tune shifts for off-momentum particles.

Table 2.3.5 displays the tune shift for a particle with a 6.3 π mmmr ($60\pi/\beta\gamma$) oscillation amplitude, accompanied by a momentum offset of 0.3%, generated by a zeroth harmonic multipole contribution of one unit. This tune shift scales as $A^{(n-1)/2}$ where A is the amplitude and n is the field index in equation 2.3.4.

Table 2.3.5: Tune shift for a particle with an oscillation amplitude corresponding to 60 π mmmr and a momentum offset of 0.3% arising from one unit of the multipole component indicated in the left column. CF and Q refer to contributions from the combined function and quadrupole magnets respectively.

		Systematic		Random (rms)	
n	Multipole	$\Delta\nu$(CF)	$\Delta\nu$(Q)	$\Delta\nu$(CF)	$\Delta\nu$(Q)
3	Octupole	0.0170	0.0003	0.0017	0.0000
4	10-pole	0.0122	0.0002	0.0012	0.0000
5	12-pole	0.0074	0.0001	0.0007	0.0000
6	14-pole	0.0079	0.0001	0.0008	0.0000
7	16-pole	0.0033	0.0001	0.0003	0.0000
8	18-pole	0.0048	0.0001	0.0005	0.0000
9	20-pole	0.0015	0.0000	0.0002	0.0000

2.3.5 Tracking calculations

The tune vs. amplitude analysis presented above provides a guide as to the allowed multipole content of the magnets making up the Recycler. However, the Recycler is required to circulate beam for several hours and long term behavior in the presence of the full collection of misalignment and field errors is best understood through tracking simulations.

Performance in the presence of a mixture of alignment and magnetic field errors in the Recycler is tested by launching an array of particles at different amplitudes in the presence of the full array of errors described in sections 2.3.2-4. Particles are tracked with betatron oscillation amplitudes relative to a corrected closed orbit. Following introduction of errors the tune is adjusted to the nominal tune for a zero momentum offset particle using the phase trombone. The criterion for acceptable performance is survival over 10^5 turns (1 second of real time) with an oscillation amplitude corresponding to 60 π mmmr over the full momentum range of $\pm$0.3%. The emittance of the recycled beam is expected to lie in the 20-25 π mmmr range, while 0.3% corresponds to the momentum acceptance of the stochastic cooling systems.

Specifically, particles are launched with a horizontal displacement "A" and a vertical displacement $\sqrt{\beta_y/\beta_x}\,A$, i.e. the particle has equal horizontal and vertical emittance. In translating into acceptance the displacement is referred to a horizontal beta function of 65 m ($x_{Launch} = \sqrt{\beta_x/65}\,A$). Particle are tracked with a constant momentum offset of,

$\Delta p/p$, which is varied over the range ±0.3%. Net chromaticities in both planes are set to -2, the correct sign to combat the bunched-beam head-tail instability. Particles with amplitudes varying from 15 mm to 35 mm are considered. Simulations are performed for five different seeds with a maximum of 100,000 turns tracked.

Combined function multipole component errors used in these simulations are given in table 2.3.6. As a starting point application of a criterion of detuning of less than 0.03 at 60 π mmmr was applied to table 2.3.5 in the presence of a 0.3% momentum offset. These multipoles were observed to result in a dynamic aperture somewhat less than the goal of 60π. As a result the multipole composition was varied with the set presented below leading to acceptable behavior. This set provides the basis of the current magnet specification as described in section 2.3.6. Further iteration on this set is anticipated. Multipole component errors used for the quadrupole magnets are given in table 2.3.7. Performance is relatively insensitive to these multipoles (at the factor of three level). Note that all systematic multipoles are modeled with the same sign. This is the most pessimistic assumption possible because it results in the maximum detuning with amplitude. It is worth noting that in the absence of any ≥8-pole errors the aperture of the Recycler is in excess of 100 π mmmr over the entire specified momentum range.

Table 2.3.6 Combined function magnet field multipoles used in the tracking simulations represented in figure 2.3.4. All multipoles are given in Fermilab "units" as referenced to the dipole component.

Multipole Component	Normal (Systematic)	Normal (Random)	Skew (Systematic)	Skew (Random)
Quadrupole	1.0	1.0	1.0	1.0
Sextupole	0.5	1.0	0	0.5
Octupole	0.5	0.5	0	0.5
10-pole	0.2	0.5	0	0.5
12-pole	0.1	0.5	0	0.5
14-pole	0.1	0.5	0	0.5
16-pole	0.1	0.5	0	0.5
18-pole	0.1	0.5	0	0.5
20-pole	0.1	0.5	0	0.5

Table 2.3.7: Quadrupole magnet field multipoles used in the tracking simulations represented in figure 2.3.4. All multipoles are given in Fermilab "units" as referenced to the quadrupole component.

Multipole Component	Normal (Systematic)	Normal (Random)	Skew (Systematic)	Skew (Random)
Quadrupole	0	8	0	0
Sextupole	0.5	0.5	0	0.5
Octupole	0.2	0.5	0	0.5
10-pole	0.1	0.5	0	0.5
12-pole	0.1	0.5	0	0.5
14-pole	0.1	0.5	0	0.5
16-pole	0.1	0.5	0	0.5
18-pole	0.1	0.5	0	0.5

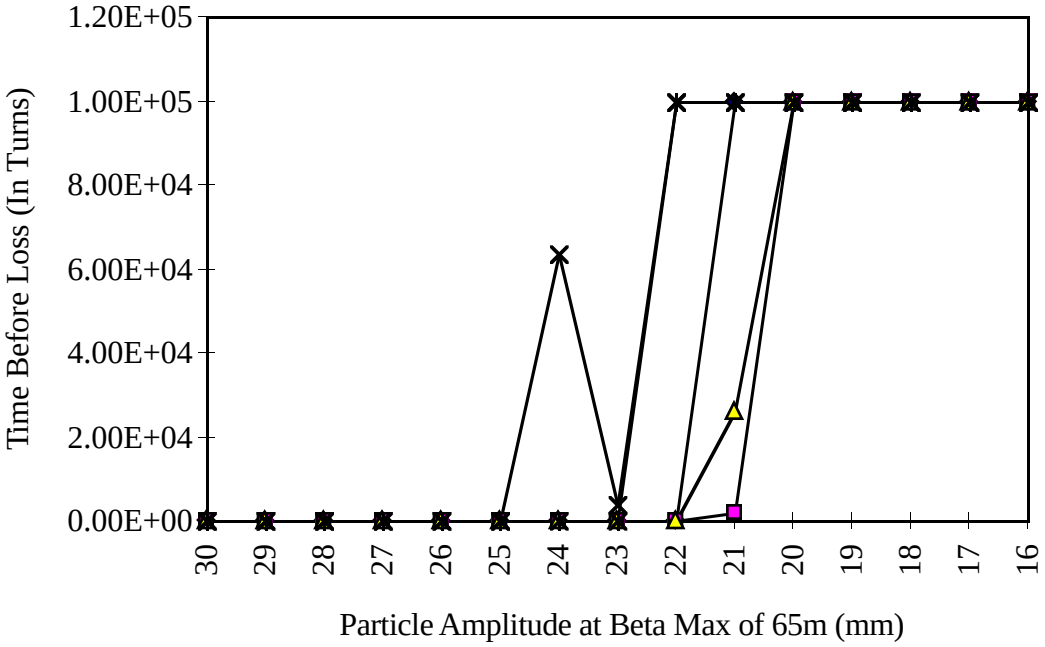

Figure 2.3.4: Survival plot for the Recycler. The number of turns survived, up to 100,000 turns, is shown as a function of the launch amplitude for five different collections of systematic and random alignment and magnetic field errors and a momentum offset of 0.3%.

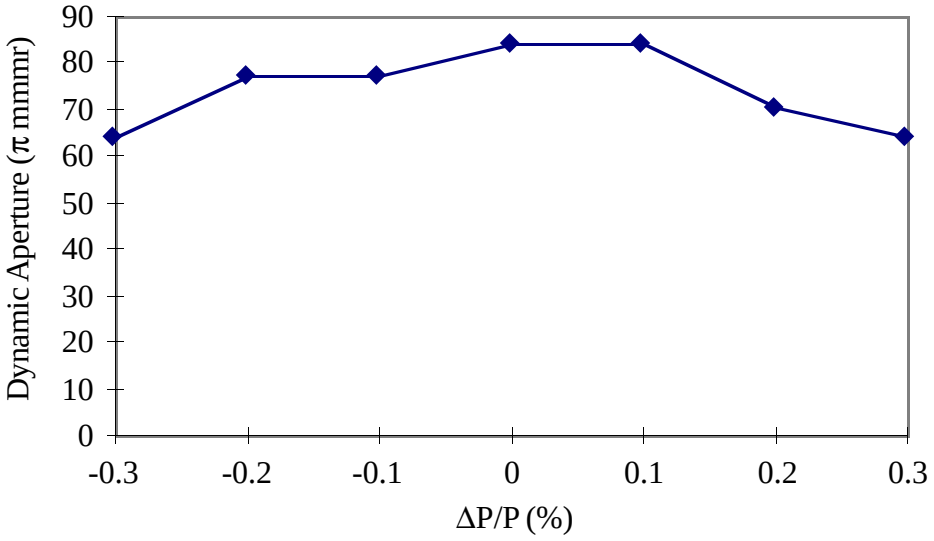

Figure 2.3.5: Dynamic aperture as a function of momentum offset over the full momentum range of the antiproton stack. This calculation is based on 100,000 turn survival and incorporates the full set of misalignment and field quality errors described in the text.

Figure 2.3.4 is a survival plot displaying how many turns a particle survives in the Recycler as a function of initial amplitude for each of five seeds. If the dynamic aperture of the machine is defined as the smallest amplitude particle that did not survive for 100,000 turns, then the dynamic aperture for the Recycler is predicted to be 22±1 mm, corresponding to a normalized emittance of 64±6 π mmmr.

Figure 2.3.5 shows the dynamic aperture as determined by 100,000 turn particle survival as a function of the momentum offset. This plot indicates that an aperture in excess of 60 π mmmr is maintained over the full momentum spread expected in the antiproton stack. Further tracking of up to 10^6 turns is currently being undertaken to understand longer term trends.

Particle tracking is also utilized to study the variation of the horizontal and vertical tunes as a function of oscillation amplitude. Figure 2.3.6 shows the tune space location as a function of amplitude for particles with a 0.3% momentum offset. Comparison with table 2.3.5 shows that the vertical tune shift with amplitude is nearly completely accounted for by the 0.5 unit systematic octupole component assumed in the tracking, while the other multipoles conspire to keep the horizontal tune shift small.

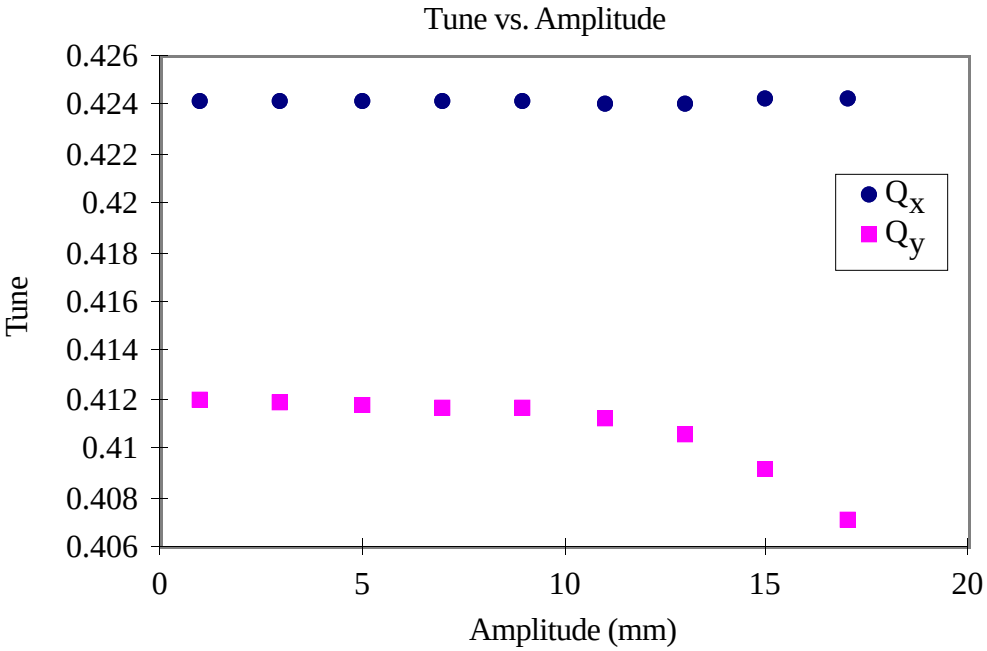

Figure: 2.3.6: Tune vs. amplitude for the set of multipoles given in Table 2.3.6 as determined through tracking.

2.3.6 Magnetic performance specification

Magnet performance specifications have been developed based on the analyses described in the above sections. The detailed performance specification is given in MI-0170 and is summarized here.

Tolerances have been specified for both systematic and random strength variations in the dipole, quadrupole, and sextupole field components, overall magnetic field uniformity across the required aperture, and allowed multipole composition. Criterion applied in deriving these tolerances are as follows:

1. Uncorrected closed orbit distortion due to magnetic field imperfections < 3 mm.

2. Beta function error due to magnetic field imperfections < 2%.

3. Tune relative to the nominal value within 0.1

4. Uncompensated minimum tune separation due to magnetic imperfections < .005

5. Tune variation with amplitude <.01 out to 20 mm.

6. Chromaticity within range of the sextupole correction system.

7. Beam survival at 20 mm oscillation amplitude for 5 seeds at 10^5 turns over the full ±0.3% range of momentum offsets.

Tolerances are summarized in tables 2.3.8 and 2.3.9 below.

Table 2.3.8: Magnet strength tolerances for Recycler combined function magnets.

Performance Measure	Tolerance (Systematic)	Tolerance (Random, rms)
Absolute bending strength of long combined function magnet	$5x10^{-4}$	$5x10^{-4}$
Ratio of short/long bending strength in combined function magnets	$5x10^{-4}$	$5x10^{-4}$
Ratio of gradient to nominal dipole in combined function magnets	$2x10^{-4}$/inch	$1x10^{-4}$/inch
Ratio of sextupole/dipole in long combined function magnets	$1x10^{-4}$/inch^2	$1x10^{-4}$/inch^2
Field flatness over ±20 mm	$\pm1.5x10^{-4}$	$\pm1.5x10^{-4}$

Table 2.3.9: Allowed multipole components, in Fermilab units, for combined function magnets. For quadrupole and sextupole components, the number listed is relative to the nominal design value.

Multipole Component	Normal (Systematic)	Normal (Random)	Skew (Systematic)	Skew (Random)
Quadrupole	1	1	1	1
Sextupole	0.5	1	-	0.5
Octupole	0.5	0.5	-	0.5
10-pole	0.2	0.5	-	0.5
12-pole	0.1	0.5	-	0.5
14-pole	0.1	0.5	-	0.5
16-pole	0.1	0.5	-	0.5
18-pole	0.1	0.5	-	0.5
20-pole	0.1	0.5	-	0.5

2.3.7 Required correction systems

Correction strategies and/or systems will be required to compensate for the magnetic field imperfections and misalignment effects described above. Systems or strategies are required for closed orbit correction, tune and chromaticity adjustment, coupling correction, and higher order resonance correction.

It is proposed that the closed orbit be corrected through adjustment of the transverse positions of a limited number of gradient magnets as described in section 2.3.2. No active correction elements are included in the design other than in the injection and extraction areas. As discussed in section 2.3.2 the uncorrected closed orbit is expected to show peak excursions of up to ~15 mm. A model in which fifteen gradient magnets are chosen to be moved was analyzed and shown to produce a corrected orbit distortion of <1 mm (rms) with peak distortions under 3 mm. The maximum transverse movement required is typically 2 mm, well within the range of tolerable mechanical motion allowed.

Tune adjustment is provided in the MI-60 phase trombone as described in section 2.2. Five families of two adjustable magnets each are provided. A total tuning range of ±0.5 is achievable with no perturbation of the optical functions outside the trombone region.

A chromaticity control (sextupole) magnet system will be incorporated into the Recycler. The incorporation of a design systematic sextupole component into the long combined function magnets will produce an uncorrected chromaticity in the Recycler of -2 in both transverse planes. A correction system is specified that allows adjustment of the chromaticity over a ±5 range relative to nominal in each plane. The total required strength of focusing and defocusing sextupoles as a function of chromaticity is given in table 2.3.10. As is shown a total strength (B"L) of 425 kG/m is required. Such a correction system will be implemented by utilizing unused Main Ring sextupoles. It is proposed to utilized two sets of sextupoles, 8 focusing and 16 defocusing, each to provide chromaticity control in the Recycler. Each set will be constituted of several pairs of magnets separated by 180° of phase in order to nullify any contribution to the third order resonant driving term.

Table 2.3.10: Sextupole strength required to achieve the Recycler chromaticities listed in the left hand columns. B"L is the integrated strength and $N_{F,D}$ is the number of magnets in each family. It is proposed to utilize a system in which N_F=8 and N_D=16.

$\Delta\xi_H$	$\Delta\xi_V$	$N_F(B"L)_F$ (kG/m)	$N_D(B"L)_D$ (kG/m)
+5	0	176	-69
0	+5	34	-355
+5	+5	211	-424

As described in section 2.3.1 coupling due to systematic and random skew quadrupole components, and due to alignment errors could be significant in the Recycler. Global coupling will be controlled via two skew quadrupole circuits. The location of these magnets depends on details of the lattice and will not be defined until the lattice is frozen. All tracking simulations performed to date incorporate uncompensated coupling.

2.3.8 Summary

Calculations presented in this section have shown that the Recycler ring can achieve the design specification for storage of beam with a $40\,\pi$ mmmr admittance and a momentum spread of 0.3%. This performance requires magnets built to tolerances listed in section 2.3.6, alignment at the level described in section 2.3.2, and correction of the closed orbit. Magnet requirements are dictated by the allowable orbit and beta function distortions, and by the dynamic aperture in the presence of higher order magnetic multipoles.

It is anticipated that once full length prototype Recycler magnets have been measured the studies described here will be expanded more systematically to construct a performance model of the real Recycler ring.

2.4. Beamlines and Beam Transfers

The desired functionality of the Recycler ring requires the addition of three 8 GeV proton and antiproton transfer lines. These transfer lines are shown on the right side of figure 2.4.1. The MI-32 and MI-40 proton injection and abort lines are used during commissioning and tune-up. The MI-22 and MI-32 antiproton transfer lines between the Main Injector and the Recycler are used for normal Tevatron Collider operations.

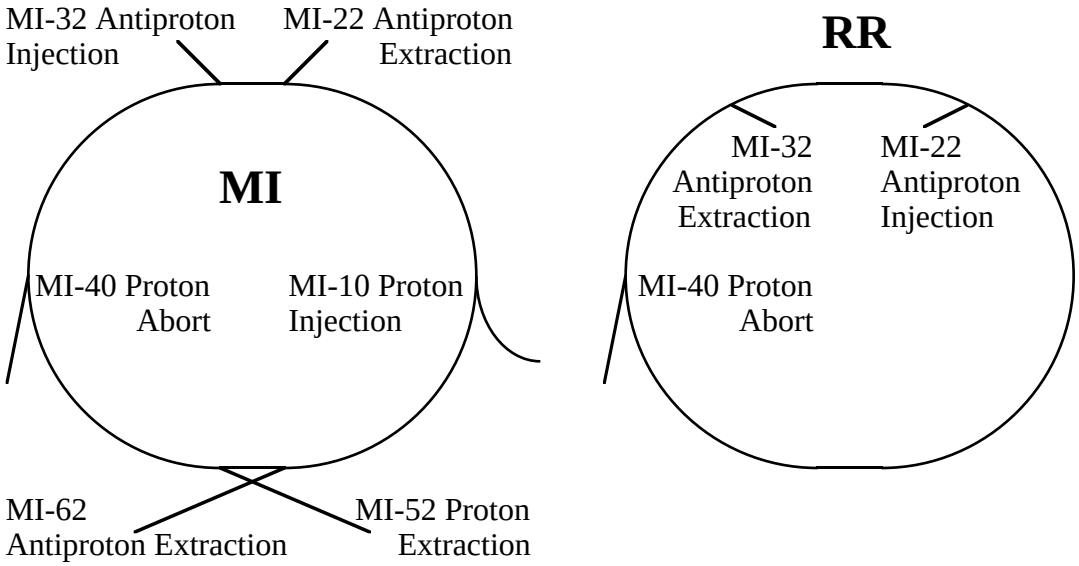

Figure 2.4.1: Sketch of the Main Injector (MI) and Recycler ring (RR) beam transfer lines. Note that the transfer lines at the MI-22 and MI-32 straight sections link the two rings together for injection and extraction of both antiprotons and protons.

2.4.1. Maximum Acceptable Kicker Ripple

The parameters which must be specified in order to design the kickers for these transfers are the kicker amplitude, rise/fall time, and flattop ripple magnitude. The allowed magnitude of kicker flattop ripple is determined by the amount of emittance growth which is considered acceptable. The equation describing the fractional emittance increase due to a position or angular misalignment normalized to the beam rms size or divergence respectively is

$$\frac{\varepsilon}{\varepsilon_o} = 1 + \tfrac{1}{2}\left(\frac{\Delta}{\sigma}\right)^2 \quad . \quad (2.4.1)$$

According to equation (2.4.1) a given kicker amplitude error Δ causes more emittance growth $\varepsilon/\varepsilon_o$ as the initial beam divergence σ or emittance ε_o decreases. Using conservative numbers for the initial emittance and the acceptable level of emittance growth, table 2.4.1 displays the relevant parameters which determine the percentage kicker amplitude ripple or error. The dependence of emittance growth on kicker error is plotted in figure 2.4.2.

Table 2.4.1: Anticipated parameters dictating the acceptable level of kicker amplitude error or ripple during flattop.

Parameter	Value
Maximum emittance growth (95% Invariant π mmmr)	0.2
Minimum initial emittance (95% Invariant π mmmr)	10
Maximum kicker error / beam divergence (equation 2.4.1)	0.2
Beta function at the kicker magnet (m)	54
Minimum beam divergence at a kicker magnet (μrad)	57
Maximum deflection angle in a kicker (μrad)	12.0
Kicker amplitude in all transfer lines (mrad)	1.0
Maximum percentage kicker ripple/error magnitude (%)	±1.2

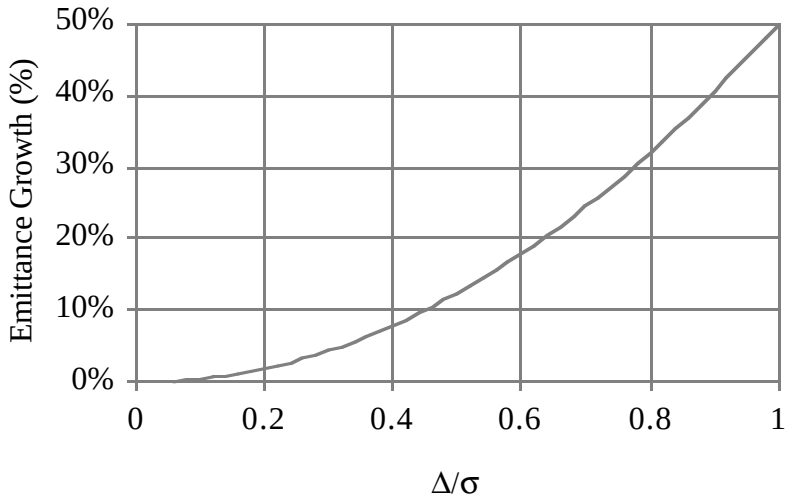

Figure 2.4.2: Fractional emittance growth as a function of the transfer angle or position error normalized to the rms beam divergence or size.

2.4.2. Role of Each Recycler Transfer Line

MI-32 Proton MI to RR: Used for commissioning and beam line tune-ups, the ability to easily inject protons into the Recycler from the Main Injector is necessary for efficient startup and operation. One positive aspect of the positioning of this transfer line is the fact that once the Main Injector is commissioned to its abort dump (which is the first half turn of the ring), Recycler commissioning can also start.

MI-40 Proton Abort: Used only during commissioning or other proton applications in which high intensities of beam can cause radiation safety or ground water activation problems, this abort line is basically identical to the Main Injector line. Since there is no emergency abort scenario envisioned, the kicker pulse length need only be 1.6 μsec in order to fulfill its ALARA mission. In the unlikely situation of multiple proton batch injection into the Recycler ring, multiple abort line transfers can be programmed to

eliminate this beam. Figure 2.4.4 shows the geometry of this abort line showing the ring quadrupoles, the horizontal kicker, and the vertical Lambertson magnet.

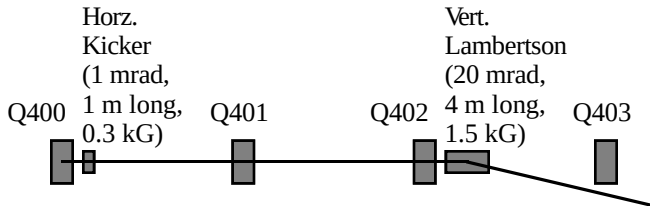

Figure 2.4.4: Elevation view of the Recycler ring MI-40 proton abort extraction geometry. The horizontal kicker deflects the extracted beam by 1 mrad into the bend field region of the vertical Lambertson magnet.

MI-22 Antiproton MI to RR: This transfer line directs antiprotons from the Main Injector and delivers them into a clockwise trajectory in the Recycler ring. The antiprotons are either enroute from the Accumulator or have been recycled from the Tevatron Collider. The maximum beam pulse length in either case is 1.6 μsec.

MI-32 Antiproton RR to MI: This transfer line directs cooled and formed antiprotons from the Recycler ring and delivers them into the Main Injector ready for acceleration and transfer into the Tevatron Collider. The kicker flattop must be at least 1.6 μsec.

2.4.3. Kicker and Lambertson Placement

In the Main Injector, it is possible to use the same kicker at MI-30 for both transfer lines at MI-32 and MI-22. By using a Recycler kicker at MI-20 for recycled antiproton injections at MI-22, the Recycler kicker at MI-22 away from any service buildings can be eliminated. This choice of kicker location is dictated by the fact that there is available space in that service building for the kicker hardware. Not only does the eliminate the civil construction cost of building a dedicated kicker building, but it also symmetrizes the two transfer lines about MI-30. As required, the betatron phase advance between the MI-20 and the MI-22 Lambertson is an odd multiple of 90°. Similarly, the kicker at MI-32 can be eliminated by using the MI-40 abort kicker. Therefore, the number of kickers is reduced from 6 to 3, a factor of 2 reduction. This scenario is sketched in figure 2.4.5. The advantages of this scheme are reduced cost and reduced Recycler ring impedance.

The details of the positioning of the MI-30 kicker in the Main Injector and the associated antiproton injection and extraction Lambertsons are sketched in figure 2.4.6. Since MI-22 and MI-32 are three half cell straight sections, the Main Injector Lambertsons are placed in those locations. In the Recycler there is so much free space between the gradient magnets that Lambertsons easily fit even in bend cells. The only catch is the leading gradient magnets at 216 and 328 need to be half (mirror) magnets in order for the extracted beam to clear with a 20 mrad kick.

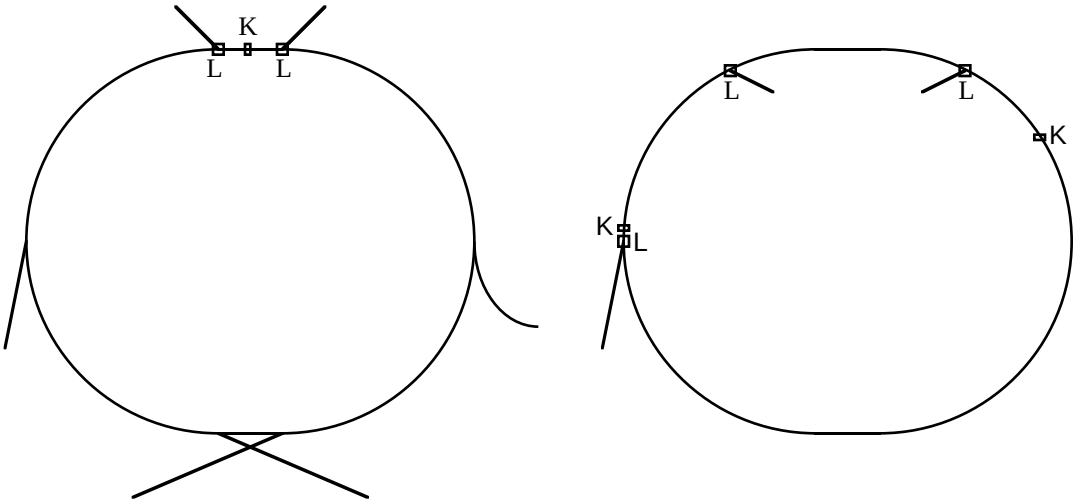

Figure 2.4.5: Sketches of the Main Injector (left) and Recycler ring (right) transfer lines in which only the new Lambertsons and kickers needed for Recycler ring operations are depicted. The displayed scenario assumes that kicker systems can be shared to service all of the transfer needs for a factor of 2 reduction in the number of systems.

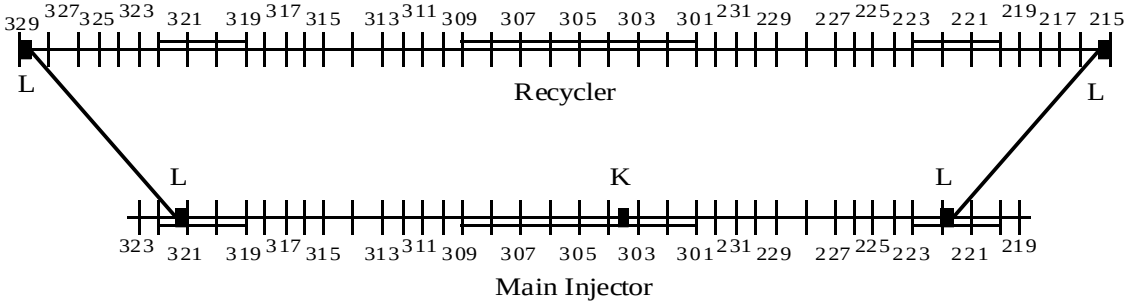

Figure 2.4.6: Sketch of the precise locations of the kickers and Lambertsons for the antiproton injection and extraction lines at MI-22 and MI-32.

Lattice designs and beam envelope calculations of the MI-22 and MI-32 transfer lines have been carried out [D. Johnson, MI Note 161]. The beam trajectories and full widths for the two machines and antiproton transfer directions are shown in figures 2.4.7 through 2.4.10. In figure 2.4.7 the antiproton recycling transfer from the Main Injector to the Recycler via MI-22 is shown from the point of view of the Main Injector. The closed orbit between the kicker and Lambertson is distorted with a pair of correction dipoles in order to optimize the use of horizontal aperture. The kicker launches the extracted beam on an opposite distortion which leads the beam into the Lambertson extraction channel. Both beams are assumed to have a transverse normalized 95% emittance of 40 π mmmr. The top and bottom of the plot are at the horizontal aperture of the Main Injector. In figure 2.4.8 the recycled antiprotons are shown in the Recycler ring just downstream of the injection Lambertson. In this case the horizontal aperture of the Recycler is explicitly indicated, and the beams are assumed to have an emittance of 20 π mmmr.

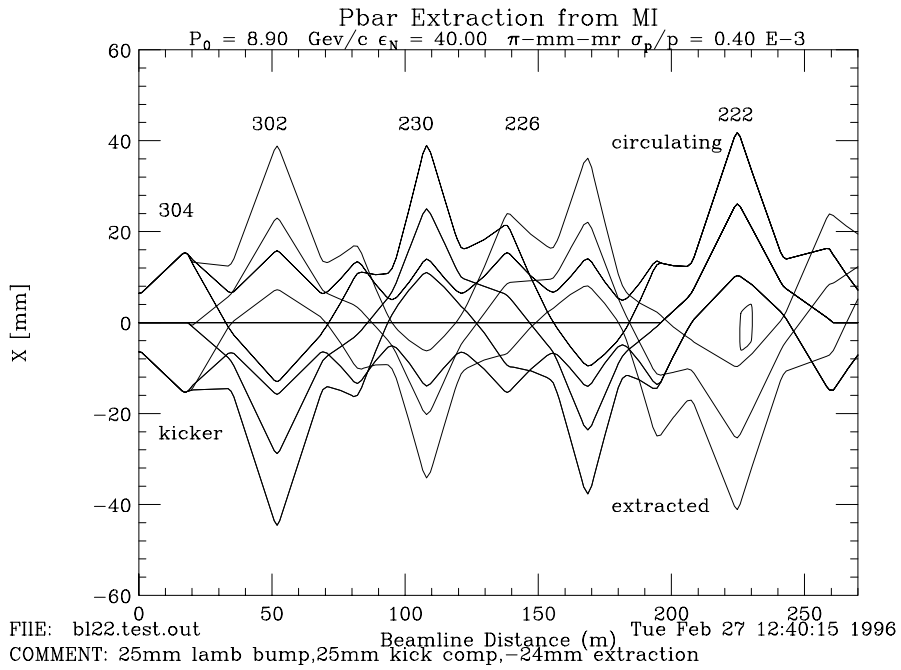

Figure 2.4.7: Beam trajectories and full widths of the stored and extracted beam in the Main Injector during antiproton recycling transfers from the Main Injector to the Recycler. The Main Injector horizontal aperture is at the extrema of the Y-axis of the plot.

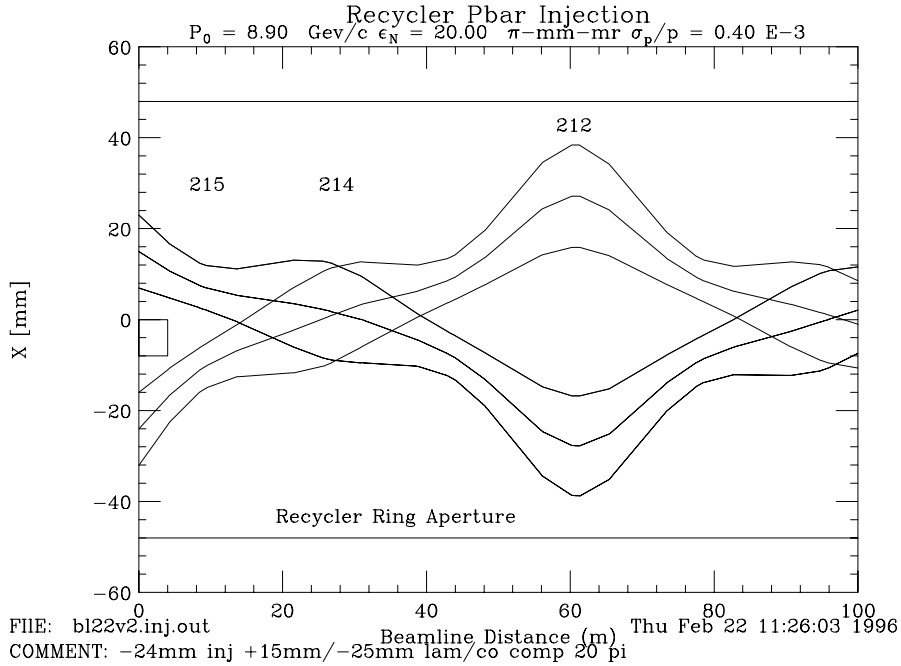

Figure 2.4.8: Beam trajectories and full widths of the stored and injected beam in the Recycler during antiproton recycling transfers from the Main Injector to the Recycler.

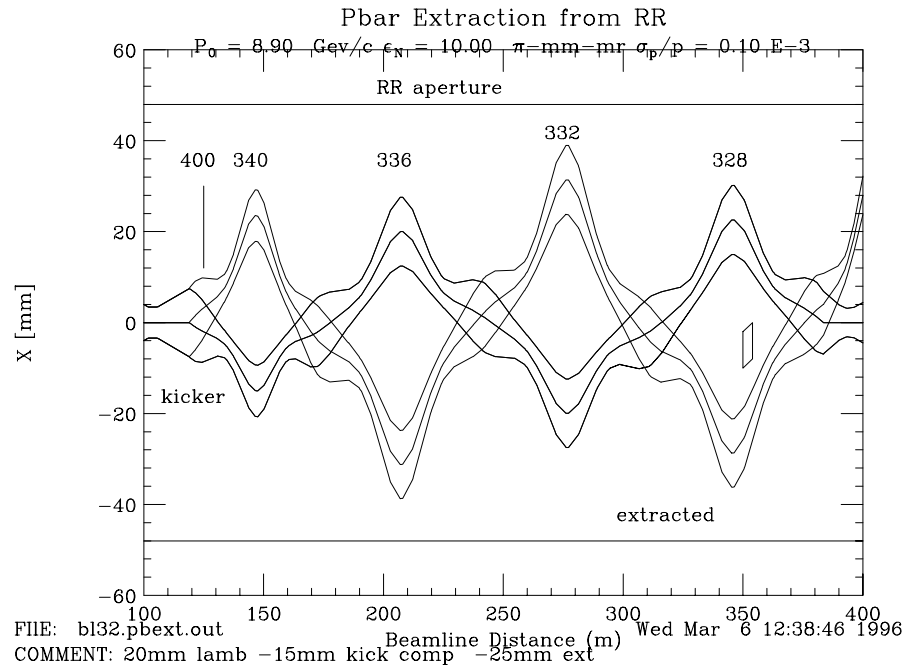

Figure 2.4.9: Beam trajectories and full widths of the stored and extracted beam in the Recycler during transfers of cooled antiprotons from the Recycler to the Main Injector.

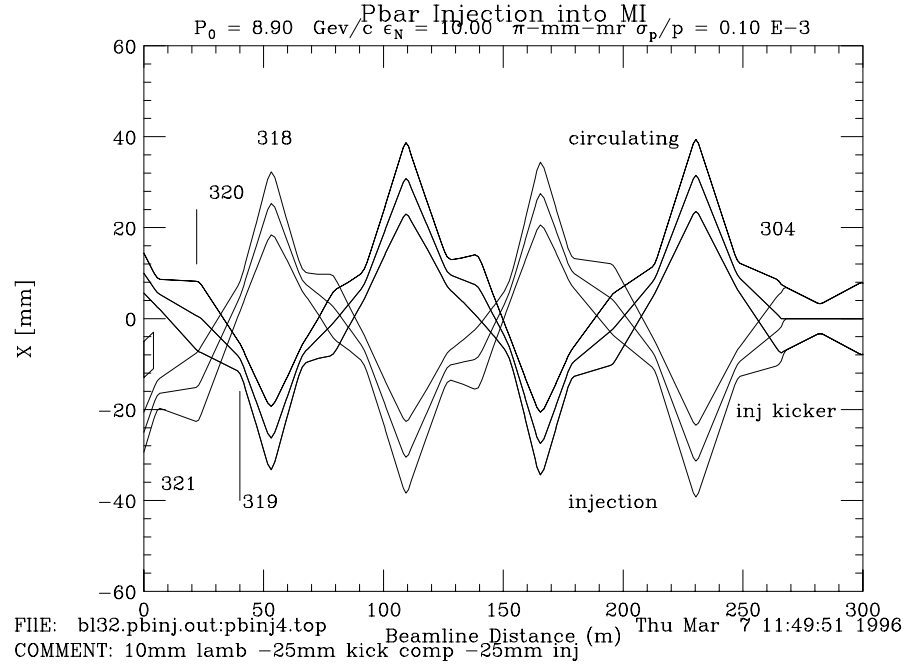

Figure 2.4.10: Beam trajectories and full widths of the stored and injected beam in the Main Injector during transfers of cooled antiprotons from the Recycler to the Main Injector. The Main Injector horizontal aperture is at the extrema of the Y-axis of the plot.

Extraction of cooled antiprotons from the Recycler for ultimate injection in the Tevatron Collider takes place via the MI-32 transfer line. In figure 2.4.9 the closed orbit and extracted beam orbits are shown between the kicker and Lambertson. A transverse normalized 95% emittance of 10 π mmmr was used to calculate the full beam widths of both the circulating and extracted beams. The beam trajectory and size after the transfer in the Main Injector is shown in figure 2.4.10.

2.4.4. Kicker and Lambertson Requirement Summary

In the transfer scenarios described in this design all kickers have an integrated kick of 300 Gauss-meters. The maximum kicker length in all of these scenarios is approximately 4 meters. In all cases the flattop duration of the kicker is at least 1.6 μsec. The rise and fall times for the two Recycler and one Main Injector kickers can be as large as 1-2 μsec. The minimum repetition interval for firing the kickers is anticipated to be 20 sec for antiproton transfers. Within the scope of Fermi III the proton injections are also limited to this interval.

In order to minimize the impedance effects of the two kickers in the Recycler, the beam tubes should be shielded or coated as much as possible. A reasonable criterion would be for the coating to slow down the rise and fall times by approximately 5-10%. Because of the slow rise times in these kickers, a rather thick coating can be used.

The Lambertsons are of the permanent magnet variety. Since there is a vertical correction magnet next to each vertically bending Lambertson, the tolerance on the field strength can be relaxed to as much as 1% (though in construction a manufacturing tolerance of 0.1% will be employed). The nominal bend angle of the Lambertsons is ±22 mrad.

2.4.5. Beam Synchronous Clocks and Beam Transfers

From the very beginning of accelerator operations at Fermilab, the transfers of beams from one accelerator to another has been complicated by the large number of transfer lines and beam dumps. As the years have gone by, especially with the addition of the Antiproton Source, the complexity of beam transfers has increased dramatically. With the addition of the Main Injector and Recycler, this trend definitely continues. Figure 2.4.11 contains a diagram of all of the beam destination options.

Since the advent of the Tevatron accelerator in the early 1980's, beam transfers between accelerators have generally taken advantage of beam synchronous clocks. Presently realized for the Main Ring and Tevatron, beam synchronous clock base frequencies are integer sub-harmonics of the machine RF (RF/7) while also synchronous with machine revolution frequency, each having 159 clock ticks per revolution. Similar in operation to TCLK, events exactly synchronous with a machine's revolution frequency (RF/1113) are coded onto each of these clocks and are denoted by the hexadecimal codes $\$AA_{MRBS}$ and $\$AA_{TVBS}$. The existing capability to transfer beam from any particular RF bucket of one machine to any particular bucket of another machine will be retained for the planned Recycler. Conceptually expressed, desired transfers between machines are allowed (or manipulated) to occur as the respective revolution events come into particular time (better stated as RF) alignment. Actual transfers are thereupon initiated by unique coded beam synchronous events that are placed constantly with respect to the

revolution events. Required kicker timing is provided by beam sync timer modules that reference the unique transfer event and provide desired delay in machine revolutions and fractions thereof.

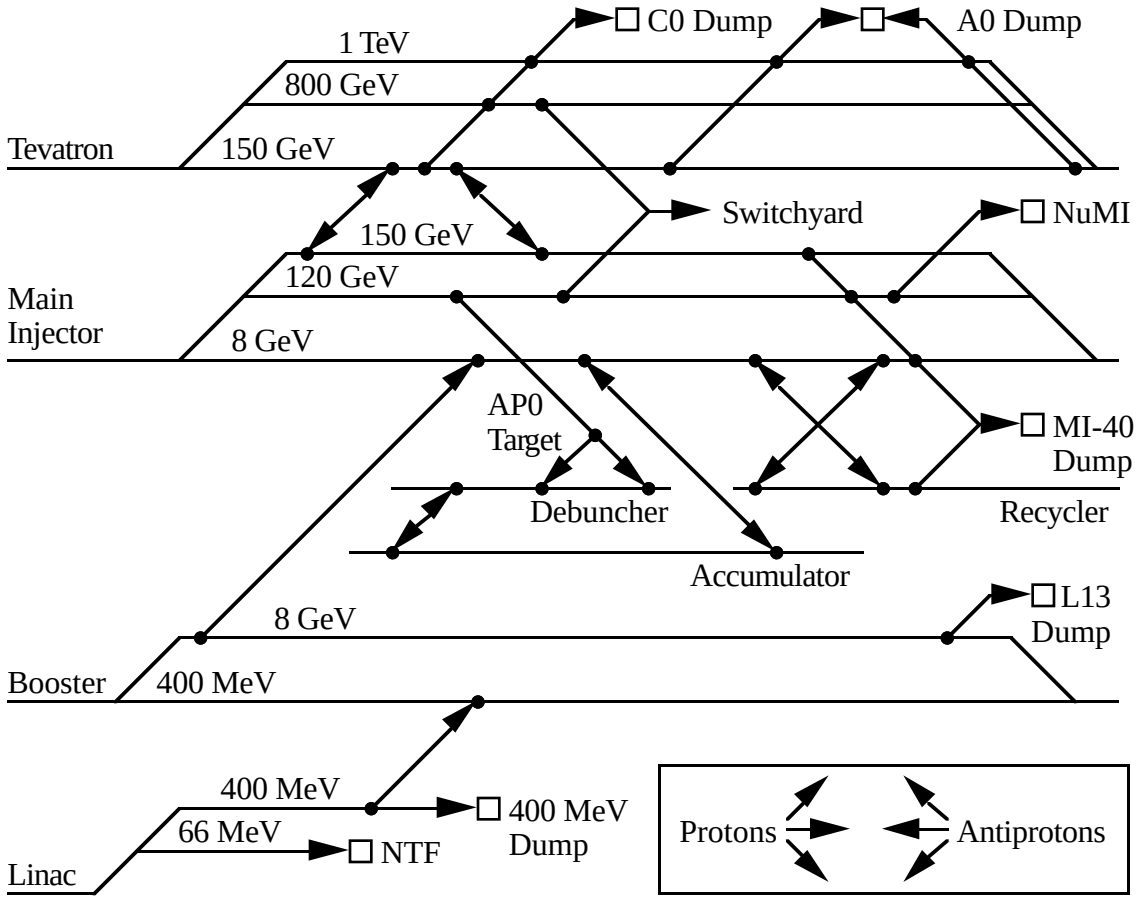

Figure 2.4.11: Map of all of the beam destination options at Fermilab after construction and commissioning of the Main Injector and the Recycler.

Transfers between the Recycler and Main Injector, which will require transfer cogging of the Main Injector RF, are relatively uncomplicated since the 53 MHz harmonic numbers of each machine both equal 588. Booster or Accumulator transfers to these larger machines are slightly more complicated in that their harmonic numbers are 84. However, transfers are simplified by the fact that the Booster and Accumulator harmonic numbers are exactly 1/7th that of the Recycler or Main Injector and that beam in either the Booster or Accumulator is, at least initially, uniformly distributed in longitudinal space.

The Recycler will require a new RF system and a derivative beam synchronous clock, RRBS, to facilitate beam transfers and circulating beam diagnostics. For this clock, $AA_{RRBS} is the assigned revolution marker event and there are 84 clock ticks per revolution. Development and installation of the new RRBS clock is judged as straightforward in that RRBS architecture will largely duplicate that of other beam synchronous

clocks. RRBS will be distributed from MI-60 to all Main Injector service buildings and to the Booster via fiber optic links.

Careful coordination of the Booster, Recycler, Main Injector, and Accumulator RF systems is fundamental to achieving successful transfers of beam. The fundamental 53 MHz reference of the Recycler RF system is to be considered as a fixed reference at 8 GeV to which other systems transfer cog and phase lock. While the operation of the Accumulator RF system has historically been independent, better synchronism strategies with the Main Injector need to be developed. The Recycler RF system will routinely provide appropriate barrier buckets for acceptance of beam while also partitioning fractions of circulating beam for extraction.

2.4.6. Beam Synchronous Transfer Events

A variety of new beam sync transfer events have been designated to effect desired transfers of particle beams to and from the Recycler. These events are temporally denoted by Sn_{xxBS}, with n ranging up from one, and with the subscript denoting the specific beam sync clock. Proper generation of these events ties closely with Recycler operating scenarios previously described and the TCLK resource. Details relative to the assignment and generation of these events are described hereafter. Discussion is facilitated by first describing the general sequence of TCLK and beam sync events on a per scenario basis. BES denotes the "Booster Extraction Sync" pulse signal presently generated by the Booster low-level RF timing hardware. It is also worthwhile to note that all beam sync transfer events are detected and mirrored as TCLK events with typical related time skew of 100 nanoseconds or less. This mirroring of beam synchronous transfer events in the Tevatron Clock has proven useful for diagnostic purposes.

S1: Main Injector Protons to the Recycler
$T6 --> $2D --> $16 --> BES --> $S1$_{MIBS}$ --> $S3$_{MIBS}$

S2: Recycler Protons to the Main Injector
$T4 -->$S3$_{RRBS}$ --> $2F

S3: Accumulator P-Bars to the Recycler
$T7 --> $9A --> $2D --> $7A$_{MIBS}$ --> $S4$_{MIBS}$

S4: Recycler P-Bars to the Main Injector
$T5 --> $2A --> $S4$_{RRBS}$
(Multiple sequences of $T5 Recycler cycles and $2A Main Injector cycles are necessary to fill the Tevatron.)

S5: Tevatron P-Bars to the Recycler
$CE --> $T8 --> $T9 --> $T7 --> $2A --> $T10 --> $25 --> $S2$_{MIBS}$ --> $T11 --> $T12 --> $T13 --> $S4$_{MIBS}$
(Multiple sequences of $T7 Recycler and $2A Main Injector cycles are necessary to empty the Tevatron of p-bars once the Tevatron is at 150 GeV.)

$S1$_{RRBS}$: Initiate Proton Transfer from Recycler to Main Injector - This transfer event will be generated in a typical fashion by having a TCLK timer channel output sync up with the first available decoded AA_{RRBS}$ event to form the $S3$_{RRBS}$ event request. $T4 appears to be the natural reference. It could also process the output of a timer channel with a $2D reference with a state machine to form the appropriate event request.

$S3_{RRBS}$: Initiate Antiproton Transfer from Recycler to Main Injector - This transfer event will be generated by having a TCLK timer output sync up with the first available decoded AA_{RRBS} event to form the $S4_{RRBS}$ event request. $T5 appears to be the natural reference though it may be too far away in time. It could also process the output of a timer channel with a $2A reference with a state machine to form the appropriate event request.

$S1_{MIBS}$: Initiate Beam Transfer from Booster to Main Injector - Generation of this event would require some state machine processing of the BES pulse from the Booster. For the general case, the occurrence of any Main Injector reset and the occurrence of any Booster reset except $17 would cause $S1_{MIBS}$ to be generated. It is necessary to have BES at MI-60, the location of the Main Injector RF system and the MIBS source, if the $S1_{MIBS}$ event is to be accurate. State processing of the $1F event might also serve as the event request for $S1_{MIBS}$. The possibility of timing the injection kicker at MI-10 with BES, as alternative to $S1_{MIBS}$, remains as a viable option.

$S2_{MIBS}$: Initiate Antiproton Transfer from Tevatron to Main Injector - Transfer cogging and diagnostic concerns again suggest this transfer event to be best placed on the MIBS rather than the TVBS clock. This event will be generated by having a TCLK timer channel output sync up with the first available decoded AA_{MIBS} event to form the $S2_{MIBS}$ event request. New event $T10, which occurs when the Tevatron ramp has reached 150 GeV after the deceleration process, is likely the best reference for the timer channel. Some state machine processing of the actual event request signal is likely.

$S3_{MIBS}$: Initiate Proton Transfer from Main Injector to Recycler - This transfer event will be generated by having a TCLK timer channel output sync up with the first available decoded AA_{MIBS} event to form the $S3_{MIBS}$ event request. $T6 appears to be the natural reference. It could also condition the output of a timer channel with a $2D reference with a state machine to form the appropriate event request.

$S4_{MIBS}$: Initiate Antiproton Transfer from Main Injector to Recycler - This transfer event is somewhat special in that two TCLK timer channels, one for each of the related S3 and S5 scenarios, are necessary to support event generation. The or'd timer channel outputs will sync up with the first available decoded AA_{MIBS} event to form the $S4_{MIBS}$ event request. For the S3 scenario, either $T7 or $9A appear to be the natural reference for the first timer channel, the choice depending on their relative position in time. Some state machine processing is anticipated. For the S5 scenario, the aforementioned $T11 might serve as a reference for the second timer channel. One could also consider $T13 which occurs when the Main Injector ramp has reached 8 GeV after the deceleration process. As for the previous case, some state machine processing is probably required.

2.5. Vacuum Issues

Stainless steel beam tubes in which the vacuum is maintained with lumped ion-sputter pumps is the traditional technology used in the hadron accelerators at Fermilab. Though an aluminum alternative is under serious consideration, this report will discuss a stainless steel system in which innovations are applied to bring down the cost without invoking unreasonable technical risks. An important factor affecting the design of the system is

the need for high reliability storage of the antiprotons. With the stated goal of surviving lightning strikes and power outages of up to an hour, manual sector valves and low outgassing rate beam tubes are required.

2.5.1. Beam Intensity Lifetime Requirement

The required beam intensity lifetime is determined by modeling the evolution of antiproton intensity in the Recycler assuming injections from the Tevatron and Accumulator. At the beginning of each collider cycle the Recycler contains the antiprotons recycled from the Tevatron. Every hour after the start of a collider store antiprotons stacked in the Accumulator are injected into the Recycler. It is assumed that the stacking rate is 20×10^{10} antiprotons/hour.

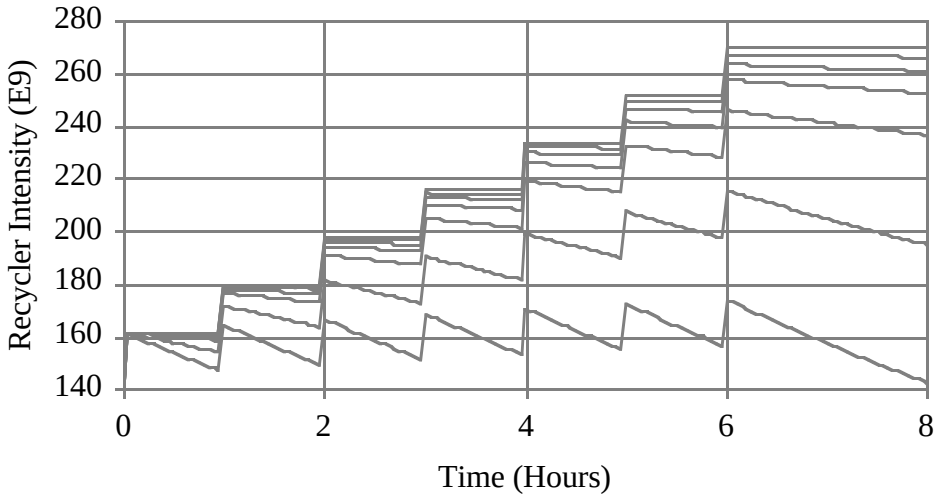

Figure 2.5.1: Assuming beam intensity lifetimes of infinity (top), 500, 200, 100, 50, 20, and 10 hours (bottom), evolution of the antiprotons injected from the Tevatron (recycled) and the Accumulator (stacked).

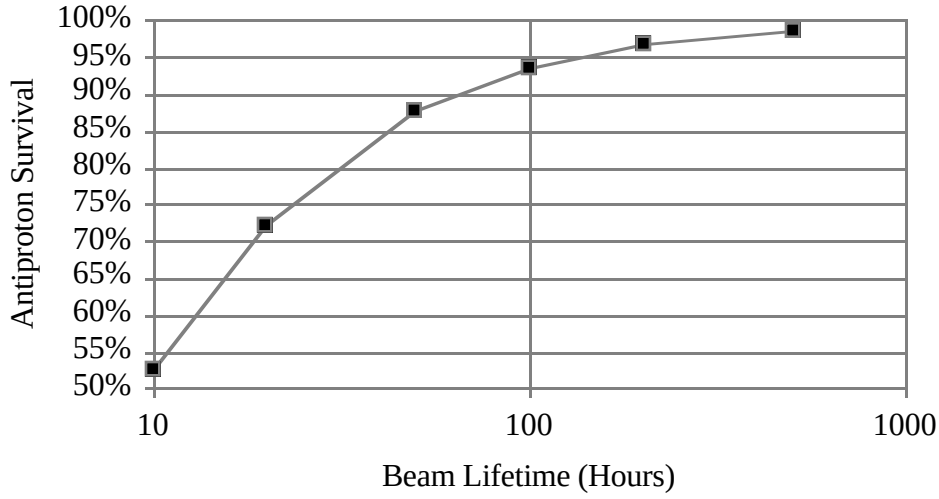

Figure 2.5.2: Fraction of the injected antiprotons (both recycled and stacked) which survive to the start of the next Tevatron Collider store.

The results of this model, for a range of beam intensity lifetimes, are displayed in figure 2.5.1. Note that using a criterion in which 95% survival is satisfactory over the 8 hours between the start of Tevatron Collider stores, it is evident that beam intensity lifetimes of 100 hours or greater are required in the Recycler. Integrating each of these curves, the percentage of recycled and stacked antiprotons available for luminosity generation in the next Tevatron Collider store can be calculated. The results of these integrations are shown in figure 2.5.2. Again, it is evident that a beam intensity lifetime of 100 hours or greater is necessary to support the antiproton storage mission of the Recycler.

2.5.2. Ion Trapping Requirement

The relativistic antiproton beam in the Recycler is composed of individual antiprotons which periodically collide with electrons circulating around residual atoms in the vacuum chamber. These electrons rebound away from the atoms with approximately 2 eV of kinetic energy [P. Zhou, Ph.D. thesis, 1993]. The momentum transfer to the ionized molecules is negligible. Because the ions are positively charged, they are attracted by the antiproton beam. In fact, because the ions are necessarily formed inside the transverse potential well of the antiproton beam, they will be trapped. Unless some mechanism is introduced to eliminate these trapped ions, the ion density will increase until it is equal to the beam density.

The rate at which the ion density increases R_i is determined by the equation [M. Reiser, "Theory and Design of Charged Particle Beams", pg. 273]

$$R_i = n_g \, n_b \, \sigma_i \, v \quad , \quad (2.5.1)$$

where n_g is the gas density, n_b is the beam density, σ_i is the ionization cross-section, and v is the beam velocity. The standard relationship between the gas density and the partial pressure P of the gas in question is

$$n_g[m^{-3}] = 3.54 \text{x} 10^{22} \; P[\text{Torr}] \quad . \quad (2.5.2)$$

The ionization cross-section depends on the velocity of the beam and the atomic properties of the gas in question. In the case of the Recycler the equation used to calculate the cross-section can be written in the approximate form

$$\sigma_i[m^2] = 1.9 \text{x} 10^{-24} \, A_1 \left\{ \text{Ln}\left(7.5 \text{x} 10^4 \, A_2 \, \gamma^2 \right) - 1 \right\} \quad , \quad (2.5.3)$$

The parameters A_1 and A_2 are molecule specific. The value of γ is 9.45 at a kinetic energy of 8.000 GeV. The results of calculations of ionization cross-section are listed in table 2.5.1.

Table 2.5.1: Values of the parameters A_1 and A_2 [M. Rudd, et. al., Rev. Mod. Phys. **57**, 965 (1985)] and the cross-sections themselves of relevant gasses in the Recycler vacuum system.

Gas	A_1	A_2	σ_i [m^2]
H_2	0.71	2.5	2.1×10^{-23}
N_2	3.8	0.52	1.0×10^{-22}
CO	3.7	0.54	1.0×10^{-22}

Assuming a peak Recycler antiproton intensity of 4×10^{12} in a circumference of 3.3 km, the peak longitudinal beam density λ_b is 1.2×10^9 antiprotons/m. The beam velocity is 3×10^8 m/s. Therefore, given assumptions justified later in this section for the vacuum partial pressures, the rate at which the longitudinal ion densities are growing can be calculated. The results of these calculations, and the estimation of the time it takes for the ion density to equal the beam density, are listed in table 2.5.2.

Table 2.5.2: Ion production rate calculations based on partial pressure predictions and an antiproton beam intensity of 4×10^{12}. The neutralization time of the beam for each gas does not assume the existence of the other gas.

Gas	Pressure [nTorr]	Gas Density [m^{-3}]	Ionization Rate [$m^{-1}\ s^{-1}$]	Neutralization Time [s]
H_2	0.1	3.5×10^{12}	2.6×10^7	46
$CO+N_2$	0.002	7.1×10^{10}	2.6×10^6	460

The average transverse rms beam size σ_r in the Recycler is 2.3 mm. Given a Gaussian transverse beam distribution and longitudinal density λ_b the beam density is described by the equation

$$n_b(r) = \frac{\lambda_b}{2\pi\,\sigma_r^2} \exp\left[-\frac{r^2}{2\sigma_r^2}\right] \quad . \qquad (2.5.4)$$

Therefore, the peak density at the beam center is 3.5×10^{13} antiprotons/m^3. If the beam has been neutralized to an ion density equal to the beam density, then using equation 2.5.2 we know that the effective peak pressure seen by the beam due to the trapped ion cloud is 3.5×10^{13} molecules/m^3, or a pressure of 1 nTorr. This calculation is an over estimate, since it ignores the fact that trapped ions can become multiply ionized, thereby neutralizing the space charge of the beam with fewer ions.

The pressure implication of the neutralized ion cloud around the antiproton beam will become evident later in the section. There are two other effects from these ions. First, a coherent instability can develop due to the electromagnetic coupling between the transverse oscillations of the antiprotons and those of the ions. Second, the ions will induce an incoherent tune spread due to the static transverse electrostatic field generated by the ion cloud.

The ion cloud has the same transverse dimensions as the beam, since the probability density of ionization has the same profile as the transverse beam density distribution. Therefore, equation 2.5.4 also describes the ion cloud density distribution. The radial electric field E_r generated by this distribution is

$$E_r(r) = \frac{e\lambda_b}{2\pi\varepsilon_o r}\left\{1 - \exp\left[-\frac{r^2}{2\sigma_r^2}\right]\right\} \quad , \quad (2.5.5)$$

where ε_o is the free space permittivity 8.854×10^{-12} F/m. The radial space charge force F_r is found by plugging equation 2.5.5 in the Lorentz equation to obtain

$$F_r(r) = \frac{e^2\lambda_b}{2\pi\varepsilon_o r}\left\{1 - \exp\left[-\frac{r^2}{2\sigma_r^2}\right]\right\} \quad . \quad (2.5.6)$$

At a radius small compared to the rms cloud radius this equation reduces to

$$F_r(r) = \frac{e^2\lambda_b}{4\pi\varepsilon_o\sigma_r^2} r \quad . \quad (2.5.7)$$

But this is the same force equation as found in either the horizontal or vertical plane of a quadrupole magnet. Converting this result into the form of a quadrupole gradient error ΔK yields the result

$$\Delta K = \frac{e^2\lambda_b}{4\pi\varepsilon_o\sigma_r^2}\frac{1}{P_o v} = \frac{r_o\lambda_b}{\left(\gamma\beta^2\right)\sigma_r^2} \quad , \quad (2.5.8)$$

where P_o is the antiproton beam momentum, r_o is the classical radius of the proton 1.53×10^{-18} m, and the quantities γ and β are the relativistic beam energy and velocity respectively (with the respective values of 9.45 and 0.9945). Plugging in all of the number expressed so far for the factors in the rhs form of equation 2.5.8 yields a space charge gradient of 3.7×10^{-5} m^{-2}.

The tune shift $\Delta\nu$ due to this gradient error is expressed as

$$\Delta\nu = \frac{1}{4\pi}\oint \beta(s)\Delta K\, ds \quad , \quad (2.5.9)$$

where the integral is evaluated around the circumference of the ring. Assuming a constant average beta function β_{ave} around the ring of 30 m, substituting equation 2.5.8 into equation 2.5.9 yields the result

$$\Delta\nu = \frac{r_o \lambda_b}{\left(\gamma\beta^2\right)\sigma_r^2}\frac{\beta_{ave} C}{4\pi} = \frac{3 r_o \lambda_b C}{2\pi\beta\,\varepsilon_N} \quad , \quad (2.5.10)$$

where C is the circumference of the ring and ε_N is the normalized 95% emittance. The value of the peak tune shift at the antiproton beam intensity of $4x10^{12}$ and full neutralization is 0.29, a value which is approximately two orders of magnitude too large for a stored beam. Therefore, it is imperative to employ methods for eliminating ions from the beam.

Three methods are planned for the Recycler. The first is the use of a coherent transverse beam closed orbit oscillation at the resonant frequency of the ion oscillation about the beam centroid. The transverse dampers installed in the Recycler to combat coherent instabilities are planned to have electronics capable of exciting this closed orbit oscillation, just as in the Accumulator. The second is to maintain a gap in the longitudinal beam distribution to destabilize the ions. This requires the constant use of a set of barrier bucket pulses to maintain an empty section of beam azimuth. The third is to employ clearing electrodes to sweep away ions from the beam potential well. In the Recycler there are two beam position monitors in each half cell which will be used as clearing electrodes.

2.5.3. Ion Clearing with a Longitudinal Gap in the Beam

Maintaining a gap in the beam distribution destabilizes low mass ions due to the fact that the time periodicity of the instantaneous beam current has the same effect on the ions as if the ions were circulating in a circular accelerator experiencing a comparable lattice. Assume that the beam is not neutralized, and that the ions have thermal kinetic energies. Then only the electric field from the beam has a significant impact on the ion motion. Equation 2.5.7 describes the radial force due to electric field of the antiproton beam. Since this force is attractive, an ion of mass M undergoes a radial oscillation about the beam centroid described by the differential equation

$$\ddot{z} + \frac{e^2 \lambda_b}{4\pi\,\varepsilon_o\,\sigma_r^2\,M} z = 0 \quad . \quad (2.5.10)$$

Let ω_i be the ion angular frequency indicated in this harmonic oscillator equation. At the antiproton intensity of $4x10^{12}$ molecular hydrogen H_2 has a ion angular frequency of $4x10^6$ rad/s. At this rate the small amplitude H_2 ion undergoes 7.13 transverse oscillations for every one antiproton revolution around the Recycler. If T_b is the length of the beam distribution and T_g is the length of the gap, then the matrix equation describing the one-turn map of the ion coordinates (z,v) is

$$\begin{pmatrix} z \\ v \end{pmatrix}_{n+1} = \begin{pmatrix} \cos(\omega_i T_b) & \frac{1}{\omega_i}\sin(\omega_i T_b) \\ -\omega_i \sin(\omega_i T_b) & \cos(\omega_i T_b) \end{pmatrix} \begin{pmatrix} 1 & T_g \\ 0 & 1 \end{pmatrix} \begin{pmatrix} z \\ v \end{pmatrix}_n \quad . \quad (2.5.11)$$

The stability of the ions is determined by the condition that the trace of the one-turn matrix

$$\begin{pmatrix} \cos(\omega_i T_b) & T_g \cos(\omega_i T_b) + \frac{1}{\omega_i}\sin(\omega_i T_b) \\ -\omega_i \sin(\omega_i T_b) & \cos(\omega_i T_b) - \omega_i T_g \sin(\omega_i T_b) \end{pmatrix} \qquad (2.5.12)$$

be

$$\left|\cos(\omega_i T_b) - \tfrac{1}{2}\omega_i T_g \sin(\omega_i T_b)\right| \le 1 \quad . \qquad (2.5.13)$$

Let $A = \omega_i T_g/2$ and $\phi = \omega_i T_b$. The magnitude of this equation for various choices of A over the full 2π range of ϕ is shown in figure 2.5.3. Note that the ion motion is unstable when the curve is greater than unity. Since ϕ depends critically on the precise beam intensity, it is very hard to control accurately enough to always guarantee that the it is in a region of instability. On the other hand, for values of A of approximately 5 or greater, the ion is generally unstable independent on the detailed beam intensity.

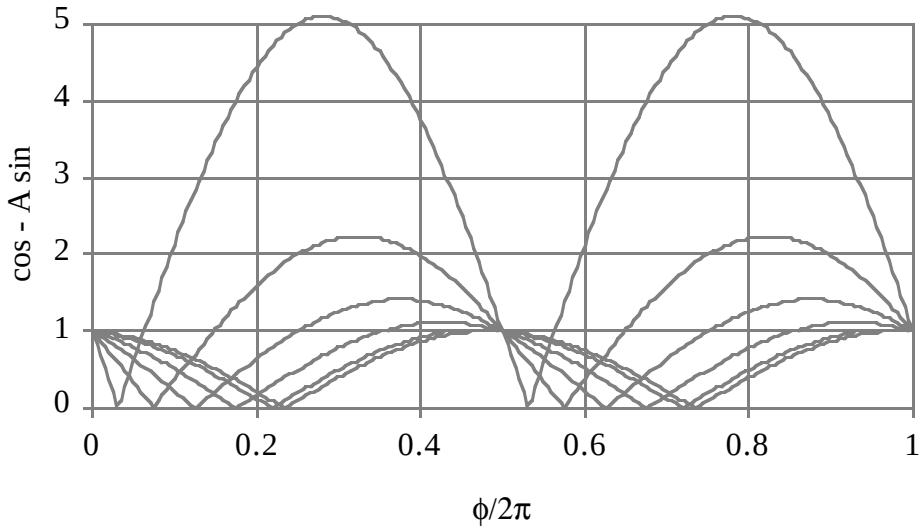

Figure 2.5.3: Map of equation 2.5.13 for various choices of the defined parameter A over the full 2π range of ϕ. The values for A are 5 (top), 2, 1, 0.5, 0.2, and 0.1 (bottom).

For the case again of molecular hydrogen H_2, the value of A for a 2 μsec long ion clearing gap is 5. For the minimum operational current when only the recycled beam is in the accelerator A drops to 2 for the same size clearing gap. As will be seen in the sections on intrabeam scattering and stochastic cooling, it is desirable to compress the beam longitudinally as much as possible, to at most half of the Recycler circumference. Under these conditions with only recycled antiprotons the factor A is again greater than 11. For stacking from an empty Recycler, assuming transfers of intensities greater than or equal to 2x1011 antiprotons, if the 1.6 μsec beam pulse length from the Accumulator is maintained with barrier buckets the minimum value for A is greater than 6. On the other

hand, with an atomic number of 28, either CO or N_2 are almost always expected to be stable in the presence of the ion clearing gap.

For unstable ions the growth rate of their oscillation amplitudes about the beam is

$$\tau = \frac{T_o}{\cosh^{-1}\left(\left|\cos(\omega_i T_b) - \frac{1}{2}\omega_i T_g \sin(\omega_i T_b)\right|\right)} \quad , \quad (2.5.14)$$

where T_o is the revolution period of the antiprotons in the Recycler. For values of A and f where the beam motion is unstable the value of the growth rate is calculated and plotted in figure 2.5.4. Note that the for most of the phase space the growth time is approximately equal to the revolution period.

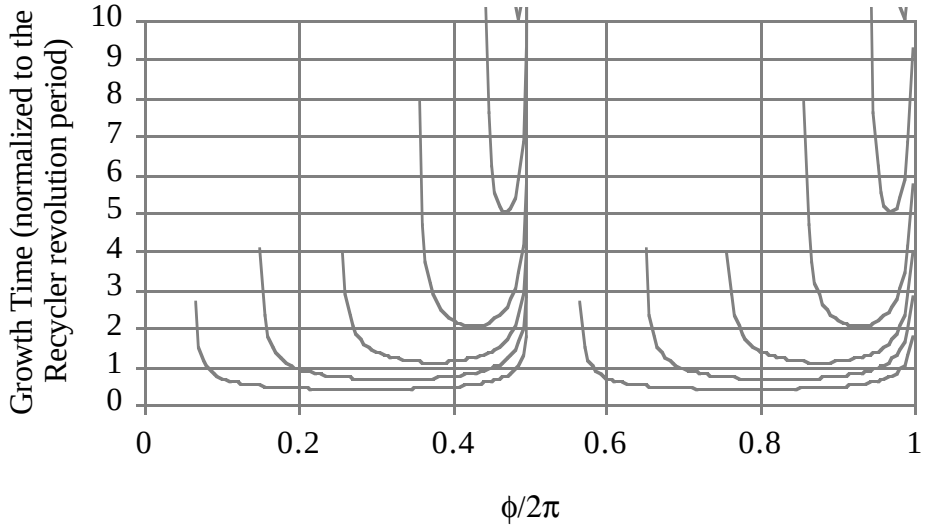

Figure 2.5.4: Map of equation 2.5.14 when the beam motion is unstable. The values for A are 5 (bottom), 2, 1, 0.5, 0.2, and 0.1 (top).

If it is assumed that the ion amplitude growth time is also the characteristic time it takes for the ion to be cleared from the beam, then the equilibrium ion longitudinal density λ_i is described by the equation

$$\lambda_i = R_i \tau \quad . \quad (2.5.15)$$

For the case of $\tau=T_o$ and the value of R_i for H_2 listed in table 2.5.2, the equilibrium ion longitudinal density is 291 H_2 ions/m! It should be pointed out that larger amplitude ions see a net field which is different from that assumed in the above linearized theory. In the cases of marginal growth linearized growth rates the net reduction in focusing experienced by the ions may slow down or even halt their escape from the beam.

2.5.4. Ion Clearing with Clearing Electrodes

In the case of H_2 where ϕ and A do not lead to unstable oscillations around the antiproton beam, and for the case of CO and N_2 in general, another method of ion clearing is required. This is the purpose of the clearing electrodes. A pair of clearing electrodes on opposite sides of the vacuum chamber with opposite voltage generate a transverse electric field. When that electric field is greater than the maximum radial electric field generated by the beam, any ions between the electrodes are stripped away from the beam.

The electric field generated by the beam is described by equation 2.5.5. Taking the derivative of the electric field with respect to radius and setting the result equal to zero, the radius at which the electric field is maximum is calculated to be

$$r_{max} = 1.585\,\sigma_r \quad . \quad (2.5.16)$$

Substituting this result into the electric field equation yields the result

$$E_{max} = \frac{0.45 e\,\lambda_b}{2\pi\varepsilon_o\,\sigma_r} \quad . \quad (2.5.17)$$

With an antiproton intensity of $4x10^{12}$ in the Recycler, the maximum radial electric field is found to be 675 V/m. The largest effective separation d of the clearing electrodes across the vacuum chamber is 9.5 cm. The minimum voltage across the electrodes is related to this separation and the maximum radial electric field according to

$$V_{min} = E_{max}\,d \quad . \quad (2.5.18)$$

Plugging in the above number, the minimum voltage per electrode is approximately 32 V.

The ions are traveling with kinetic energies determined by their temperature, which is equal to room temperature 300°K. Table 2.5.3 contains a summary of the ion velocities, and for future reference when ion propagation in the gradient magnets are discussed their cyclotron orbit in a 1.5 kG magnetic field.

Table 2.5.3: RMS thermal ion velocity and rms cyclotron orbit radius as a function of gas species assuming room temperature. The cyclotron orbit radius assumes the 1.5 kG magnetic field in the Recycler gradient magnets. The overvoltage is the amount of additional voltage required to accelerate an rms ion into the negative electrode, thereby eliminating the ion from the beam.

Gas	Atomic Mass	rms Velocity [m/s]	rms Cyclotron Radius [mm]	Overvoltage [V]
H_2	2	1113	0.15	0.0013
$CO+N_2$	28	297	0.58	0.0013

In order to assure that the ions leave the beam while they ballistically traverse the clearing electrodes, an additional accelerating voltage greater than the above 32 V is

necessary. The electrodes are 1' long. Assume that a particle traveling at the rms velocity straight down the center of the vacuum chamber must be deflected enough to strike the negative electrode. The additional voltage required per electrode for each species of gas to perform this task is listed in the right most column of table 2.5.3. It is truly negligible.

Table 2.5.4: Mean free path calculation assuming the effective molecular diameter to be $2x10^{-10}$ m. The point of this calculation is to verify that the ion motion in the beam is ballistic in nature, since the mean free path is much longer than the vacuum chamber and the distance between clearing electrodes.

Gas	Pressure [nTorr]	Gas Density [m^{-3}]	Mean Free Path [m]
H_2	0.1	$3.5x10^{12}$	$2.3x10^{6}$
$CO+N_2$	0.002	$7.1x10^{10}$	$1.1x10^{8}$

As shown in table 2.5.4, the motion of ions is not significantly affected by other ions in the range of pressure that is found in the Recycler vacuum system. Therefore, it is not unreasonable to assume that a molecule ionized in the beam will travel unmolested longitudinally with an rms speed listed in table 2.5.3. This geometry, with the approximate relative geometry between two clearing stations in a Recycler half cell, is shown in figure 2.5.5.

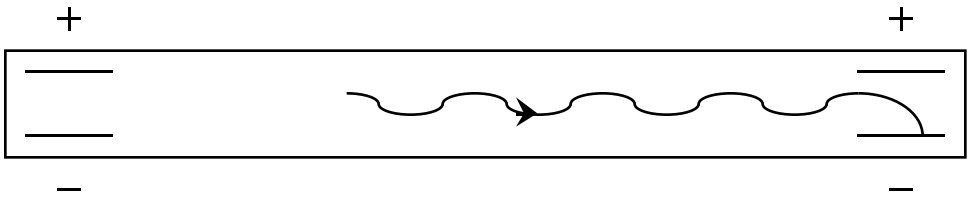

Figure 2.5.5: Sketch of an ionized molecule with an initial longitudinal velocity in a geometry very similar to that inside a Recycler half cell.

The clearing electrodes act as a black hole, eliminating every ion that traverses them. If the distance between the clearing electrodes is L_{ce}, and the rms velocity of an ion is σ_v, then the average time τ it takes an ion heading toward a particular electrode to be eliminated from the beam is

$$\tau = \frac{L_{ce}}{\sigma_v} \quad . \quad (2.5.19)$$

Plugging this result into equation 2.5.15 yields an estimate of the equilibrium average trapped ion density between the clearing electrodes. Using previously present values for the relevant parameters, the calculations this average ion density for each gas species is listed in table 2.5.5. The worst case density is 10,000x lower than expected at neutralization.

Table 2.5.5: Calculation of the equilibrium ion longitudinal density assuming a distance between clearing stations of 6 m.

Gas	Clearing Time [ms]	Ion Density [m^{-1}]
H_2	5.3	$1.4x10^5$
$CO+N_2$	20	$5.2x10^4$

The Recycler vacuum system also has gradient magnets. When a gas molecule is ionized inside the magnet, the ions do not simply propagate out at their thermal velocities. As shown in table 2.5.3, the ions execute very tight horizontal cyclotron oscillations around the magnetic field lines. If these magnets were pure dipoles, the only mechanism for ion transport to the clearing electrodes would have been ExB drift generated by the space charge radial electric field of the beam. At the radial field maximum of 675 V/m, for a relatively improbable ion more than a sigma away from the beam center, the drift velocity is 675 / 0.15= 4500 m/s. But the small amplitude ions see an order of magnitude smaller electric field, and for the case of low beam intensity the electric field is yet again another order of magnitude smaller. On the other hand, that still leaves a factor of 100x lower density than expected if the beam were completely neutralized. But this is the factor of 100x that was needed to reduce the tune spread effects of the ion cloud to manageable levels.

In addition, the gradient portion of the Recycler bend magnets introduce ∇B drift. As an ion executes horizontal cyclotron orbits, the gradient in the dipole field causes these orbits to have a horizontal position dependent radius of curvature. This causes the particle to drift longitudinally. The drift velocity v_d depends on the cyclotron radius r_c, the field gradient g, and the cyclotron frequency f_c according to the equation

$$v_d = \pi f_c \, g \, r_c^2 \quad . \quad (2.5.20)$$

Table 2.5.6 contains the results of this calculation for the gas species of interest. The gradient for the normal cell Recycler gradient magnets is 2.5 m^{-1}. Note that compared to the neutralizing ion density of $1.2x10^9$ m^{-1}, the H_2 density in the magnet is almost unaffected whereas the $CO+N_2$ density is a factor of 20x below neutralization. Taking into account the fact that the gradient magnets make up approximately half of the ring, this indicates that with clearing electrodes only that $CO+N_2$ neutralization can be avoided. The combination of a gap and electrodes seems to be needed for H_2.

Table 2.5.6: Calculation of the equilibrium ion longitudinal density in a gradient magnet assuming ∇B drift as the mechanism for trapped ion loss. The expected average equilibrium ion densities in the magnets are also calculated.

Gas	Cyclotron Freq. [MHz]	Drift Speed [m/s]	Magnet Ion Density [m^{-1}]
H_2	1.1	0.19	$5.2x10^8$
$CO+N_2$	0.082	0.22	$5.2x10^7$

2.5.5 Vacuum Specification

The beam tube vacuum pressure requirement is determined by antiproton intensity lifetime, antiproton emittance growth, and ion trapping considerations. The emittance growth rates should be small compared to the anticipated intrabeam scattering growth rates. The intensity lifetime should be long enough insure that the stacking rate necessary to achieve the required antiproton intensity is not increased by more than a few percent. Because vacuum pressures always improve with time, the specification quoted in this section will apply to the initial pressure needed for reasonable operations.

The transverse normalized 95% emittance growth rate is determined by multiple Coulomb scattering with the nuclei of the residual gas in the beam tube. Assuming a relativistic beam, the equation describing this growth rate can be written as

$$\dot{\varepsilon}_n = \frac{3\langle\beta\rangle}{\gamma_r}\left(\frac{15\,\mathrm{MeV}}{mc^2}\right)^2 \frac{c}{L_{rad}} \quad , \quad (2.5.21)$$

where $<\beta>$ is the average beta function of the accelerator, γ_r is the relativistic energy of the beam, and L_{rad} is the radiation length of the gas at a given temperature and pressure. Radiation length values at standard temperature (0 °C) and pressure (760 Torr) are listed in table 2.5.7.

Table 2.5.7: Radiation lengths for the two constituent molecules commonly found in a high vacuum stainless steel system such as that expected for the Recycler ring.

Gas	Radiation Length (g/cm^2)	Density @STP (g/l)	Radiation Length (m)
H_2	61	0.090	6800
$CO+N_2$	38	1.25	300

Table 2.5.8: Normalized 95% emittance growth rate for each component gas in a high vacuum system assuming a total pressure of approximately 1 nTorr and a standard ratio of 5:1 between hydrogen and nitrogen/carbon monoxide.

Gas	Partial Pressure (nTorr)	Radiation Length (m)	Emittance Growth Rate (π mmmr/hr)	Emittance Growth Time (hrs)
H_2	0.1	5.2×10^{16}	0.05	200
$CO+N_2$	0.002	6.0×10^{15}	0.05	200

Assuming an average beta function value of 30 m and a kinetic energy of 8 GeV, the emittance growth rates for the same constituent vacuum gasses are listed in table 2.5.8. Note that the measured and expected ratio of hydrogen to nitrogen/carbon monoxide is set at 50:1. As will be shown later, these pressures are the result of measured outgassing

rates and calculated pumping speeds. In order to calculate an emittance growth time, a base emittance of 10 π mmmr is assumed.

The stochastic cooling system is anticipated to have an emittance cooling time of approximately 4 hours. From table 2.5.8 it is can be shown that maintaining an average $CO+N_2$ partial pressure of less than 0.1 nTorr is necessary for Recycler operations.

Table 2.5.9: Nuclear interaction lengths for the two constituent molecules commonly found in a high vacuum stainless steel system.

Gas	Nuclear Int. Length (g/cm^2)	Density @STP (g/l)	Nuclear Interaction Length (m)
H_2	51	0.090	5700
$CO+N_2$	88	1.25	704

Table 2.5.10: Intensity lifetime due to nuclear interactions with each component gas in a high vacuum system.

Gas	Partial Pressure (nTorr)	Nuclear Interaction Length (m)	Antiproton Loss Time (hrs)	Antiproton Loss Rate (10^{10}/hrs)
H_2	0.1	4.3×10^{16}	40,000	0.0063
$CO+N_2$	0.002	1.4×10^{17}	250,000	0.0010

The other consideration is particle lifetime. The two mechanisms which remove particles from the ring are nuclear interactions and large angle Coulomb scattering (Rutherford scattering). Nuclear interactions are typically broken down between elastic and inelastic scattering. Though a portion of the elastically scattered particles would stay in the accelerator, it is easier to take the worst case assumption that they are all lost. In that case the total cross-sections, characterized as a nuclear interaction length, is used. Table 2.5.9 contains the nuclear interaction lengths for the expected constituent gasses in the vacuum tube. In table 2.5.10 the lifetime and particle loss rates are calculated using a base intensity of 250×10^{10} antiprotons in the Recycler.

Single large angle Coulomb scattering angles greater than the angular acceptance of the Recycler occur with a frequency described by the equation

$$\sigma_{el} = \frac{2\pi r_p^2 Z^2}{\gamma_r^2} \frac{\beta_y}{A_y} \quad . \quad (2.5.22)$$

The lifetime associated with this cross-section is

$$\tau_{el} = \frac{1}{n_{gas} \sigma_{el} \beta c} \quad , \quad (2.5.23)$$

and $r_p = 1.535 \times 10^{-18}$ m. The results of these calculations are listed in table 2.5.11.

Table 2.5.11: Intensity lifetime due to large angle Coulomb scattering.

Gas	Partial Pressure (nTorr)	Cross-Section (mbarns)	Antiproton Loss Time (hrs)	Antiproton Loss Rate (10^{10}/hrs)
H_2	0.1	17	30,000	0.008
$CO+N_2$	0.002	870	30,000	0.008

In conclusion, even though its partial pressure is lower than the hydrogen, the $CO+N_2$ is comparable in both the particle loss and the emittance growth rate. A partial pressure less than $1x10^{-10}$ Torr is desirable for those species.

2.5.6. Outgassing of Stainless Steel

The spacing and pumping speed of the lumped ion-sputter and titanium sublimation pumps in a traditional Fermilab system is determined by the outgassing rate of gas molecules from the surface of the stainless steel vacuum tube. Because the cost of the vacuum system scales with the number of pumps, minimizing this outgassing rate is very desirable.

Upon chemically cleaning a stainless steel tube and performing a 150°C bake after system assembly, a hydrogen surface outgassing rate of $1x10^{-12}$ T-l/cm^2-sec is achievable. At this point the only other gas in the system is $CO+N_2$, which comes dominantly from the ion pumps and ion gauges. The hydrogen comes from diffusion of molecules out of the bulk of the stainless steel material. The key to reducing the cost of the Recycler vacuum system is to eliminate this bulk hydrogen.

High concentrations of hydrogen exist in stainless steel because of one step in it's production, when the steel is quenched in a hydrogen atmosphere. It has been found [R. Calder and G. Lewin, Brit. J. Appl. Phys. **18**, 1459 (1967)] that the hydrogen can be removed by heating the stainless steel in a good vacuum ($<10^{-6}$ Torr) at a temperature of approximately 500°C. Using this technique, measurement results at Fermilab with a 30 m test vacuum system have found surface outgassing rates of $2x10^{-13}$ T-l/cm^2-sec, even though it turns out that the ultimate pressure during the bake was only 10^{-3} Torr and multiple vacuum accidents during studies. More details concerning the hydrogen degassing oven and its operation can be found in chapter 3.

The calculation of time and temperature vs. hydrogen degassing of stainless steel is rather straightforward. Assume that an infinite slab of stainless steel of thickness d is placed in a perfect vacuum and heated to some temperature T. The one dimensional diffusion equation describing this situation is

$$D\frac{\partial^2 c}{\partial x^2} = \frac{\partial c}{\partial t} \quad . \quad (2.5.25)$$

The diffusion coefficient D as a function of some typical outgassing temperatures is plotted in figure 2.5.6. The initial condition is that the stainless steel is uniformly saturated with hydrogen at some initial concentration c_o. As compared to an atmospheric hydrogen concentration of $1.4x10^{-4}$ T-l/cm^3, the initial concentration found in 300 series

austentic stainless steels is 0.3 T-l/cm^3. Outside of the slab it is assumed that a perfect vacuum exists. The solution of the differential equation with these boundary conditions can be written in terms of an infinite sum

$$c(x,t) = c_o \frac{4}{\pi} \sum_{n=0}^{\infty} \frac{1}{(2n+1)} \sin \frac{\pi(2n+1)x}{d} \exp\left[-\left(\frac{\pi(2n+1)}{d} \right)^2 D t \right] \quad . \quad (2.5.26)$$

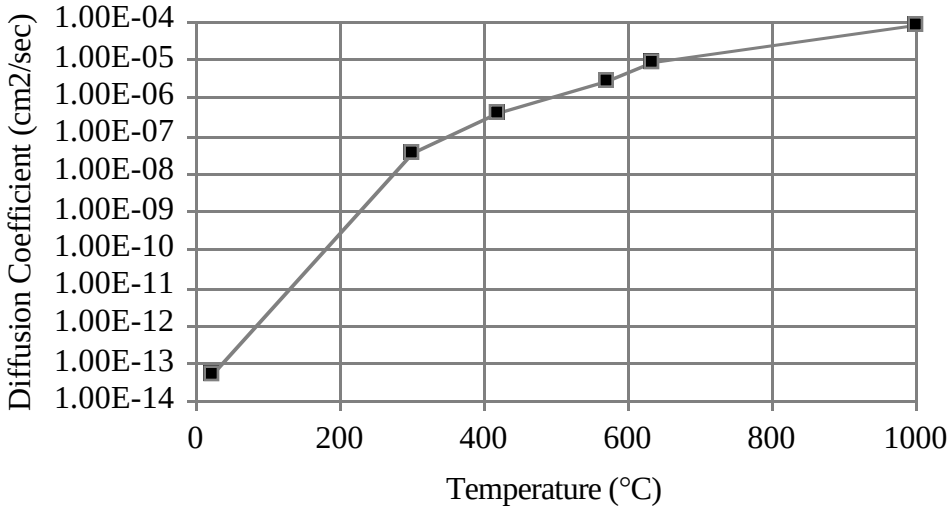

Figure 2.5.6: Hydrogen diffusion rate as a function of temperature in stainless steel. The data points are at typical degassing temperatures. The lines are for the purpose of interpolation.

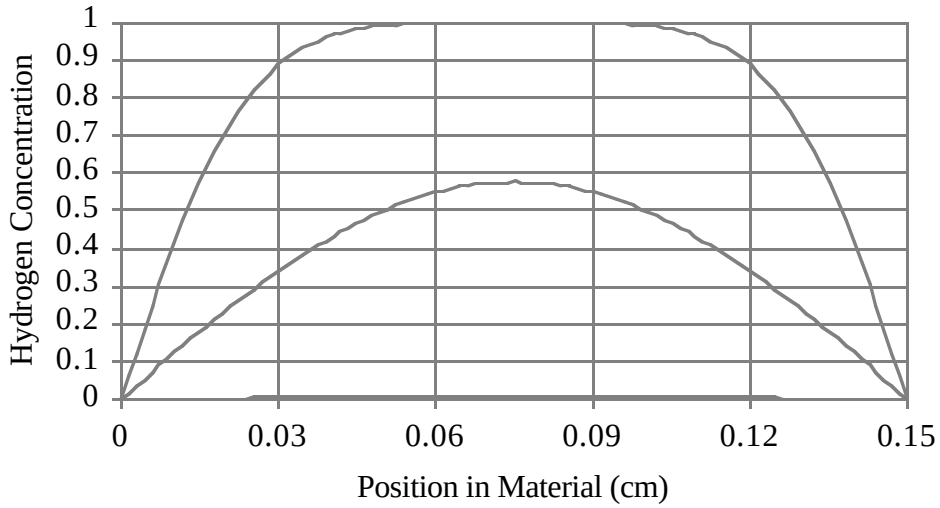

Figure 2.5.7: Hydrogen concentration profile across the beam tube wall as a function of time at 500°C. In the beginning the concentration is uniform and scaled to unity. The curves show the concentration profiles after 60 sec, 10 minutes, and 1 hour. After 3 hours the concentration is 1×10^{-7}.

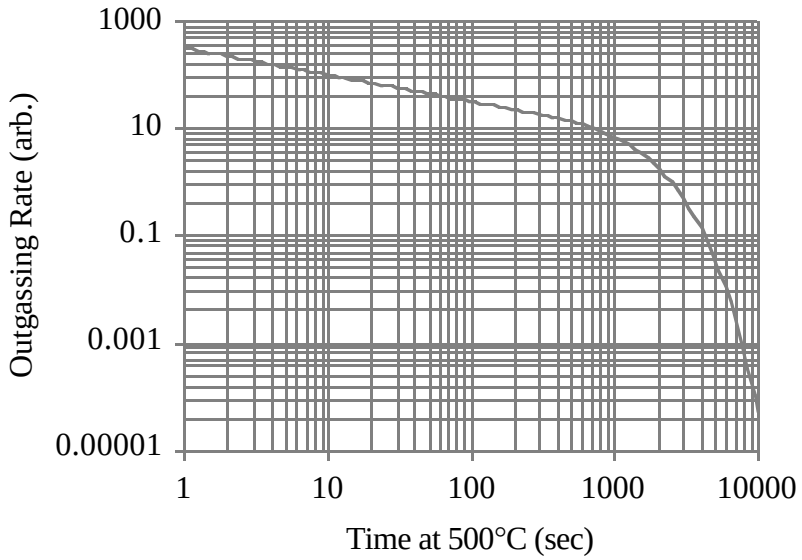

Figure 2.5.8: Hydrogen outgassing rate after cooldown as a function of the time spent at 500°C for degassing.

For the case of Recycler vacuum chamber, using a diffusion coefficient of 1×10^{-6} cm^2/sec (500°C) and a thickness d of 0.065" (approximately 1.5 mm), the concentration profile through the vacuum tube wall as a function of position in the wall and time at temperature is plotted in figure 2.5.7.

The surface outgassing rate σ_q of hydrogen from either surface is simply the derivative of the hydrogen concentration at the surface times the diffusion coefficient

$$\sigma_q(t) = D\left(\frac{\partial c}{\partial x}\right)_{x=0} = \frac{4c_o D}{d}\sum_{n=0}^{\infty}\exp\left[-\left(\frac{\pi(2n+1)}{d}\right)^2 D t\right] \quad . \quad (2.5.27)$$

Figure 2.5.8 contains a plot of the surface outgassing rate after cooldown as a function of time the vacuum tube was degassed at 500°C. The plan is to bake the tubes at 500°C for 6 hours with an oven pressure less than 1×10^{-6} Torr to guarantee full degassing.

2.5.7. Pressure Calculations

The pressure P(z) at some azimuth z around the ring is calculated using the differential equation

$$c\frac{d^2P}{dz^2} - s\,P = -q \quad , \quad (2.5.28)$$

where c(z) is the specific conductance of the vacuum tube, s(z) is the linear pumping speed, and q(z) is the specific outgassing rate. If these coefficients of the differential equation are piecewise constant, then the solution in any section of vacuum tube is

$$P(z) = A\exp\left[\sqrt{\frac{s}{c}}\,z\right] + B\exp\left[-\sqrt{\frac{s}{c}}\,z\right] + \frac{q}{s} \qquad . \quad (2.5.29)$$

Just as in the case of dispersion function lattice calculations, this solution lends itself to matrix calculations on the basis vector (P,Q,1), where Q(z) is the flow rate of gas down the tube at the azimuth z.

In a lumped stainless steel system the pumps and beam tubes are treated as separable (similar to the concept of separated function magnets). Therefore, in a vacuum tube the pumping speed is zero. The specific conductance of the elliptical cross-section beam tube can be written as

$$c[m-l/s] = 1.30\frac{(a[cm]\,b[cm])^2}{\sqrt{a^2+b^2}}\sqrt{\left(\frac{T[^\circ K]}{300}\right)\left(\frac{28}{M}\right)} \qquad , \quad (2.5.30)$$

where a and b are the half width and half height of the inside surface of the vacuum tube, T is the temperature of the system, and M is the atomic mass of the gas molecules (the equation is referenced to room temperature and the atomic mass of nitrogen).

Table 2.5.12: Parameters expected to describe the vacuum system in the Recycler ring. This spacing corresponds to three 30 liter/sec pump (either ion or titanium sublimation) per half cell, where the pumping speed (assuming ion pumps) was derated to account for saturation and low pressures at the pump.

Parameter	H_2	CO/N_2
Lumped Pump Pumping Speed (L/s)	30	10
Surface Outgassing Rate (T-L/s-cm^2)	2×10^{-13}	1×10^{-15}
Distance between Lumped Pumps (m)	5.75	5.75
Total Width of Elliptical Pipe (inch)	3.75	3.75
Total Height of Elliptical Pipe (inch)	1.75	1.75
Molecular Mass of the Gas	2	28
Specific Conductance (m-L/s)	100	28
Specific Outgassing Rate (T-L/s-m)	4.4×10^{-10}	2.2×10^{-12}
Pressure at Lumped Pumps (nTorr)	0.084	0.0013
Pressure Halfway between Pumps (nTorr)	0.100	0.0016
Average Pressure (nTorr)	0.096	0.015

To convert from the surface outgassing rate σ_q to the specific outgassing rate q it is necessary to multiply σ_q by the surface area per unit length. For an elliptical beam pipe

$$q[T-l/s-m] = 100\pi\sqrt{2(a[cm]^2+b[cm]^2)}\;\sigma_q[T-l/s-cm^2] \qquad . \quad (2.5.31)$$

Table 2.5.12 contains an example of typical parameter values used for calculating the Recycler vacuum performance. The ion pumps to be used are 30 liter/sec pumps, but the actual pumping speeds are derated because of the low pressures and assuming that the

pumps are nitrogen saturated during pumpdown. The majority of the pumps are of the titanium sublimation variety, which have much lower ultimate pressure and much higher typical pumping speeds. The present titanium sublimation pumps are also planned to have a speed of 30 liter/sec. Figures 2.5.9 and 2.5.10 show the dependence of pressure on position in the beam tube. Note that the average pressures described are much lower than assumed in the lifetime discussions above.

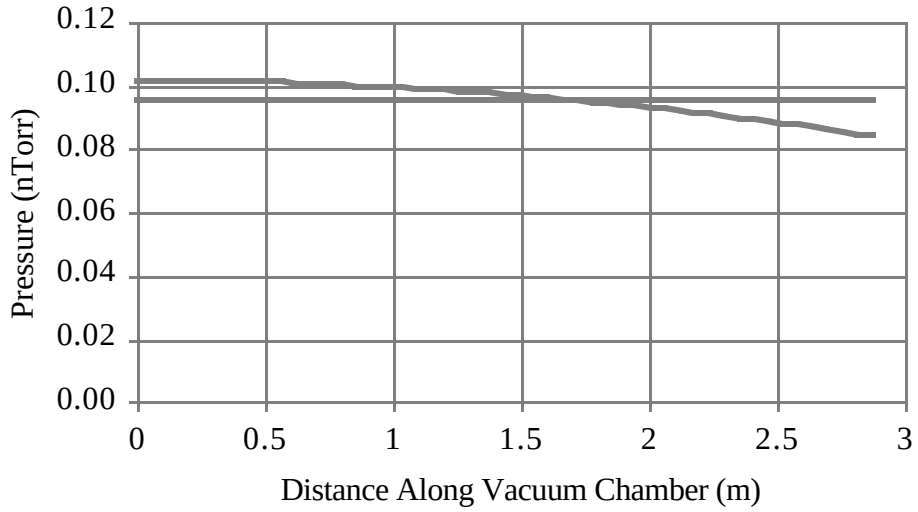

Figure 2.5.9: Hydrogen partial pressure as a function of distance along the vacuum tube. The origin is the symmetry point halfway between any two pumps. The parameters which generated this figure are listed in table 2.5.12. The horizontal line designates the average pressure.

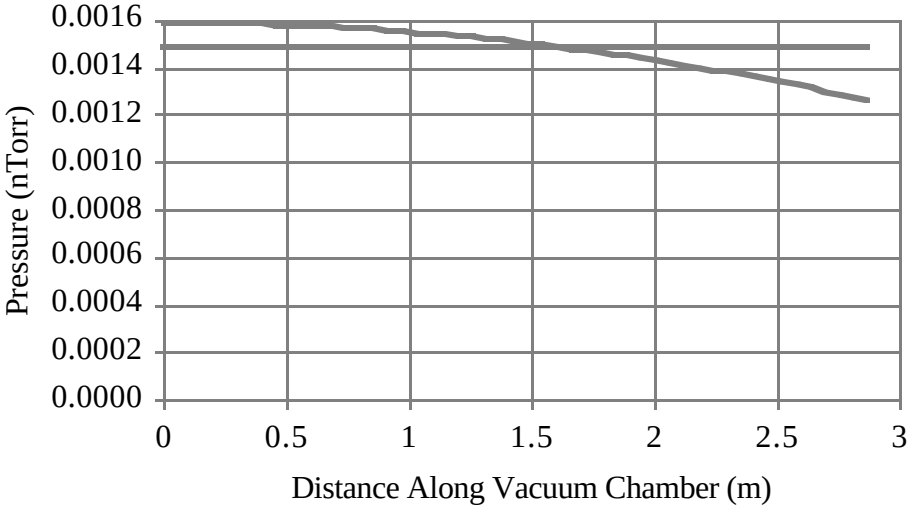

Figure 2.5.10: $CO+N_2$ partial pressure as a function of distance along the vacuum tube. The origin is the symmetry point halfway between any two pumps. The parameters which generated this figure are listed in table 2.5.12. The horizontal line designates the average pressure.

2.5.8. Magnetic Shielding

There are many sources of time-dependent magnetic fields which if left unshielded would modulate the closed orbit position and tune of the Recycler beam. Therefore, it has been decided to generate a hermetic seal of magnetic shielding around the Recycler vacuum chamber. In order to save money the insitu bake insulation and the magnetic shielding have been merged into the same effort. Because of this link to the insitu insulation, and because of the need to integrate the shielding with the vacuum fabrication, magnetic shielding is one of the responsibilities of the vacuum Recycler group. A sketch of the geometry of the magnetic shielding and insitu bake insulation is displayed in figure 2.5.11. The regions of vacuum chamber occupied by magnets do not require shielding due to the thick flux return they employ.

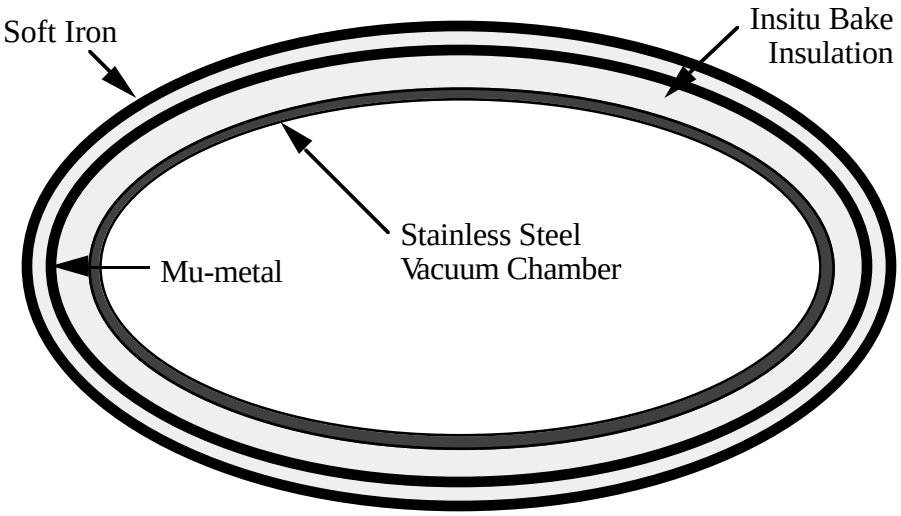

Figure 2.5.11: Sketch of the integrated magnetic shielding and insitu bake insulation for the Recycler ring.

.

The dominant sources of stray time-dependent magnetic fields at the Recycler tunnel position are:

1) Main Injector magnet fringe fields. These have been measured to be no more than 2 Gauss at the Recycler position [A. Mokhtarani & P. Mantsch, MTF-94-0052 (1994)].
2) Main Injector magnet bus bypasses. By calculating the dipole field generated by a pair of busses near the wall at the Main Injector elevation, a maximum field of 2 Gauss is calculated.
3) Uncompensated quadrupole loop current. The focusing and defocusing quadrupole circuits are each single loops around the tunnel. Therefore, the net current difference between these loops will generate a net magnetic flux through the wetland inside the Main Injector. More important, it would generate approximately 4 Gauss at the Recycler beam pipe.

4) High current cables in trays. One example would be Lambertson cables. Estimates generate fields as high as 5 Gauss.

In order to firm up these estimates and to identify any unanticipated source of field, a flux measurement experiment is being designed for the Main Ring tunnel at the comparable elevation of the Recycler. Another purpose of this test is to measure the actual field attenuation one obtains from magnetic shielding. There is some doubt as the validity of more detailed calculations of magnetic shields in the milliGauss field range. It is because of these doubts that only semi-quantitative calculations are presented below.

A system capable of shielding the beam to an extent comparable to the dipole field strength criterion is necessary. The fields in the gradient magnets is specified to have a maximum allowable error of $5x10^{-4}$ in a field of 1.5 kG. This corresponds to approximately 1 Gauss over roughly 4 m. In order to assure that systematic or random effects from the time dependent fields are negligible, especially in alignment sensitive regions such as the stochastic cooling pickups, a stray field goal at the Recycler beam of 10 mG has been specified.

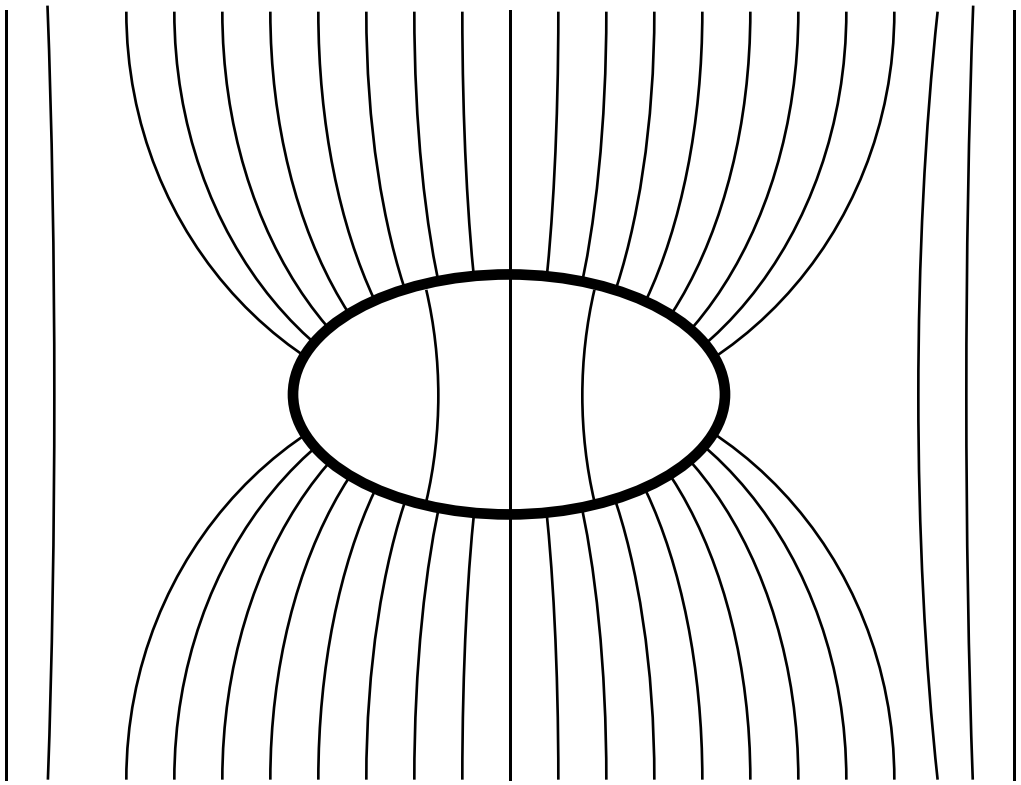

Figure 2.5.12: Sketch of magnetic field lines from the tunnel being drawn into the soft iron shield around the beam pipe. Note that due to the finite permeability of the iron, approximately 0.1% of the flux continues through to the beam.

When a layer of soft iron is wrapped around an otherwise non-ferric material such as the beam pipe, the higher permeability of the iron pulls magnetic flux lines from an area

approximately double the width of the iron geometry. In the case of the Recycler, this covers an area almost 8" across. The plan is to use a layer of soft iron which is 6 mils thick. Therefore, the peak magnetic field in the soft iron is approximately 670 times larger than the ambient field. Since the saturation field of the soft iron is 20 kG, this puts an upper limit on the magnetic field at the Recycler of 30 Gauss. This is 5-10 times higher than anticipated. In specific locations in which there are known or discovered high magnetic field generating devices, extra shielding can be added to prevent the soft iron from going into saturation.

The problem with the above solution is that even when not in saturation, the soft iron has a finite permeability of approximately 3000-5000. Therefore, some fraction of the ambient tunnel magnetic flux still penetrates to the beam. For time-dependent fields the maximum level of attenuation is approximately 1000x. It is for this reason that mu-metal is inserted as an addition layer between the beam pipe and the soft iron.

The disadvantage of mu-metal is that it's saturation level is on 8 kG. On the other hand, it's permeability is in the range of 12,000-400,000. At fields up to 3 kG and frequencies up to 60 Hz, field attenuation factors of 100,000x are achievable [Amuneal Manufacturing Corp., "Complete Guide to Magnetic Shielding"]. The plan for the Recycler is to use a mu-metal layer which is 4 mil thick. Over basically the same area, the maximum residual field inside the soft iron which the mu-metal can shield is 2 Gauss. By design, this field matches the leakage expected through the soft iron just as it begins to seriously saturate.

The power spectrum of the magnetic fields in the tunnel below 60 Hz should be dominated by 0.5 Hz from the basic Main Injector ramp plus the first 10-100 harmonics needed to reproduce the more complex, non-sinusoidal current waveforms found in most correctors, busses, and specialty devices (such as Lambertsons). At these frequencies both the soft iron and mu-metal still behave as if exposed to a constant magnetic field.

2.6. RF System

The Recycler RF system which generates the longitudinal phase space gymnastics described in section 2.1 is composed of four 50Ω gaps driven by wideband amplifiers. The bandwidth of the net system is from 10 kHz to 100 MHz. The upper cutoff frequency corresponds to a voltage rise-time or fall-time of a few nanoseconds, far faster than actually necessary. The low frequency cutoff is composed of two poles, one from the gap inductance and the other from the amplifiers. Because there is no DC response in the system, two concerns need to be considered. The first is the amount of droop in the square voltage pulse during its duration. The second is the amount of baseline offset between the voltage pulses which can accelerate or decelerate beam particles which should be drifting.

The amount of droop can be calculated fairly easily. Using a simulation program to calculated response functions, as the two pole high pass filter response shown in figure 2.6.1, the resultant accelerating voltage waveform is presented in figure 2.6.2. For pulse lengths less than 1 μsec the droop is well less than 10%. This level of droop has only a small quantitative effect on the bucket height.

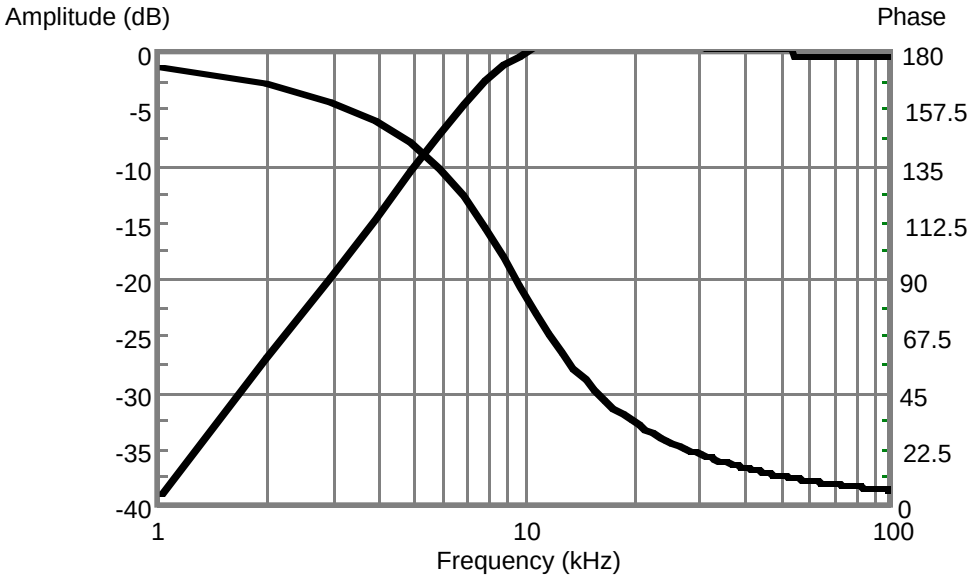

Figure 2.6.1: Two pole response function simulating the lower bandwidth limit of the accelerating gap and power supply.

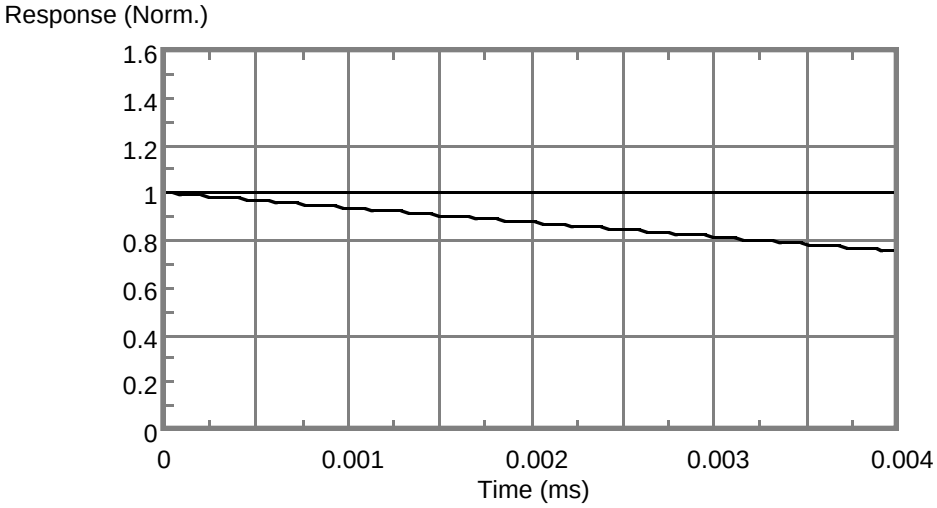

Figure 2.6.2: Calculation of the droop and the original pulse as a function of time. Note that for the most part pulse lengths of 1 μsec and less are envisioned, which infers that droops of less than 10% should be expected.

The first rule for suppressing baseline offsets is to always generate pairs of voltage pulses with equal and opposite areas, so that the net area is zero. This insures that there is no DC component in the drive signal. As can be seen in figure 2.6.3, after the pair of pulses the baseline voltage is at zero again. But note that inside the barrier bucket the drift region contains a nonzero residual voltage.

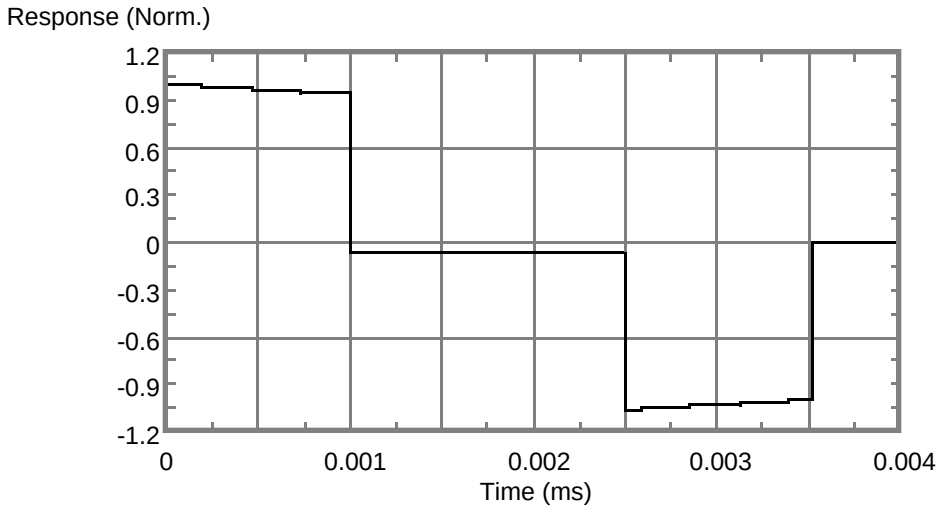

Figure 2.6.3: Calculation of the response to a barrier bucket pair constraining a 1.5 μsec batch with 1 μsec voltage pulses.

Another potential problem is the total impedance of 200Ω associated with the four gaps. The peak antiproton beam current envisioned is approximately 50 mA. Multiplying this current by the total impedance yields a beam loading waveform with a peak voltage of 10 V. Though this sounds like a small number, it is in fact enough to distort longitudinal phase space and cause a non-uniform beam distribution in the gap.

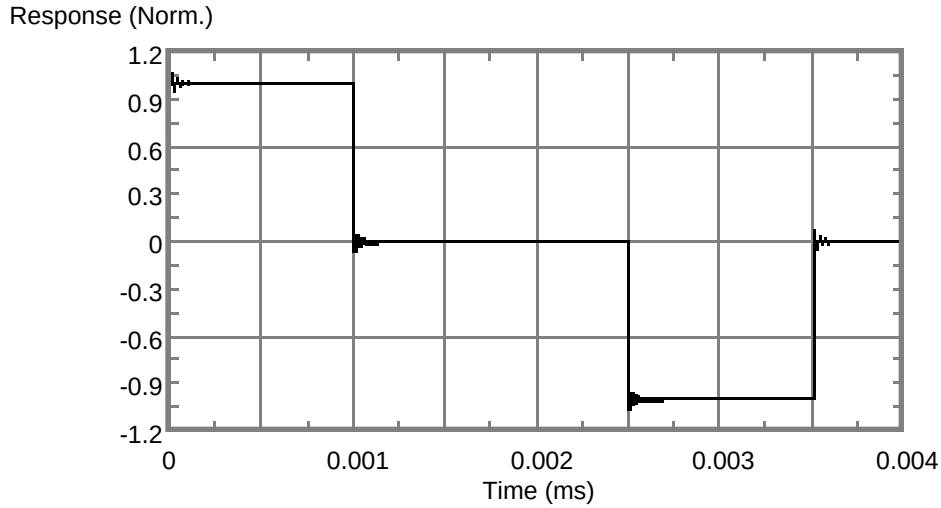

Figure 2.6.4: Calculation of the response to a barrier bucket pair constraining a 1.5 μsec batch with 1 μsec voltage pulses, but this time with a gap feedback system in operation with a loop gain of 10.

To fix the above three concerns simultaneously a feedback loop is envisioned. By comparing the gap voltage and the input to the amplifiers, the error signal is amplified

and added back into the amplifier. In this way the errant voltage from the low frequency bandwidth limit and the beam loading voltage can be corrected. Figure 2.6.4 shows the result of the inclusion of such a feedback system with a loop gain of 10. Figure 2.6.5 contains a block diagram of the feedback system.

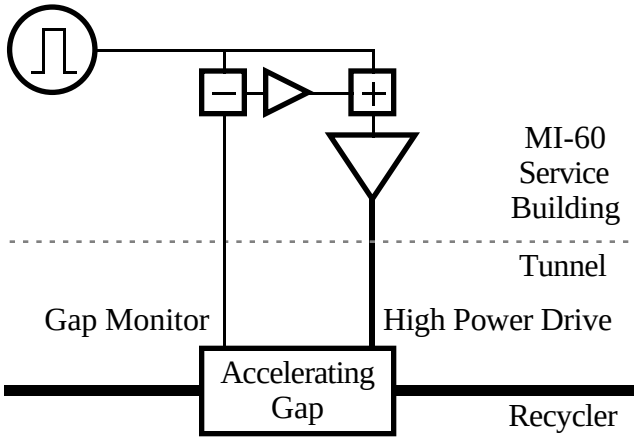

Figure 2.6.5: Block diagram of the feedback system around each gap/amplifier designed.

2.7. Impedances and Instabilities

Because the beam is unbunched, the instabilities which are expected to be a problem are not complicated. The two instabilities to be potentially concerned about are the transverse resistive wall instability and the longitudinal microwave instability.

2.7.1. Impedance Budget

The dominant sources of accelerator impedance in the Recycler ring are the beam position monitors, the kicker magnets, the accelerating cavities, and the resistance of the vacuum tube itself. At first one could assume that the impedance budgets of the Main Injector and the Recycler are the same at

$$\frac{Z_{\parallel}}{n} = 1.6\ \Omega \qquad Z_{\perp} = 2.2\ \mathrm{M}\Omega / \mathrm{m} \qquad .$$

However, the impedance will be dramatically less in the Recycler. For instance, there are no laminated Lambertson magnets, the kickers are slower and hence have a thicker coating, and there are no high-Q, high impedance RF cavities.

The beam impedance is dominated by the space-charge impedance. Calculation (K.Y. Ng) of the magnitude of this space charge impedance at a debunched beam intensity of 2.5×10^{12} yields the result

$$\frac{Z_{\parallel}}{n} = 12\ \Omega \qquad Z_{\perp} = 420\ \mathrm{M}\Omega / \mathrm{m}$$

2.7.2. Resistive Wall Instability

The resistive wall instability involves long wavelengths, and therefore does not depend on whether beam is bunched or coasting. Because the Recycler vacuum tube is the same material and cross-section as the Main Injector, the results obtained for the Main Injector for the instability growth time can simply be scaled with respect to the beam intensity. At an intensity of 1×10^{13} antiprotons, a growth time of approximately 3.6 ms, or 300 turns, is expected in the absence of space charge impedance or Landau damping. Note that a tune below the half integer was chosen to minimize the severity of the instability. Calculations including the space charge impedance and Landau damping indicate that the beam is in fact stable, and feedback systems are not necessary.

2.7.3. Microwave Instability

The minimum rms momentum spread in the Recycler will be 0.3 MeV. At that momentum spread the beam intensity is approximately 250×10^{10}. The threshold longitudinal impedance for microwave instability is given by

$$\left|\frac{Z_{\parallel}}{n}\right| < 0.68\pi\, Z_o \frac{|\eta|\gamma_r R}{N r_p}\left(\frac{\sigma_e}{E_o}\right)^2 \quad , \quad (2.7.1)$$

where $r_p = 1.5 \times 10^{-18}$ m and $Zo = 377\ \Omega$. Plugging in the rest of the numbers for the Recycler a threshold impedance of 70 Ω is found. The only impedance larger than this is from the four 50 Ω RF cavities at low frequencies below 1 MHz. If a problem did occur, the RF cavity feedback described above would suppress it.

2.8. Intrabeam Scattering

Intrabeam scattering, or Coulomb interaction between antiprotons, is the dominant heating mechanism which, when balanced against cooling forces from stochastic cooling, determines the equilibrium emittance achievable in the Recycler. Since each collision conserves energy, it is possible that as the thermal energy of one plane increases, which is related to the emittance in that plane, the emittance in another plane decreases, much as the temperatures of two heat reservoirs tend toward equilibrium. However, the potential for coupling some of the directed longitudinal beam energy into either longitudinal or transverse thermal motion in general leads to an overall increase in the phase space volume of the beam as a result of Coulomb interactions.

From simple kinematic arguments, it is possible to show that below transition, Coulomb collisions can lead to an equilibrium between the emittances of all planes, while above transition no such equilibrium is possible, that is, the emittance in all planes continues to increase. This comes about because the effective longitudinal temperature is proportional to the slip factor η, which implies a negative temperature above transition. The negative temperature is another manifestation of the negative mass instability.

Since the Recycler is well below transition, it could be expected that such an equilibrium is possible: i.e. the emittance of one plane increases while that of another

decreases. However, this is only partly true due to two mitigating factors. First, since there is a distribution of energies and angles among colliding particles, the transition from equilibrium to growth conditions is gradual. A completely stationary equilibrium is only achievable at non-relativistic energies. Second, Mtingwa and Bjorken have shown that the overall phase space volume can only remain stationary if a specific condition on lattice parameters is satisfied everywhere which, in general, is usually never true for a given lattice. Stated in physical terms, whenever Coulomb scattering occurs in the presence of gradients, either in configuration or velocity space, work is effectively done on the distribution, namely, emittance growth occurs.

The original work on this subject was carried out by Piwinski, and later work, based on an alternative, but equivalent approach, was carried out by Mtingwa and Bjorken. The latter work is often cited, because of the generality of the analysis, however certain approximations are typically made in the literature which do not permit immediate application of this analysis to beams below transition. Using the most general expressions from these references, it can be shown there is still some discrepancy between Piwinski`s work and that of Mtingwa and Bjorken regarding the conditions necessary for thermal equilibrium. However, we have extensively studied these two formulations and have found that the quantitative differences between these models are small. In the following analysis, we assume there is no transverse coupling, and that all particle distributions are Gaussian.

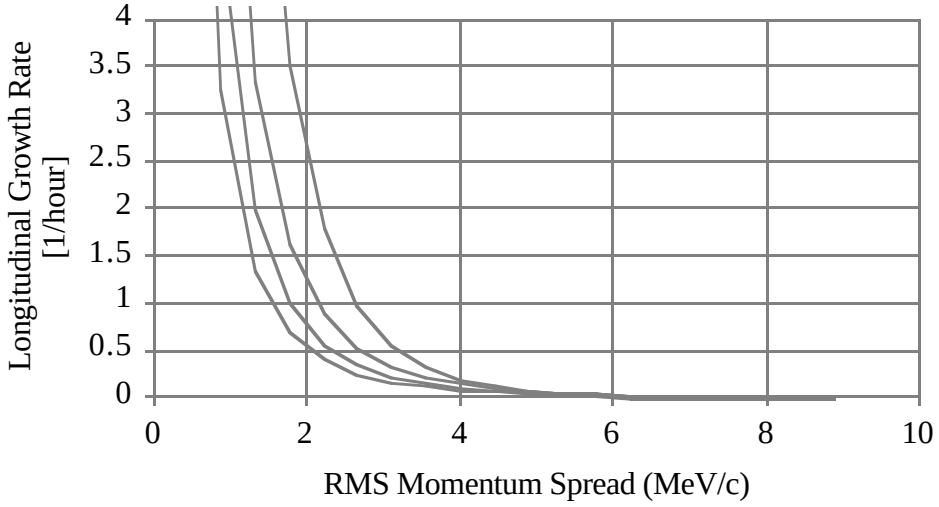

Figure 2.8.1: Longitudinal intrabeam scattering growth rates as a function of transverse emittance and momentum spread. The different curves are for transverse normalized 95% emittances of 5 (top), 10, 15, and 20 π mmmr (bottom). The beam intensity was 7×10^{12} antiprotons.

For the Recycler, there are two regimes of interest: a relatively high momentum spread regime in which stochastic cooling is used, and a regime with small where electron cooling is relevant. For large momentum spread, emittance growth times are shown in figure 2.8.1.

Inverse growth rates for the longitudinal plane are plotted as a function of momentum spread for various fixed transverse emittances (normalized, 95%). In figure 2.8.2, we plot the dependence of the horizontal scattering rates vs. momentum spread. At sufficiently small momentum spreads, it is possible that slight cooling of the horizontal emittance can occur through coupling to the relatively cold longitudinal plane. Note that since we have neglected coupling in this analysis, and there is no vertical dispersion, there is little coupling between the longitudinal and vertical planes. The vertical plane usually is cooled, but with very long cooling times. Hence it will be ignored in this analysis. In this regime, the sum of the horizontal and longitudinal inverse growth rates is approximately constant, although the net overall phase space volume increases, due to the presence of gradients. A small amount of longitudinal cooling is expected, as the transverse plane heats. In the limit of small momentum spread the situation is reversed where the longitudinal plane is strongly heated, while the horizontal plane can be measurably cooled.

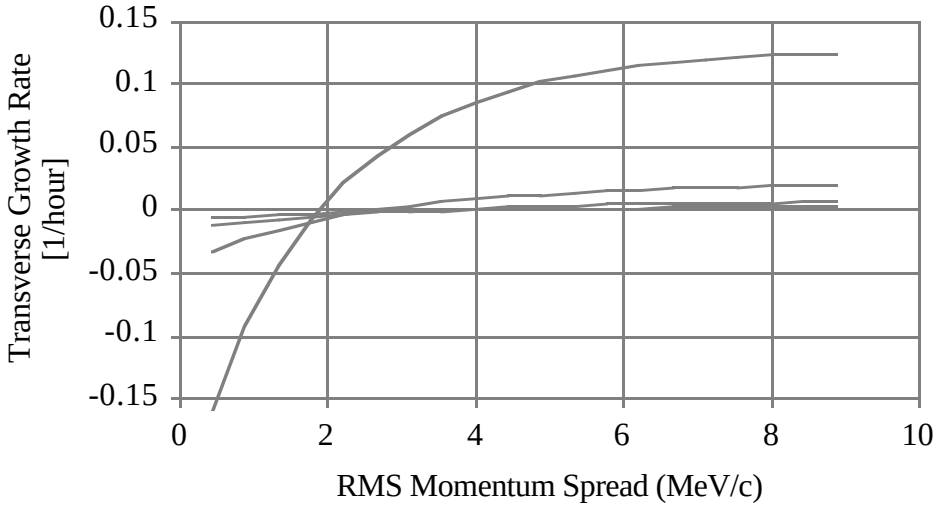

Figure 2.8.2: Transverse intrabeam scattering growth rates as a function of transverse emittance and momentum spread. The different curves are for transverse normalized 95% emittances of 5 (top on right edge), 10, 15, and 20 π mmmr (bottom on right edge). The beam intensity was 7×10^{12} antiprotons.

It should be noted that the actual equilibrium achieved is a balance between stochastic cooling and diffusion caused by scattering, all of which are non-Maxwellian processes; that is, tails will develop on the distributions as the energy-dependent diffusion and drag forces come to equilibrium in detailed balance. As such, the actual equilibrium must be found by the solution of a time-dependent Fokker-Planck approach.

It is worthwhile to note that the regime predicted for the Recycler in which some degree of transverse cooling is possible has not yet been investigated experimentally. It would be valuable to carry out a series of experiments in the Fermilab Accumulator, which can access the regime below transition.

2.9. Stochastic Cooling

The stochastic cooling systems in the Recycler ring are discussed in section 2.1 and chapters 3 and 4. The general picture one acquires is that the horizontal and vertical betatron cooling systems are not controversial and relatively straightforward. On the other hand, the momentum cooling system is critical, where cooling strength and momentum aperture are key design parameters. In this section the system parameters for both the betatron and momentum cooling systems are reviewed. To set the stage, the interaction between intrabeam scattering and stochastic cooling is explored explicitly first.

2.9.1. Intrabeam Scattering and Barrier Bucket Compression

The calculations of intrabeam scattering in the previous section indicate that the momentum growth rate for a fixed normalized 95% transverse emittance of 10 π mmmr is quite fast for the anticipated beam currents. In addition, the rate of increase in growth rate with diminishing rms momentum spread is very well described by the approximation

$$\alpha_{IBS} = \frac{k}{\left(\frac{\sigma_p}{P}\right)^3} \quad , \quad (2.9.1)$$

where $k=1.3\text{x}10^{-11}$ hr^{-1} at an antiproton beam intensity of $7\text{x}10^{12}$. Both the calculated and fit dependencies of intrabeam scattering growth rate on rms momentum spread are plotted in figure 2.9.1. Assuming a stochastic cooling/intrabeam scattering model in which distribution shapes are constant and rms momentum spread is an adequate parameterization of the beam temperature, a cooling system with a momentum cooling time of 1 hour can only reduce the rms momentum spread to approximately 2 MeV at the current of beam intensity of $7\text{x}10^{12}$. The engineering form of the equation can be written as

$$\alpha_{IBS}[hr^{-1}] = 0.093\frac{I_b\,[mA]}{\left(\sigma_E\,[MeV]\right)^3} \quad , \quad (2.9.2)$$

The cubic nature of the dependence of intrabeam induced growth time on rms energy spread suggests a Recycler stacking scenario in which the cooled beam distribution is always compressed in order to maintain the largest energy spread inside the energy aperture of the momentum cooling system. This time agile compression of the azimuthal distribution of the beam is carried out with the barrier bucket RF system.

Rough calculations [G. Jackson, MI-Note 164] indicate that a 0.5 hour momentum cooling time for a 21 mA instantaneous current antiproton beam with an rms energy spread of 2.7 MeV is sufficient for the beam distribution expected at any time in the Recycler ring during Run II.

As a result of the curve in figure 2.9.1, barrier bucket compression aimed at maintaining a large momentum spread at the expense of higher peak current will be systematically employed in the following scenario. Because of other side benefits, such

as more efficient ion clearing due to the beam distribution gaps and the ease and flexibility of beam transfers, the RF system which generates these barrier voltage pulses is a key component in the Recycler.

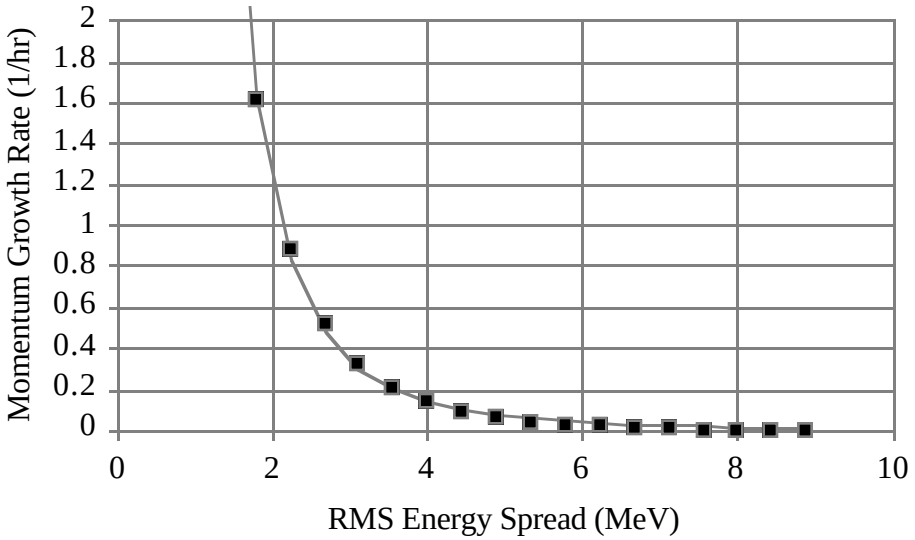

Figure 2.9.1: Calculated intrabeam scattering driven momentum growth rate in the Recycler ring as a function of momentum spread. The normalized 95% transverse emittance is 10 π mmmr and the antiproton intensity is 700×10^{10}. The points are calculated values while the line is the result of an inverse cubic fit.

2.9.2. General Considerations

The momentum cooling was chosen to be a filter cooling system. Non-overlapping Schottky bands are a requirement for this type of cooling system. The betatron cooling systems (horizontal and vertical) do not use any filters and the Schottky bands overlap slightly. The effect of these requirements is described in the section on Bandwidth below.

To minimize the phase errors in the cooling system ("bad mixing") the cooling signal is transmitted across the ring (from Q215 to Q111). Between these two locations particles traverse about 1/6 of the ring and accumulate approximately 1/6 of the phase slip. The signal will be transmitted with a modulated laser signal.

2.9.3. Bandwidth

The most important design choice concerns the system bandwidth. The maximum frequency that can be used without encountering Schottky band overlap is

$$\frac{\Delta p}{p} \eta f_{max} T_o \leq 1 \quad , \quad (2.9.3)$$

where

$$\eta = \frac{1}{\gamma_t^2} - \frac{1}{\gamma^2} \quad , \quad (2.9.4)$$

γ_t is the Recycler relativistic transition energy, and γ is the relativistic beam energy. The revolution period T_o is determined mostly by the circumference of the Main Injector tunnel. The maximum cooling frequency f_{max} is therefore inversely proportional to the momentum spread.

The equilibrium momentum spread is determined by the balance between the cooling rate and the heating rate from external mechanisms. Intrabeam scattering is expected to be the dominant heating mechanism longitudinally. Since stacked beam is trapped between two RF barriers and both the cooling and heating rate depend on the separation between the barriers (barrier bucket compression), the momentum spread depends on the choice of the amount of bucket compression. However, the choice is limited by the necessity of retaining adequate longitudinal phase space for injecting and recycling antiprotons. For a given choice of bucket compression, the required momentum spread is determined by the need to maintain the loss from diffusion at a level that is small compared to the stacking rate. Calculations indicate that a momentum spread of ±20 MeV/c will adequately retain the beam with a cooling system bandwidth of 0.5 to 2.0 GHz. It is tentatively planned to achieve this bandwidth with two separate cooling systems: one operating from 0.5 to 1.0 GHz and one operating from 1.0 to 2.0 GHz.

The transverse cooling system limitation of the maximum frequency comes from the "bad mixing" between pickup and kicker. For a momentum spread of ±20 MeV/c a cooling bandwidth of 2.0 to 4.0 GHz is appropriate. The transverse heating rate from intrabeam scattering is quite small, and the transverse emittance will probably be determined by other mechanisms. It is probably undesirable for the transverse emittance to be smaller than 10π because of the increase in longitudinal intrabeam scattering that results from low emittance beams. On the other hand, the equilibrium emittance will not be much less than 10 π mmmr if the beam heating rate is 1 π mmmr/hr. For this reason, a maximum beam heating rate (from all sources other than the cooling system) has been specified to be a maximum of 1 π mmmr/hr.

2.9.4. Stability

The gain of the longitudinal cooling system is limited by stability considerations. It has been assumed that errors in the gain function will limit the gain to a value 10 dB below the stability limit. This assumption is thought to be somewhat (but not overly) conservative in light of experience with similar systems in the Antiproton Source.

The betatron cooling systems are stable well past the optimum gain and should not present any unusual stability problems.

2.9.5. Simulation Description

The simulation of the stacking process is derived from the Fokker-Planck simulation used to design the momentum cooling for the Antiproton Source. The simulation assumes a coasting beam and neglects the transverse motion. The line density in the simulation is computed from the total beam in the stack divided by the sum of the barrier bucket compression and 1/2 the pulse width. The RF stacking and unstacking are

assumed to be perfectly adiabatic and with negligible emittance dilution. The bucket height (20 MeV) is treated as a hard aperture: particles that escape from the barrier bucket are lost.

Thus, the model used for the cooling process is exactly correct for a machine with an infinite voltage RF barriers and a finite momentum aperture. This model should be perfectly adequate for the dense portion of the antiproton stack. However, for particles that have larger momentum offsets, this approximation underestimates the time spent under the influence of the barrier and overestimates the particle density. For example, the stack is contained between two barrier voltage pulses that capture 139 eV-sec. The simulation, with infinite height buckets, contains only a total of 112 eV-sec.

Intrabeam scattering is incorporated in an average way with the addition of an energy independent diffusion constant

$$D = \frac{2\sigma_p^2}{\tau_l} \quad , \qquad (2.9.5)$$

where σ_p is the momentum of the beam and τ_l is the calculated intrabeam scattering heating time. The value of σ_p varies somewhat in the stacking process, but the variation is not included in the simulation. It is adequate to use the final value of σ_p. The value of D is, however, scaled to account for the changing intensity of the stored beam.

The system gain function is calculated using ideal components. Gain errors are introduced by multiplying the response function of a broad-band (Q=1) resonator centered at mid-band. No frequencies outside the nominal cooling band are considered: it is assumed that these frequencies contribute no net heating or cooling. The resulting gain functions are shown in figures 2.9.2 through 2.9.4.

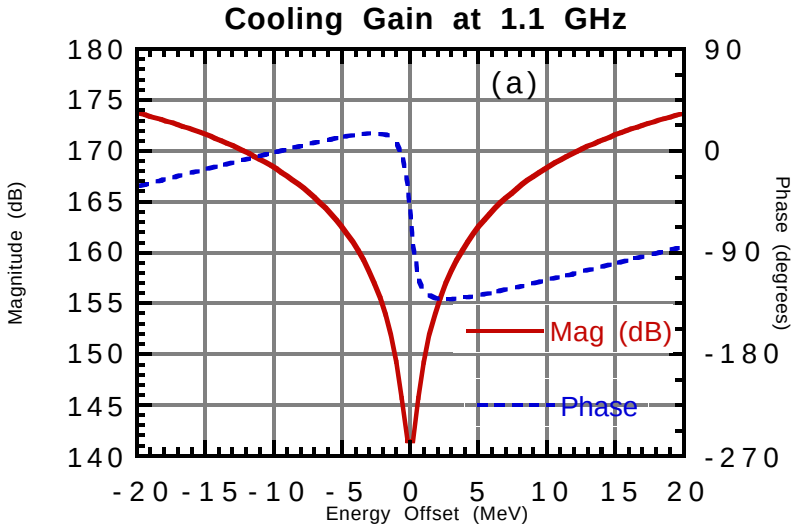

Figure 2.9.2: Momentum cooling gain functions for the Schottky band at 1.1 GHz.

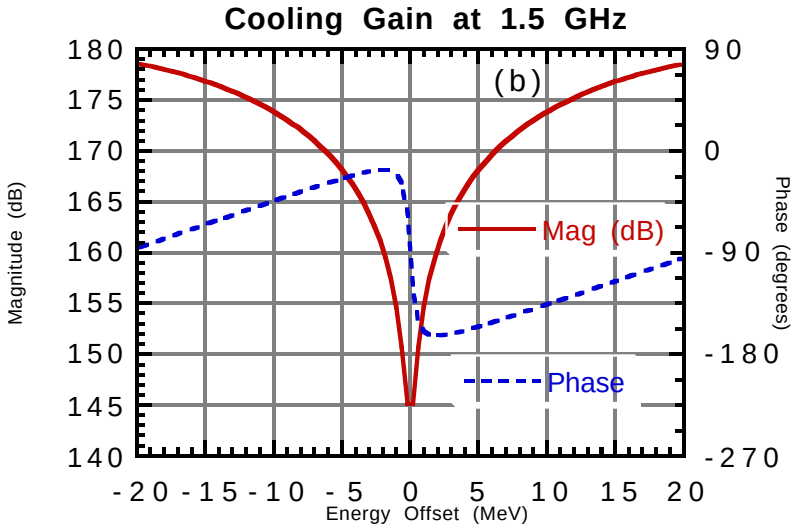

Figure 2.9.3: Momentum cooling gain functions for the Schottky band at 1.5 GHz.

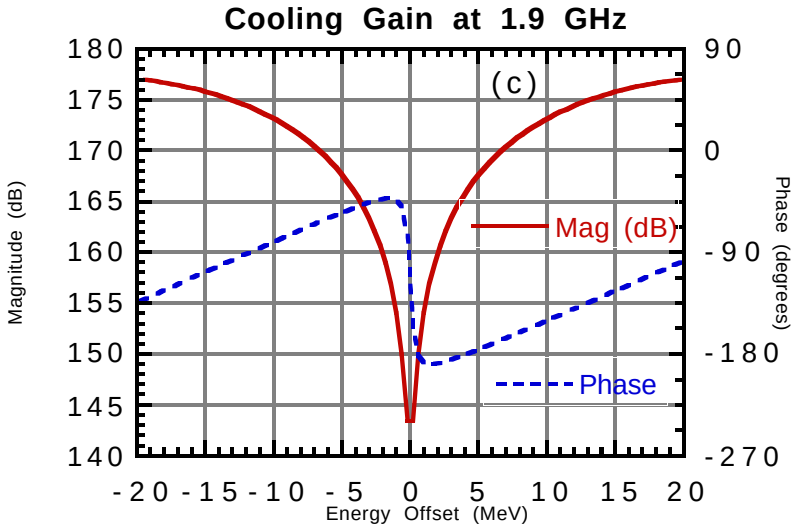

Figure 2.9.4: Momentum cooling gain functions for the Schottky band at 1.9 GHz.

The transverse cooling simulation is also based on a coasting beam approximation assuming that the particle momenta are constant. This assumption is not correct because: 1) the momentum cooling system changes the particle momenta, 2) the beam intensity and distribution changes as the beam is stacked, and 3) the RF changes the particle momenta. A proper calculation of the evolution of the distribution function would have to take into account both the longitudinal and transverse degrees of freedom. If, however, the distribution function can be written as a product of distribution functions for the

longitudinal and transverse coordinates, the coasting beam approximation should be accurate. The momentum distribution is taken from the longitudinal stacking calculation and input to the transverse calculation. The transverse cooling is calculated for particles of a fixed momentum (but time varying density). Any new beam that is injected is assumed to have the same transverse distribution as the beam already present. The results of this calculation are shown below and are self-consistent with the above assumptions.

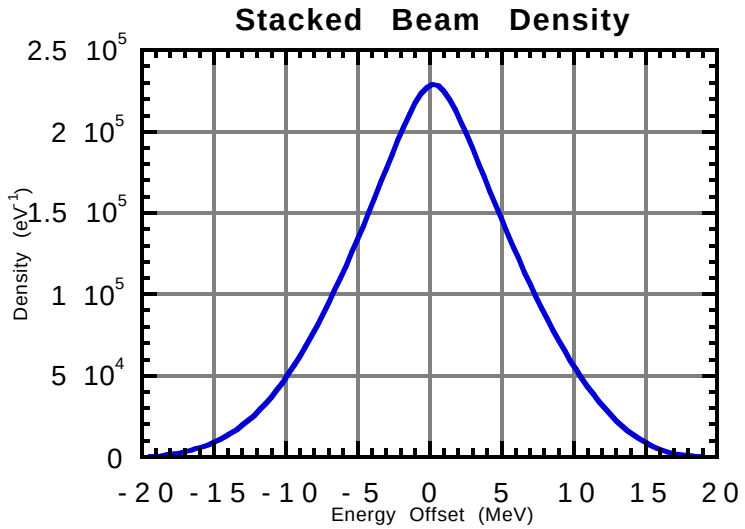

Figure 2.9.5: Longitudinal density profile obtained after 8 hours of stacking.

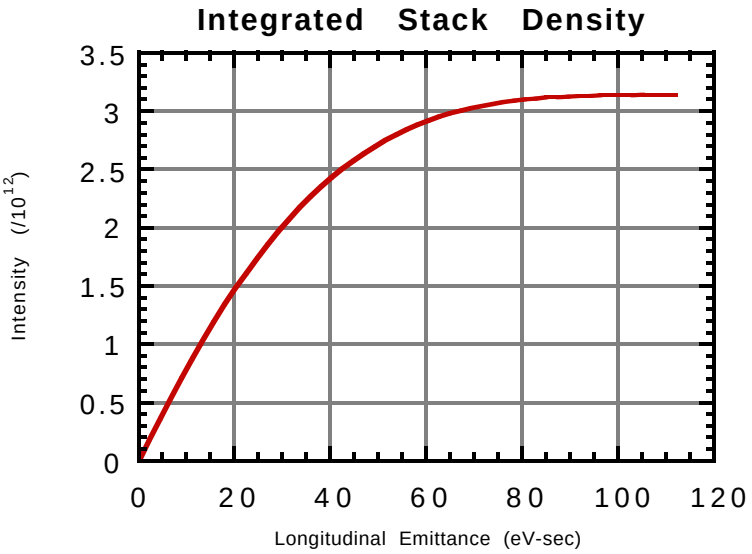

Figure 2.9.6: Integrated density profile obtained after 8 hours of stacking.

The transverse heating rate (from mechanisms other than the cooling systems) is critical. The simulation assumes that this rate is 1 π mmmr/hr. The longitudinal cooling system is specified to contribute less than 0.1 π mmmr/hr to the total.

2.9.6. Simulation Results

The final momentum distribution obtained is shown in figure 2.9.5. This distribution is integrated and shown in figure 2.9.6. As discussed above, the particle density is overestimated at high values of the momentum offset.

The stack size versus time in the cycle is shown in figure 2.9.7. Also shown is the cumulative stacking efficiency: the total stack size divided by the amount of beam injected in the current cycle. The maximum stack size is 3×10^{12} and the overall stacking efficiency for the cycle is about 98%.

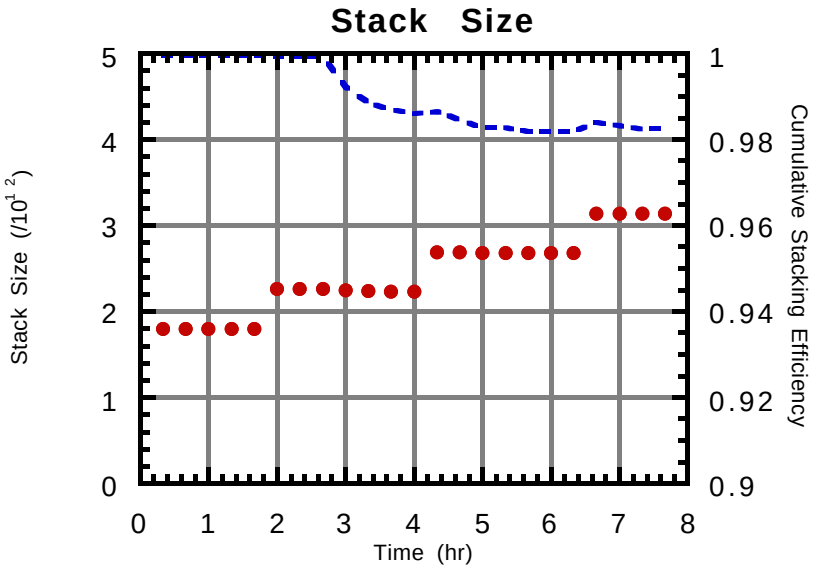

Figure 2.9.7: The stack size begins at t=0 at about $1.8\text{x}10^{12}$ antiprotons and grows to more than $3\text{x}10^{12}$ antiprotons after 7 hours of stacking. The cumulative stacking efficiency is equal to the current beam intensity divided by the sum of the initial beam and subsequent injections. The cumulative stacking efficiency exceeds 98% at the conclusion of the stacking cycle.

The simulation of the cooling of transverse emittance of the beam is shown in figure 2.9.8. The initial emittance of the beam is taken to be 30 π mmmr (100%). The beam cools rapidly initially and then grows as the intensity increases and the cooling rate decreases. The fraction of the beam that is contained within the 10 π mmmr emittance design goal is shown in figure 2.9.9. At the conclusion of the 8 hour stacking cycle virtually all of the beam is within this emittance.

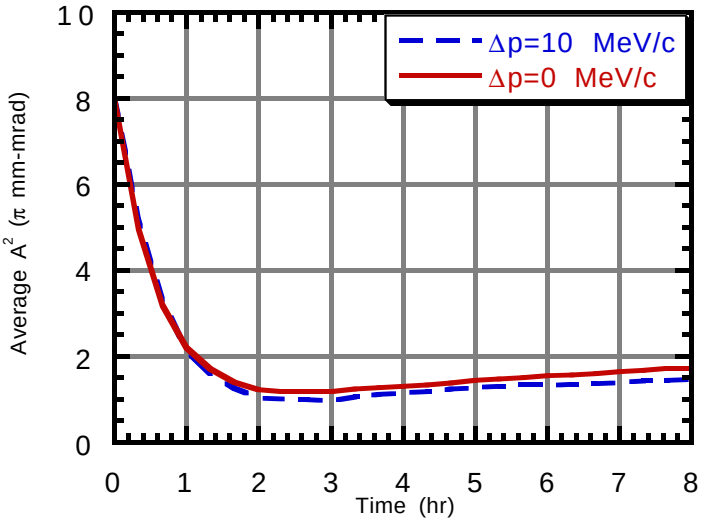

Figure 2.9.8: The evolution of the average amplitude-squared of the beam betatron motion. The beam emittance (95%) is approximately 3x the average amplitude-squared. The recycled beam cools rapidly initially until it reaches a minimum after which it grows because of the increasing intensity.

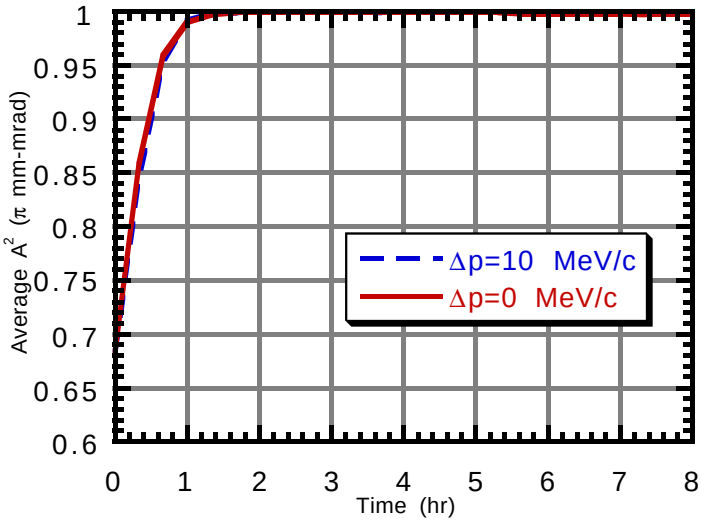

Figure 2.9.9: The fraction of the beam contained in a 10 π mmmr emittance (100%). The fraction becomes nearly 100% after 2 hours of cooling.

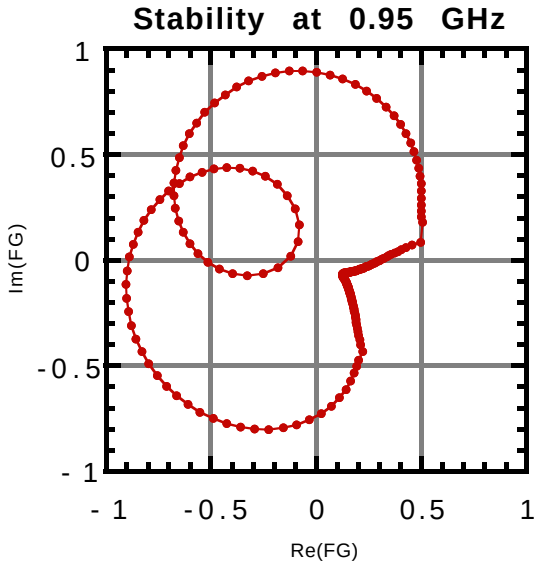

Figure 2.9.10: Stability diagram for the Schottky bands at 0.95 GHz at 7:40 (just before transfer to the Tevatron). The curve is a parametric plot of the real versus imaginary parts of the product gain (G) and beam feedback (F) functions. The points are spaced at 0.4 MeV intervals. The gain has been chosen so that the curve crosses the real axis at 0.3.

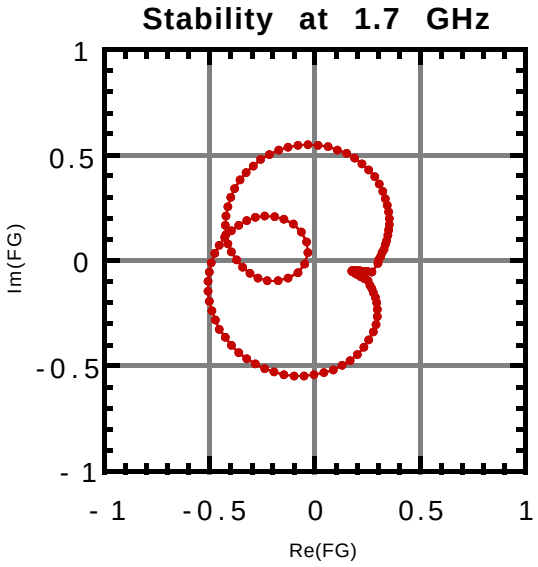

Figure 2.9.11: Stability diagrams for the Schottky bands at 1.7 GHz at 7:40 (just before transfer to the Tevatron). The curve is a parametric plot of the real versus imaginary parts of the product gain (G) and beam feedback (F) functions. The points are spaced at 0.4 MeV intervals. The gain has been chosen so that the curve crosses the real axis at 0.3.

The stability diagrams for the two momentum cooling system bands are shown in figures 2.9.10 and 2.9.11 for the time 7:20 - just before transfer to the Tevatron. This case is the one with the lowest stability margin. The stability criterion is that the curve cross the real axis with an intercept less than 1. The gain function has been scaled in the simulation so that the stability curve passes through the point (0.30,0.0). The stability margin, particularly in the lower band, is sensitive to phase errors in the gain function. However, it is believed that the designed stability margin is large enough that unanticipated phase errors can be tolerated.

The stability criterion as stated is actually unduly restrictive in that it is sufficient but not necessary. However, the more general stability criterion is not of practical importance for these systems.

2.9.7. Specifications: Longitudinal

The specifications for the momentum cooling system are given in Table 2.9.1.

Table 2.9.1: Momentum Cooling System Specifications

	Band 1	Band 2	
Pickups (PU)			
Beta Function at PU	35	35	m
Beam Transverse Emittance	10	10	π mmmr
Beam Size	22.68	22.68	mm
Number of Pickups	16	32	
PU Impedance	100	100	Ω
PU Gap	30	30	mm
Pickup Width	40	40	mm
PU Sensitivity	0.84	0.84	
PU Combiner Loss Factor	2	2	dB
Number of Tanks	1	1	
PU Repeat Length	12	7	cm
Overall Tank Length	2.32	2.64	m
Electronics			
Lower Frequency	0.5	1	GHz
Upper Frequency	1	2	GHz
Maximum Noise Figure	1	1	dB
Nominal Pickup Temperature	293	293	°K
Nominal Electronic Gain	116	101	dB
Notch Depth	30	30	dB
Notch Dispersion	20	20	ppm
Max Gain Ripple (Small Scale)	10	10	dB
Max Gain Variation (Large Scale)	3	3	dB
Nominal Noise Power	2	2	W
Nominal Schottky Power	6	3	W
Nominal Total Power	8	5	W
Amplified Rated (Saturated) Power	100	100	W
Kickers			
Number of Kickers	16	32	
Kicker Impedance	100	100	Ω
Kicker Gap	30	30	mm
Kicker Width	40	40	mm
Kicker Sensitivity	0.84	0.84	
Kicker Loss Factor	2	2	dB
Number of Kicker Tanks	1	1	
Overall Tank Length	2.32	2.64	m
Maximum Transverse Growth Rate	0.1	0.1	π mmmr/hr

2.9.8. Specifications: Transverse

The specifications for the betatron cooling systems are given in Table 2.9.2.

Table 2.9.2: Transverse Cooling System Specifications

Pickups (PU)		
Beta Function at PU	35	m
Beam Transverse Emittance	10	π mmmr
Beam Size	22.68	mm
Number of Pickups	32	
PU Impedance	100	Ω
PU Gap	30	mm
Pickup Width	22.5	mm
PU Sensitivity	0.83	
PU Combiner Loss (2 GHz)	2	dB
PU Combiner Loss (4 GHz)	2	dB
Number of Tanks	1	
PU Repeat Length	4.5	cm
Overall Tank Length	1.84	m
Electronics		
Lower Frequency	2	GHz
Upper Frequency	4	GHz
Maximum Noise Figure	1	dB
Nominal Pickup Temperature	293	°K
Electronic Gain	86	dB
Max Gain Ripple (Small Scale)	10	dB
Max Gain Variation (Large Scale)	3	dB
Nominal Noise Power	0	W
Nominal Schottky Power	2	W
Nominal Total Power	2	W
Maximum (Saturated) Power	50	W
Kickers		
Beta Function @ Kicker	35	m
Number of Kickers	32	
Kicker Impedance	100	Ω
Kicker Gap	30	mm
Kicker Width	22.5	mm
Kicker Sensitivity	0.62	
Kicker Loss(2 GHz)	2	dB
Kicker Loss(4 GHz)	2	dB
Number of Kicker Tanks	1	
Overall Tank Length	1.84	m

3. Technical Components

In this section the specific technical scope of the Recycler upgrade of the Main Injector project is described. For each category of components technical specifications and counts are reviewed.

3.1. Magnets (WBS 3.1.1)

Except for a small number of dipole and quadrupole correction magnets, all magnets in the Recycler ring and its associated injection and extraction beamlines are of the permanent variety. In this section the shape, weight, placement, strength, and tolerances of the magnets are described.

3.1.1. Recycler Ring Overview

In the Recycler ring there are 9 unique major magnet types, all of which are permanent magnets. Table 3.1.1 contains name definitions for the magnet types. The two magnet categories which make up the majority of the magnets are gradient dipoles and pure quadrupoles. Figure 3.1.1 and 3.1.2 contains engineering cross-sectional drawings of these two categories.

Table 3.1.1: The definition of names representing magnet types.

Type	Name	Description
1	RGF	Focusing Gradient Dipole in a Normal Bend Cell
2	RGD	Defocusing Gradient Dipole in a Normal Bend Cell
3	RGS	Gradient Dipole in a Dispersion Suppression Cell
4	RQM	Straight Section Quadrupole
5	RQS(1-8)	MI-60 Trim Quadrupoles
6	RQPT(0-4)	MI-60 Phase Trombone Quadrupoles
7	RLA	Lambertsons at the Ends of Transfer Lines
8	RMG	Mirror Gradient Dipole near MI-30 Recycler Lambertsons
9	RVD	Vertical Dipoles for Transfer Lines

The number of gradient magnets in the ring, along with the design multipole strengths and lengths, are listed for each type of gradient magnet in table 3.1.2. Note that only the normal cell magnets in the region of nominal dispersion contain a sextupole component of the magnetic field in order to combat the natural chromaticity of the uncorrected lattice. It turns out that the present version of the Recycler lattice, version 10, has equal gradient and bend in the focusing and defocusing dispersion suppression gradient magnets. Therefore there are only three pole piece shapes in all of the gradient magnets in the Recycler ring.

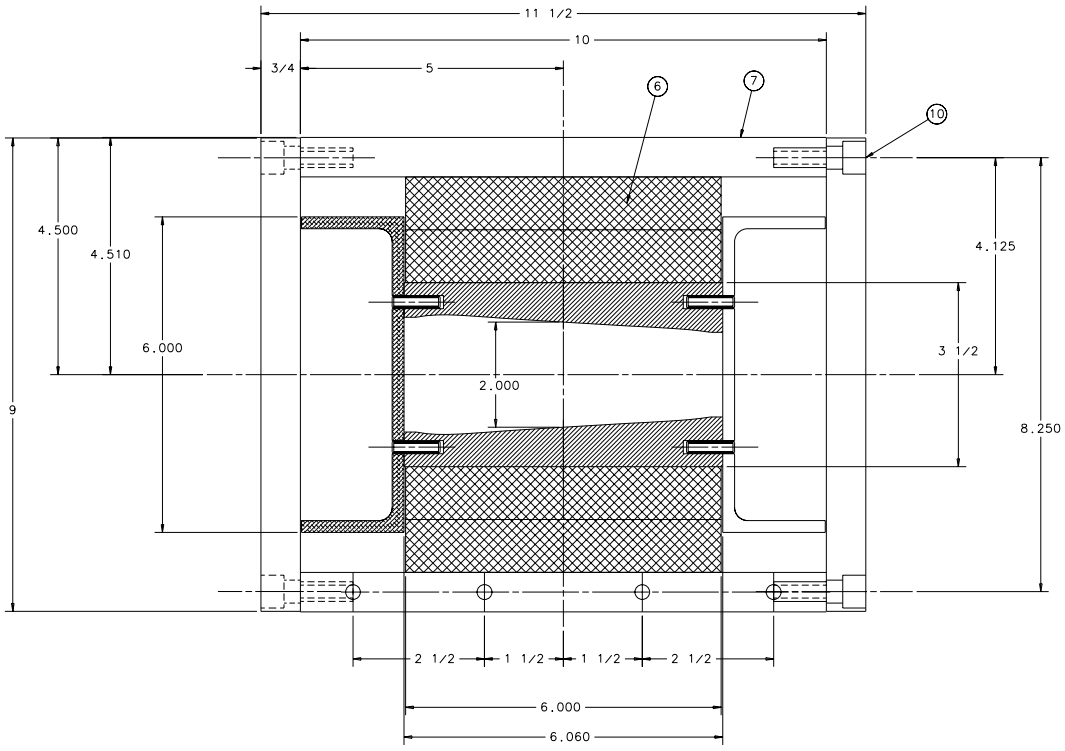

Figure 3.1.1: Gradient magnet profile. These magnets are composed of double bricks on top and bottom.

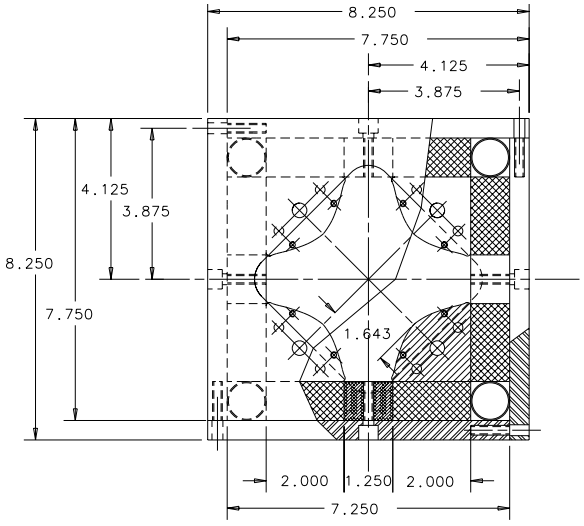

Figure 3.1.2: Quadrupole magnet profile. These magnets are composed of twin cut bricks behind each pole.

The same information for the main quadrupoles in the ring is displayed in table 3.1.3. Note that the focusing and defocusing quadrupoles are identical except for a 90° rotation (or brick polarity reversal during fabrication).

Table 3.1.2: Number, magnetic lengths, and magnetic multipoles of gradient magnets in the Recycler ring. The dispersion suppression focusing and defocusing magnets are now identical. Therefore, there are only three different shape gradient magnet pole pieces in the entire ring.

Name	Length (m)	Number	B_0 (kG)	B_1 (kG/m)	B_2 (kG/m^2)
RGF	4.267	108	1.4494	3.515	3.566
RGD	4.267	108	1.4494	-3.365	-5.997
RGS	2.845	128	1.4494	7.877	0

Table 3.1.3: Number, lengths, and magnetic multipoles of quadrupole magnets in the Recycler ring. Note that only one pole shape is required in order to produce all of the magnets.

Name	Length (m)	Number	B_0 (kG)	B_1 (kG/m)	B_2 (kG/m^2)
RQM (F)	0.5	28	0	26.816	0
RQM (D)	0.5	28	0	-25.640	0

Table 3.1.4: List of the vernier quadrupoles needed on either side of the MI-60 straight section to correct the lattice function distortions caused by the horizontal bypass of the Recycler around the Main Injector RF cavity power tubes.

Name	Length (m)	Number	B_0 (kG)	B_1 (kG/m)	B_2 (kG/m^2)
RQS1	0.5	2	0	6.041	0
RQS2	0.5	2	0	-10.232	0
RQS3	0.5	2	0	-12.926	0
RQS4	0.5	2	0	19.763	0
RQS5	0.5	2	0	-7.001	0
RQS6	0.5	2	0	-4.235	0
RQS7	0.5	2	0	-9.580	0
RQS8	0.5	2	0	4.291	0

At MI-60 the straight section is empty of specialty components except for the four RF cavities. Because of the cost of a distributed quadrupole circuit for betatron tune control of the Recycler, it has been decided to employ the phase trombone method of tune control. By adjusting 5 families of quadrupoles in the MI-60 straight section, the phase advances in the horizontal and vertical planes are independently adjustable while simultaneously maintaining the same Twiss parameter values at the ends. By keeping the end Twiss parameters constant, no lattice mismatches result and the straight section actually appears as a phase trombone. In table 3.1.5 the different settings of the phase

trombone quadrupoles are displayed. While holding the maximum beta function in the straight section to under 200 m, a tune range of ±0.5 tune units in either plane can be realized. This maximum beta function value represents an almost doubling of the beam size. A 3" diameter round beam tube will be used in the MI-60 straight section to preserve the admittance of the entire ring.

The initial implementation of these quadrupoles, as well as the two skew quadrupoles required to cancel coupling globally, will be electromagnets - trim quadrupoles reused from the Main Ring and powered by reused Main Ring trim power supplies. A possible later improvement would be to replace the electromagnets with a system to roll adjacent permanent magnet quadrupoles in a counter-phased manner using stepping motors. This would enhance the the high reliability mission of the Recycler. Lattice calculations show that in the rolling scheme three short magnets are required to implement each variable strength quadrupole, but these magnets can also serve as the skew quadrupole correction.

To adjust the beam position and angle through the Lambertson magnets during injection and extraction, and to permit aperture scans, we will install both horizontal and vertical four-bumps at each Lambertson in the Recycler, a total of 24 magnets. These will be reused Main Ring trim dipoles powered by Main Ring trim power supplies. At 8 GeV the Main Ring trims are sufficiently strong, even shimmed to a larger aperture.

Table 3.1.5: Phase trombone quadrupole strengths at MI-60 in a lattice in which the standard phase advance per cell in each transverse plane is maintained.

Name	Length (m)	Number	B_0 (kG)	B_1 (kG/m)	B_2 (kG/m^2)
RQPT0	0.5	2	0	-36.676	0
RQPT1	0.5	4	0	32.033	0
RQPT2	0.5	4	0	-34.601	0
RQPT3	0.5	4	0	32.679	0
RQPT4	0.5	2	0	-32.827	0

3.1.2. Transfer Line Overview

There are also a significant number of permanent magnets employed in the three transfer lines associated with the Recycler. The two transfer lines between the Main Injector and the Recycler at MI-30 have the largest number of magnets associated with them, since the transfer occurs over a segment of the tunnel which is bending. Table 3.1.6 contains a summary of the permanent magnets envisioned for both lines. The mirror gradient magnets are required in the Recycler and the beam line at the first (otherwise) normal defocusing gradient dipole downstream (upstream) of the Lambertson. The problem is that the transfer is taking place in a normal arc cell, and the distance between the Lambertson and the first permanent magnet gradient magnet is too small to have both a ring and matching beamline gradient magnet stacked on top of one another. Since the mirror dipoles can be constructed such that there is only 0.75" of flux return for each magnet between the ring and transfer line beam pipes, the minimum separation of 4.5" at the leading edge of the magnets can be accommodated.

Table 3.1.6: Total number of magnets of each type required in both transfer lines at MI-30 between the Main Injector and the Recycler.

Name	Length (m)	Number	B_0 (kG)	B_1 (kG/m)	B_2 (kG/m^2)
RLA	4.064	4	1.5232	0	0
RVD	4.267	4	1.4494	0	0
RMG	4.267	4	1.4494	-3.365	-5.997
RQM (F)	0.5	4	0	26.816	0
RQM (D)	0.5	2	0	-25.640	0
RGS	2.845	8	1.4494	7.877	0

The transfer lines and the abort line all require vertical bends beyond that provided by the Lambertson magnets. The strength, length, and aperture of these magnets match the normal gradients in the ring. Therefore the plan is to copy the design, substituting a new pole shape to produce a dipole field.

In the proton abort line three 20 mrad permanent magnet dipoles and two quadrupoles are necessary. In addition, a mirror dipole or permanent magnet Lambertson is also needed. These counts are summarized in table 3.1.7.

Table 3.1.7: Total number of magnets of each type required in the Recycler abort line.

Name	Length (m)	Number	B_0 (kG)	B_1 (kG/m)	B_2 (kG/m^2)
RQM	0.5	4	0	26.816	0
RLA	4.064	2	1.5232	0	0
RVD	4.267	3	1.4494	0	0

3.1.3 Permanent Magnet Design Features

The basic design of the permanent magnet dipole is shown in figure 3.1.3. It is a 1.5 kG gradient (combined-function) dipole with a 2 in. gap at the center, a 5.5 in. horizontal aperture and a 3.5 in. horizontal good-field aperture. Overall dimensions are 9.5 in. high by 11.5 in. wide by approximately 13 ft. long. The weight is typically 2000 lb. The magnets are straight and the sagitta of the beam inside a magnet is typically 1 cm. The beam pipe dimensions under vacuum are approximately 1.75 in. vertically and 3.75 in. horizontally. The precise parameter values for each of the individual gradient magnet types appear in table 3.1.8.

The design is a so-called “hybrid” permanent magnet in which the field is driven by permanent magnet material and the field shape is determined mainly by steel pole pieces. The field quality, which is shown in figure 3.1.4, is designed to give a vertical magnetic field error of less than 1×10^{-4} across the designated good field region. The permanent magnet bricks drive flux into (from) the pole tips from the top (bottom) (see figure 3.1.5). The entire assembly is enclosed in a flux return shell 0.75” thick. Solid "bar stock" components are used throughout rather than laminations. The pole tip steel is 1008 low

carbon steel and the flux return is construction grade (A36) steel. The design field harmonics which correspond to the design shape shown in figure 3.1.4 are listed in table 3.1.9.

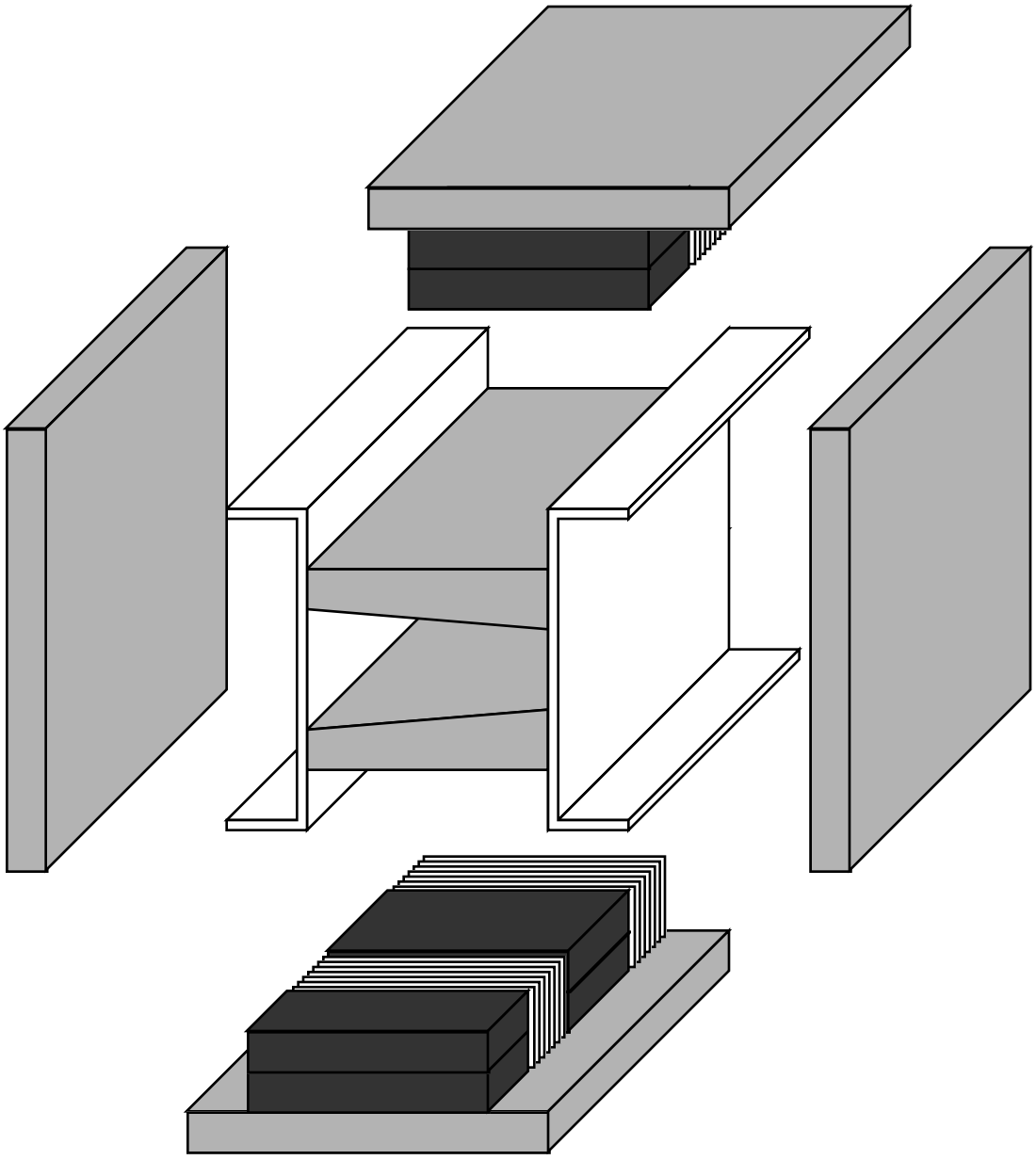

Figure 3.1.3: Permanent magnet gradient dipole components shown in an exploded view. For every 4" wide brick there is an 0.5" interval of temperaature compensator material composed of 10 strips.

Table 3.1.8: Design and physical parameters of Recycler focusing (RGF), defocusing (RGD), and dispersion suppresser (RGS) gradient magnets.

Parameter	RGF	RGD	RGS
Magnet Width (in.)	11.5	11.5	11.5
Magnet Height (in.)	9.0	9.0	9.0
Physical Length (in.)	175.0	175.0	119.0
Total Weight (lb.)	2691	2691	1800
Magnetic Length (in.)	168.0	168.0	112.0
Bend Angle (mrad)	21	21	14
Beam Sagitta (mm)	10	10	5
Flux Return Weight (lb.)	1496	1496	1017
Pole Tip Weight (lb.)	302	302	202
Ferrite Brick Weight (lb.)	710	710	461
Compensator Weight (lb.)	133	133	86
Aluminum Weight (lb.)	50	50	34

Table 3.1.9: Calculated magnetic field harmonics for the Recycler arc cell focusing gradient magnet pole shape design.

N	Normal	Skew	N	Normal	Skew
1	10000	-0.07	7	0.02	-0.02
2	610.03	0	8	0	0.01
3	15.21	-0.06	9	0.04	0.01
4	-0.11	0	10	0.01	-0.02
5	-0.1	-0.02	11	-0.07	0.01
6	0.01	-0.01			

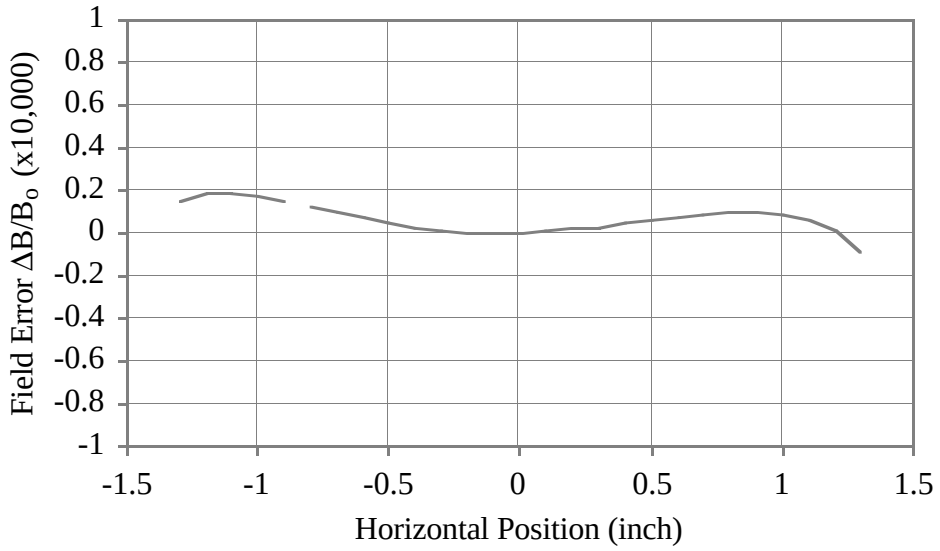

Figure 3.1.4: Design magnetic field imperfection across the horizontal aperture of a Recycler gradient magnet. Generated by Poisson, the ripple in the field is due to the finite extent of the poles and the trapezoidal approximation of the pole shape.

As shown in figure 3.1.6, the end fields of the magnets are terminated by flux clamp/end plate assemblies which are magnetically connected to the flux return shell. These plates prevent the stray flux from leaking out and saturating the mu-metal/soft iron shielding of the beam pipe between magnets. The end plates are removable to allow access to the ends of the pole tips for field quality shimming operations.

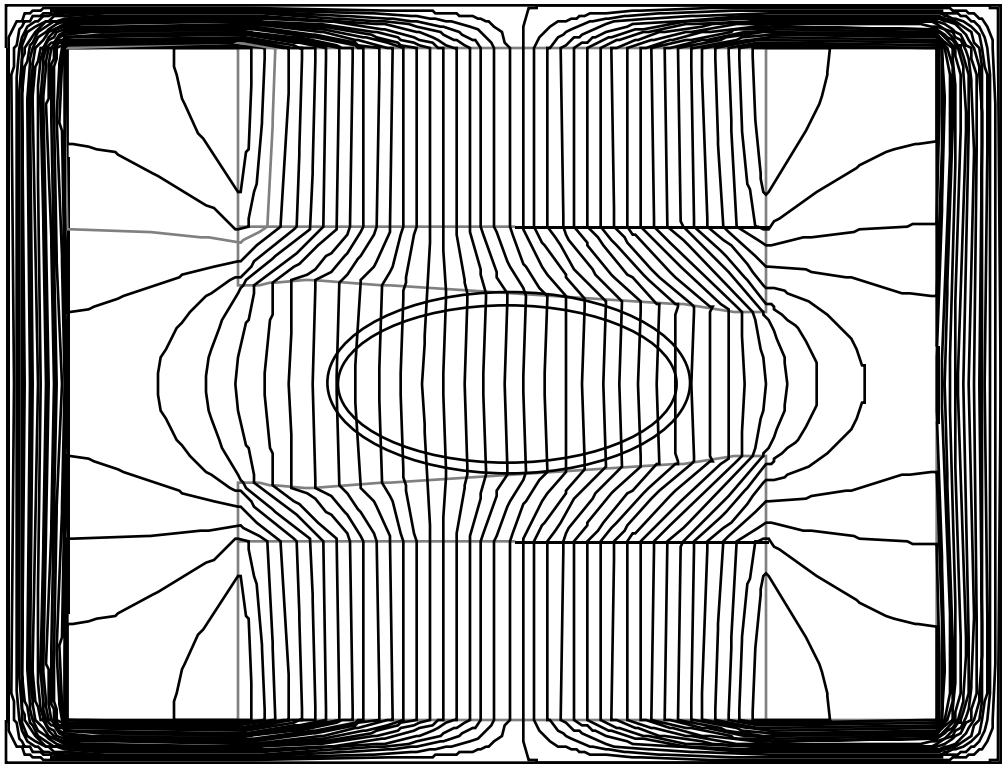

Figure 3.1.5: POISSON field map of a Recycler gradient dipole.

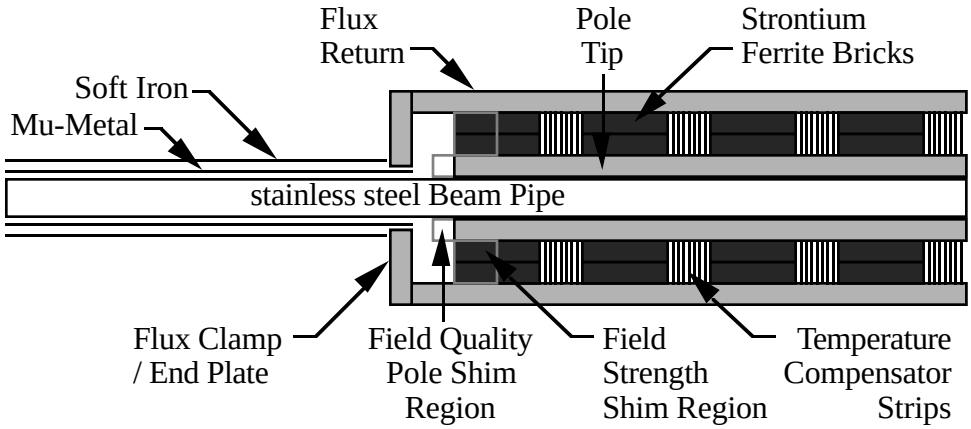

Figure 3.1.6: Side view of magnet, showing transition from magnetic shielding of naked beam pipe to magnet flux return. Also indicated are the regions at the ends of the pole tips devoted to shimming the field shape, and the ends of the ferrite bricks which are used to trim the strength of the magnet by adjusting the total amount of magnetic material.

3.1.4. Permanent Magnet Material

We have chosen Type 8 Strontium Ferrite (Type 8 Strontium Ferrite data sheets & specifications from Arnold, Crucible, and Hitachi) as the permanent magnet material because of its low cost and high stability over time, temperature, and radiation. Strontium ferrite is the material of choice in automotive applications and is available at low cost in standard grades and sizes from multiple vendors. It has documented stability in applications such as NMR magnets and is commonly used in ion pumps in accelerator applications. Materials from the three major U.S. vendors were evaluated and performed well in the R&D program.

3.1.5. Magnetization and Strength Trimming

Ferrite bricks are shipped unmagnetized from the foundry and are magnetized immediately prior to assembly using a 2 Tesla dipole. The bricks are individually measured and assembled into "kits" each containing a specified total magnetic strength of brick. The magnet design is such that a magnet fully loaded with bricks of nominal strength is 3~5% stronger than required. Dummy bricks, fractional bricks and spacers are used to control the total strength of the "kits" to correct for brick-to-brick and lot-to-lot variations. A final strength trim is accomplished by adjusting the amount of ferrite at the ends of the magnet.

3.1.6. Temperature Compensation

The intrinsic temperature coefficient of the Ferrite material (-0.2%/°C) is canceled [Dallas 1995 PAC papers on permanent magnets by Bertsche & Ostiguy, Foster & Jackson] by interspersing a "compensator alloy" (Carpenter Technologies Compensator 30 type 4 data sheets from Telcon data sheet, Eagle Alloys, Sumitomo Heavy metals) between the ferrite bricks above and below the pole tips. The compensator is an iron-nickel alloy with a low Curie temperature and therefore a permeability which depends strongly on temperature. This shunts away flux in a temperature dependent manner which can be arranged to null out the temperature dependence of the ferrite. We find that the degree of temperature compensation is linearly related to the amount of compensator material in the magnet. Thus the degree of compensation can be "fine tuned" to the required accuracy by adjusting the amount of compensator at the ends of the magnet in a manner similar to the strength trimming with the ferrite. For example, a 20-fold reduction of the temperature coefficient (from 0.2%/°C to 0.01%/°C) requires that the amount of compensator in the magnet be adjusted correctly to 1 part in 20. This poses no difficulties for production.

The range and accuracy of the required temperature compensation is determined by the expected variation in tunnel temperature. Data from the Main Ring tunnel during a typical period of operations can act as a guide to predict Main Injector tunnel temperatures. Figure 3.1.7 contains data from a Main Ring sector which had the maximum temperature variation during the time plotted. Note that a ±1°C temperature variation is a pessimistic estimate.

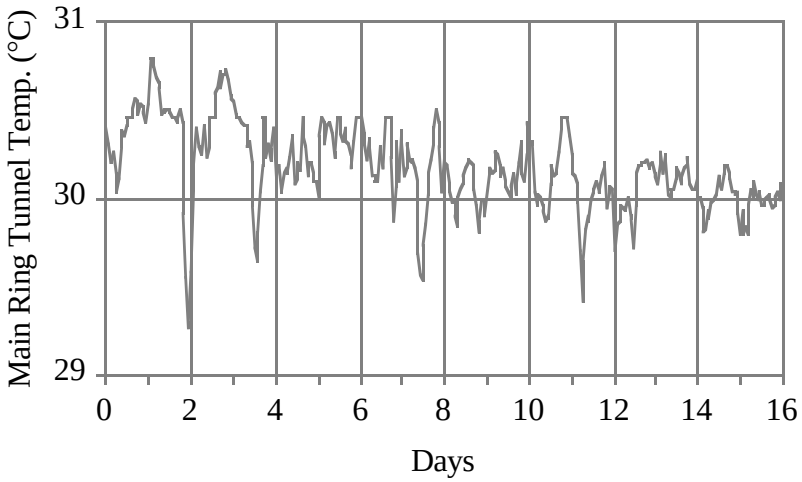

Figure 3.1.7: Measured Main Ring tunnel temperature during a typical period of operations. Note that on the second day the Main Ring was turned off for a few hour access.

The ultimate limit to the temperature range of the compensation technique is set by the nonlinearities of the opposing temperature coefficients. The ferrite material appears to be highly linear over the relevant temperature range. However, the compensator material tends to become weaker as it approaches its effective Curie temperature of approximately 55°C. Figure 3.1.8 indicates the degree of compensation achieved on a test magnet using ferrite and compensator materials from the 8 GeV line production (low bidder) vendors. Note that the maximum deviation is $\pm 1 \times 10^{-4}$ over the range 31± 7 °C.

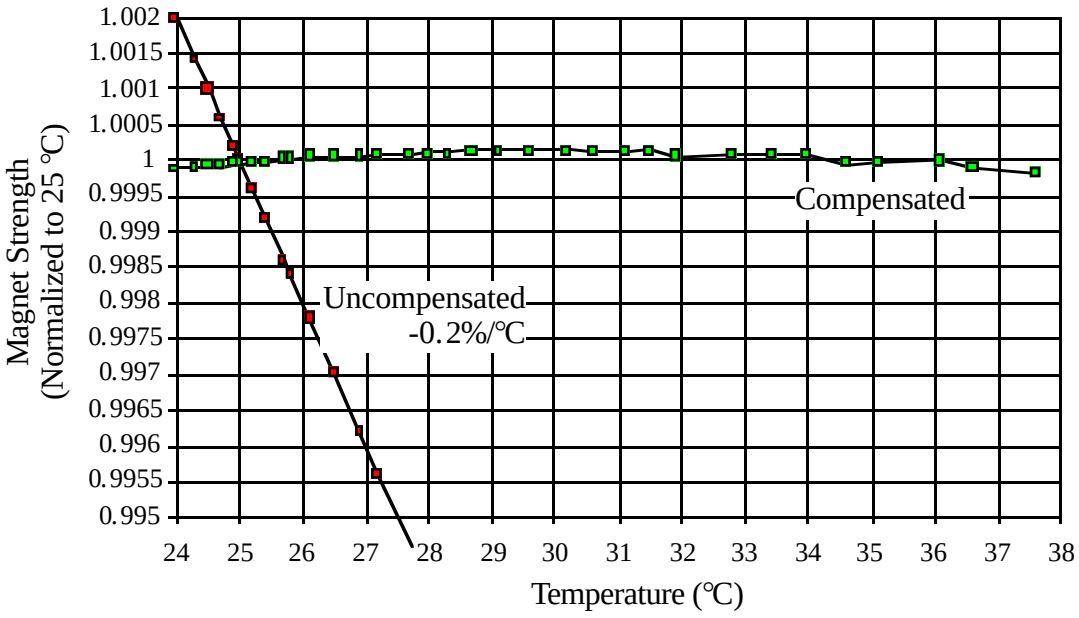

Figure 3.1.8: Field strength vs. temperature for a stability test magnet using pre-production samples from the selected vendors for compensator alloy and ferrite.

3.1.7. Magnet Assembly

The assembly sequence is as follows (see figure 3.1.3). The pole pieces are pinned and bolted to the aluminum U channel side members hold them in place to make a box structure. The bricks are placed on the back of the pole pieces, interleaved with the strips of compensator. The magnetic forces hold them in place. The top and bottom flux return plates are lowered onto the assembly using meachanical fixturing to control the operation in the presence of strong magnetic forces. The side flux returns are then moved to their places using the fixturing and bolted to the top and bottom plates. The steel end plates are installed and bolted to the flux return.

After the initial assembly each magnet's field strength and shape will be measured at the assembly facility. On the basis of this shape measurement, the steel shim pieces described below will be machined to trim the field shape as needed. In parallel the magnet will be placed in a large freezer and cooled to 0 degrees C to stabilize it against further temperature excursions (see section 3.1.9 Stabiliy Issues) during installation. On removing the magnet from the freezer the temperature and strength will be measured immediately. Assuming that the magnet is correctly compensated, the strength trimming can be determined from this measurement. After the magnet warms to room temperature, the strength will be remeasured to verify that it is correctly compensated, then the end shims will be installed and the appropriate bricks added or removed to trim the strength. A final measurement will confirm that the correction was successful and document the final configuration.

3.1.8. Field Quality

The field quality of the Recycler magnets must be adequate for a storage ring, i.e. roughly $\Delta B/B = \pm 0.01\%$ over a good-field aperture chosen to be 1.75 in. horizontal by 3.5 in. vertical, or $\pm 0.02\%$ over ± 25 mm in the performance simulations. The basic manufacturing strategy is to maintain construction tolerances of a few times 0.001 in. for the iron pole tips of the magnets, which is sufficient to achieve roughly 0.1% field defect over the aperture. The field shape is then trimmed to an accuracy of 0.01% using additional metal pieces on the ends of the magnet pole tips. This procedure is considerably simplified since only the integrated field is of interest, and the shims only have to work at a single level of excitation (no saturation effects).

3.1.9. Stability Issues

In order to address the issue of long-term stability of strontium ferrite, 10 test dipoles "stability test magnets" were built and subjected to a variety of environmental conditions which could possibly have an impact on the magnetic stability. The effects studied included varying the ferrite and compensator suppliers (most of the stability magnets were built with Hitachi bricks and Carpenter type-4 compensator), heating and cooling effects, radiation, partial demagnetization of the bricks, and simple aging.

One effect which has so far been demonstrated to have an immediate and irreversible effect on the magnet strength is cooling below 0°C. A magnet was cooled from room temperature (20°C) to 10°C, and no decrease in strength was seen when warmed back up to room temperature. However, on freezing to 0°C, the magnet lost 0.05% of its original

strength on warm-up. It was then cooled to -20 C, and it lost 0.1% of its original strength. This magnetization loss appears to be a one-time effect, provided one does not cool the magnet below the previous coldest temperature it has experienced. Thus, the magnet was cooled a second time to -20 C, and did not suffer any additional degradation in strength. This effect has been observed on two different magnets.

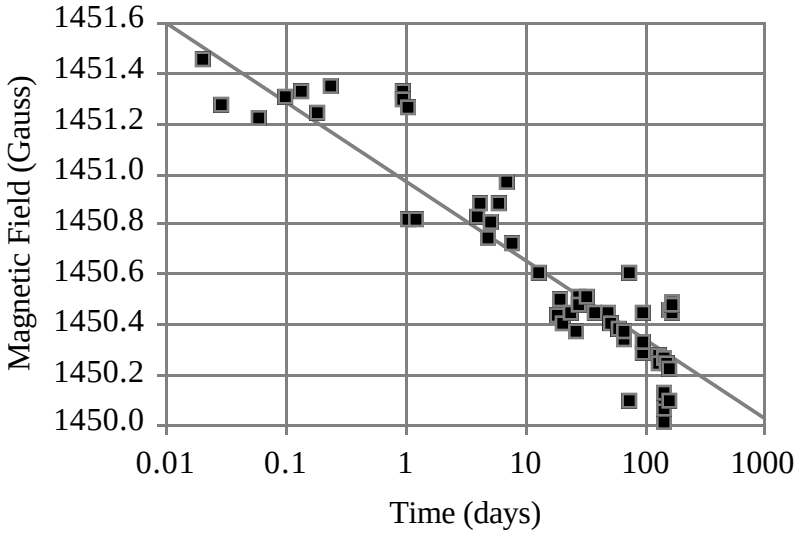

Figure 3.1.9: Field strength vs. time of a stability test magnet. Over 4 decades the data follows an expected log-time dependence. The line represents a log-time decay rate of 2.2×10^{-4}/decade.

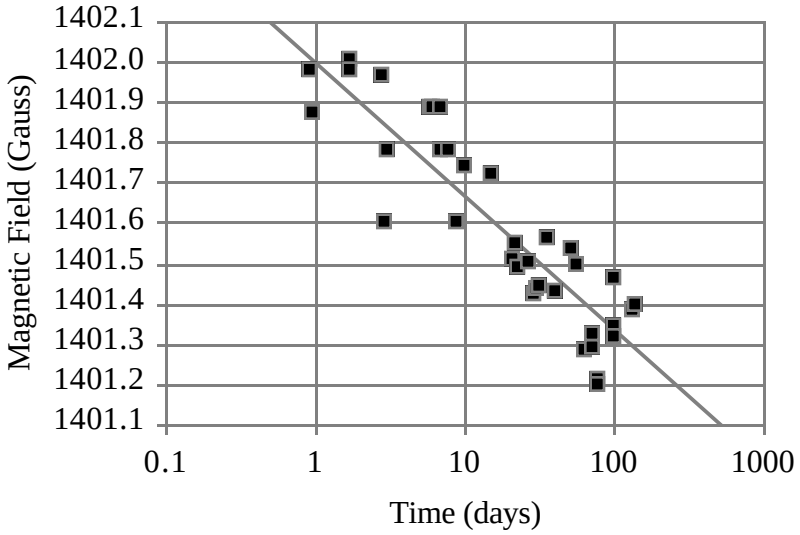

Figure 3.1.10: Field strength vs. time of a stability test magnet. This magnet was composed of bricks which were demagnetized by 5% before assembly. The line represents a log-time decay rate of 2.4×10^{-4}/decade.

Some magnets were monitored for aging by measuring their strength (at the midpoint of the aperture, using an NMR probe) as a function of time since production. The data, shown for two magnets in figures 3.1.9 and 3.1.10, is consistent with an expected log-time aging [Kronenberg & Bohlmann, J. Appl. Phys. **31**, 82S (1960); Street & Wooley, Proc. Phys. Soc. **A62**, 562 (1949)], and the present upper limit on aging derived from this data (2.5×10^{-4}/decade) corresponds to less than 0.05% of field change over a 20-year life span for the magnets. Aging at this level can be easily accommodated by changing the energy of the Booster, Main Injector, Debuncher, and Accumulator rings to match the central energy of the Recycler.

One magnet was irradiated by a source putting out approximately 0.8 Mrad/hour for 268 hours. Taking into account down time, the net average flux to the magnet was about 0.3 Mrad/hour for about 100 Mrads. The observed change in magnet field is approximately 0.5 Gauss out of 1465 Gauss, or $\sim 3 \times 10^{-4}$ which is within the range of allowed variation. No change was seen in a series of low level initial doses. In addition, mechanical disturbance such as dropping the magnet had no measurable effect above 0.3 Gauss.

One concern voiced in some project reviews was the potential for strength demagnetization of the Recycler permanent magnets due to the A.C. component of the stray fields in the tunnel from Main Injector components. A 1 m long prototype of an arc cell focusing gradient magnet was exposed to 100 magnetic field ramps generated by a Helmholtz coil. With an estimated field in excess of 10 Gauss, no observable field loss (to an accuracy of 1×10^{-5}) was observed.

Another review concern was changing of the field magnitude or shape from the 150°C in-situ bake of the vacuum system. ANSYS calculations of the bake procedure predict that the permanent magnet bricks never exceed 40°C due to thermal insulation around the beam pipe and heat transport through the aluminum and steel components out to the air. In order to verify theoretical predictions that this temperature is not harmful to the magnetic field of gradient magnets, the 1 m long prototype magnet was heated to a uniform temperature of 60°C. No field strength or quality changes were observed.

3.1.10. Magnet Measurement Requirements

A rotating coil probe has been built for measuring all of the dipole and gradient magnets for the 8 GeV and Recycler projects. This probe is a Morgan-style probe, having windings sensitive to dipole through 14-pole. It is 16 feet in length, which allows measurements of integrated strength of all the anticipated magnets. Morgan probes have the advantage of cleanly separating dipole, quadrupole, and higher-order harmonics, an essential feature for measuring gradient magnets. The probe has been tested on the two pre-production magnets, and has demonstrated the ability to meet the specified requirements of measuring the integrated strength to better than 2×10^{-4} and the harmonics to about 0.2 units (0.2 parts in 10,000 at 1 in.). An additional probe with a tangential winding geometry is being considered to improve the sensitivity to higher magnetic field multipoles.

A redundant measurement system will use a single stretched wire to scan the horizontal aperture. This device will provide a second measurement of the strength, but will also map the field shape in a region inaccessible to the Morgan coil (beyond

|x|>0.8 in.). This stretched wire system has been in use in measuring Main Injector quadrupoles.

A Hall probe measurement system to measure the central field as a function of the longitudinal position will be necessary. A similar system is used in the Main Injector dipoles. The field strength profile of the magnet as a function of distance inside the magnet must be generated with sufficient resolution to determine the bend center to approximately 0.5".

3.1.11. Field Shape Tuning

Using the two full length gradient magnets already produced for the 8 GeV line project, studies have been performed attempting to identify an algorithm for tuning the field harmonics to a level required by lattice and beam stability criterion. Because these magnets do not change in field, end packs shaped to eliminate unwanted field harmonic amplitudes are relatively simple to employ. Tests show that field deviations across the aperture as large a 0.1% can be corrected.

We now have experience with constructing identical models of full length Recycler gradient magnets. Figure 3.1.11 shows the multipole difference between two magnets built identically. Repeated measurements were performed on each magnet, and the difference RMS is shown to give one a feeling of the expected error bars on these measurements. The dominant error is in the normal gradient, which is easily tuned with end shims discussed in the next paragraph. The skew multipole differences are generated by a pole potential imbalance caused by unequal brick strengths behind the top and bottom poles (before equalization was carried out). In experiments with equalization the transfer function between brick strength and skew multipole strength has been measured. The results of these measurements scaled to the observed difference in these two magnets are also displayed. The dominant source of skew moment is this easily correctable pole potential imbalance.

As shown in figure 3.1.12, the shimming is presently accomplished by adding extra sections of gradient poles which are shaped longitudinally in order to generate the required multipole correction. These shapes are generated by measuring the field deviation in each magnet, using the measurement program to generate an input file for a computer controlled wire EDM machine, cutting a piece of normal pole piece, and then mounting the extra pole pieces (one top and one bottom) on one side of the magnet. The lower the multipole moment, the bigger a multipole correction can be made for a given average shim thickness. As can be seen in figure 3.1.11, the higher the multipole moment the smaller the multipole error which can be generated with expected fabrication imperfections.

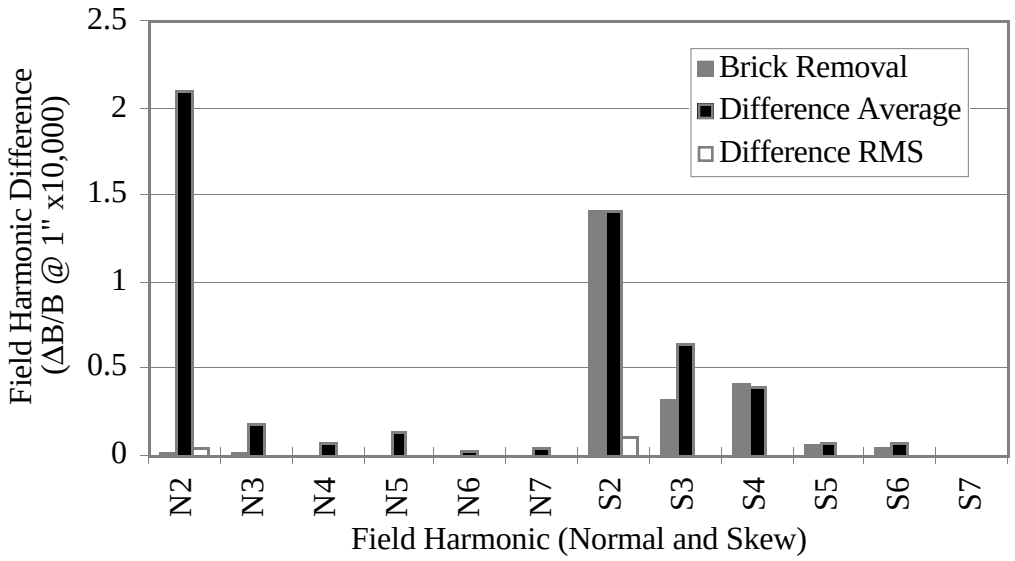

Figure 3.1.11: Difference in magnet field quality due to difference in magnet fabrication measured on two identical full length Recycler prototype gradient magnets.

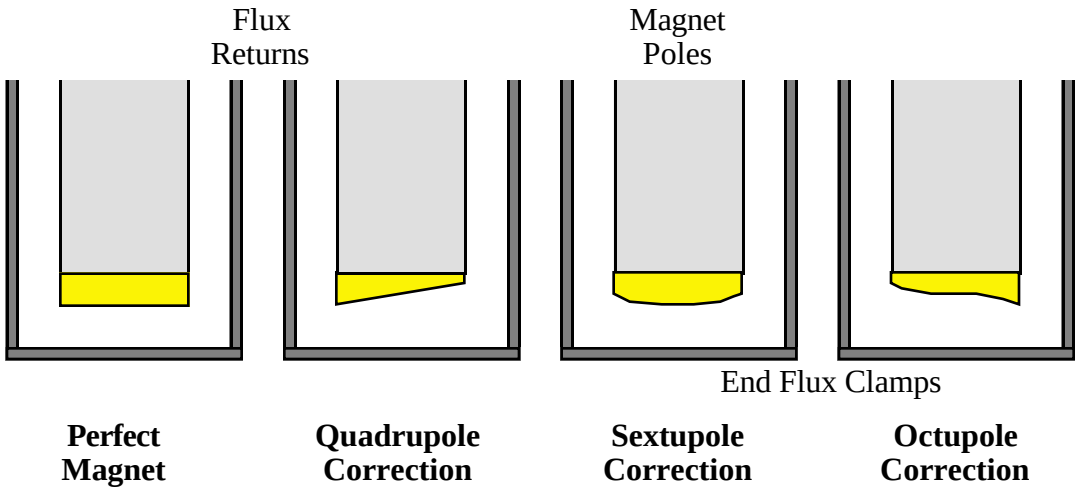

Figure 3.1.12: Sketch of the scheme used to correct any measured field shape errors. Using these prototype shapes and linear superposition, a very good correction algorithm has been generated and measured.

3.1.12. Recycler Magnet Key Performance Specifications

The table below contains the basic key specifications for the Recycler permanent magnets. These are discussed, justified, and quantified at exhaustive length in MI-Note #150. Many of the values listed in this table, such as the design lifetime, are rather arbitrary and are intended to guide engineers and technicians toward an appropriate level of care and ruggedness.

Table 3.1.10: Miscellaneous magnet performance specifications. Many of the specifications are quite far from anticipated parameter values and do not present concerns.

Design Lifetime	30 years
Operating Temperature	20°C (68°F) to 35°C (95°F)
Storage Temperature	5°C (41°F) to 50°C (120°F).
Humidity	0%-100%
Corrosion Resistance	All parts resistant, plated, or painted.
Bakeout Compatibility	Beam Pipe @ 150°C, Magnet @50°C
Temperature Stability of Field Strength	±0.05% full spread over 10-35°C
Temperature Stability of Field Shape	< ±1 unit in any multipole for ±10°C
Time Stability	$\Delta B/B < 0.05\%$/yr.
Radiation Resistance	$\Delta B/B < 1\%$ for 1E9 Rads
Shock & Vibration	$\Delta B/B < 0.1\%$ from normal handling
Radiation Activation	Comparable to steel/copper magnets
Good-Field Aperture	±1.25" at $\lvert \delta By/B_0 \rvert$ <1E-4
Dipole Vertical Aperture	2.0" between the pole tips (at X=0)
Quadrupole Pole Tip Radius	1.643" (XY = 1.350 in^2, same as MI)
Magnet Sagitta	Zero (straight magnets)
Beam Sagitta Inside Dipole	~1cm
Field Uniformity in Z	±5% (random) or better
Bend Center uncertainty	±1cm in Z (measured and surveyed)
Field Strength Modification	possible in range [+3%,-5%].
Field Shape Modification	+/- 10 units (modify end shims)
Magnetic Field in Flux Return	<1 Tesla
Magnetic Shielding of Beam Pipe	2-layer (μ-metal + iron foil)
Termination of End Fields	via Flux Clamp / End Plate of Magnets
End Fields	< 5 Gauss 2.5 cm past end of magnet
Beam Pipe Fixturing	allows ±1cm horiz. range of motion
Survey Fiducials	8 "nests" at corners of magnet
Mechanical Rigidity (sag)	< 0.020" for 25% , 75% support points

3.1.13. Permanent Magnet Quadrupoles

One type of permanent quadrupole is required for the Recycler. The standard design has the same 1.643" pole tip radius as the Main Ring/Main Injector quadrupoles. All Recycler quadrupoles are 0.5 m long. Different strengths are implemented with different brick concentrations and flux shorting shims.

The quadrupoles have a hybrid design analogous to the gradient dipole. The field shaping is provided by machined steel pole tips and the field is driven by strontium ferrite bricks. The version which is currently under fabrication for the 8 GeV line and Recycler R&D is shown in figure 3.1.13. Temperature compensation of the ferrite is provided by

interspersing strips of compensator alloy between the bricks along the length of the magnets. The overall strength of the magnet is trimmed by adjusting the amount of permanent magnet material behind each pole tip, and the field shape is trimmed by adding steel shims to the ends of the pole tips. A steel flux return shell surrounds the magnet, and "flux clamp" end plates are used to terminate the field at the ends of the magnet.

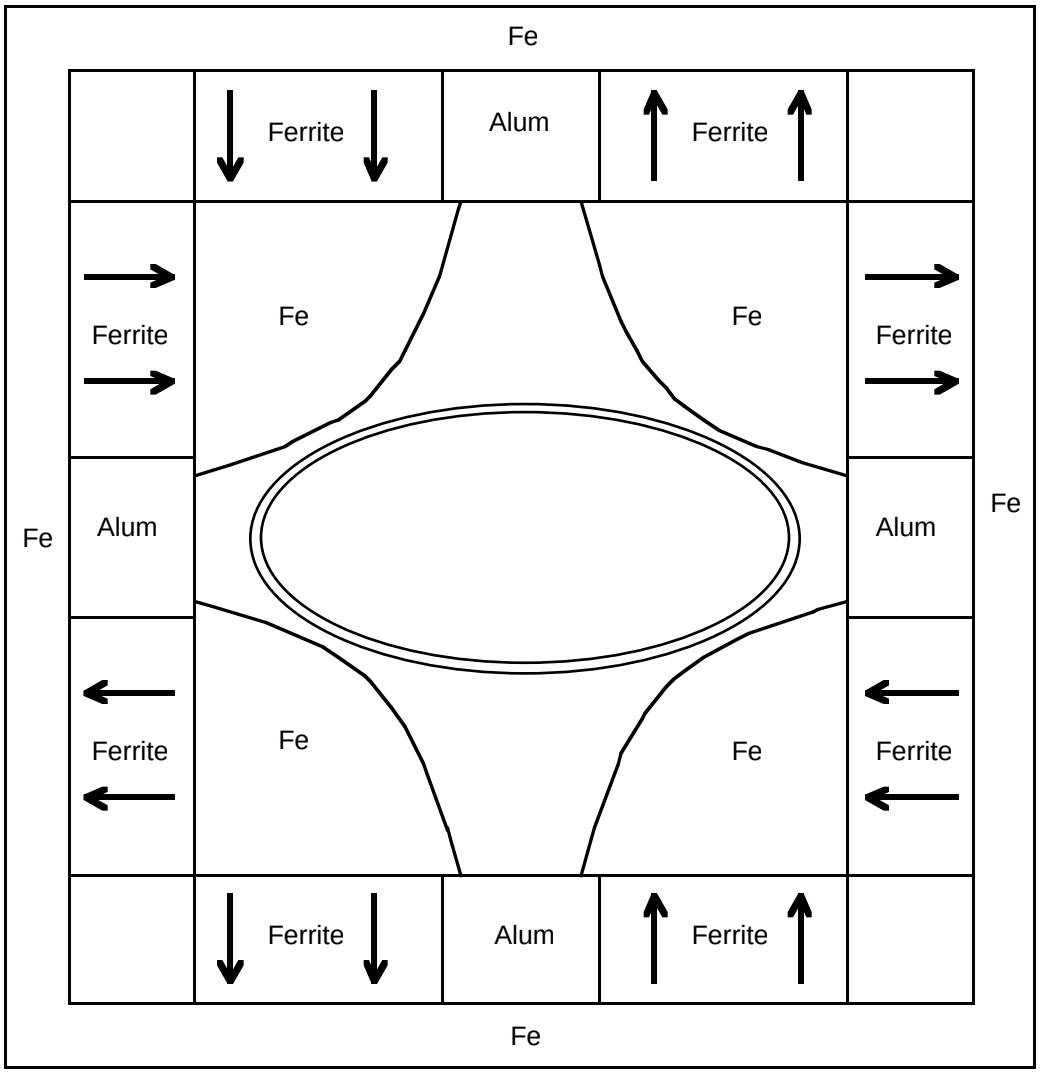

Figure 3.1.13: Cross-section of a rectangular quadrupole magnet.

3.1.14. Permanent Magnet Lambertsons

Transfer lines to and from the Recycler and 8 GeV line require a total of six Lambertson magnets. A standard design (2 kG, 3m long) has been adopted which provides a 21 mrad bend for the 8.9 GeV/c extracted or injected beam. In the typical

application the circulating beam is in the field-free region and is kicked horizontally outwards into the bend region where it is deflected upwards or downwards.

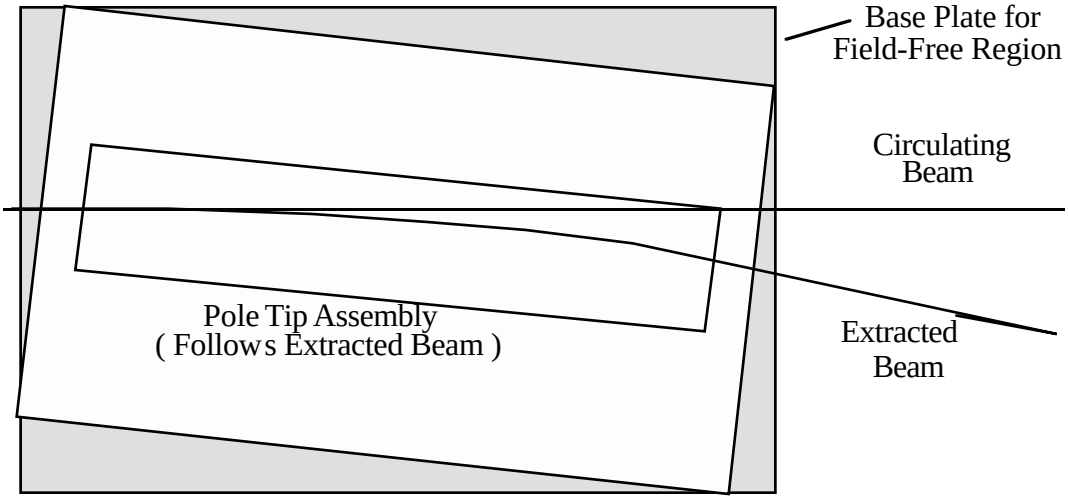

Figure 3.1.14: Side view of a Lambertson magnet showing the stored and extracted beam trajectories, and the slant in the extraction channel to minimize sagitta effects.

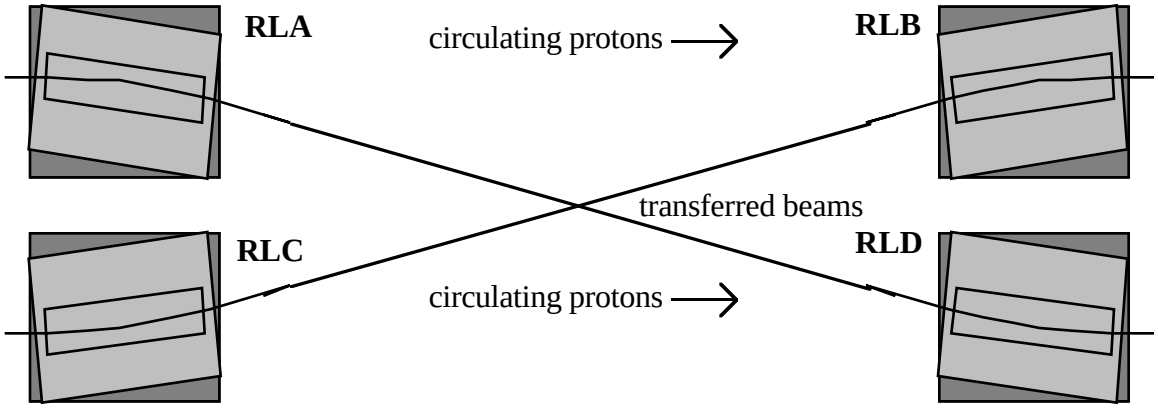

Figure 3.1.15: Lambertson construction geometries required to service all of the beam transfer needs of the Recycler.

To minimize sagitta and economize on magnet aperture, the pole tip assembly for the bend region follows (to first order) the trajectory of the deflected beam. The pole tip is therefore not parallel to the field-free trajectory, but is offset and canted by 1/2 of the bend angle or approximately 10 mrad. See fig. below. This is easily accomplished since the cutout of the field free region is machined out of the solid plates used to piece together the "base plate" of the Lambertson. See figure 3.1.14 for a sketch of the Lambertson geometry.

Two polarities of permanent-magnet Lambertsons are required: one which deflects counterclockwise protons (and clockwise antiprotons) downwards, and one which deflects them upwards. For each polarity there are two possible orientations of the "base

plate" containing the field-free cutout: one which deflects incoming beam from the left, and another from the right. Figure 3.1.15 summarizes these options.

Two successful prototype permanent Lambertsons (2.2 kG and 3.55 kG, each 1m long) have been produced and tested. The bend field uniformity was adequate and the average field in the "field-free" region was <0.5 Gauss. The cross-sectional view of the permanent Lambertson is shown in figure 3.1.16.

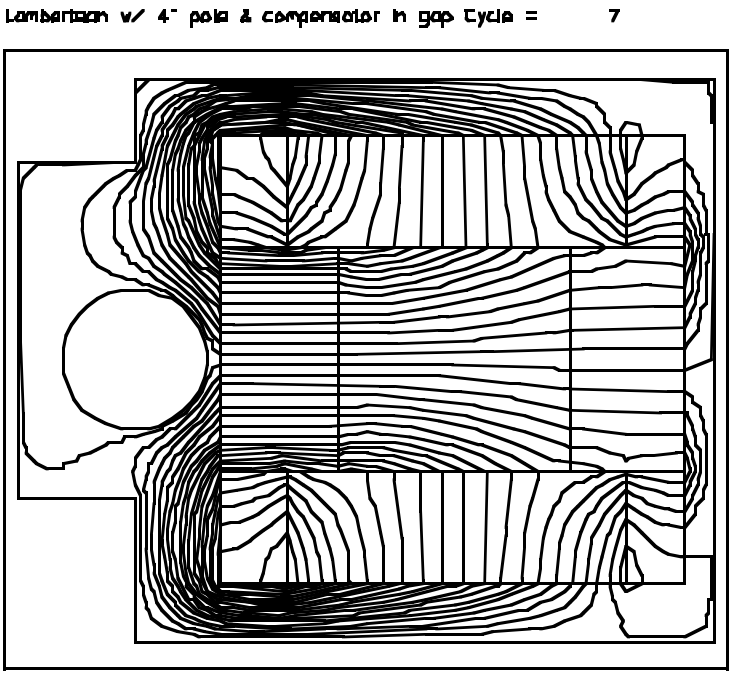

Figure 3.1.16: Permanent Lambertson magnet cross-section with POISSON field map superimposed. The field free circular region is the circulating beam aperture. The horizontal field in the extracted beam line steers the beam up or down. Three bricks drive flux into the central solid pole piece, one from the back and one from each side (top and bottom in the figure).

3.1.16: Magnet Hangers and Installation

The hangers and installation for the Recycler are presently being modeled within the permanent magnet 8 GeV line project. It is expected that the magnets will be cheaper and easier to install than their Main Injector counterparts. For instance, each gradient dipole weighs approximately 1 ton, as compared to 20 tons in the Main Injector. The cross-section of the magnets are much smaller, and the magnets are shorter. The quadrupoles are expected to weigh approximately 200 lbs. each.

In most locations around the ring it is expected that the hangers will be bolted to the unistrut sections welded to the iron bars captured in the concrete tunnel walls. In a few locations where the tunnel shape changes or where Main Injector transfer lines to the Booster, Accumulator, and Tevatron exist, it will be necessary to build some more elaborate hangers.

3.2. Vacuum (WBS 3.1.2)

There are 104 cells in the Recycler ring. Because of the low outgassing rates accessible with the hydrogen degassing technique described in chapter 2, a vacuum pressure two orders of magnitude lower than the Main Injector can be achieved with the same number of pumps. In this discussion the type, placement, and processing of Recycler ring vacuum components are reviewed.

3.2.1. Geometry Overview

In the Main Injector there are 6 ion pumps per cell and the length of vacuum sectors is approximately 500' (150 m). In the Recycler there will be one ion pump per cell, for a total of 104 ion pumps. Between the ion pumps there will be 5 titanium sublimation pumps (TSPs) per cell to achieve an average of pressure of approximately 1×10^{-10} Torr. The benefit of TSPs are lower cost and lower ultimate pressures. Since the length of normal cells is 34 m and the length of dispersion cells is 26 m, the longest vacuum sector possible if the isolation valves are spaced every 8 cells apart is 270 m. Therefore, the total number of sector valves is $104 \div 8 = 26$. Figures 3.2.1 through 3.2.3 contain sketches of the vacuum system in normal arc cells, straight section cells, and dispersion suppression arc cells.

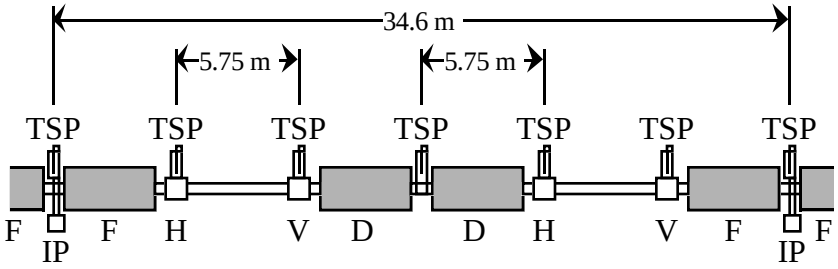

Figure 3.2.1: Sketch of the vacuum system in a normal arc cell. The horizontal (H) and vertical (V) beam position monitors have attached to them titanium sublimation pumps (TSP) in order to maintain a low average pressure and to minimize the number of welds in the tunnel.

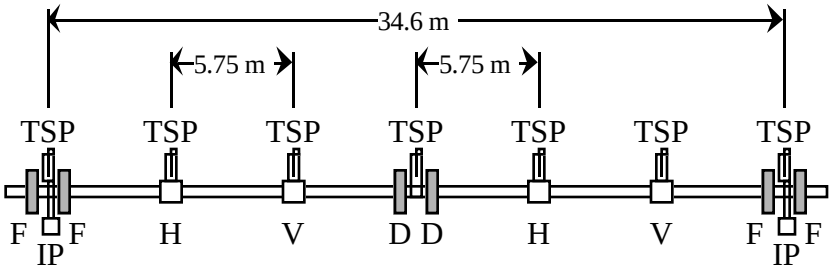

Figure 3.2.2: Sketch of the vacuum system in a normal straight section cell. Except for the fact that the quadrupoles are much shorter than the gradient magnets in the normal arc cell, nothing is different with respect to figure 3.2.1.

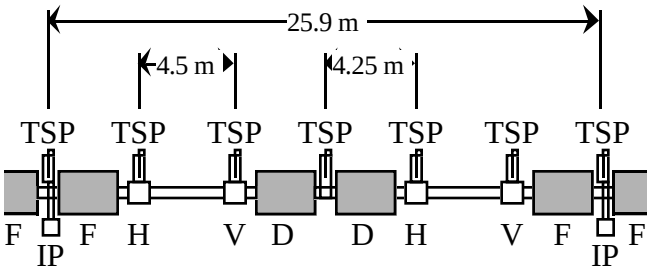

Figure 3.2.3: Sketch of the vacuum system in a dispersion suppresser cell.

With the exception of the MI-60 phase trombone straight cells which need additional vertical aperture and hence a round 3" O.D. beam tube, the Recycler vacuum tube is a 1.75" inside height by 3.75" inside width ellipse. It is produced by crushing a standard 3" O.D. beam tube with a wall thickness of 0.065".

3.2.2. Beam Position Monitor Assemblies

In order to minimize the cost of the vacuum system, it is necessary to minimize the number of welds in the tunnel. This means generating as many pre-fabricated assemblies in industry and staging areas as possible. In addition, if possible it is good to merge multiple functionalities into the same component. For instance, the beam position monitor (BPM) can also act as an ion clearing electrode. Another possibility which will depend on further surface physics research by personnel at FNAL, LBNL, and KEK is the use of titanium electrodes in order to get ion pumping from the BPM electrodes.

Because both protons and antiprotons are injected into the Recycler for operations, commissioning, and studies, the beam position monitors need to be bi-directional. Capacitive split-tube electrodes are optimum in a geometry where the transverse beam size is comparable to the electrode dimensions. Capacitive electrodes are also perfect for the creation of ion clearing electrodes. In order to minimize the impedance effects of the BPMs, the electrodes are shaped to match the vacuum chamber, the outer wall of the BPM is the same shape as the electrodes and only large enough to stand off the 700 V of ion clearing voltage. For the same reasons, the gaps between the electrodes and the vacuum chamber wall are as small as possible without compromising the capacitance (and hence sensitivity) of the electrodes.

As can bee seen in figures 3.2.1 through 3.2.3, in every Recycler half cell there are always two BPMs separated by a straight, unoccupied section of vacuum pipe. At each of these BPM locations a bellow is required to absorb the length increase which occurs in the vacuum system when it is insitu baked at 150°C. In order to simply the beam pipe positioning stands and installation, the bellows are always located to the outside of both BPMs. As shown in figure 3.2.4, between the BPMs and bellows are TSPs. The TSP port is a rectangular slot 4" long and 1" high centered on the horizontal edge of the chamber (see figure 3.2.5). The horizontal edge of the vacuum chamber supports the minimum of the image current distribution, so therefore this geometry has the lowest impedance impact while simultaneously maximizing the conductance to the pump itself.

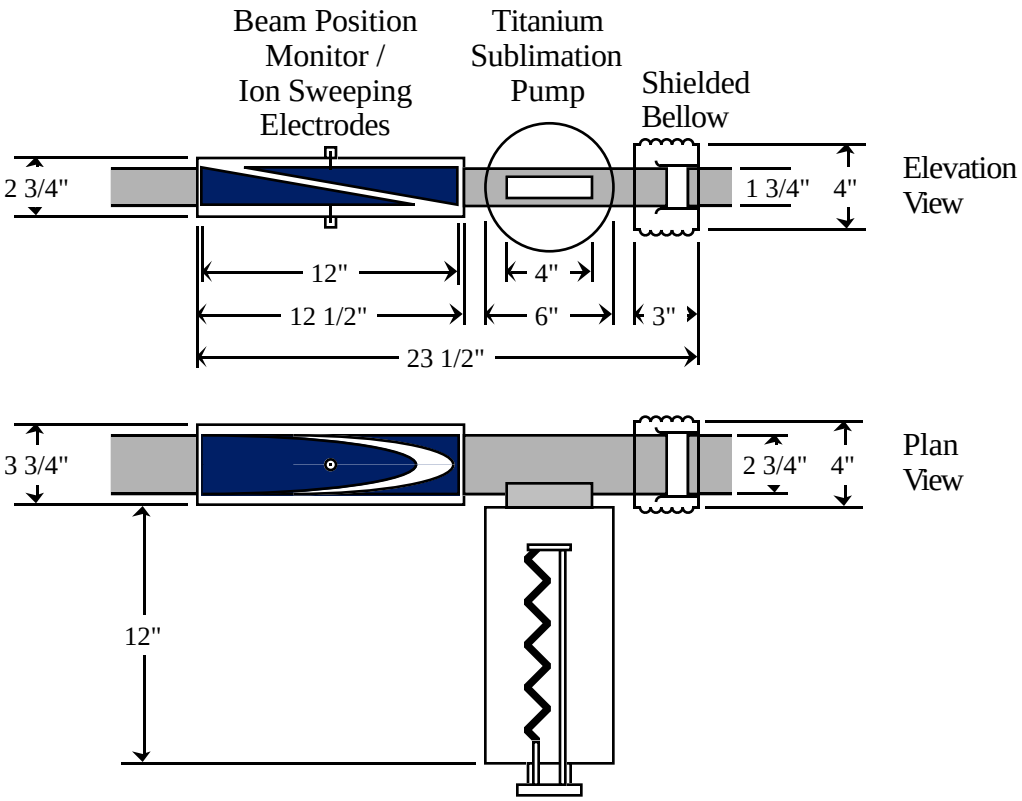

Figure 3.2.4: Elevation and plan views of the BPM assemblies which each include a TSP and shielded bellows. A vertical BPM is shown, which is on the downstream side of each half cell. The horizontal BPM, which is placed on the upstream side of each half cell, has a horizontally sensitive electrode and the entire assembly is rotated left for right.

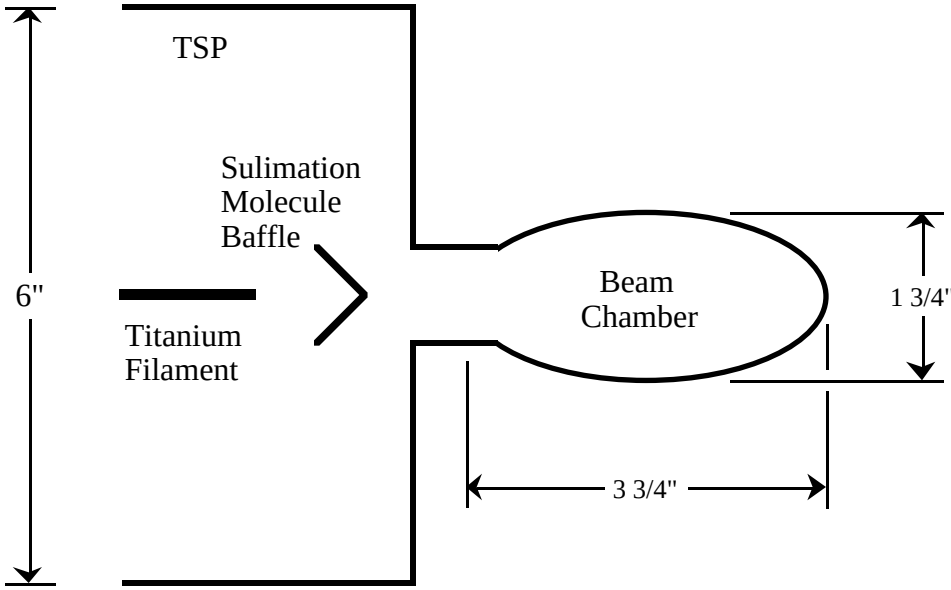

Figure 3.2.5: Beam's eye cross-section view of the TSP and its connection to the beam tube.

3.2.3: Hydrogen Degassing Oven

Before the hydrogen degassing is performed, the tubing is washed and cleaned internally with solvents. The tubing is then sent over to a former superconducting coil collar hydraulic press used for crushing the pipe into the correct elliptical shape. The design profile has an inner full height of 1.75 in. and a full width of 3.75 in.

In order to achieve this vacuum system configuration and achieve an average vacuum of approximately $1x10^{-10}$ Torr, it is necessary to hydrogen degas every component. The test oven shown in figure 3.2.6 will be used for specialty pieces such as 1.5" diameter tubing for gauges. The 3" diameter tubing used to generate the vacuum chamber itself needs to be processed at a rate of approximately one half cell per day in order to keep up with the projected rate of magnet production. This criterion requires three 20' pipes per day. As shown in figure 3.2.7, by creating a new oven which has a 12" diameter, a total of six pipes per day could be processed. Since the processing requires that the tubing stay at a temperature of 500°C for approximately 12 hours (or 900°C for 30 minutes for those who prefer the higher temperature approach) and the time constant of the heating and cooling is approximately 4 hours, one batch of six pipes per day is a convenient processing rate. This requires that a technician spend approximately 1 hour per day to empty the previous day's tubing, clean the oven, load the next batch, and then start the control system computer which automatically performs the processing.

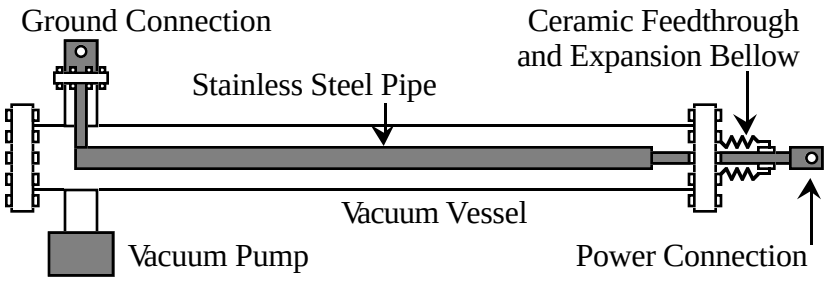

Figure 3.2.6: Sketch of the test oven which will still be used to process specialty tubing.

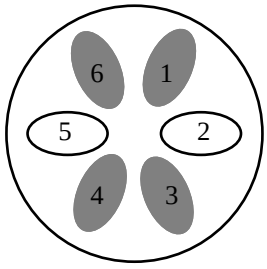

Figure 3.2.7: Profile of the crushed 3" tubing in the 12" diameter production oven proposed to generate an average of 2 half cells of tubing per day.

It is also necessary to hydrogen degas the tubing which makes up the beam position monitors, the titanium sublimation pumps, and also the shielded bellows. The split-plate capacitive pickups are created with the same 3" diameter tubing that makes up the rest of the vacuum system, unless the titanium electrode option is utilized. The 4.5" diameter tubing which forms the vacuum wall around the pickup electrodes, the 6" diameter tubing for the titanium sublimation pumps, and the bellows themselves are all hydrogen degassed before assembly. After the monitor, pump, and bellow has been assembled they are again baked to 500°C in order to burn off any surface hydrocarbons from the forming and assembly of the monitor, while simultaneously hydrogen degassing all of the miscellaneous steel parts such as end plates.

3.2.4. Shielded Bellows

As shown in figure 3.2.4, associated with each BPM there is a bellow assembly. The bellows are shielded in a manner identical to the Main Injector. The reason for so many bellows is the 150°C bakeout which is necessary for initial vacuum commissioning. The coefficient of elongation of stainless steel tubing is 16 μm/m-°C. A normal half cell is 17 m long. Therefore, the 120°C temperature rise associated with the in-situ bake leads to a change in length of the beam tube of 33 mm or 1.25". Given that bakes are not expected to occur very often, a compression ratio of 2:1 is acceptable. Therefore, each half cell needs at least 2.5" of uncompressed bellow. Therefore, 2" of bellow at the horizontal BPM and 2" of bellow at the vertical BPM generate more than enough temperature change capacity. The other purpose of the bellows is to absorb approximately 0.5° of bend per bellow, since the pipe segments are straight.

3.2.5. Insitu Bake System

After installation of the vacuum system it is necessary to heat it to 150°C for approximately 24 hours in order to purge the system of water vapor. But the entire 3.3 km circumference of the Recycler cannot be baked simultaneously. Instead, each vacuum sector is baked independently. As stated earlier, each vacuum sector is composed of 8 cells, or 16 half-cells.

The vacuum system is heated with the use of a pair of coaxial heaters. The coaxial geometry is used because of measurements performed on the 1 m long Recycler prototype gradient magnet where a DC 50 Amp current caused a 16×10^{-4} field relative field deviation across the magnet aperture. By using a coaxial geometry, it can be assured that no field change will occur due to leakage fields from the heater conductors.

The thermal insulation around the vacuum chamber is integrated with the magnetic shielding around the chamber. As part of this system, there are 2 layers of insulation. In addition, the shining surface finish of the magnetic shielding also reflects back some heat.

In order for this scenario to work, a couple of conditions must be observed. First, the magnetic shielding around the beam pipe discussed in the next section must be electrically insulated from the beam pipe. Second, in order to evenly heat the vacuum chamber it is necessary to put in flexible copper ground straps across bellows to act as current bypasses. Thermal conduction through the stainless steel tubing is sufficient to heat the bellows.

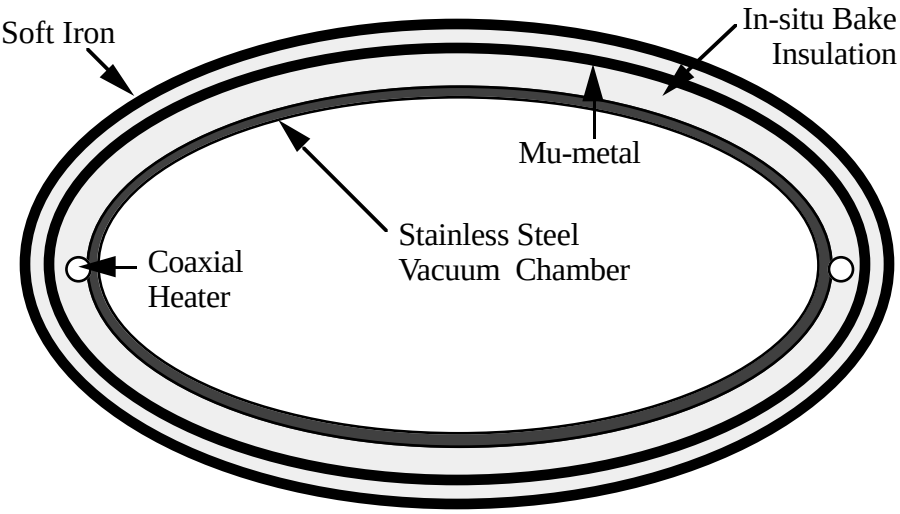

Figure 3.2.8: Sketch of the portable power supply connected across a vacuum sector used to heat the vacuum system to 150°C.

3.2.6. Magnetic Shielding

Figure 3.2.8 contains a sketch of the magnetic shielding around the beam pipe at the edge of a permanent magnet. In order to prevent the Recycler beam from reacting to the Main Injector ramp, a hermetic magnetic seal around the Recycler vacuum chamber is required. In order to achieve a magnetic field reduction factor of 1000x, a layer of 4 mil thick mu-metal inside a 6 mil thick layer of soft iron is employed.

Between the vacuum chamber and mu-metal, and between the mu-metal and soft iron, are layers of thermal insulation. Not only is this insulation needed for the insitu bake system, but it is necessary to keep the mu-metal and soft iron from coming into contact in order to get the full magnetic field attenuation effect.

3.2.7. Beam Pipe Hangers

It is necessary to build hangers specifically for the vacuum system due to the long distances between the magnets. The magnets themselves act as vacuum chamber hangers. In the center of the long sections between magnets the vacuum chamber hanger holds the pipe in a fixed position. During bakes the vacuum chamber lengthens toward the bellows near the beam position monitors. The hangers connected to these monitors have sliding joints which allow this expansion. Similarly, the pipe can slide within the magnets, but is held fixed at the end of the magnets at the 1 m short straights between the magnets. Figure 3.2.8 contains a sketch of this geometry.

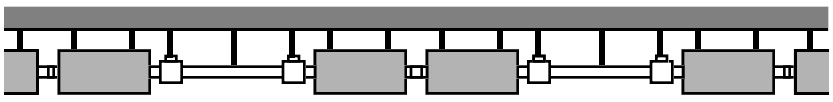

Figure 3.2.8: Magnet and vacuum chamber hangers for a normal cell. Note that the magnets themselves also act as vacuum chamber stands.

3.3. Power Supplies (WBS 3.1.3)

A total of 48 dipole correctors are needed in the Recycler ring and its dedicated transfer lines. The power supplies for these dipole correctors are only for limited orbit control around each of the 3 Lambertsons at MI-30 and MI-40 and their associated transfer lines. In addition, correctors are also needed at the kicker at MI-20. In order to generate an arbitrary position and angle in each plane, 8 dipole channels are required at each Lambertson in the Recycler. In addition, 4 horizontal and 4 vertical dipoles each separated by 90° of phase advance are necessary at each transfer line to adjust the position and angle into/out of the line. See figure 3.3.1 for a sketch of the locations of these correctors. At 6 Amps per channel and using the Main Ring corrector magnets, a deflection of 0.5 mr is achievable. Applied near a beta function maximum of approximately 50 m, a closed orbit motion of 25 mm is possible. Vertically this exceeds the 7/8" half height of the elliptical vacuum tube. The half width of the beam tube is just under 1-7/8", so only half the horizontal aperture can be probed by the beam center.

These power supplies are already existing Main Ring "ramped corrector" controllers which are not going to be used in the Main Injector. The correction magnets will also come from the Main Ring.

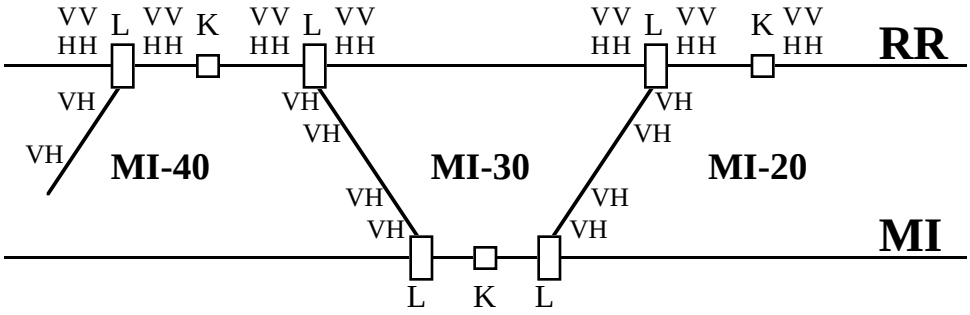

Figure 3.3.1: Locations of the horizontal (H) and vertical (V) dipole correctors in relationship with the kickers (K) and Lambertsons (L) required for the Recycler ring.

The ramped corrector power supplies are also used for three other powered magnet applications. The most important in the MI-60 phase trombone. Between each of the quadrupole pairs at MI-60 (and between the end quadrupoles and their partnered dispersion suppresser gradient magnets) a Main Ring correction quadrupole is installed. These 9 quadrupoles have enough strength to implement a phase trombone with a tuning range of greater than ±0.1 tune units.

Also at MI-60 two skew quadrupoles from the Main Ring will be transfered to the Recycler in order to implement global decoupling tuning. Because there are 6 corrector channels per chasis and the phase trombone only uses nine, the two skew quadrupoles will be plugged into the spare chassis channels.

Finally, 24 Main Ring sextupoles will be installed in the Recycler and powered individually with ramped corrector channels. At MI-20 and MI-50 two chassis each will be installed. In each pair of chassis 8 channels are dedicated to defocusing sextupoles

and 4 are dedicated to focusing sextupoles. In all of the above applications the 6 Amp output of the ramped corrector power supplies is sufficient.

3.4. RF Systems (WBS 3.1.4)

The Recycler RF system is both very simple and highly complex. Because the Recycler ring is fixed energy, coordinated control of voltage, synchronous phase, radial position, tuning angle, cavity resonant frequency, grid bias, etc. is not necessary. On the other hand, the barrier bucket manipulations outlined in chapter 2 represent a quantum leap in phase agility and computer control.

3.4.1. High Level System

The RF cavities for the Recycler acceleration system are actually 50Ω ceramic gaps which have sufficient inductance to pass frequencies above 10 kHz. Four of these cavities are used to generate the needed peak voltage of 2 kV.

Connected to each of these cavities is a 5 kW amplifier and a gap monitor signal which feeds back into the feedback system which insures fidelity to the programmed waveform and suppression of beam loading voltages. The amplifiers have a highpass cutoff frequency of 10 kHz and a lowpass cutoff frequency of 100 MHz. All of the amplifier feedback electronics and control electronics are in the MI-60 service building.

3.4.2. Low Level System

Most of the hardware, firmware, and software necessary for the Recycler RF system is already being generated for the Main Injector RF system. Therefore, the estimation of manpower and hardware do not represent as large a level of extrapolation as might be expected.

The system revolves around a very advanced direct digital synthesizer VME module which allows computer coordinated frequency changes which are phase continuous. By programming frequency ramps, arbitrary relative phases can be generated between neighboring synthesizers. Since all synthesizers run off of the same clock, frequency synchronization is a digital control with no phase lock loops or feedback systems necessary. By sending this 52.8 MHz sinusoid through a comparator and a divide by 588 counter, a turn marker can be generated which is extremely phase agile. By sending that pulse into a module which under computer control generates a pulse of arbitrary length and height, the full capability of the RF system described in chapter 2 is realized.

The Direct Digital Synthesizer (DDS) VXI LLRF platform component offers performance improvement and new implementation options for transfer synchronization. The DDS includes an AD21062 SHARC DSP, Harris Numerically Controlled Oscillators (NCO), and RF parts for SSB modulation. The DDS has three RF outputs; $RF_1=A\sin(\omega t+\Phi_1)$, $RF_2=A\sin(\omega t+\Phi_2)$, and $RF_3=A\sin(\omega t+\Phi_3)$. Under DSP control, the outputs are frequency and phase agile, with controlled Φ_n and its first through third derivatives. The ωt term is determined from a 720 Hz MDAT input, filtered, and updated at 100 kHz identically for all RF outputs. The DSP updates Φ_n with 16.66 kHz and 100 kHz components that include absolute and relative phase terms. Φ_n registers also sum a $\Delta\Phi_n$ term for phase control at precise rates. This specifies cogging processes

directly in the fundamental unit of interest, instead of the present cogging system's $\Delta\Phi_{cog} = \int\Delta\Phi\ dt$, taken over the cogging interval.

For the Recycler, two DDS modules are employed in parallel to generate six independent phase-variable waveforms which can be used to generate and manipulate barrier buckets. Figure 3.4.1 contains a block diagram of this system. All six waveforms are created by sending the DDS channel sine waves into comparators which generate pulses at 52.8 MHz. The divide-by-588 circuit generates a single pulse each turn, which in itself triggers an arbitrary waveform generator. All six waveforms are then summed before being delivered to the high level RF system.

Unlike the Main Injector, the Recycler store beams for long periods of time. Therefore, an added constraint for Recycler operations is that the phase and amplitude noise of the pulses be very small. Measurements of the spectral purity of the output of the comparator are very promising.

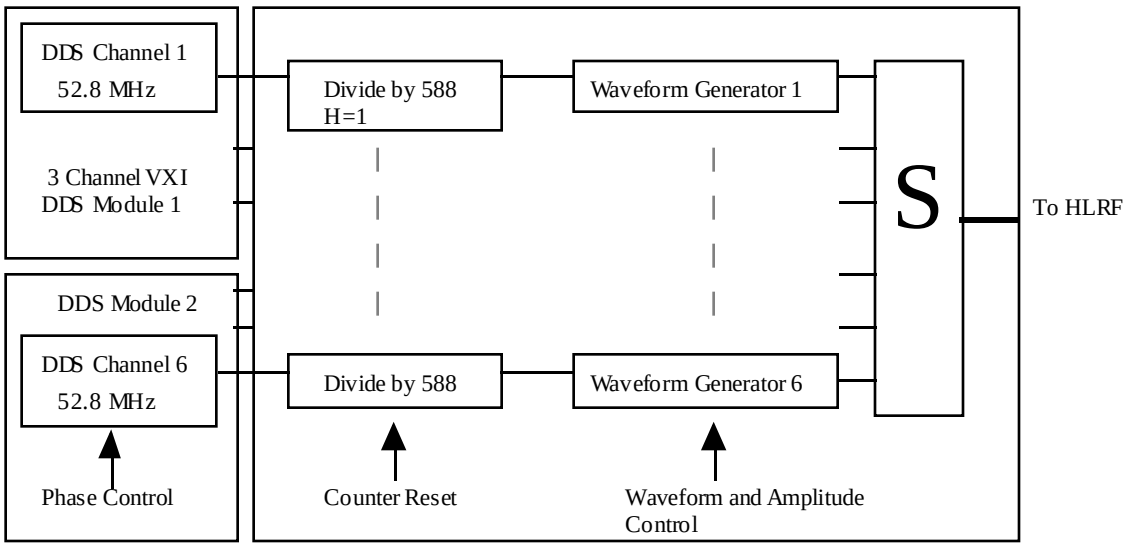

Figure 3.4.1: Block diagram of the Recycler low-level RF system.

3.6. Kickers (WBS 3.1.6)

The specifications for the kicker magnets needed for Recycler operations are listed in table 3.6.1. In order to keep costs low, the kicker in the Recycler ring should build on the Main Injector design experience as much as possible.

Table 3.6.1: Specifications for the Recycler magnet kickers and the transfer kicker in the Main Injector for injection/extraction with respect to the Recycler.

Location	Direction	Kick	Risetime	Falltime	Flattop	Recharge
RR-20	Horz	300 G-m	1-2 μs	1-2 μs	1.6 μs	10 sec
MI-30	Horz	300 G-m	1-2 ns	1-2 μs	1.6 μs	10 sec
RR-40	Horz	300 G-m	1-2 μs	1-2 μs	1.6 μs	10 sec

A design which comfortably attains the specifications has been produced. Parts from old Main Ring systems and the production of systems similar enough to the Main Injector to share spare capacity have been designed. No unusual technology was invoked to reach the above parameters.

3.7. Stochastic Cooling (WBS 3.1.7)

There are 4 stochastic cooling systems envisioned for the Recycler ring. The two transverse systems are 2-4 GHz bandwidth betatron cooling systems. Providing momentum cooling are a pair of systems; a 1-2 GHz and 0.5-1 GHz filter cooling system.

3.7.1. Pickup and Kicker Placement

As shown in figure 3.7.1, an amplitude modulated laser beam is used to cut a chord across a potion of the ring to transmit the signals from the pickups to the kickers. The laser beams should propagate down evacuated tubes in order to prevent excessive laser attenuation during periods of poor weather. Another benefit of laser propagation through an evacuated tube is the insensitivity of time-of-flight to humidity and air pressure changes.

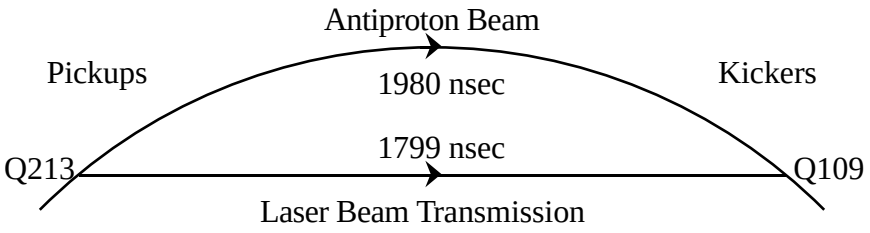

Figure 3.7.1: The chord cut by the stochastic cooling systems in order to minimize the bad mixing between the pickup and kicker.

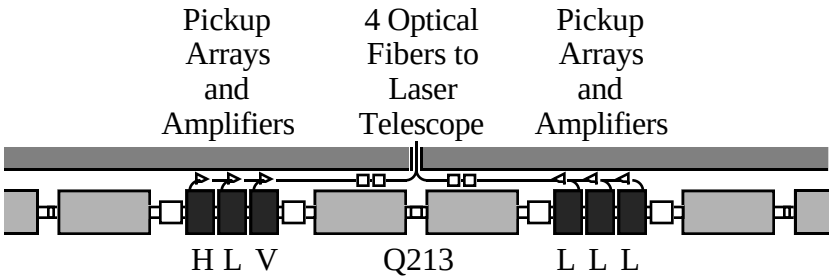

Figure 3.7.2: The relative placement of the horizontal (H), vertical (V), and momentum (L) pickup tanks with respect to the magnets. Note that the pre-amplifiers are attached to the tanks, while the laser driver for the optical fiber signal transmission are placed over the permanent magnets in order to obtain some radiation shielding from Main Injector losses.

The placement of the pickup tanks around Q213 is shown in figure 3.7.2. The pre-amplifiers are attached to the pickup tanks, while the power amplifiers and optical fiber transmitters are placed over the permanent gradient magnets for radiation shielding against Main Injector losses. At Q109 the relative tank placements are identical, and the fiber optic receiver and power amplifiers are again over permanent gradient magnets. The final power amplifiers, planned to be travelling wave tubes (TWTs), are attached to the kicker tanks themselves.

3.7.2. Arrays and Tanks

The number of pickup and kicker tanks and pickup and kicker electrodes are listed in table 3.7.1. As the frequency of the system increases, the size of the electrodes and their spacing along the beam shrink. Therefore, the higher frequency systems have a higher longitudinal density of electrodes.

Table 3.7.1: Number of pickup and kicker tanks and electrodes required to fulfill the cooling requirements outlined in chapter 2.

Plane	Band (GHz)	Pickup Tanks	Kicker Tanks	Pickup Electrodes	Kicker Electrodes
Horz	2-4	1	1	32	32
Vert	2-4	1	1	32	32
Mom	1-2	2	2	32	32
Mom	0.5-1	2	2	16	16
	Total	6	6		

The standard length of a tank is 48". A typical array is 1 m long. Therefore, only three tanks per half cell fit into an unmodified section of Recycler lattice.

3.7.3. Laser Telescope

The laser telescope is composed of two passive elements per beam, each pair on either side of the telescope. First, in order to minimize the laser beam divergence the beam radius is increased via large aperture telescope lens systems at either end of the evacuated tubes. With a 20:1 expansion ratio, the laser beam can be as large as 2" in diameter. Second, the transitions of the laser light from fiber optic cable to air and back are accomplished with a light launcher composed of a polished fiber end coupled to a point-to-parallel collimating lens.

As shown in figure 3.7.3, there are also X-Y micro-positioning stages to move the light launcher transversely with respect to the beam expander and to steer the entire beam in either dimension. These stages are operated via remote control and/or feedback loops to set and maintain a high quality optical link across the arc of the Recycler.

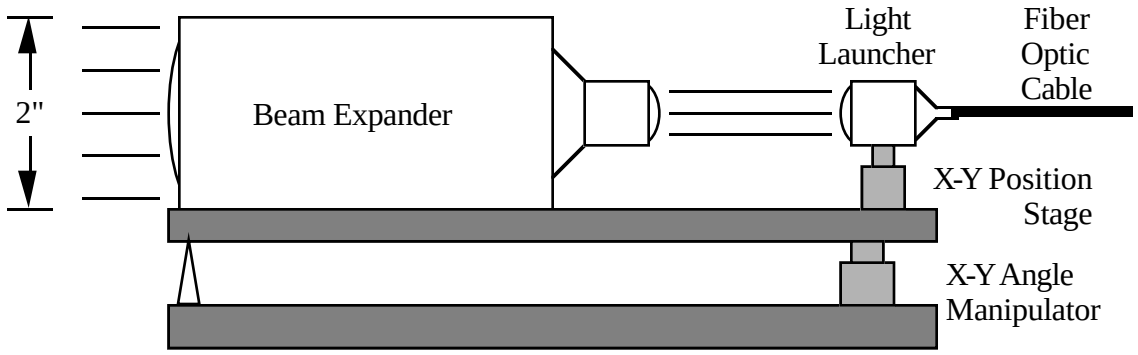

Figure 3.7.3: Sketch of the optics involved in the laser telescope. The passive optical hardware is identical on both sides of the telescope.

3.8. Instrumentation (WBS 3.1.8)

The Recycler Ring instrumentation will closely resemble much of the Main Injector instrumentation. The beamline intensity monitors and both the longitudinal and transverse wideband detectors will be identical. Some changes will occur in the transverse Schottky system to take advantage of the stationary revolution frequency of the Recycler. A commercial beam current measurement system will be purchased. Due to costs and unusual beam signals, the beam position monitor system is very unique.

3.8.1. Beam Position Monitor System

The BPM (Beam Position Monitor) detectors will be used for both position information and ion clearing. In the Recycler ring 416 detectors located at the 1/3 and 2/3 boundaries of each half cell will provide 8 detectors per betatron wavelength in both the horizontal and vertical planes. Split-plate detectors will provide output linear with displacement in one plane at a time. Three flavors of detector will be required: one horizontal and one vertical elliptical detector, covering most of the ring; and one round detector, rotated to measure the desired plane. Detector edges will be rounded to prevent arcing of the ion-clearing high voltage.

The BPM system will have two measurement modes. The first measures injected beam from the Booster or Main Injector, while the second measures the closed orbit of the stack. The beam stack in the Recycler will be DC beam, except for an injection gap equal to 1/7th of the circumference. For both modes, the resulting harmonics of the 89.8 kHz revolution frequency lead to an AC-coupled pulse for low frequency processing.

The low and medium frequency response of the detector resembles that of a highpass filter. The low frequency corner is inversely proportional to both the terminating resistance and the system capacitance. For long cable runs terminated in high impedance, sensitivity is inversely proportional to the cable capacitance. These two factors dictate the use of high-impedance pre-amplifier buffers in the tunnel. A series resistance before the pre-amp reduces the system bandwidth and noise. The radiation resistance of possible pre-amp candidates is being tested in the Booster dump. Manufacturer testing [Analog Devices, Inc., Radtest Data Service, November 1995] claims radiation resistances of 25-

50 and 200 kRad for two possible chips. Other possibilities, including discrete transistors, are being considered.

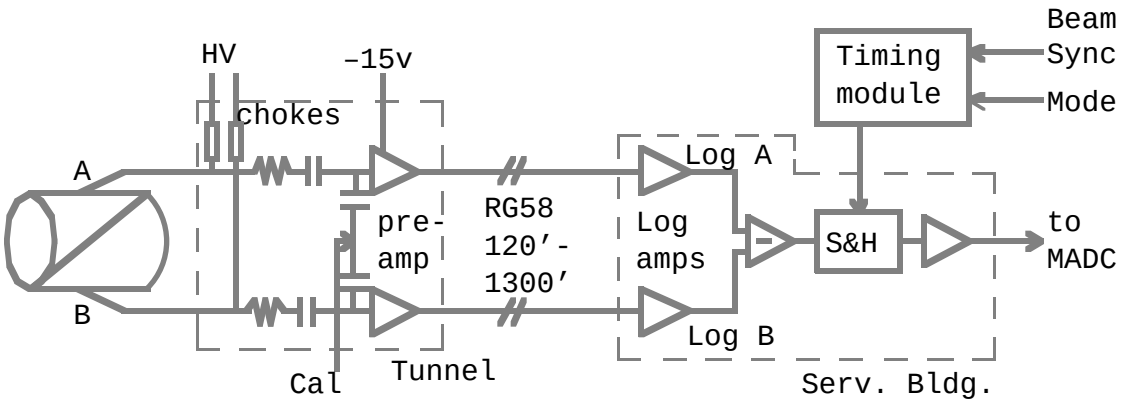

Figure 3.8.1: Block Diagram of the Recycler BPM System.

Short cables will connect detector feedthroughs to a small shielding box for the pre-amps and other components. The box, shared by two neighboring detectors, may be mounted above the Recycler magnets for enhanced radiation shielding. A high resistance couples the high DC voltages to the detector plates for ion clearing. The high voltages are daisy-chained for all the detectors in a sector. Current monitoring takes place at the source of these voltages, in the service buildings. A calibration signal, resembling a typical signal pulse, will also be daisy-chained throughout a sector. When activated, it will be loosely coupled equally to the two signal paths.

The low signal frequencies enable use of inexpensive RG58 50Ω cable for the 120'-1300' cable runs. Additional cables are needed for the two pre-amp DC supplies, the ion-clearing high voltage, and the calibration signal. Dual use of cables for DC and AC signals is being considered. Figure 3.8.1 contains a sketch of the BPM system.

The cost constraints of the Recycler project and the nature of the detector signals demand a new, inexpensive processing scheme and control system interface. Innovations in analog processing technology and the Fermilab control system make that possible.

The position can be derived from the signals of a linear detector by

$$\frac{x[mm]}{b[mm]} = \left(\frac{A-B}{A+B}\right) \approx \frac{Ln10}{2}\left(\log A - \log B\right) \quad , \quad (3.8.1)$$

where A and B are amplitudes of the two plate signals and b is the detector radius. Recent improvements in logarithmic amplifiers [Analog Devices, Inc., AD640 and AD608 data sheets, Analog Devices Design-In Reference Manual, 1994] enable a large dynamic range and high bandwidth. Laboratory tests on a simulated Recycler signal show a dynamic range near 50 dB. These chips approximate the log function. Log nonconformance, which leads to errors, is expected to fall within the accuracy specification. Subtraction by a differential op-amp results in a voltage which is converted

to position after system (detector and electronics) offset subtraction and scaling. This can be carried out in the control system.

The position signal will be digitized using standard MADC-compatible ADCs from the Controls Department. The result is interfaced to the control system with the CAMAC 290 MADCs. The differing signal occurrence times at the BPMs (a range of 2 μs per sector for both protons and antiprotons) and the two operating modes (injection and stack) require a sample-and-hold circuit with correct timing. From the 1.6 μs minimum signal length, acquisition time, and other factors, it is anticipated that 6 distinct timing signals are needed per house. These will be created with CAMAC 279 modules, synchronized to the Recycler Ring Beam Sync clock.

The digitized signals are converted into ACNET database devices with scaling as described above. Standard acquisition types will be available, including "snapshot" (closed-orbit), "flash" (single-turn), and turn-by-turn (TBT). Note that only one TBT channel is possible per MADC, and current plans call for two MADCs per house. An application page will control acquisition modes and timings, as well as calibrations done during beam-off times.

3.8.2. Beam Loss Monitor System

The Recycler Ring will use the beam loss monitor system of its neighbor, the Main Injector. There will be no additional monitoring for the Recycler.

3.8.3. Longitudinal Wideband Pickup

One resistive wall current longitudinal pickup will be built for the Recycler and placed in the MI-30 region. The design will be identical to that used for the Main Injector. It will be used for studies and any possible longitudinal monitoring systems.

The basic design of this resistive wall current monitor is to insert a ceramic gap shunted with resistance in the vacuum pipe and measure the voltage induced by the beam wall current [R. Webber, "Longitudinal Emittance an Introduction to the Concept and Survey of Measurement Techniques Including Designing of a Wall Current Monitor", AIP Acc. Instr. Conf. Proc. #212, 1989]. The ultimate bandwidth of such a detector is limited by the spreading of the electric field lines between the beam and the image charge on the inside wall. For the monitor's 5" circular aperture and the relativistic Recycler beam, the bandwidth limit is 23 GHz.

In practice the detector response is difficult to maintain above the microwave cutoff frequency of the beam pipe, estimated to be 1.4 GHz for the 5" diameter. Spurious electromagnetic energy, generated by various discontinuities and guided along the beam pipe, corrupts the image current signal. Microwave absorber material is placed inside a 6" vacuum pipe up and downstream of the detector to reduce this noise by 20 dB. The absorbing material is an epoxy-based Resin Systems RS4825 core. It is placed outside a 5" aperture ceramic sleeve to preserve vacuum specifications without lessening the absorbing properties. This solution is cheaper and more readily available than the previous vacuum-friendly absorber.

The detector maintains a 3 kHz low frequency cutoff with a series of toroids shunting the resistance across the gap. An impedance of 1Ω (122 resistors of 112Ω each) terminates a radial transmission line formed by the 140 mil ceramic gap. Four signal

pickoff points spaced evenly around the gap are summed to reduce position dependence and azimuthal signals. The result is a position-independent longitudinal monitor with ±1 dB flat response from 3 kHz to 6 GHz, as measured with a tapered 50Ω transmission line test setup. An identical, reciprocal port can be used for calibration.

3.8.4. Transverse Wideband Pickups

The Main Injector transverse wideband pickup design will be used in the Recycler. Two pickups, one for each plane, will be placed at MI-30 for studies purposes.

Standard striplines are planned for both the horizontal and vertical planes. Feedthroughs at both ends will be used to observe both proton and antiproton signals. The plate length of 55", $\lambda/4$ at 53 MHz, will be used to increase signal and to maximize doublet separation when viewing proton injections. In the frequency domain, zeroes in transmission will occur at those frequencies where the plate is $\lambda/2$ long.

3.8.5. Transverse Profile Monitors

The Ionization Profile Monitor (IPM) system [Zagel, J., "Fermilab Booster Ion Profile Monitor System Using LabView", AIP Acc. Instr. Conf. Proc. #333, 1994], used in the Booster and Main Ring/Main Injector, is planned for the Recycler Ring. Two systems are needed to handle the transverse planes. The IPM uses a microchannel plate to collect and amplify ions produced when the beam passes through residual gas in the detector. The high quality vacuum in the Recycler may necessitate an intentional, localized, calibrated gas leak at the IPM detector.

The 8 kV clearing field of the Booster IPM sweeps the ions across the 10 cm aperture onto a microchannel plate, which amplifies the current and deposits it onto a grid of 1.5 mm spaced conductors etched into a printed circuit card. The current induced in each conductor is amplified, digitized, and stored each turn. The amplifiers have a gain of 2.5 X 10^6 volts per amp and 100 kHz bandwidth. The digitizers are commercial 4 channel 12 bit VME cards which have 64 Kwords of memory for each channel. A National Instruments MXI adapter is used to access the VME cards with a Macintosh computer running LabView software. The Main Ring IPMs use a 20 kV clearing field across the 10 cm aperture with 0.5 mm conductor spacing on the collection grid.

A flying wire system is not being included due to the high reliability demanded of the Recycler ring. The possibility of the failure mode of the wire getting stuck in beam was considered too great.

3.8.6. Transverse Schottky Monitor

The Recycler Ring transverse Schottky monitor system [Chou, P., "Transverse Schottky Detector for Antiproton Recycle Ring", internal Fermilab note] will be similar to the new Main Ring system but with much higher sensitivity. The primary system output is a two channel (for two planes) spectrum analyzer display in the main control room. Various beam parameters can be calculated from information provided by transverse Schottky signals, including fractional tune, transverse emittance, momentum spread, chromaticity, and presence of trapped ions [Peterson, D., "Schottky Signal Monitoring at Fermilab", AIP Acc. Instr. Conf. Proc. #229, 1990].

The two Schottky detectors, to be located at MI-30, will be round, split-plate capacitive pickups. A box in the tunnel will contain a transformer, designed to resonate the detector at 79.263 MHz and to couple to the output cable. The resonant frequency was chosen at the harmonic number n=882.5, halfway between the first two harmonics of the Main Injector RF system. A bandwidth of 90 kHz (one revolution harmonic) requires a loaded quality factor Q_L=880. To enable this high Q and maintain stability, suitable feedthroughs must be found and temperature drift effects must be small. The detector sensitivity is given by

$$S_{\perp} = \frac{l}{2bc}\sqrt{\frac{R_o\,\omega_c\,Q_o}{C_t}} \qquad , \quad (3.8.2)$$

where l is length, nominally 40 cm, b is aperture radius, c is speed of light, R_o is the receiver's 50Ω termination, ω_c is radian resonant frequency, Q_o is unloaded Q, and C_t is total capacitance. Design calculations estimate a sensitivity of 22 Ω/mm, much higher than the Main Ring system (0.9 Ω/mm) and comparable to the Tevatron's (27 Ω/mm). Low-loss heliax 50Ω cables will be used to bring the signals upstairs.

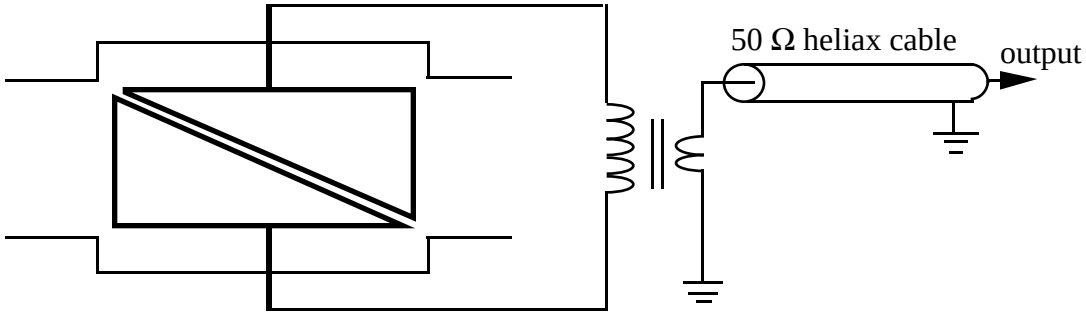

Figure 3.8.2: Sketch of the Recycler transverse Schottky electrical model. The split plate pickup provides a linear position response function. The system is resonated at 79.263 MHz (n=882.5).

The Schottky receiver down-converts the signal bandwidth to baseband for use with a low frequency spectrum analyzer. A Trontech ultra-low noise amplifier provides 60 dB of gain. Variable attenuators tune the gain. Custom crystal bandpass filters from Piezo Technology, Inc. set the signal bandwidth at 100 kHz. The local oscillator signal might be generated by a Main Injector injection frequency oscillator, if available, or a fixed custom oscillator. Unlike the Main Ring/Main Injector, the Recycler energy is constant at 8.9 GeV. Thus, its revolution harmonics will remain fixed and no frequency tracking is needed. A mixer down-converts the signal before a final low-pass filter and gain stage. A long length of RG-8 low loss cable brings the outputs to the Main Control Room and the spectrum analyzer. Given that a horizontal and vertical system are needed, this implies 2 cables to the control room and two channels of FFT capable digitizers.

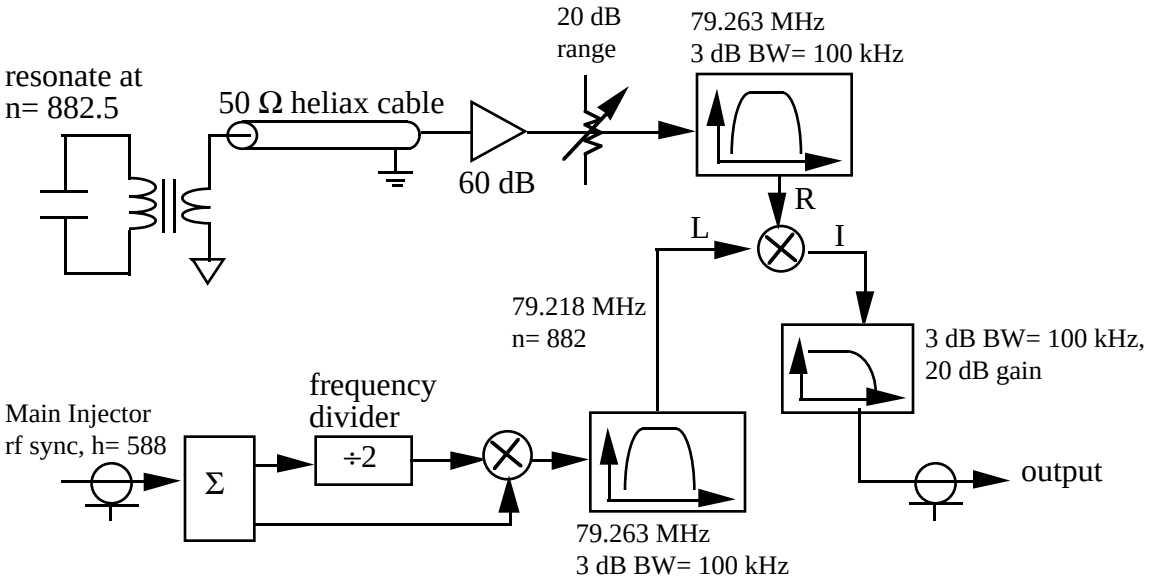

Figure 3.8.3: Sketch of the beam processing electronics which conditions the RF signal from the detector to a low frequency signal a signal analyzer can measure.

3.8.7. Ring Current Monitor (DCCT)

The DC Current Transformer, or parametric current transformer, uses the second harmonic detection principle to measure the DC beam current in series with an AC transformer to extend the bandwidth (Unser, K., "The Parametric Current Transformer, a beam current monitor developed for LEP", AIP Acc. Instr. Conf. Proc. #252, 1991). Fermilab does have a number of versions of the DCCT, but a commercial version will be purchased for a Recycler unit at MI-30. The Bergoz current monitor (Bergoz, Parametric Current Transformer data sheet) is 4.25" long and offers several apertures from 2" to 7". At this time, a 3" pipe is anticipated at MI-30. A ceramic break is required for use with the Bergoz monitor. Radiation damage can be reduced by selecting the radiation hard sensor option and locating the tunnel front-end electronics (maximally 5 m from the sensor) where radiation dosage is less than 10^4 rad/year.

The DC current monitor is relied upon for absolute beam current calibrations. The Bergoz monitor specifies a frequency response from DC-20 (optionally 100) kHz, dynamic range of 2 X 10^7 for each full scale range, resolution optionally to 0.5 μA, and absolute accuracy and linearity of 0.05% and 0.01%, respectively. The ±10V output is digitized and interfaced to the controls system with the MADC.

3.8.9. Toroids

Toroid systems are AC-coupled intensity monitors that are cheaper than DCCTs and appropriate during transient events such as injections and extractions. The present toroid design used Pearson Electronics, Inc. model number 3100 current monitors. The aperture is 3.5" and the output signal is 0.5 volts/amp into 50Ω with a bandwidth of 40 Hz to 7 MHz. At the toroid output the signal is 85 mV for 10^{10} ppb. The toroid is electrically isolated from ground in the enclosure and good quality cable such as LDF4-50A is

required to avoid noise problems. The toroid must be placed over a ceramic break in the vacuum pipe. To reduce the RF energy radiated into the environment a ground connection is required across the break but external to the toroid.

The signal is transported to the service building where the electronics amplifies, limits the bandwidth, and integrates the signal to provide a voltage representing the total charge. The present design [Vogel, G., "Toroid Integrator User Guide", internal Fermilab note] in use includes a baseline subtraction circuit, a fixed length integration window, and an A/D and D/A used to form a sample and infinite hold. The toroid integrator has a bandwidth of 100 Hz to 400 kHz and selectable gains of $2x10^{11}$, $2x10^{10}$, and $2x10^{9}$ particles/volt.

There are 6 toroid systems required due to the addition of the Recycler Ring. Figure 3.8.4 shows the relative locations of these systems. For each transfer between the Main Injector and the Recycler there are 3 toroids; one to determine the initial intensity, one record the transfer line intensity, and finally one to measure the final intensity. For the abort line there is an initial intensity and an abort line intensity.

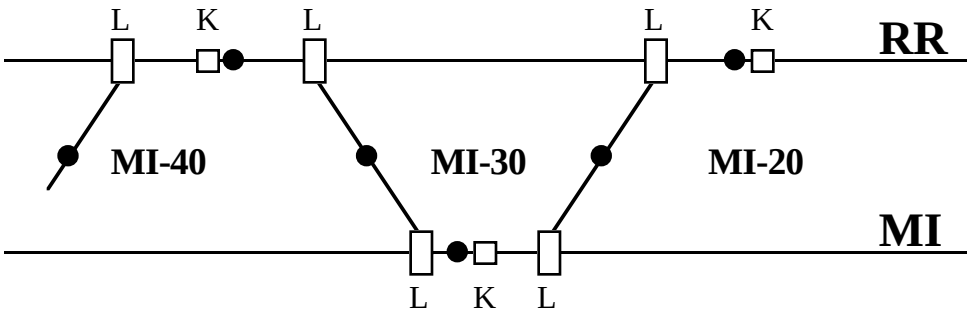

Figure 3.8.4: Sketch of the placement and number of toroids in the Main Injector and Recycler to service the instrumentation needs of the Recycler transfers. The Lambertsons (L), kickers (K), and toroids (black dots) are shown with respect to the service building the reside in.

3.9. Controls (WBS 3.1.9)

Controls requirements have been the focus of a number of cross-departmental discussions. Because of the novel nature of many of the technologies employed in the Recycler ring, it is important that a thorough exploration of hidden demands on controls be identified. Just as in the case of beam instrumentation, it is vital for efficient commissioning of the Recycler that all control software and hardware be installed and tested before actual accelerator commissioning commences. Below is the result of these scope explorations.

3.9.1. Stochastic Cooling System

Existing equipment will be moved from the present Tevatron bunched beam stochastic cooling R&D implementation. CAMAC equipment now residing at F0 TeV crates \$60, \$61, \$62 will be moved to their new locations at MI-20 and MI-30.

3.9.2. Power Supplies

The two kickers in the Recycler and one kicker in the Main Injector will need power supply controllers - CAMAC C118 cards and beam synch triggers supplied by C279 cards. All associated Lambertsons are built with permanent magnets and do not require power supply controls.

There are a number of dipole correctors required in the Recycler ring and its transfer lines. Around each of the 3 Recycler Lambertsons a 4-bump orbit offset is required in both planes. This requirement alone involves 24 correctors. In the transfer and abort lines another 20 correctors are required. Figure 3.3.1 contains a sketch of the corrector count and placement.

In addition to the dipole correctors, the phase trombone quadrupoles, the two skew quadrupoles at MI-60, and the correction sextupoles at MI-20 and MI-50 are also powered with Main Ring ramped corrector chasis.

All correctors will utilize existing MR corrector power supplies and existing corrector coils, each chassis controls 6 correction elements. A total of 8 of these supplies are required: 2 at MI-20, 4 at MI-30, and 2 at MI-40. It should be noted that additional bulk power supply control in addition to what CAMAC 053 cards can provide is required. Six CAMAC 118 cards will be included to cover this need.

3.9.3. RF Systems

The low level RF system developed for the Recycler RF system, which is a copy of the VXI MI LLRF system, will be located at MI-60. It will need an accelerator controls ethernet connection to the VXI platform.

3.9.4. GPIB Interfaces

Stochastic cooling, RF, and instrumentation all need GPIB connections. There will be an interface at MI-20, MI-30, and MI-60 (assuming up to 32 devices per connection). A high speed and reliable VME based interface will be used.

3.9.5. Vacuum System

There will be one ion pump for every 2 half cells (104 total) for the Recycler itself. There will also be 4 pumps for each of the transfer lines (16 total). Each pump requires control and monitoring. No automatic valves (other than the safety critical devices) will be allowed in the Recycler in order to eliminate the chance of accidental antiproton stack loss. All of the valves will be manually operated. The positions of these manual valves will not be electronically monitored. Instead, valve motion will only be allowed via the insertion of keys which can only be removed when the valves are in the out position. The keys are put in a low-tech key tree to make up a permit. The requirement for gauges is two ion gauges per vacuum sector (every 8 cells for a total of 13 sectors and 26 gauges). CIA crates are the best way to effect control of Recycler pumps. Spare control channels are available in planned Main Injector CIA crates at 4 of the 6 service buildings. Two CIA crates (and ARCNET controllers) will be purchased for the other service buildings. One CIA card can control 6 pumps. Some spare gauge channels will be used by the Recycler. Sharing CIA crate space with the Main Injector vacuum system will not

present any software problems. Summary of ring and transfer line (XL) pumps and their geographical position are summarized in table 3.9.1.

Table 3.9.1: Summary of the Recycler pump controller locations around the ring. Transfer line (XL) pumps are also included in the count.

Service Bldg	# of Cells	Ring Pumps	XL Pumps	Total Pumps
MI-10	16	16	0	16
MI-20	16	16	0	16
MI-30	20	20	8	28
MI-40	16	16	2	18
MI-50	16	16	0	16
MI-60	20	20	0	20
Totals	104	104	10	114

3.9.6. Beam Position Monitors (BPM)

It is possible to support the Recycler BPM system with existing multiplexed ADC (MADC) and CAMAC 290 card controllers dedicated to this function. Scans of the closed orbit can occur every 1 to 2 seconds. Turn-by-turn beam position acquisition is also supported. For turn-by-turn data taking, the MADCs (and controllers) must be fast enough to accommodate the Recycler's 90 kHz revolution frequency. A minimum 12 bit resolution for the MADC has been specified.

There is one horizontal and one vertical BPM every half cell, for a total of 416 Recycler ring beam position measurements. Intensity signals will not be provided by the BPM RF modules. Horizontal and vertical monitors are distributed to separate MADCs to facilitate acquiring turn-by-turn data. This will require at least two MADC systems per house (service building). Connection to the sample and hold analog outputs of the BPMs should be direct and use 16 twisted pair cable for direct connection to the MADC. Avoiding use of an Analog Entry Box will save costs.

Table 3.9.2: Summary of BPM MADC system counts and locations.

Service Bldg	# Cells	Horz BPMs	Vert BPMs	XL BPMs	Total BPMs
MI-10	16	32	32	0	64
MI-20	16	32	32	0	64
MI-30	20	40	40	28	108
MI-40	16	32	32	8	72
MI-50	16	32	32	0	64
MI-60	20	40	40	0	80
Totals	104	208	208	36	452

Associated control of BPM data acquisition requires generation of a "sample" signal triggered by a RRBS event. Also required at each service building are four CAMAC

279 cards listening for the sample event to provide appropriately timed triggers to the BPM module's sample-and-hold (S&H) circuit. The data taking mode of the CAMAC 290 cards is controlled by TCLK events and software. A timing resolution of 1 μsec is required for BPM signal sampling.

There are also BPMs associated with each of the transfer lines. These are included in table 3.9.2 as "XL BPM", with half being horizontal and the other half vertical. The ring beam sync timing will also serve to trigger the S&H circuits of the transfer line BPMs.

3.9.7. Control System Front Ends

Recycler controls requirements do not require an additional front end computer. Specialized instrumentation systems such as residual gas ionization profile monitors using Macintosh computers running the LabView software are connected directly to the ethernet link around the ring.

3.9.8. Accelerator Control Consoles

An MI-30 control room for Recycler commissioning and electron cooling research, development, and eventual commissioning will need two consoles.

3.9.9. Beam Permit System:

Because of the precious nature of antiprotons, the beam permit system will only be applied to protons during commissioning. The Recycler beam permit system status will be applied to the beam switch sum box (BSSB) to adjudicate injection of protons. CAMAC 200 cards, input panels, and repeaters will be installed at each of the 6 Main Injector service buildings and the main control room. All equipment should be available from the MR system after decommissioning. The beam permit will be physically implemented with a spare optical fiber.

3.9.10. Recycler Ring Beam Sync Clock (RRBS)

The low level RF system will provide: a revolution marker (53 MHz/588); 7.5 MHz (53 MHz/7), and 53 MHz. Various CAMAC modules are necessary for clock generation and have been added to the WBS. These will be located at MI-60 and include two CAMAC 377 cards, a CAMAC 280, 175, and 276 card. These signals will be supported ring-wide and at the main control room, so at least 12 fiber repeaters are necessary. RRBS will use a spare optical fiber.

3.9.11. Software

Unlike the Main Injector, in which most systems existed previously in the Main Ring, the Recycler relies on new subsystems, new geometries, and hence new software. Because of the traditional tendency to underestimate software manpower requirements, serious discussions of the scope of software requirements have been held. Below are the results of these discussions.

Database entries: The stochastic cooling system gets transferred from the Tevatron. Everything else is created new. Because of the use of permanent magnets, the non-

existence of distributed corrector systems, and the lack of utilities, the total number of database entries is <1000. A new "R" index page will be created and R:xxxxxx database entries will be facilitated.

Applications: After studying the applications driving the other Fermilab accelerators, a list of programs relevant to the Recycler ring has been developed. Some of the applications are rather generic, such as DataLogger, vacuum readback, and parameter pages. The orbit control/magnet move program is very important, and is already applied to Fermilab accelerators. With the addition of the Recycler lattice to the program database, it will be able to function with minimal modification. Similarly, the stochastic cooling software already exists from the Tevatron Collider bunched beam cooling effort. New programs for low level RF control and beam position measurement must be written. Just as the number of database entries is orders of magnitude smaller than other accelerators, the number of application programs is similarly low.

3.10. Safety System (WBS 3.1.10)

The additional safety system components necessary to support the Recycler are quite limited. To insure the termination of the coasting beam in the Recycler, two gravity activated fail safe vacuum isolation gate valves will be used. These valves are necessary because permanent magnets cannot be readily turned off and interlocked.

3.11. Utilities (WBS 3.1.11)

Besides a limited amount of conventional power, the only utility being used by the Recycler is LCW. The subsystems which consume this water are described below. All usages are in service buildings. Note that the total water flow required by the Recycler is approximately 40 gallons/minute. There are sometimes leaks in the Main Ring that are larger than this!

3.11.1. Dipole Corrector Supplies

The dipole correctors supplies at MI-10, MI-30, and MI-40 require 4 gallons/minute per chassis. Each chassis services 6 correctors. Table 3.11.1 summarizes this usage.

Table 3.11.1: Summary of LCW water usage rates at each service building in which a need exists for the ring and its dedicated transfer lines.

Location	# Chassis	LCW Need
MI-20	4	6 gal/min
MI-30	4	16 gal/min
MI-40	2	8 gal/min
MI-50	2	8 gal/min
MI-60	2	8 gal/min

3.11.2. Stochastic Cooling Traveling Wave Tubes

The stochastic cooling kickers at MI-30 are driven by traveling wave tubes (TWT) which require a couple of gallons per minute per tube. Given that there are three cooling channels, a total of approximately 6 gal/minute is required.

3.11.3. Moving Existing LCW Pipes

There are a limited amount of valves, pipes, and air dehumidifiers which have already been installed in the MI-60 straight section which will have to be moved because of the addition of the Recycler. In addition, in order to build the MI-22 and MI-32 transfer lines between the Main Injector and Recycler the LCW headers in the regions between Q212 & Q222 and Q320 & Q330 need to be moved.

4. Civil Construction

In this section the civil construction associated with the Recycler project is described. The purpose of this work is to construct both the penetrations for the stochastic cooling fiber optic cables and the laser telescopes for signal transmission between the pickup and kicker tanks.

4.1. Stochastic Cooling Penetrations

The penetrations for the stochastic cooling system are situated at Main Injector quadrupole locations Q213 and Q109. As shown in figure 4.1.1, a 2" diameter pipe between the berm toe line and the tunnel is inserted in order to provide a conduit for alignment control cables and fiber optic signal transmission lines. This pipe is placed in a hole bored by a drilling crew.

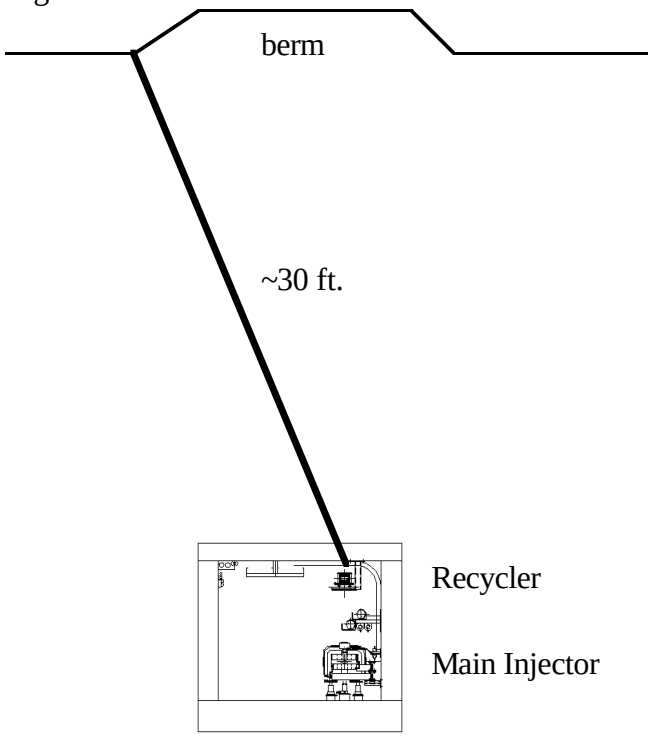

Figure 4.1.1: Tunnel and berm cross-section with a 2" diameter conduit for stochastic cooling signal transmission via optical fibers. In addition, the alignment control cables for aiming the laser beams and the electrical service for the required pumps and motion control must also fit in the conduit.

4.2. Stochastic Cooling Telescope

Approximately 8' below the surface near Q213 the horizontal, vertical, and two momentum stochastic cooling signals, transmitted as AM modulation on four separate laser beams, are aimed toward the Q109 location. The transition from optical fiber to a 1" diameter laser beam (and back to fiber optic again) is accomplished with commercial optical components. All of these components are passive and do not require power. The

lasers are aimed through a window into an evacuated pipe for signal transmission. The pipe has a diameter of 18" and is 3/16" thickness stainless steel coated for cathodic corrosion protection.

In order to aim the laser beams, it is necessary to have remote piezoelectric motion control. The power, control, and diagnostic readback cables for aiming come from the tunnel. The exact location of this optical transition/aiming hardware is at present designed to be approximately 8' underground. In order to assure maximum stability against transverse pipe motion, the pipe is buried below the frost line. Because the aiming mechanism is below ground, and that hardware must be installed and maintained, a manhole accessed underground enclosure is required on both sides of the telescope. These enclosures require sump pumps in order to keep the aiming hardware and optical fibers dry. The power for the sump pumps also comes from the tunnel via the stochastic cooling penetrations discussed in section 4.1. A sketch of an enclosure appears in figure 4.2.1.

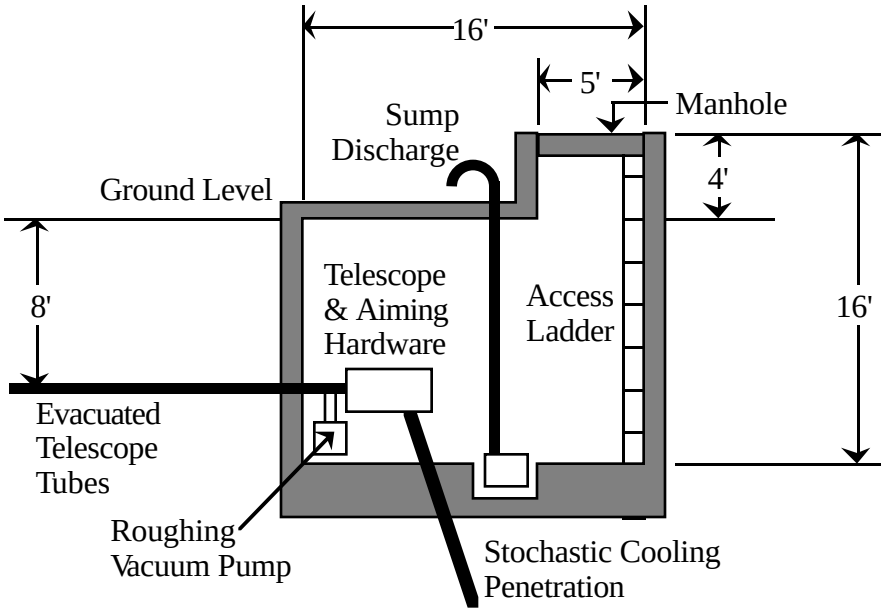

Figure 4.2.1: Sketch of one of the enclosures required at each end of the stochastic cooling signal telescope. One inexpensive model for this enclosure is a sewer access manhole constructed of round, pre-fabricated concrete components.

Therefore, the civil construction implications of the stochastic cooling telescope are; 1) the excavation of an 8 ft. deep and 1800 ft. long trench for burial of the signal transmission pipes, and 2) the construction of two human accessible underground enclosures on either side of the telescope.